

Model-driven design of synthetic microbial communities for the upcycling of One-Carbon feedstocks



Sara Benito Vaquerizo

Propositions

1. A mathematical model of metabolism is never complete, neither should it be.

(this thesis)

2. The pH is the main limitation for the feasibility of synthetic microbial communities.

(this thesis)

3. The bias of artificial intelligence models mirrors societal inequalities.

4. The translation of the intrinsic mechanisms of nature into practical knowledge is the only way to drive scientific progress.

5. ChatGPT is a friend, not a threat, even for teachers.

6. Gender equality faces three crucial barriers: history MANipulation, inherited power structures and economic interests.

7. Putting things into perspective is used to justify the unjust.

Propositions belonging to the thesis, entitled

Model-driven design of synthetic microbial communities for the upcycling of One-Carbon feedstocks.

Sara Benito Vaquerizo

Wageningen, 23 June 2023

**Model-driven design of synthetic
microbial communities for the
upcycling of One-Carbon feedstocks**

Sara Benito Vaquerizo

Thesis committee

Promotors

Prof. Dr V.A.P Martins dos Santos
Personal chair at Bioprocess Engineering
Wageningen University & Research

Prof. Dr M. Suarez Diez
Personal chair at the Laboratory of Systems and Synthetic Biology
Wageningen University & Research

Co-Promotor

Prof. Dr D.Z. Machado de Sousa
Personal chair at the Laboratory of Microbiology
Wageningen University & Research

Other members

Prof. Dr M. H. Zwietering, Wageningen University & Research
Dr H. De Wever, VITO, Mol, BE
Dr F.R. Bengelsdorf, University of Ulm, DE
Dr R. Kleerebezem, Delft University of Technology, Delft

This research was conducted under the auspices of the Graduate School VLAG (Advanced studies in Food Technology, Agrobiotechnology, Nutrition and Health Sciences).

Model-driven design of synthetic microbial communities for the upcycling of One-Carbon feedstocks

Sara Benito Vaquerizo

Thesis

submitted in fulfilment of the requirements for the degree of doctor
at Wageningen University
by the authority of the Rector Magnificus,
Prof. Dr A.P.J. Mol,
in the presence of the
Thesis Committee appointed by the Academic Board
to be defended in public
on Friday 23 June 2023
at 4 p.m. in Omnia Auditorium.

Sara Benito Vaquerizo

Model-driven design of synthetic microbial communities for the upcycling of One-Carbon feedstocks,

271 pages.

PhD thesis, Wageningen University, Wageningen, the Netherlands (2023)

With references, with summary in English and Spanish

ISBN 978-94-6447-700-9

DOI <https://doi.org/10.18174/630256>

Contents

1	Introduction	1
2	Renewable methanol and formate as microbial feedstocks	15
3	Modeling a co-culture of <i>Clostridium autoethanogenum</i> and <i>Clostridium kluyveri</i> to increase syngas conversion to medium-chain fatty-acids	33
4	Genome-scale metabolic modelling enables deciphering ethanol metabolism via the acrylate pathway in the propionate-producer <i>Anaerotignum neopropionicum</i>	61
5	Model-driven evaluation of the feasibility of Clostridia communities to produce even and odd-chain fatty-acids from syngas	95
6	Model-driven approach for the production of butyrate from CO ₂ /H ₂ by a novel co-culture of <i>C. autoethanogenum</i> and <i>C. beijerinckii</i>	123
7	A structured evaluation of genome-scale constraint-based modeling tools for microbial consortia	155
8	Discussion	191
	Summary	205
	Resumen	209
	References	213
	List of publications	257
	Overview of completed training activities	261
	About the author	265
	Acknowledgements	267

Chapter 1

Introduction

1.1 Circular bio-based economy

By 2050, world population is expected to increase up to 9.7 billion [1]. As a consequence, waste generation is estimated to rise from 2 to 3.4 billion tons a year (70 %), outpacing population growth ($\approx 20\%$) by more than double [2]. The energy demand is also projected to increase nearly 50% in the next thirty years [3]. Yet, the majority of global primary energy consumption and source of commodity chemicals relies on fossil fuels, such as oil, coal and gas. Fossil fuels are not sustainable and their continue use is dramatically accelerating climate change and affecting public health [4]. Hence, it is imperative that we find and implement alternative processes for the sustainable production of fuels and commodity chemicals.

The primary goal of the Paris agreement for climate change is to reduce carbon emissions by 45% by 2030 and, ultimately, become carbon neutral by 2050 [5]. More than 70 countries -including the highest polluters- have set a net-zero target, which would mean already a 76% reduction of global emissions. 2050 is still far away, but 2030 is around the corner. This leaves seven years to develop solutions and to deploy them in a competitive manner. Thus, we need to start taking action on promising solutions now.

Specifically, we need to radically change the way we manage our natural resources, how we use and make products, and what do we do with the waste later on. This can be achieved with a transition towards a circular bio-based economy, a structured solution approach that tackles climate change, biodiversity loss, waste, and pollution [6], enhancing the use of renewable natural capital, minimizing waste and replacing non-renewable/fossil-based products currently in use [7]. The resulting bio-based products would contain biogenic carbon originated from sustainable feedstocks such as biomass or wastes, and thus, the final CO_2 emissions is biogenic CO_2 that is considered carbon-neutral [8]. Considering our net-zero target and the need to implement circular approaches, research is now needed to explore promising solutions. In this regard, microbial conversion of C1 feedstocks is envisioned as the way forward.

1.2 One-carbon (C1) feedstocks

Since the 1980s, the production of biofuels from agricultural feedstocks (grains, seeds and sugars) has largely increased as a sustainable technology to mitigate climate change [9, 10]. Despite some examples where biofuels and animal feed were produced from the same process [11], the use of agricultural substrates still raises concerns and disapproval as they compete with food production and endanger biodiversity [12, 13]. To avoid this competition, the use of waste streams and lignocellulosic biomass as feedstocks to produce sustainable biofuels and chemicals is also being explored as a potential alternative. However, the hydrolysis of lignocellulosic biomass leads to complex mixtures, difficult to break down and that require further separation and processing, ultimately requiring larger facilities and higher energy costs for transportation than the previous technology [14]. Nevertheless, gasification of these complex mixtures allows for the conversion of carbon in the original source to synthesis gas. Synthesis gas -syngas- is a mixture of CO, H₂, CO₂ and traces of CH₄ and other gases.

One-carbon (C1) gases can also directly be obtained as off-gas in steel-mill industries, and from the sequestration of carbon from the atmosphere. Due to their low production cost and high availability, they have gained attention as preferable feedstocks for the sustainable production of fuels and chemicals. In fact, the production of bioethanol from C1 gases is now at industrial scale [13, 15–17].

Formate and methanol are other C1 feedstocks particularly interesting since they are miscible, which circumvents gas-liquid mass transfer limitations associated to gaseous feedstocks [18]. Formate (and CO) can be obtained from the electrochemical reduction of CO₂ [19], via photoreduction of CO₂ [20] or via hydration of syngas [21], among others. Methanol is produced from syngas, usually obtained by means of steam reforming of natural gas [22], and it can be used as energy carrier for hydrogen storage and conservation [23].

1.3 Microbes as cell factories for the production of high-value chemicals

Plant biomass can be used to produce many natural products that have an important role as biofuels, chemicals, pharmaceuticals or flavors. In fact, plant-derived biofuels represent the most abundant source of renewable fuels [24]. However, their production rate often fluctuates due to changes in climate and frequently result in low productivities. The fluctuations also affect the prediction of productivities, which introduces risk and volatility in the supply chains. Besides, these solutions

are tied to a particular location which also makes them more susceptible to geopolitical disturbances (e.g., sunflower in Ukraine). Chemocatalytic processes, such as the Fischer-Tropsch synthesis can convert syngas to synthetic fuels [25], but they present some limitations. For instance, these processes require high purity level of syngas to avoid poisoning of the catalyst, strict CO/H₂ ratios, and high operational costs associated to the high temperature and pressure operations [26]. Alternatively, the use of microbes as cell factories to produce high-value chemicals is gaining attention, as they present several advantages over plants and chemocatalytic processes [13, 27, 28]. In general, microbes have high specificity, required when the target is a specific product [29], they can grow in a more controlled environment than plants, since they are not dependent on weather, and their production does not fluctuate. They are not tied to grow on a specific location as their operational units can be set everywhere. Microbes are low-priced and can be genetically modified, which often leads to higher productivities. Besides, they can handle better than chemical catalysts the variations of CO/H₂ ratios, and are also more resistant to impurities (e.g. sulfides), reducing the need for highly-priced pre-treatment of syngas [27].

1.4 Microbial conversion of C1 feedstocks

Methylotrophs are able to grow on C1 compounds such as methane, methanol, methylamine, formaldehyde, formate, formamide or carbon monoxide [30]. *Methylobacterium extorquens* is a facultative aerobic methylotroph that grows on methanol and methylamine as well as others C2-C4 compounds, and it is highly used to study methylotrophy [31]. Formatotrophs use formate as carbon source or for reducing power. *Cupriavidus necator* is one of the most studied native formatotrophs, it can grow on formate as sole carbon source and autotrophically using the Calvin-Benson-Bass-ham (CBB) cycle to fix CO₂ with addition of H₂. It is highly used as a platform for the production of polyhydroxyalkanoate (PHA) [32].

Formatotrophs and methylotrophs can naturally grow aerobically on formate and methanol via the serine cycle (*M. extorquens*), CBB, Ribulose Monophosphate (RuMP) Cycle, Dihydroxyacetoneformate (DHA) Cycle, reductive glycine (rGly) pathway and synthetically via the formolase pathway [13]. rGly has been recently discovered in anaerobic bacteria (*Desulfovibrio desulfuricans*) [33]. Previous studies stated that it is the most efficient route to assimilate formate aerobically (1 ATP/pyruvate) [19, 34–36], outperforming other natural pathways [13]. Thus, recent studies have focused on implementing this pathway synthetically in model organisms and natural formatotrophs and methylotrophs for biomass production [37–40]. For instance, *Escherichia coli* cannot grow on C1 feedstocks, neither aerobically nor anaerobically, but recent efforts have successfully proved the ability of *E. coli* to grow on formate

and methanol [41–47] via the rGly pathway. This pathway was also implemented into the model organism *Pseudomonas putida* for assimilation of methanol, formate and CO₂ [40], and in yeast for growth on formate [48]. Growth on formate was demonstrated via the same pathway in *C. necator* [39], where the yield through the rGly pathway was for the first time proven to exceed yield of the Calvin cycle [38].

While aerobic microbial growth on methanol and formate has shown potential for biomass production, its use as a platform for valuable products is less explored. Furthermore, the toxicity events associated to formate and methanol present a challenge [13]. Anaerobic microbial conversion of C1 feedstocks has been proven to have a higher energetic efficiency than the aerobic conversion [13], and it has already led to the successful production of valuable products at industrial scale [17, 49, 50].

Acetogens are anaerobic bacteria that can use CO, CO₂/H₂, methanol and formate via the Wood-Ljungdahl (WL) pathway [51]. Some acetogens could possibly use the rGly pathway for autotrophic growth as they harbour the genes of the rGly pathway [33] and was already demonstrated in *Clostridium drakei* [52]. Acetogens can therefore grow on syngas converting it into acetate, ethanol, and traces of formate, 2,3-butanediol or lactate. Few acetogens also have the ability to produce butyrate, caproate, butanol and hexanol [53]. *Clostridium autoethanogenum* is the acetogen usually used as chassis for syngas fermentation. For instance, for the upcycling of waste-derived CO/CO₂ into ethanol, that is now a product successfully commercialized [49]. However, the low water solubility of gases limits mass transfer and, consequently, microbial growth and productivity. This is a limitation that could be overcome using miscible substrates (i.e., formate or methanol). Acetogens also present energy limitations, since they operate at a thermodynamic edge. In the WL pathway, formate is converted to formyl-tetrahydrofolate investing one molecule of ATP that is recovered by producing acetate via substrate level phosphorylation. Hence, the WL pathway and subsequent acetogenesis have a net zero ATP production. Thus, acetogens have to rely on additional mechanisms to generate ATP, and that is the coupling between the Na⁺-translocating ferredoxin:NAD⁺ oxidoreductase (Rnf) complex or the reduced ferredoxin:H⁺ oxidoreductase (Ech) and the ATP synthase. The free energy change of the electron transport chain in the former complex system (Rnf/Ech-ATP synthase) is coupled to the translocation of ions, creating an electrochemical ion gradient across the membrane that is used to generate ATP through the ATP synthase [54]. The net ATP production per mol of acetate and ethanol produced from CO₂ and H₂ is only 0.3 and 0.14 - 0.15, respectively [55]. CO is more energetically favourable, with a net ATP production per mol of acetate and ethanol of 1.5 and 1.7, respectively. Acetogens oxidize CO to CO₂ (that enters the WL pathway) generating reducing equivalents. Yet, part of the CO₂ is lost. The utilization of H₂ can reduce the loss of carbon, and should increase the production of reduced products, which makes the use of syngas (CO, H₂ and

CO₂) more attractive [56]. Energy barriers in acetogens limit the range of products to simple, short-chain molecules (ethanol and acetate) and, therefore, strategies are needed to obtain products of higher value from C1 feedstocks.

1.4.1 Microbial cultures in Biotechnology: Synthetic microbial communities for enhanced production of added-value chemicals

Since few years ago, the use of metabolic engineering strategies have been implemented in acetogens, enabling the increase of ethanol and 2,3-butanediol production [50, 57], the production of ethyl acetate from ethanol [58], or the production of acetone and isopropanol in pure acetogen cultures [59]. However, pure cultures often present difficulties to fully utilize complex substrates, have reduced fitness, may lead to contamination and are product specific, which limit its application [60].

Open-mixed cultures can utilize complex, cheap and impure substrates leading to more products, and are more stable and robust than pure cultures. In addition, the metabolic burden of costly metabolites can be overcome due to the introduction of division of labour, in which complex tasks are distributed between community members for mutual gain [61]. The production of medium-chain fatty-acids (MC-FAs; C6-C8) has been achieved by mixed cultures from CO and from real syngas effluents [62, 63]. Regardless of these advantages, in open mixed-cultures microbes often compete for the same substrate and there can be inhibitory events due to unknown species or interactions, which might affect the control and predictability of these systems [60].

The use of synthetic microbial communities is emerging as a potential strategy to tackle the shortcomings of pure and open-mixed cultures. Synthetic microbial communities comprise communities of generally two to three species, selected *a priori* for a specific purpose. Synthetic communities are often designed forcing a direct cross-feeding of metabolites to optimize substrate consumption or to produce a product of interest that would otherwise not be obtained from the same substrate by the two species separately. In addition, unwanted by-products, competence among members or inhibition occurrences are significantly reduced and often avoided, compared to open mixed cultures. Ultimately, members of the community can be replaced, added or removed in a modular way to fulfill the process needs (Fig. 1.1), which is an advantage that open-mixed cultures do not have [60].

Fig. 1.1, which illustrates the work of this thesis, shows how the product portfolio of a synthetic microbial community can be tuned from even- to odd-chain fatty-acids and their respective alcohols by the addition of a microbe that brings a different phenotype (production of propionate), or by the replacement of a microbe that re-

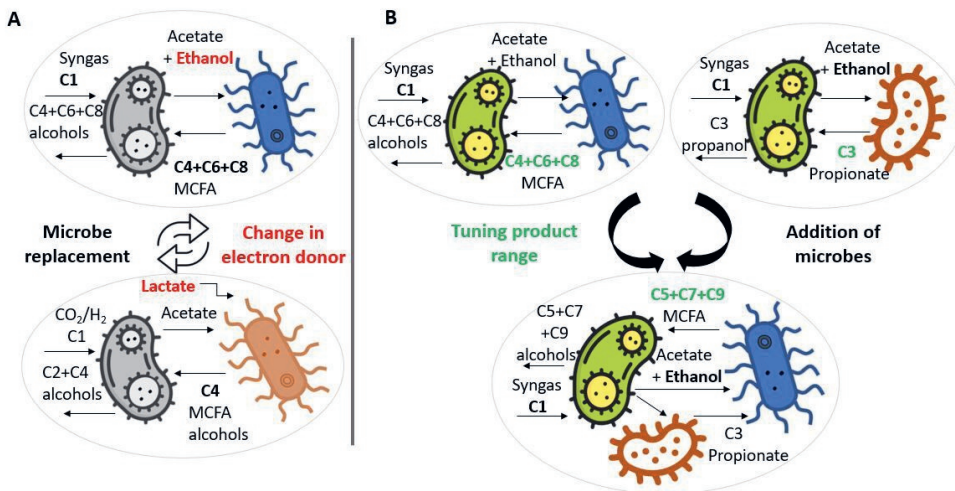


Figure 1.1: Modular approach for the design of synthetic microbial communities for C1 conversion to added-value chemicals. Microbes can be replaced (A) or added (B) targeting products of different chain-lengths.

quires a different electron donor to ethanol (lactate). Owing to these advantages, synthetic microbial communities have flourished in the past decade showing their potential to produce added-value chemicals from the conversion of numerous substrates (monosaccharides, polysaccharides, alcohols and C1 feedstocks), and going beyond the products obtained by pure cultures [64–70]. For instance, the production of even-chain fatty acids (C4–C8) and alcohols from syngas was demonstrated by co-cultivation of the acetogens *C. autoethanogenum* or *Clostridium ljungdahlii* and the chain-elongator species *Clostridium kluyveri* [64, 65, 68]. Another example is the production of MCFAs from CO₂/H₂ by *C. autoethanogenum* and the solventogen *Clostridium beijerinckii* [70], and the production of odd-chain MCFAs from CO by a tri-culture of the acetogen *Acetobacterium wieringae* JM, the propionate-producer *Anaerotignum neopropionicum* and *C. kluyveri* (chapter 5, Fig. 1.1).

Despite the numerous advantages, synthetic microbial communities present limitations that still impede their industrial implementation. Most of the previous examples showed robust and stable communities since they were grown under conditions where all members survived, e.g., same pH range. However, often optimal conditions differed favouring growth in detriment of production, or favouring the accumulation of intermediates rather than final products.

1.5 Computational approaches to increase the potential of microbial systems

Some of the drawbacks and limitations of microbial systems as cell factories can be addressed with the support of computational approaches. Genome-scale constrained-based metabolic modeling is the computational approach commonly used to study microbial systems through genome-scale metabolic models (GEMs). GEMs represent the list of metabolic reactions, metabolites and genes retrieved from the annotation and curation of microbial genomes. GEMs have been shown to be potent tools in biotechnology and health applications for pathway design, pathway evaluation, process characterisation, chassis optimisation and media design [71, 72]. For instance, the use of metabolic modeling led to the identification of targets for the increase of oil production in oleaginous yeasts [73]. The construction of the GEM of *C. autoethanogenum* shed light into the energy metabolism of anaerobic gas fermentation in acetogens [74]. Recently, GEMs have also been used to study functional reprogramming of cancer cells at the pathway level [75]. In the past decades, the construction of microbial GEMs has rapidly increased due to the enlarged availability of sequenced genomes [72]. Genomes are sequenced and subsequently annotated through bioinformatic tools that are constantly being improved and expanded. CarveMe, ModelSEED, KBase, Raven, AuReMe [76–80], among others, are tools that automatically construct a draft model from annotated genomes, incorporating in some cases the genome annotation step [81]. The output draft models require a following manual curation and refinement to improve their quality and completeness [82]. Often, there is a preference for the use of reduced GEMs, known as core models. They represent a small and essential part of the metabolism including the central carbon and energy metabolism, and additional pathways related to phenotypes of interest (e.g., substrate utilization or product formation). While information of secondary metabolism or amino acids pathways is lost, the use of core models is often preferable since it reduces computational time and complexity (e.g., dynamic modeling), futile cycles are avoided, and have shown similar predictability to full models [83].

GEMs are studied using Constrained-Based Reconstruction and Analysis (COBRA) techniques available in several packages, such as COBRA Toolbox and COBRAPy [84, 85]. In these approaches, the information contained in a GEM is translated into a mathematical problem; a stoichiometry matrix (S) and a vector representing the flux through all of the reactions in a network (v). This matrix represents the stoichiometry of every metabolite and every reaction. The stoichiometry of reactants is represented with a ‘-’, and the stoichiometry of products with a ‘+’ in the matrix. GEMs have different type of reactions; metabolic reactions, transport and extracellular reactions. Intracellular reactions take place inside the cell (i.e. the cy-

tosol). Transport reactions represent the flux of a metabolite from the intracellular compartment to the extracellular compartment, and vice versa. Extracellular reactions represent the uptake rate of substrates or the production of metabolites. The reversibility of the reactions is represented with bounds, which symbolize the maximum flux that one reaction can have ($\text{mmol gDW}^{-1} \text{h}^{-1}$) and the flux direction. When a reaction has a negative flux, this indicates that the flux goes in reverse direction, and the other way around. In addition, GEMs have a biomass synthesis reaction, representing the growth rate (h^{-1}). Additionally, more constraints can be applied to, for example, define the substrate uptake rate or block flux through a specific reaction. Flux Balance Analysis (FBA) [86] is one of the mathematical approaches most commonly used to simulate scenarios with GEMs. FBA assumes steady-state ($S.v=0$), and fluxes are computed under the specified constraints maximizing a predefined objective function; normally, the biomass synthesis reaction. FBA requires the definition of an objective function, as a way to mimic the most common cellular objective, cell growth. Objectives can be modified, and one can maximize production of a product of interest or the uptake of a specific substrate. However, this can result in an overestimation of the objective function, that could be far from reality. Flux Variability Analysis (FVA) [87] is an alternative approach that can overcome some of the FBA limitations. FVA gives the maximum and minimum flux that satisfies a defined % of the maximum objective function. Flux sampling [88] is a promising approach that instead of maximizing a predefined objective function, inspects the feasible solution space by generating probability distributions of steady-state metabolic fluxes under specified conditions [89]. FBA, FVA and Flux sampling are meant to represent continuous systems where a steady-state is reached.

Dynamic FBA (dFBA) [90], an extension of FBA, is an approach that uses FBA to update the flux of the extracellular environment, and kinetics to calculate the concentration of substrates and products over time. These approaches have been successfully implemented to represent non-continuous environments (i.e., batch, fed-batch) with pure cultures for unraveling principles of microbial metabolism, designing strategies to increase desired products, substrate conversion or microbial growth [72, 91, 92].

Several algorithms identify possible genetic interventions targeting the production of a desired product, and coupling growth and production [93, 94]. There are also extensions of GEMs that aim to improve the predictability of these models. Enzyme-constraints GEMs (ecGEMs) [95] for example, include enzyme kinetics and abundances, and GEMs of metabolism and gene expression (ME-models) [96] include the synthesis of the gene expression and calculate the optimal proteome allocation for a specified phenotype. The predictability of GEMs can be increased by the addition of information in the form of constraints based on transcriptomics, proteomics and genomic data.

1.5.1 Metabolic modeling of microbial communities

In the past decade, genome-scale, constrained-based metabolic modeling has also been extended to model microbial communities of two to more than hundred individuals for biotechnology, medicine and bioremediation applications [97, 98]. Modeling communities brings additional complexity to mathematical formulations compared to the modeling of single species. The simulation of continuous environments requires the creation of a community model. This is achieved by the extension of the stoichiometric matrix with the integration of single species models as single compartments, and a common extracellular compartment through which they share metabolites with one another. In single species models, the flow of metabolites is represented with specific fluxes ($\text{mmol gDW}^{-1} \text{h}^{-1}$), and growth rate is calculated for 1 g of biomass. In community models, each species have their own relative abundance with respect to the total biomass of the community. To account for this, the flow of extracellular metabolites is represented as environmental fluxes ($\text{mmol (L)}^{-1} \text{h}^{-1}$) and the relative abundance would be integrated as part of the biomass synthesis reaction, or transforming environmental fluxes to specific fluxes when calculating intracellular fluxes of each species, and vice versa. In continuous environments (e.g. chemostat), balanced growth of species and the community can be assumed; thus, the mathematical problem becomes a linear problem. cFBA is one of the approaches that best predict continuous environments and assumes balanced growth [99]. The main difference among all type of approaches is the consideration of the objective function. Many tools optimize the community growth or/and the species growth rates (MMT, MICOM, OptCom) [100–102]. Yet, the selection of the objective function in static approaches is not unanimous, and some approaches (e.g. OptCom) [102] do not consider balanced growth of species and communities in environments where steady-state is assumed (e.g. chemostats). A solution to this is the use of approaches that do not require the maximization of an objective function (e.g. Flux sampling). Non-continuous environments can be simulated with dynamic approaches. In these approaches, the species can grow at a different growth rate, and single GEMs are not integrated in the same stoichiometric matrix, but treated separately, and dFBA can be applied. In general, dynamic approaches differ again in the selection of the objective function. Some opt for the maximization of the community growth rate (DyMMM) [103], some others follow a bi-level approach and require the definition of a second objective, usually the species growth rate (e.g. d-OptCom) [104], or a priority list of objectives [105]. Finally, spatiotemporal approaches aim to represent 2D dimensional surface environments (e.g. Petri dish) informing on the spatial distribution of extracellular metabolites, biomass of species and uptakes rates at any given time point (e.g. COMMETS) [106]

In the past decade, several tools became available that aimed to model contin-

uous, dynamic and spatiotemporal environments using GEMs [99]. Although some tools still need some refinement, they have been used to design new co-cultures, gain access to microbial metabolism and to suggest genetic interventions for increased production [51, 70, 107–109].

1.6 Thesis objectives and outline

In this thesis I aim to i) gain understanding into principles of cellular metabolism of C1-fixation, ii) guide experimental designs for the conversion of C1 substrates to added-value chemicals by synthetic microbial communities, and iii) focus on strategies to increase the production of even- and odd-chain medium-chain fatty-acids (MCFAs) in these systems. To these ends, I assess the state-of-the-art of microbial C1 conversion and bioproduction, construct GEMs of individual species and community GEMs of synthetic communities, validate those GEMs with experimental data, and run simulations to guide new experimental designs. To achieve these objectives I apply FBA, dFBA, flux sampling, constraint-based optimization algorithms, GEM reconstruction tools and community modeling approaches and tools, that were also evaluated.

In **chapter 2**, I (along with my co-workers) review the mechanisms of microbial C1 conversion. We compare the energetic efficiency of the bioproduction of biomass and products between the aerobic and anaerobic conversion of C1 feedstocks. We also describe and compare the biomass, acetyl-CoA and pyruvate yield of the assimilation of methanol and formate via natural and synthetic pathways using the core model of *E. coli* and FBA. Finally, we discuss the challenges of using methanol and formate as microbial feedstocks.

In **chapter 3**, **chapter 4** and **chapter 5** I describe how we follow a modular approach by assembling different combination of microbes to target the production of even- and odd-chain products from syngas. First, a co-culture of an acetogen and a chain elongator species was proven to produce even-chain fatty-acids (**chapter 3**, **chapter 5**). Next, the incorporation of a propionate-producing species proved the shift of products from even- to odd-chain fatty-acids (**chapter 4**, **chapter 5**).

In **chapter 3**, a community GEM of a co-culture of *C. autoethanogenum* and *C. kluyveri* is constructed. Then the co-culture GEM is used to model the conversion of syngas to even-chain fatty acids comparing with available chemostat data using an expanded cFBA with Flux Sampling. This requires the scaling of specific fluxes to environmental fluxes by the incorporation of the relative abundance (biomass species ratio). The relative abundance are calculated from microscopic observations and from RNAseq reads. I identify the effect of the relative abundance on the production and consumption of cross-feeding metabolites. Finally, I identify strategies

to optimize the production of MCFAs.

In **chapter 4**, I present the first GEM of the propionate producer *A. neopropionicum* for its further incorporation in a community that targets the production of odd-chain fatty acids. The GEM is validated with experimental data of growth experiments on several substrates using Flux sampling and fermentation of ethanol (+ acetate) in batch using dFBA. The GEM serves to clarify the mechanisms of the acrylate pathway for propionate production. The annotation and construction of the model served to identify key metabolic elements of this species and to understand their role in the metabolism.

In **chapter 5**, I present the community GEMs of the acetogen *Acetobacterium wieringae* JM and *C. kluyveri*, and of *A. wieringae* JM, *A. neopropionicum* and *C. kluyveri*. The assessment of these two communities (a co-culture and a tri-culture) shows the shift of products from even- to odd-chain by the incorporation of *A. neopropionicum*. I assess the feasibility of the communities at different species ratios and growth rates with cFBA, and identify possible designs for the optimization of even- and odd-chain fatty acids using cFBA with Flux Sampling. As the GEM of *A. wieringae* JM was not available yet, I present the newly constructed model that was built using the GEM of *C. autoethanogenum* as scaffold.

In **chapter 6**, modeling is used to design a community able to produce butyrate from CO_2 and H_2 . For this, I assess growth on single and a combination of two carbon sources on the GEM of the solventogens *C. beijerinckii* and *C. acetobutylicum* to choose the potential candidate to co-assimilate acetate using FBA. Batch experiments confirm growth on the proposed candidates (acetate and glycerol/lactate) in *C. beijerinckii*. Then, the feasibility of a co-culture of *C. autoethanogenum* and *C. beijerinckii* on several combinations of species relative abundances, growth rates, CO_2/H_2 ratios and lactate feed rates is assessed with cFBA with FBA and Flux sampling. A wide range of conditions initially confirmed the feasibility of the co-culture which was subsequently established. The co-culture produces mainly butyrate and isobutyrate, a newly identified product.

In **chapter 7**, we highlight the potential of using community modeling for alternative processes and systems other than microbial C1 re-valorization. We assess the state-of-the-art of available community modeling tools/approaches to model static, dynamic and spatiotemporal environments. We qualitatively assess the tools and approaches evaluating features that covered the FAIR principles. Additionally, we quantitatively test top candidate tools/approaches in regard to their performance in reproducing available experimental case studies of synthetic microbial communities in the three environments. We base our evaluation in small communities of two species and tools that used GEMs and COBRA methods. Finally, we identify the strengths, weaknesses and challenges of using these tools and suggest recommendations for future developments and improvements of the tools.

Finally, in **chapter 8**, I discuss how these chapters contribute to meet the objectives of this thesis and what aspects still need to be tackled. I highlight the potential and challenges of using synthetic microbial communities for the upcycling of C1 feedstocks, as well as the ones pertaining to the use of GEMs and metabolic modeling of microbial communities, giving recommendations to address some limitations. I assess the future perspectives of synthetic microbial communities, evaluate their current status, and give recommendations for achieving their future scale-up.

Chapter 2

Renewable methanol and formate as microbial feedstocks

2

Charles A.R. Cotton*, Nico J. Claassens*, Sara Benito-Vaquerizo*, Arren Bar-Even
Published in: Curr. Opin. Biotechnol. 62, 168-180 (2020).

doi.org/10.1016/j.copbio.2019.10.002

* Contributed equally

2.1 Abstract

Methanol and formate are attractive microbial feedstocks as they can be sustainably produced from CO₂ and renewable energy, are completely miscible, and are easy to store and transport. Here, we provide a biochemical perspective on microbial growth and bioproduction using these compounds. We show that anaerobic growth of acetogens on methanol and formate is more efficient than on H₂/CO₂ or CO. We analyze the aerobic C1 assimilation pathways and suggest that new-to-nature routes could outperform their natural counterparts. We further discuss practical bioprocessing aspects related to growth on methanol and formate, including feedstock toxicity. While challenges in realizing sustainable production from methanol and formate still exist, the utilization of these feedstocks paves the way towards a truly circular carbon economy.

2.2 Introduction

To expand the share of commodity and fine chemicals produced biologically, it is vital to identify alternative microbial feedstocks to replace sugars and agricultural products, the use of which erodes food security and threatens biodiversity [110, 111]. One carbon (C1) compounds have recently gained attention as alternative

feedstocks for microbial growth. These compounds are naturally abundant (e.g., methane [112]), cheap to produce (e.g., methanol from methane [113]), or available as industrial by-products (e.g., carbon monoxide [114]). C1 compounds can also be produced from CO₂ and renewable energy, which is critical for the establishment of a sustainable circular carbon economy. For example, carbon monoxide and formate can be produced by electrochemical or photochemical reduction of CO₂ [115, 116]. Also, H₂, produced electrochemically and photochemically [117], can be reacted with CO₂ to generate formate [118], methanol [119], and methane [120].

Cultivation of microorganisms on C1 gases – methane, carbon monoxide, and H₂/CO₂ – has been explored in numerous studies and reviewed elsewhere (e.g., [28, 112, 114, 121, 122]). However, all C1 gases suffer from the common challenge of low water solubility, which limits mass transfer and thus microbial productivity [123, 124]. In contrast, formate and methanol are completely miscible, bypassing the mass transfer barrier and potentially supporting higher microbial productivities. Another major advantage of these two compounds is that, unlike the C1 gases, they can be easily stored and transported. This enables a spatial and temporal decoupling of the abiotic feedstock production from the biotic feedstock consumption, an important feature that serves to insulate microbial growth and bioproduction from fluctuations in the availability of renewable energy.

Cultivation of microbes on methanol has already been extensively explored, both scientifically and commercially [125]. Already 50 years ago industrial production of microbial proteins from methanol was pursued to supply human and animal nutrition [126]. However, until recently, the source of methanol was always considered to be fossil methane rather than CO₂. In contrast with methanol, formate has been largely neglected as a potential industrial feedstock, due to its relatively high price. The only exceptions were proposals to use formate as an auxiliary carbon source to supplement the cell with reducing power and thus boost bioproduction [127]. With developments in electrochemical, photochemical, and catalytic methods of generating formate, interest in its use as a microbial feedstock is rising [19, 128, 129].

In a recent study, we used experimentally measured growth parameters to calculate the energetic efficiencies associated with the microbial conversion of different carbon sources into biomass and products [130]. We showed that methanol and formate outperform other C1 compounds as microbial feedstocks (Fig. 2.1). Specifically, the energetic efficiency by which anaerobic acetogens convert methanol and formate into a product is 80-90%, rather than 60-80% when cultivated on H₂/CO₂ or carbon monoxide. Aerobically, the energetic efficiency of converting methanol and formate into biomass can reach 50%, while for other C1 feedstocks it lies in a range of 20-40%. The high efficiencies associated with microbial growth on the miscible C1 compounds are key to their commercial use.

Here, we aim to provide an overview of microbial cultivation on methanol and

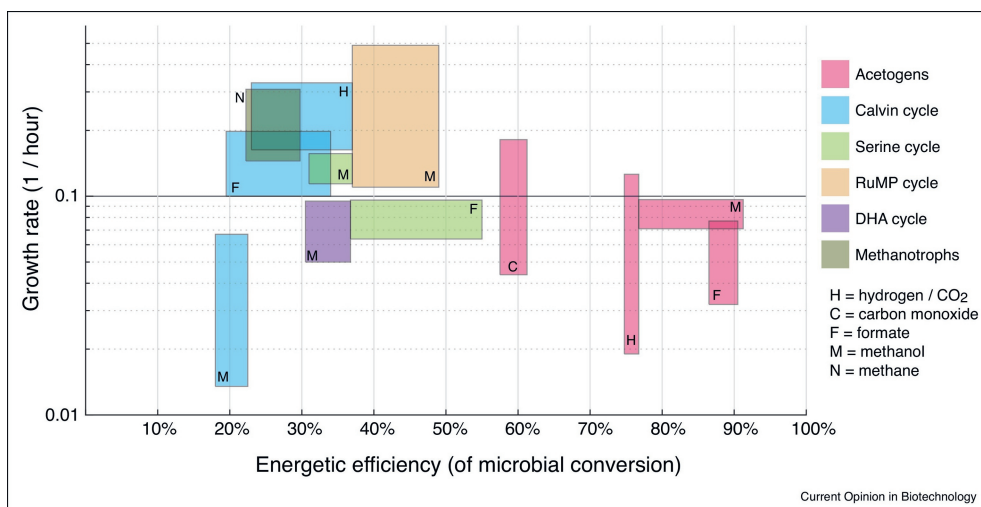


Figure 2.1: Methanol and formate support higher energetic efficiencies under both aerobic and anaerobic conditions. Rectangles represent the 25-75% percentile values as calculated using experimentally measured values for mesophilic microorganisms ($\leq 49^{\circ}\text{C}$) as available in ref. [130]. Energetic efficiency was calculated as the fraction of the combustion energy of the substrate that is retained in the product (for acetogens) or biomass (for aerobic microbes). Detailed explanation of the calculations is provided in ref. [130]

formate. First, we discuss anaerobic growth of acetogens on these C1 compounds. Next, we analyze aerobic microbial growth on methanol and formate, starting with natural pathways and their variants and ending with synthetic pathways that might enable more efficient growth and bioproduction. Finally, we discuss specific technical challenges associated with microbial cultivation on methanol and formate.

2.3 Anaerobic growth of acetogens on methanol and formate: hidden treasure?

Bioproduction with acetogens is thoroughly researched and commercially exploited using gaseous C1 feedstocks, i.e., H_2/CO_2 and CO [131–133]. In contrast, only a small number of acetogens have been tested for growth on methanol and formate, which can be directly assimilated into the reductive acetyl-CoA pathway (Fig. 2.2). As compared to the gaseous feedstocks, the miscible carbon sources support higher energetic efficiencies of bioproduction (Fig. 2.1) [130]. For example, in the model acetogen *Acetobacterium woodii*, the energetic efficiency of acetate production from methanol and formate is 89% [134, 135], considerably higher than 74% with H_2/CO_2 [136].

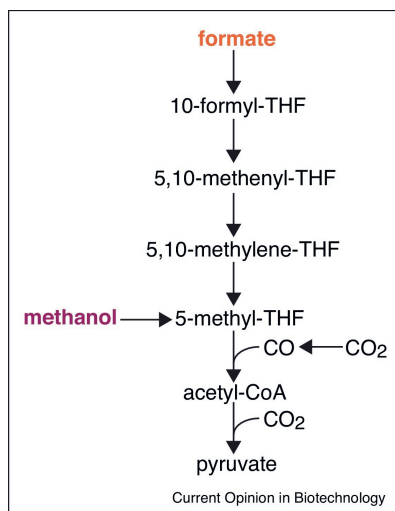


Figure 2.2: Formate and methanol are directly assimilated into the reductive acetyl-CoA pathway. Acetogens can integrate the miscible C1 carbon sources in the reductive acetyl-CoA pathway without the production of other metabolic intermediates, e.g., formaldehyde.

While little data is available regarding the growth rate of acetogens on methanol and formate, it seems to be in same range as for H_2/CO_2 : 0.03-0.08 h^{-1} for formic acid and 0.07-0.1 h^{-1} for methanol vs. 0.02-0.1 for H_2/CO_2 (Fig. 2.1) [130]. Similarly, acetogenic growth on carbon monoxide and methanol are comparable (Fig. 2.1); for example, the growth rate of *Eubacterium limosum* on methanol, 0.11 h^{-1} [137], is close to that on carbon monoxide, 0.165 h^{-1} [138].

The toxicity of methanol and formate for acetogens has never been comprehensively tested. Acetogens are commonly tested for growth on these feedstocks at concentrations ranging between 10 mM and 100 mM. The maximal reported concentrations tested are \approx 500 mM methanol and \approx 150 mM formate [139]. At these concentrations, methanol had some inhibitory effects on growth, whereas growth on formate resulted in a long lag phase [139]. While the cause of these inhibitory effects remains elusive, it is important to emphasize that some of the major toxicities associated with methanol and formate are completely avoided in acetogens. Specifically, methanol is assimilated directly into the tetrahydrofolate system without the formation of the highly reactive intermediate formaldehyde (Fig. 2.2), which is the major cause of methanol toxicity in aerobic methanol assimilation [113]. Similarly, anaerobic acetogens, which do not use respiratory proteins, avoid the toxic effects associated with formate inhibition of cytochrome c oxidase [140].

One of the major barriers that limits the use of acetogens for bioproduction is their highly restricted product spectrum [141], which, in many cases, requires challenging metabolic engineering to expand [121]. Exchanging the gaseous substrates $H_2/CO_2/CO$ with methanol and formate could provide an easier way to broaden this product spectrum. For example, *E. limosum* and *Butyrivacterium methylotrophicum* cultivated on methanol produce butyrate as a major product [142, 143]. A systematic characterization of how the product profile of acetogens shifts when gaseous substrates are replaced with miscible ones is still missing. Once performed, such analysis could point towards novel bioproduction opportunities with considerable economic prospects.

2.4 Aerobic growth on methanol and formate: native pathways and their variants

When compared with anaerobic conditions, cultivation of microorganisms with oxygen decreases the energetic efficiency, but dramatically expands the product spectrum as it uncouples bioproduction from generation of cellular energy [130, 131]. Aerobic growth on methanol and formate is naturally supported by four metabolic pathways: the Calvin Cycle, the Ribulose Monophosphate (RuMP) Cycle, the Dihy-

droxyacetone (DHA) Cycle, and the Serine Cycle. Yet, as we discuss below, this count might be misleading, as each of these pathways has several variants.

The Calvin Cycle is known to support growth on methanol and formate in multiple microbial lineages. In fact, aerobic growth on formate for biotechnological purposes was mostly explored with microorganisms which employ the Calvin Cycle, mainly *Cupriavidus necator* (formerly known as *Ralstonia eutropha*) [128, 144, 145]. However, the use of the Calvin Cycle for growth on either methanol or formate is characterized by a low energetic efficiency of only 20-35% (Fig. 2.1). Two main reasons explain this apparent inefficiency. First, as the physiological reduction potential of NAD^+ (-250 mV [146]) is considerably higher than that of CO_2 to formate or methanol (-420 mV and -400 mV), the complete oxidation of these C1 compounds with NAD^+ as an acceptor is energetically wasteful. Second, among the different carbon fixation pathways, the Calvin Cycle is one of the least energy efficient routes due to its high ATP consumption [147].

The RuMP Cycle and the DHA Cycle, operating exclusively in bacteria or yeasts, respectively, follow a similar metabolic strategy to enable methanol assimilation (Fig. 2.3). In both routes, methanol is first oxidized to formaldehyde, which is then condensed with a pentose phosphate to give metabolites that are reassimilated into the pentose phosphate pathway (PPP), regenerating the initial substrate and providing fixed carbon for cell growth. The RuMP Cycle converts methanol to biomass at a high energetic efficiency of 40-50%, while the DHA Cycle operates at a lower efficiency of 30-35%. The RuMP Cycle also supports a significantly higher growth rate than the DHA Cycle (Fig. 2.1). The higher efficiency of the bacterial RuMP Cycle can be explained by a lower ATP cost for glyceraldehyde 3-phosphate (GAP) formation (Fig. 3) and by the energetically wasteful oxidation of methanol with O_2 by methylotrophic yeasts using the DHA Cycle.

The RuMP Cycle nicely demonstrates that a metabolic pathway does not necessarily have a unique structural identity but rather represents a family of variants. The shared core of the RuMP Cycle consists of the enzymes 3-hexulose-6-phosphate synthase and 6-phosphate-3-hexuloisomerase, which together convert formaldehyde and ribulose 5-phosphate (Ru5P) to fructose 6-phosphate (F6P) (brown arrows in Fig. 2.3 A-D). The fate of F6P, however, differs between microbial lineages. In some microorganisms, F6P is metabolized via glycolysis and the non-oxidative PPP to regenerate Ru5P (Fig. 2.3 A,B), while in others, F6P is channeled to the Entner-Doudoroff (ED) pathway and Ru5P is subsequently regenerated from pyruvate and GAP (green arrows in Fig. 2.3 C,D). Another variation exists with regards to the production of sedoheptulose 7-phosphate, which can either be generated via the activity of a transaldolase (Fig. 2.3 A,C) or via the formation and dephosphorylation of sedoheptulose 1,7-bisphosphate (S17BP, blue arrows in Fig. 2.3 F,D). Finally, the oxidation of methanol to formaldehyde can be supported either by an

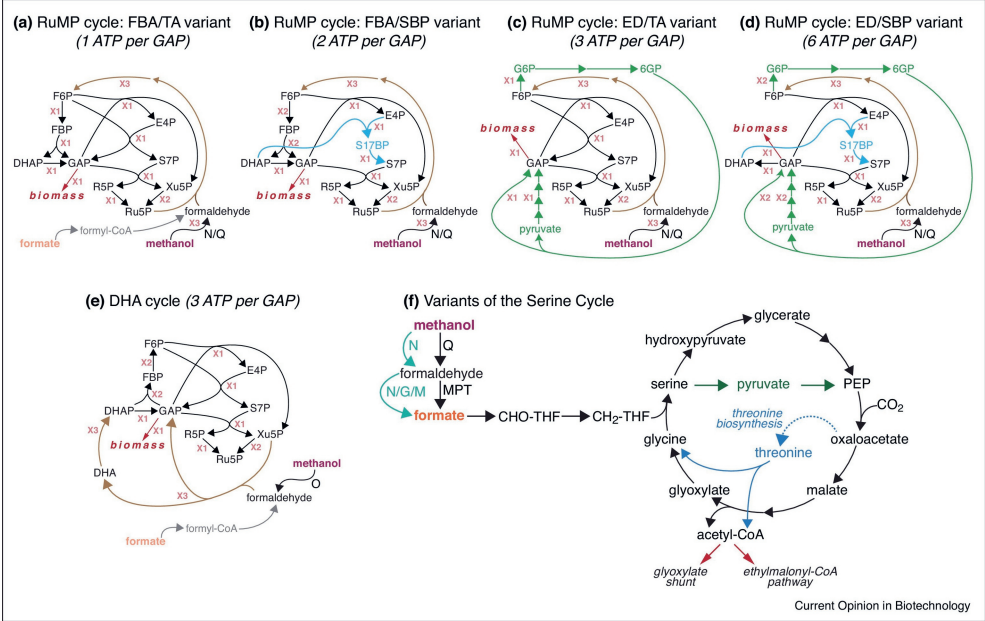


Figure 2.3: Natural pathways supporting the aerobic assimilation of methanol and formate and their structural variants. (A-D) Different variants of the RuMP Cycle, where glyceraldehyde 3-phosphate is assumed to serve as biomass precursor. Methanol oxidation to formaldehyde is supported by an NAD-dependent methanol dehydrogenase ('N') or by a PQQ-dependent enzyme ('Q'). Formate can potentially be reduced to formaldehyde via a formyl-CoA intermediate. (E) The DHA Cycle, where methanol is oxidized to formaldehyde via an O₂-dependent methanol oxidase ('O'). (F) Variants of the Serine Cycle. PQQ-dependent methanol dehydrogenase ('Q') can be replaced with an NAD-dependent enzyme ('N') and tetrahydromethanopterin ('MPT')-dependent formaldehyde oxidation can be replaced with an NAD-dependent ('N'), glutathione-dependent ('G') or mycothiol-dependent ('M') system. Serine conversion to hydroxypyruvate can be replaced with deamination to pyruvate (green arrows) and the formation and cleavage of malyl-CoA can be replaced with threonine biosynthesis and degradation (blue arrows). Assimilation of acetyl-CoA to biomass can take place either via the glyoxylate shunt or via the more efficient ethylmalonyl-CoA pathway. X1, X2 and X3 refer to the number of times a given reaction takes place in order to generate one GAP molecule (general precursor for biomass production). 'FBA' corresponds to fructose 1,6-bisphosphate aldolase; 'TA' to transaldolase; 'SBP' to sedoheptulose 1,7-bisphosphatase; 'ED' to Entner–Doudoroff pathway.

NAD-dependent enzyme or by a pyrroloquinoline quinone (PQQ)-dependent dehydrogenase [148].

Bioproduction from methanol via the RuMP Cycle has been explored mostly with the thermophile *Bacillus methanolicus* [113]. However, as genetic tools for the engineering of *B. methanolicus* and other methylotrophs that use the RuMP Cycle are limited, their use in biotechnology is restricted. To address this problem, several research groups are attempting to introduce the RuMP Cycle into biotechnological production hosts such as *Escherichia coli* and *Corynebacterium glutamicum* [149–153]. None of the attempts have so far been successful in establishing growth on methanol as sole carbon source. Yet, the combination of different strategies such as modular pathway engineering, growth-coupled selection for pathway activity, and adaptive laboratory evolution could pave the way towards synthetic methylotrophy in the near future [63, 154–156]. Bioproduction using methylotrophic yeasts that use the DHA Cycle, e.g., *Pichia pastoris* and *Hansenula polymorpha*, has been performed on industrial scale and mostly focused on the production of biomass, single-cell-protein, and, more recently, heterologous protein, while the production of smaller compounds is largely unexplored [157]. One study has attempted to introduce the DHA Cycle into the non-methylotrophic yeast *Saccharomyces cerevisiae*, but growth on methanol as sole carbon source was not demonstrated [158].

The RuMP Cycle and DHA Cycle could potentially support growth on formate if it could be reduced to formaldehyde *in vivo*. Such reduction was previously proposed, relying on the promiscuous activity of an acetyl-CoA synthetase which ligates CoA to formate to generate formyl-CoA and an (acetylating) acetaldehyde dehydrogenase which reduces formyl-CoA to formaldehyde [34, 129]. While the rate of these reactions is currently very low [129], it could be improved via enzyme engineering, allowing for the establishment of formate assimilation via the RuMP Cycle or the DHA Cycle. The Serine Cycle offers a completely different metabolic architecture to support the direct assimilation of both methanol and formate into cellular metabolism (Fig. 2.3F). Within this pathway, methanol is oxidized to formaldehyde by a PQQ-dependent enzyme, while formaldehyde is oxidized to formate via the tetrahydromethanopterin system [148]. These canonical oxidation routes could potentially be replaced with alternatives. PQQ-dependent methanol dehydrogenase might be exchanged with an NAD-dependent enzyme, which conserves more energy and hence could support higher yields. The tetrahydromethanopterin system might be replaced with a glutathione-dependent or mycothiol-dependent formaldehyde oxidation, or even with an NAD-dependent formaldehyde dehydrogenase [159]. For example, the introduction of a glutathione-dependent formaldehyde oxidation route from *Paracoccus denitrificans* enabled *Methylobacterium extorquens* to grow on methanol after the deletion of the endogenous tetrahydromethanopterin system [160].

The canonical structure of the Serine Cycle (black arrows in Fig. 2.3F) is con-

served in all microorganisms that use this pathway. Yet, alternative synthetic variants that might be more suitable for implementation in non-methylophilic biotechnological hosts have been suggested and at least partially demonstrated. For example, to bypass the formation of the highly reactive intermediate hydroxypyruvate [161], serine deamination to pyruvate was suggested and recently demonstrated in *E. coli* (green arrows in Fig. 2.3F) [34, 162]. Also, as the introduction of malyl-CoA synthetase and lyase could disrupt flux via the TCA Cycle, it was suggested that glycine could be regenerated via threonine biosynthesis and degradation (blue arrows in Fig. 2.3F) [34]. Indeed, glycine produced in this way was shown to be condensed with formate-derived 5,10-methylene-THF to generate serine in *E. coli* [163]. The product of the Serine Cycle, acetyl-CoA, can be assimilated via either the glyoxylate shunt or via the more energetically efficient ethylmalonyl-CoA pathway [148]. The replacement of the latter with the former was recently demonstrated in *M. extorquens* [164].

Microorganisms that use the Serine Cycle have been explored for multiple biotechnological applications, including high titers of the biopolymer polyhydroxybutyrate [165]. The development of versatile genetic tools (e.g., [166]) has enabled considerable expansion of the product spectrum with methanol as a feedstock; however for most products only low yields and titers have been achieved [113, 167–170].

2.5 Aerobic growth on methanol and formate: synthetic pathways

All naturally occurring aerobic methanol and formate assimilation pathways are cyclic and heavily overlap with microbial core metabolism (i.e., pentose phosphate pathway, glycolysis, and TCA Cycle). This makes their implementation in non-methylophilic hosts highly challenging, as it requires the establishment of a delicate balance between the high fluxes expected within the pathway with those that diverge from and converge into the pathway [171]. In contrast, the introduction of a linear C1 assimilation pathway should be much simpler to achieve. Indeed, two synthetic, linear methanol and formate assimilation routes – the reductive glycine (rGly) pathway and the formolase pathway – have been suggested and at least partially demonstrated.

The rGly pathway was designed as an aerobic analogue to the anaerobic reductive acetyl-CoA pathway [172]. It consists of naturally occurring, ubiquitous enzymes but is not known to support aerobic growth on methanol or formate in nature (although recently suggested to support growth under anaerobic conditions [173]). The core of the rGly pathway includes the condensation of formate with THF and

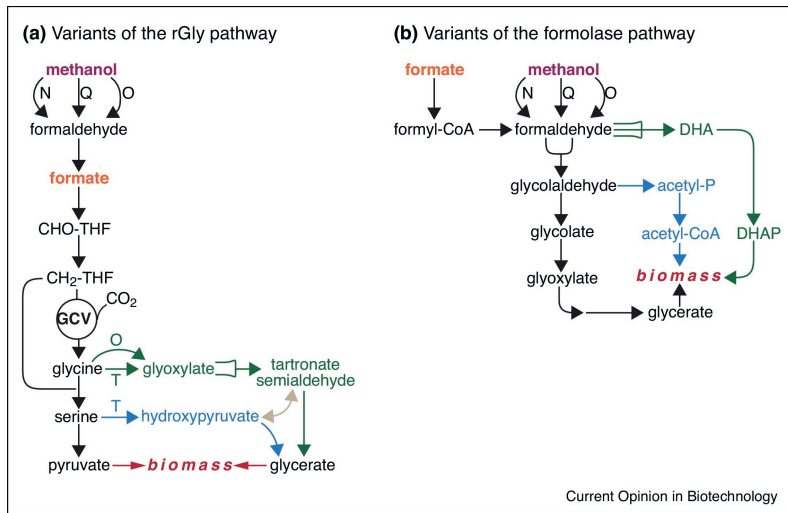


Figure 2.4: Synthetic methanol and formate assimilation pathways and their structural variants. (A) Variants of the reductive glycine pathway. Methanol can be oxidized to formaldehyde via an NAD-dependent ('N'), PQQ-dependent ('Q'), or O₂-dependent ('O') enzyme. Glycine can be converted to serine and then assimilated via deamination to pyruvate or conversion to glycerate (blue arrows). Glycine can also be converted to glyoxylate via a transaminase enzyme ('T') or an O₂-dependent oxidase enzyme ('O'). (B) Variants of the formolase pathway. Methanol can be oxidized to formaldehyde via an NAD-dependent ('N'), PQQ-dependent ('Q') or O₂-dependent ('O') enzyme. Formate can be reduced to formaldehyde via a formyl-CoA intermediate. Formaldehyde is condensed either to dihydroxyacetone (DHA, green arrows) or to glycolaldehyde. This latter intermediate can be assimilated via oxidation to glyoxylate using native enzymes, or via its conversion to acetyl phosphate using a repurposed phosphoketolase enzyme [178].

reduction to 5,10-methylene-THF (as in the Serine Cycle or the reductive acetyl-CoA pathway), followed by condensation of the latter metabolite with CO₂ and ammonia to produce glycine (Fig. 2.4A). This last transformation is catalyzed by the reversible glycine cleavage/synthase system (GCS) [174–176]. Within the initial design of the rGly pathway, glycine is condensed with another 5,10-methylene-THF to give serine, which is then deaminated to pyruvate to serve as a biomass precursor [172]. Biosynthesis of glycine and serine from formate via the rGly pathway was recently demonstrated in *E. coli* [44, 177]. In yeast, so far only production of glycine via the pathway was shown [48].

Other variants of the rGly pathway are possible and might be preferred under

some conditions (Fig. 2.4A). First, instead of deamination of serine, this amino acid can be assimilated into central metabolism as in the Serine Cycle, i.e., transamination to generate hydroxypyruvate (using, e.g., pyruvate as an amine acceptor [179]), followed by reduction to glycerate and phosphorylation to 2-phosphoglycerate. While relying on the highly reactive intermediate hydroxypyruvate, this route is more energetically efficient as it does not require the activity of energy-wasteful PEP synthase (which consumes two ATP equivalents per activation of pyruvate). Second, glycine can be assimilated into central metabolism without being converted to serine. Deamination of glycine to glyoxylate can be followed by self-condensation to generate tartronate semialdehyde which is then reduced to glycerate and phosphorylated to 2-phosphoglycerate (Fig. 2.4A). This deamination can be catalyzed either by a transaminase (using, e.g., 2-ketoglutarate as an acceptor [180]) or using an oxidase enzyme (e.g., [181]). While the latter enzyme is energetically wasteful, dissipating reducing power, its main advantage is its irreversibility, pulling formate assimilation towards glycine biosynthesis.

Another synthetic, linear C1 assimilation pathway was based on an engineered formolase enzyme, which condenses three formaldehyde molecules to generate dihydroxyacetone which is assimilated into central metabolism via phosphorylation to dihydroxyacetone phosphate [129]. This pathway can potentially support growth on methanol which is oxidized to formaldehyde [182] or on formate which is converted to formaldehyde via the generation and reduction of a formyl-CoA intermediate [129] (Fig. 2.4B). At lower formaldehyde concentrations, the formolase enzyme condenses two formaldehyde moieties instead of three, giving rise to glycolaldehyde [178, 183]. Glycolaldehyde can enter central metabolism using natural enzymes that catalyze its oxidation to glyoxylate, which is subsequently assimilated as described above (Fig. 2.4B). Alternatively, a recent study has demonstrated the use of the enzyme phosphoketolase to catalyze the conversion of glycolaldehyde to acetyl phosphate [80]. This option is especially useful for the production of compounds that directly originate from acetyl-CoA, as it bypasses the decarboxylation of pyruvate. Although all of the required enzyme activities have been demonstrated *in vitro*, the *in vivo* activity of the formolase pathway is highly constrained due to poor kinetics of the formolase enzyme [178].

2.6 Yields of aerobic assimilation of methanol and formate

To gain a deeper perspective on the yields expected with methanol and formate as feedstocks under aerobic conditions, we performed Flux Balance Analysis (FBA) [86]

using the core metabolic model of *E. coli* [184] to which we added the reactions of each assimilation pathway. We used a core model, rather than a genome scale one – including only the primary metabolic routes of the pentose phosphate pathway, glycolysis, and the TCA Cycle – as this provides a general platform to compare different routes without being overly specific to *E. coli*'s metabolism. We considered all the pathway variants described above and calculated the maximal biomass yields, as well as the maximal yields of acetyl-CoA and pyruvate, which serve as precursors in the biosynthesis of many value-added chemicals. The results are shown in Fig. 2.5. We tested, for each pathway, three different electron acceptors for methanol oxidation, which are displayed together: light shading corresponds to oxygen, intermediate shading to quinone, and dark shading to NAD^+ . This enabled us to better compare the pathways, even if naturally they use different electron acceptors.

First, we compared the predicted biomass yields to experimental values [130] which are shown in thick short lines to the left of the corresponding bars in Fig. 2.5. As expected, in most cases, the experimentally measured yields are similar to and somewhat lower than the predicted maximal yields. Surprisingly, the measured biomass yield for growth on formate via the Serine Cycle is substantially higher than the predicted yield. This could be explained by noting that the stoichiometry of central metabolism intermediates in the biomass function (of the core metabolic model) is dictated by the specific biosynthesis pathways in *E. coli* and their precursors. If native methylotrophs use different biosynthetic routes – e.g., to optimize growth yield on formate – their biomass function would differ from that of *E. coli*. This could lead to the observed yield mismatch.

Methanol is a highly reduced carbon source, more reduced (per carbon) than glucose or other canonical carbon sources. It is also more reduced than biomass. As a result, growth on methanol can generate considerably more reducing power than needed for biomass, energy (ATP production), and also bioproduction. In this case, excess electrons are channeled to the respiratory chain and dissipated wastefully. The more electrons are 'dissipated' this way the more the potential yield decreases. For example, the RuMP Cycle is expected to lead to higher electron overflow than the Serine Cycle and the rGly pathway, as the latter two fix and reduce CO_2 which serves as an electron sink. Hence, while the RuMP Cycle supports considerably higher biomass yield, the Serine Cycle and the rGly pathway outperform it for the production of the relatively oxidized acetyl-CoA and pyruvate (Fig. 2.5A). To systematically assess which methanol assimilation pathway is likely to lead to futile electron respiration, we added to the metabolic model of *E. coli* a reaction which dissipates excess reducing power. We found this reaction to carry positive flux when we used FBA to maximize methanol conversion to acetyl-CoA and pyruvate using the RuMP Cycle, the DHA Cycle, the rGly pathway, and formolase pathway (marked with a '*' sign above the respective bars in Fig. 2.5), indicating that these routes are most likely to

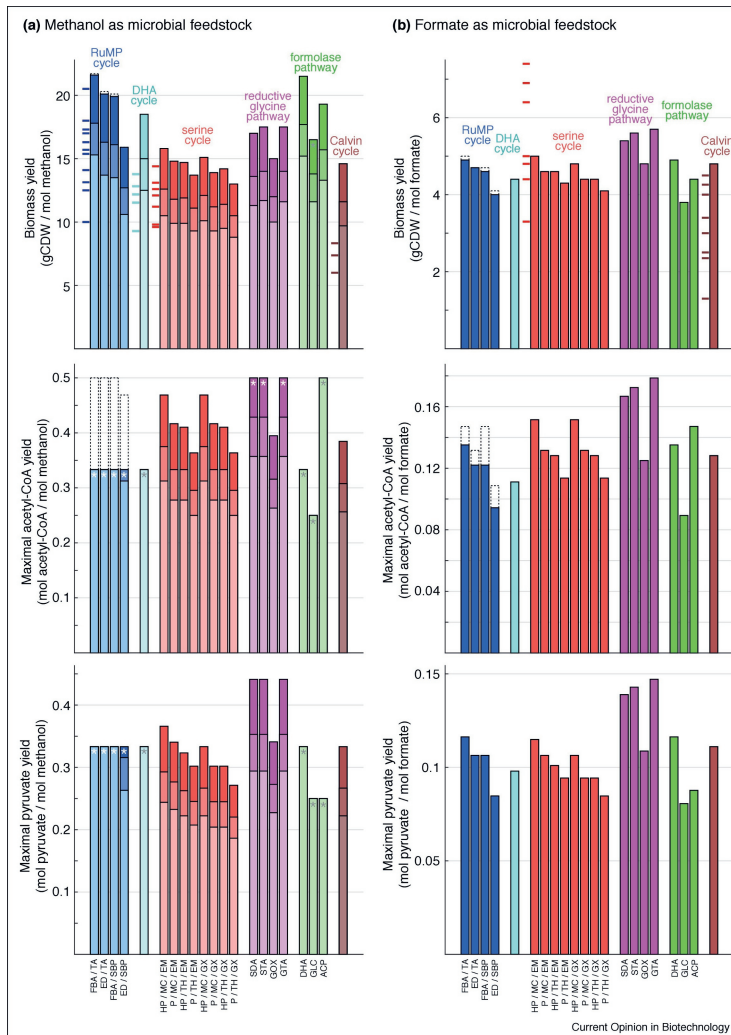


Figure 2.5: Predicted biomass and product yields using different variants of the aerobic methanol and formate assimilation pathways. We calculated yields by performing Flux Balance Analysis. Reactions of the specified assimilation pathways — illustrated in Fig. 2.3 — were added to the core metabolic model of *E. coli*. (a) Methanol as feedstock. Different shades correspond to the use of different electron acceptors for methanol oxidation: light shading corresponds to oxygen, intermediate shading to quinone, and dark shading to NAD. The ‘*’ sign corresponds to cases where methanol oxidation produces excess reducing power, as indicated by positive flux via an arbitrary NADH dissipation reaction. Dashed bars correspond to the addition of a phosphoketolase reaction (xylulose 5-phosphate + Pi → glyceraldehyde 3-phosphate + acetyl phosphate) to the model.

suffer from reduced yield for the production of relatively oxidized compounds.

The yield of acetyl-CoA from methanol can be increased when the enzyme phosphoketolase (PKT) is introduced into the cell [185]. PKT cleaves phospho-ketosugars into acetyl-phosphate and a corresponding phospho-aldosugar [186]. Therefore, PKT enables the conversion of RuMP Cycle intermediates into acetyl-CoA while bypassing glycolytic carbon loss (via pyruvate dehydrogenase). Indeed, as shown in Fig. 2.5, the predicted maximal yield of acetyl-CoA via the RuMP Cycle increases by 50% when PKT is added to the model (dashed bars).

Growth and bioproduction with formate, a much less reduced feedstock than methanol, does not lead to the formation of excess reducing power. Hence, the differences in biomass yield between the formate assimilation pathways are roughly mirrored in the acetyl-CoA and pyruvate yields and are mostly related to differences in ATP requirement (Fig. 2.5B). We assumed that formate assimilation via the RuMP Cycle, DHA Cycle, and the formolase pathway proceeds via the reduction of formate to formaldehyde [129]. However, as this reduction is energetically costly – hydrolyzing ATP for the activation of formate to formyl-CoA – the yields associated with these pathways are generally lower than those of pathways that do not depend on formate reduction (Fig. 2.5B).

Overall, the RuMP Cycle seems to be less attractive for assimilation of methanol and formate than might be expected, while the Serine Cycle seems to provide an underappreciated alternative. Still, a marked advantage of the RuMP Cycle is that it supports higher growth rates than the Serine Cycle (Fig. 2.1). The most flexible pathway seems to be the reductive glycine pathway, which supports the highest yields of biomass, acetyl-CoA, and pyruvate with formate as a carbon source as well as the highest yields of acetyl-CoA and pyruvate with methanol as a feedstock.

2.7 Practical aspects of using methanol and formate as microbial feedstocks

Currently, for economic reasons, most industrial-scale fermentations are supplied with a locally available source of bulk sugar (starch hydrolysate, cane molasses, etc.). However, such complex raw materials vary in composition from one batch to another, which can severely disrupt bioproduction (e.g., [187]). In contrast, C1 compounds, such as methanol and formate, can be used as carbon sources with inexpensive, defined media and simple nitrogen sources such as ammonia. The use of mineral (i.e., minimal) media significantly reduces downstream processing costs and reduces variation in bioprocess conditions. Moreover, C1 compounds, particularly methanol, can be used in seawater-based media [113, 188] and for wastewater

remediation [189, 190], which serve to emphasize its versatility as a microbial feedstock.

The use of methanol and formate as microbial feedstocks comes with several challenges. One of which is specific to methanol. Under aerobic conditions, growth on the highly reduced methanol greatly benefits from the supply of pure oxygen to the culture in order to provide a strong electron sink and avoid growth limitation at high cell densities [191]. This results in considerable heat production. To avoid a deleterious rise in temperature, expensive cooling is needed. It has been suggested that reducing the oxidative capacity of methylotrophs and diverting reducing power towards anaplerotic metabolism could help address this issue [125]. Alternatively, the use of thermophilic methylotrophs, e.g., *Bacillus methanolicus* that grow at maximal rate at 50°C [192], can reduce the cooling burden.

A problem that methanol and formate share is their cellular toxicity. As mentioned above, the primary cause of methanol toxicity under aerobic conditions is the high reactivity of the intermediate formaldehyde [193] that can cross-link and inactivate proteins and other macromolecules. The threshold concentration from which methanol starts to inhibit growth changes between microorganisms but 0.5-2% (v/v, i.e., 150-600 mM) seems to be an optimal concentration range while growth seems to be completely inhibited at 4-6% (v/v, i.e., 1.2-1.9 M) [194-196].

Formate toxicity is attributed to inhibition of the respiratory cytochromes [140] and may be exacerbated by the diffusion of the protonated acid across the cell membrane, which acidifies the cytoplasm and reduces the proton motive force [197]. The threshold concentration of formate above which growth is inhibited seems to be, at least to some extent, affected by the activity of formate dehydrogenase. Microorganisms that endogenously have only weak formate dehydrogenase activity, e.g., as *E. coli* [198], show severe growth impairment at formate concentrations below 100 mM [199], while those with highly active formate dehydrogenase, e.g., yeasts [200, 201], can tolerate and even benefit from concentrations of hundreds of mM. Still, some microorganisms that can grow on formate via the Calvin Cycle, and thus exhibit considerable formate dehydrogenase activity, seem to be quite sensitive to this compound, e.g., *Thiobacillus* strain A1 [202] and *Thiobacillus ferrooxidans* [203]. Fed-batch or continuous cultivation modes provide the best solutions for microbial cultivation on methanol and formate, maximizing product titer and productivity while minimizing the toxicity problem [130]. Nonetheless, within large bioreactors, in which the culture is more difficult to mix, local high concentrations of the feedstock might develop which could severely disrupt growth and bioproduction. To address this problem, large-scale designs sometimes use a system of distributed sparging. For example, the process developed by Imperial Chemical Industries avoided toxic local concentrations of methanol by using 3,000 outlets in the reactor [204, 205]. Finally, we note that the positive aspect of cultivating microorganisms on a somewhat

toxic feedstock is that the possibility of contamination by other organisms is much reduced.

2.8 Concluding remarks

A bioeconomy based on C1 compounds was previously championed as a solution to the grand challenges facing the latter part of the 20th century: food shortages, energy crises, and unsustainable production. These efforts were constrained by technological and economic factors that have changed considerably in the last decades. In the first half of the 21st century, we face the same problems with more urgency. Fortunately, research into the sustainable production of C1 compounds from CO₂ and renewable energy may soon provide technically and economically viable solutions. In this new landscape, methanol and formate could have transformative potential for bioindustry.

Methanol and formate can be assimilated into central metabolism using various metabolic routes. Anaerobic bioproduction with these feedstocks, while currently neglected, is highly promising for a specific set of products, such as ethanol, acetone, isopropanol, and short-to-medium chain fatty acids. Production of other molecules requires aerobic conditions which decouple biosynthesis from energy conservation. While naturally occurring methylotrophic microorganisms can support such bioproduction, they are mostly limited by either low efficiency pathways (e.g., Calvin Cycle) or by the lack of genetic tools for metabolic engineering (e.g., methylotrophs that use the RuMP Cycle). Engineering model biotechnological microorganisms to grow on methanol and formate is thus becoming an attractive alternative. Such efforts rely either on the introduction of existing pathways (e.g., RuMP Cycle) into non-methylotrophic hosts or on the design and implementation of new-to-nature routes. Our analysis suggests that the synthetic pathways, and especially the rGly pathway, might support higher bioproduction yield than the native ones, thus serving as good target for implementation in various microorganisms.

It is important to emphasize that yield is not the only important factor to consider when comparing different pathways or pathway variants. Pathway kinetics is as important. For example, while the formolase pathway can support high yields, the low rate of its key enzymes makes this route less attractive. The complexity of the engineering task is also very important: cyclic pathways that strongly interact with core metabolism are very challenging to implement, while establishing linear routes that operate in a more peripheral part of cellular metabolism may be more feasible. Finally, different pathways and pathway variants might be more suitable for different products. For example, production of oxidized products from methanol is better supported by pathways which also fix CO₂ (e.g., Serine Cycle or rGly pathway) than

pathways which rely solely on methanol as a carbon source (e.g., RuMP Cycle).

Establishing industrial bioprocesses that use methanol and formate as feedstocks presents specific challenges such as overheating and feedstock toxicity. Solving these issues is vital for further development of the field. Still, the advantages of using these feedstocks – production from CO₂ and renewable energy, miscibility that bypasses mass transfer barriers, easy storage and transport – suggest that further development of bioprocessing strategies with methanol and formate feedstocks could enable the emergence of a truly sustainable bioeconomy.

Conflict of interest statement

A.B.E. is co-founder of b.fab, aiming to commercialize C1 assimilation. The company was not involved in any way in the conducting, funding, or influencing the research.

Acknowledgements

The authors thank Armin Kubis and Sebastian Wenk for critical reading of the manuscript. This work was funded by the Max Planck Society and by the European Union's Horizon 2020 research and innovation programme under grant agreement No. 763911 (Project eForFuel). N.J.C. is supported by The Netherlands Organization for Scientific Research (NWO) through a Rubicon Grant (Project 019.163LW.035).

Chapter 3

Modeling a co-culture of *Clostridium autoethanogenum* and *Clostridium kluyveri* to increase syngas conversion to medium-chain fatty-acids

3

Sara Benito-Vaquerizo, Martijn Diender, Ivette Parera Olm, Vitor Martins dos Santos, Peter J. Schaap, Diana Z. Sousa, Maria Suarez-Diez
Published in: CSBJ. 18, 3255-3266 (2020).

doi.org/10.1016/j.csbj.2020.10.003

3.1 Abstract

Microbial fermentation of synthesis gas (syngas) is becoming more attractive for sustainable production of commodity chemicals. To date, syngas fermentation focuses mainly on the use of *Clostridium* species for the production of small organic molecules such as ethanol and acetate. The co-cultivation of syngas-fermenting microorganisms with chain-elongating bacteria can expand the range of possible products, allowing, for instance, the production of medium-chain fatty acids (MCFA) and alcohols from syngas. To explore these possibilities, we report herein a genome-scale, constraint-based metabolic model to describe growth of a co-culture of *Clostridium autoethanogenum* and *Clostridium kluyveri* on syngas for the production of valuable compounds. Community flux balance analysis was used to gain insight into the metabolism of the two strains and their interactions, and to reveal potential strategies enabling production of butyrate and hexanoate.

The model suggests that one strategy to optimize the production of medium-chain fatty-acids from syngas would be the addition of succinate. According to the prediction, addition of succinate would increase the pool of crotonyl-CoA and the ethanol/acetate uptake ratio in *C. kluyveri*, resulting in a flux of up to 60% of electrons into hexanoate. Another potential way to further optimize butyrate and hexanoate production would be an increase of *C. autoethanogenum* ethanol production. Blocking either acetaldehyde dehydrogenase or formate dehydrogenase (ferredoxin) activity or formate transport, in the *C. autoethanogenum* metabolic model could potentially lead to an up to 150% increase in ethanol production.

3.2 Introduction

One of the biggest challenges society faces nowadays is finding alternative processes for the sustainable production of fuels and chemicals. At present, the production of many commodities depends on fossil fuels, which is not sustainable or sugar crops, competing with human and animal food consumption [206]. To circumvent this, circular approaches are required, such as the conversion of lignocellulosic biomass or municipal waste as feedstocks to fuels and chemicals [207]. Although lignocellulosic biomass has been identified as a promising source for renewable energy and carbon [208], current technologies involving hydrolysis of this substrate result in a complex mixture of compounds that need further separation and individual processing [14]. However, gasification of these rigid materials allows for the conversion of the carbon in the original source to synthesis gas (syngas), consisting mainly of CO, H₂ and CO₂. This energy-rich syngas can be further used as feedstock for chemocatalytic processes such as Fischer-Tropsch, but microbial fermentation of syngas is gaining more attention recently as a potential production platform [27, 28]. Compared to chemical catalysts, microorganisms are more robust to variations of CO/H₂ ratio in syngas, and are also more resistant to the presence of certain impurities (e.g. sulfides), reducing the need for costly pre-treatment of syngas [27].

Acetogenic clostridia are efficient microbial hosts for syngas fermentation as they can grow on CO and CO/H₂ via the Wood–Ljungdahl pathway [209]. However, the natural product range of most acetogens is limited to a mixture of acetate and ethanol [210]. Co-cultivation of a syngas-fermenting organism with other organisms (that use the primary products of syngas fermentation) can be used to extend the range of possible products. Previously, a co-culture of *Clostridium autoethanogenum* and *Clostridium kluyveri* was described to produce medium-chain fatty acids (C4-C6) and their respective alcohols by assimilation of CO or syngas [64, 68]. *C. autoethanogenum* is an acetogenic bacterium able to produce acetate and ethanol when growing on CO or syngas [211]. *C. kluyveri* grows on acetate and ethanol via reverse- β -

oxidation, producing chain-elongated acids like butyrate and hexanoate. When *C. kluyveri* is grown in co-culture with *C. autoethanogenum* on CO, it produces butyrate and hexanoate, which are further reduced by the acetogen to the corresponding alcohols, butanol and hexanol [64]. MCFA are used to produce pharmaceutical and personal care products, animal feed additives and lubricants, among other, and can be converted chemically or enzymatically into valuable biofuel molecules such as methyl esters, methyl ketones, alkenes and alkanes [212, 213]. The theoretical maximum yield of hexanoate production in a co-culture of *C. autoethanogenum* and *C. kluyveri* is 0.056 mmol of hexanoate per mmol of CO, whereas the yield obtained in the most recent study [68] was 0.009 mmol hexanoate per mmol of CO, so there is substantial room for improvement and new strategies need to be developed.

Genome-scale, constraint-based metabolic models (GEMs) attempt to represent the complete set of reactions in a living organism, and have been used to gain better understanding of cellular metabolism, assessing theoretical capabilities or designing media and processes [72]. GEMs can be used to link the microbial consumption and production rates with cellular growth rates. Moreover, they enable linking these phenotypes with the genome content of the studied organisms and with internal phenotypes, such as metabolic fluxes that are usually difficult to measure experimentally. GEMs and their analysis with constraint-based techniques, such as flux balance analysis (FBA) for the calculation of steady-states, have been proven effective tools to devise strategies for increasing productivity of microbial fermentation processes [72, 86, 214]. Specifically, GEMs have been used to further understand the metabolism of clostridia. For instance, the GEM of *Clostridium thermocellum* allowed the design of metabolic strategies to increase ethanol production after identification of bottlenecks in central carbon metabolism that were inhibiting its production [215]. Stolyar and collaborators [216], generated a multi-species GEM by combining the GEMs of bacterium *Desulfovibrio* and archeon *Methanococcus maripaludis* S2 into a single model with a shared extracellular environment, bringing the use of GEMs to a next level. Since then, this type of community models have been used to describe metabolic interactions among community members and inter-species fluxes [217]. Li and Henson [218], recently used GEMs to compare mono-culture and co-culture systems to produce butyrate from carbon monoxide. They applied dynamic flux balance analysis (dFBA) [90] to analyze a community GEM to cover the changes in community composition over time and to assess the relative performance of these mixed cultures. The availability of GEMs for *C. autoethanogenum* [219] and *C. kluyveri* [220], enables the use of community modeling as a potential method to help optimizing the performance of this co-culture for syngas fermentation to elongated acids and alcohols.

In this study, we present a multi-species model built by combining the GEMs of *C. autoethanogenum* [219] and *C. kluyveri* [220]. The model accounts for exper-

imental measurements informing on relative species abundances and steady-state production rates of syngas fermentation products obtained in chemostat runs under different conditions for mono-culture and co-culture [68]. In order to test the model, experimental values were introduced as environmental constraints by employing community flux balance analysis (cFBA) [217, 221]. cFBA implicitly assumes equal abundances of the species when exchange fluxes are expressed on a per gDW basis. To circumvent this, and considering that in microbial communities different species can have distinct abundances, we have scaled fluxes by volumes in this study. Additionally, cFBA also assumes equal growth rates of the members of the community. In the current analysis of a co-culture in a chemostat, equal growth rates are achieved as the dilution rate ensures same growth rate for each organism [222]. Subsequently, the model was used to identify and assess strategies to optimize desired products, specifically butyrate and hexanoate.

3.3 Materials and methods

3.3.1 GEMs of *C.autoethanogenum* and *C. kluuyveri*

To represent the metabolism of *C. autoethanogenum*, the previously described GEM, iCLAU786, was retrieved in SBML (XML) format from the supplementary material provided by Valgepea et al. [219]. This model was amended with an exchange reaction to simulate acetate uptake when this is used as additional substrate (EX_AC_c). eEQUILIBRATOR [223] was used to manually verify reaction directionality: Gibbs energy released (ΔG) at pH 7.0 and ionic strength (0.1M) was computed. Reactions with $\Delta G \in [-30, 30]$ kJ/mol were considered reversible.

The GEM of *C.kluuyveri*, iCKL708, was downloaded in table format from its publication [220]. An additional reaction was added to excrete biomass, which was first included as new metabolite and as additional product in the biomass reaction BOF. Minor changes were applied affecting the reversibility of few reactions and addition of protons. Pyruvate synthase (Rck1119) was set to non-reversible in the direction of pyruvate production [224, 225]. Pyruvate formate lyase (PFL) was set to non-reversible, allowing only the production of formate and acetyl-CoA. Protons were added in the exchange of heptanoate reaction (Rck1870). eEQUILIBRATOR [226] was used to manually verify reaction directionality as in previous model. The updated model was converted to SBML level 3 version 1 standardization [227].

3.3.2 Multi-species GEM reconstruction

The multi-species GEM of *C. autoethanogenum* and *C. kluyveri* was generated by combination of single species models: iCLAU786 [219] and the updated version of iCKL708 [220], respectively, following a compartmentalized approach [216] where each species is considered a single compartment. Therefore, we consider two internal compartments: 'cytosol_auto' and 'cytosol_kluy', with 'c' and 'ck' as their respective identifier (id). Intracellular metabolites were assigned to their corresponding compartment and the flag '_c' was added to the id of metabolites belonging to 'cytosol_auto' and '_ck' to those belonging to 'cytosol_kluy'. In addition to these two internal compartments, the model has an extracellular compartment that is unique for both species. To achieve this, all metabolites that were defined as extracellular ('_e') in its original models, will be defined in the common extracellular compartment of the community model, id: '_e'. As some metabolites will appear in both species, names need to be unified and corrected to have the same naming system (namespace). Metabolites that are shared between species, will be exchanged through this extracellular compartment, being first transported from the corresponding intracellular compartment to the extracellular compartment, or vice versa. In principle, all metabolites that are present in both internal compartments and are defined in the extracellular compartment, can be exchanged, being the directionality of the associated reactions favorable to produce the exchange. However, some dependencies have been assumed in the model based on experimental evidences.

Each species has its own biomass synthesis reaction. An extra biomass metabolite was created and defined in the extracellular compartment for each species: 'BIOMASS_c_e' and 'BIOMASS_ck_e'. In addition, two extra reactions were added for each species, one to transport biomass from the intracellular to the extracellular compartment, and a second one to excrete biomass (exchange reaction). A reaction was included to distinguish the amount of H_2 excreted by *C. kluyveri*, from the amount of H_2 metabolized by *C. autoethanogenum*. The same was done for acetate. A reaction was included to distinguish the amount of acetate metabolized by *C. autoethanogenum*, from the amount of acetate produced by *C. autoethanogenum*. The model also contemplates the possible production of butanol and hexanol via butyrate and hexanoate uptake by *C. autoethanogenum*. The added reactions are a transport reaction from the external compartment to the internal compartment of *C. autoethanogenum*, reactions for production of butyraldehyde and caproaldehyde from the corresponding fatty-acids and reactions for production of alcohols from their corresponding aldehydes. Finally, the multi-species model was transformed into SBML level 3 version 1 (see supplementary material).

3.3.3 Multi-species modeling framework

In order to model the community, we have followed an approach similar to the one proposed by SteadyCom [228] and that is based on community FBA (cFBA) [221]. Environmental fluxes ($\text{mmol L}^{-1} \text{h}^{-1}$) are integrated as model constraints instead of specific fluxes ($\text{mmol gDW}^{-1} \text{h}^{-1}$), where gDW indicates grams of dry weight. The biomass reaction of each species incorporates as new term, the biomass of the relative species together with the growth rate term. In this way, we can account for species abundance in the community. The biomass of each species is calculated based on the community biomass and the species ratio. In addition to this, steady-state and equal growth rate of species are assumed.

3.3.4 Calculation of species abundances

The ratio between *C. autoethanogenum* and *C. kluyveri* in co-culture, was estimated from partitioning RNAseq reads and confirmed by cell counting in microscopy observations as two independent methods. Transcriptomic data was obtained from steady-state co-cultures grown in chemostats [68]. The Genomes of *C. autoethanogenum*: DSM 10061 (GCA_000484505.1) [229] and *C. kluyveri*: DSM 555 (GCA_000016505.1) [230] were retrieved from the European Nucleotide Archive. The genomes have similar size with sequence length 4.352.205 and 4.023.800, respectively [231]. Reads were mapped to each genome using BWA-SW (Burrows Wheeler Aligner) [232] and the ratio was calculated based on the amount of reads associated to each species.

The second method consisted of direct cell counting under microscopy observations. This led to a proportion between cell numbers of 10 *C. autoethanogenum* by 1 *C. kluyveri*. This proportion was considered to calculate the accumulated dry weight. To calculate the respective dry weights, the cellular volume of each species was calculated based on their average size. *C. autoethanogenum* is a rod-shaped bacterium with an average size of $0.5 \times 3.2 \mu\text{m}$ [211] and *C. kluyveri* cells are curved rods, with average size of $12.5 \mu\text{m}$ in length and $1.5 \mu\text{m}$ in width [233]. Cell volume was calculated following a previously proposed formula for rod-shaped cells [234]: $V = [(w^2 \cdot \pi/4) \cdot (l - w)] + (\pi \cdot w^3/6)$, with l and w indicating length and width, respectively. The associated dry weight (DW) was then derived using: $DW = 435 \cdot V^{0.86}$ [234]. Then, the dry weight of *C. autoethanogenum* was multiplied by 10 and the dry weight of *C. kluyveri* was multiplied by 1 (as the observed proportion). Finally, the biomass-species ratio was calculated based on the ratio of the accumulated dry weights. The proportion was observed to be constant among experimental conditions with CO and CO/H₂, so we assume that the relative abundances are constant for the rest of conditions too.

3.3.5 Use of experimental values to constrain the model.

Experimental measurements were converted to $\text{mmol L}^{-1} \text{h}^{-1}$. Product concentrations, measured in mM, were used to compute product secretion rates ($\text{mmol L}^{-1} \text{h}^{-1}$) by using the same hydraulic retention time (HRT) that in laboratory settings. Dilution rate is the inverse of the HRT. In steady-state conditions, growth rate is considered equal to the dilution rate and therefore, it was calculated as the inverse of the HRT and expressed in h^{-1} . In co-culture, growth rate of both species was assumed to be the same and equal to that of the community, since HRT was kept constant both, in mono-culture and co-culture experiments [222]. We have followed the usual convention in constraint-based modeling, so that uptake is represented by negative fluxes whereas production corresponds to positive fluxes. To model experimental conditions, we fix substrate uptake rates to the desired ones by setting the lower bounds of the corresponding exchange reactions to the measured values multiplied by -1 (as it corresponds to consumption). Biomass reactions were constrained with the growth rate multiplying the total biomass by the ratio of each species ($\text{gDW L}^{-1} \text{h}^{-1}$). Similarly, product formation was set to be at least 80% of the calculated product formation by modifying the lower bound of the corresponding exchange reaction. ATP maintenance reactions of each species, ATPM_auto and ATPM, were transformed to $\text{mmol L}^{-1} \text{h}^{-1}$ from the pre-set values in $\text{mmol gDW}^{-1} \text{h}^{-1}$ multiplying by the total biomass and species ratio. In cases where metabolites behave as products that are further metabolized by the other species, the transport reactions of these metabolites are forced to operate in the direction from the external compartment to the other species compartment.

Chemostat experimental data

Experimental data was collected from reactor run 3 and 4 of the recent study [68] on *C. autoethanogenum* in mono-culture and co-cultivation of *C. autoethanogenum* and *C. kluyveri* grown on CO/H_2 and $\text{CO}/\text{acetate}$. In co-culture experiments, *C. kluyveri* was inoculated in the reactor on top of *C. autoethanogenum* in a 1:20 volume ratio. The organisms were cultivated in chemostat to control environmental conditions such as pH (6.2), temperature (37°), HRT (between 1.5 to 2 days) and medium composition during the entire reactor run. A reactor run starts with inoculation of *C. autoethanogenum* in mono-culture followed by co-cultivation with *C. kluyveri* after reaching stationary phase. Total reactor volume is 1.5 L. Working volume was set between 0.75 L to 1 L. Experiments were run on different conditions of CO/H_2 and $\text{CO}/\text{acetate}$ as initial substrates. Concentrations of organic acids and alcohols in the reactor and gas composition in the outflow were tracked during the runs.

3.3.6 Model simulations

Model simulations were done using COBRAPy, version 0.17.0 [235], IBM ILOG CPLEX 128 and Python 3.6. Simulations based on changes/addition of parameters were done by constraining the associated reactions with the mentioned values. When simulations required removal of a substrate or product, flux through the associated reaction was set to 0. Constraints on the profile of fermentation products were kept unchanged when simulations were based on substrate uptake ratios in *C. kluyveri*, unless stated otherwise. For each explored condition, the solution space and the set of fluxes compatible with the measured constraints was sampled using the *sample* function in the *flux_analysis* submodule COBRAPy. Flux sampling is a method to get a distribution of fluxes [236] under specific conditions. Presented results are the average and standard deviation based on 15000 iterations generated at each condition. All additional assumptions taken into account during model simulations are listed in the supplementary material.

3.3.7 Genetic intervention strategy

OptKnock and RobustKnock [93, 237] were applied as algorithms that suggest reactions to be knocked out that can potentially increase the yield of a target reaction. The algorithms were applied to increase ethanol production in the GEM of *C. autoethanogenum* [219]. Both algorithms were integrated in a python script adapted for COBRAPy and CPLEX as solver. OptKnock identifies a set of reaction knock-outs that allows high production of a target product under the constraint of optimal growth in wild type. RobustKnock guarantees a minimal production rate by considering alternative optimal solutions that produce less of the target product. This is achieved by employing a bi-level max-min optimization. The possible reactions to be modified were adjusted in order to avoid essential reactions, reactions associated to essential genes, extracellular reactions and reactions with no associated genes. The identified mutants were further implemented in the model of *C. autoethanogenum* deleting the corresponding reactions. Each mutant was assessed at each experimental condition and compare to the wild type. The media as well as the biomass reaction were constrained using the experimental data of mono-culture experiments for those conditions [68]. Fluxes are expressed following the modeling framework. For each explored condition, the solution space and the set of fluxes compatible with the measured constraints was sampled. Presented results are the average and standard deviation based on 15000 iterations generated at each condition.

3.4 Results

The objective of this study is to find optimization strategies for the production of medium-chain fatty-acids from syngas using the co-culture of *C. autoethanogenum* and *C. kluyveri*. The generated multi-species GEM, together with the GEM of *C. autoethanogenum*, were used to assess these strategies.

3.4.1 Description and validation of the GEM of individual strains

The GEM of *C. autoethanogenum*, iCLAU786 is composed of 1108 reactions and 1094 metabolites. The model is able to simulate growth on CO or syngas as the sole carbon and energy source, producing acetate and ethanol as the main fermentation products.

The GEM of *C. kluyveri*, iCKL708 has been previously shown to predict growth on ethanol and one other organic acid (acetate, propionate, butyrate, or succinate), propanol and acetate, crotonate, and vinyl acetate, in accordance to published experimental data [233, 238–240]. The updated GEM of *C. kluyveri*, has 993 reactions and 811 metabolites. This updated model also simulates growth on acetate and ethanol uptake producing butyrate and hexanoate as the main chain-elongated products and H_2 .

3.4.2 Multi-species GEM

The multi-species GEM contains 2064 reactions and 1823 metabolites, from which 139 reactions correspond to extracellular reactions and 208 metabolites belong to the shared extracellular compartment. Fig. 3.1, shows the dependencies included in the model to describe the syngas fermentation process by the co-culture based on the experimental data [68]. $H_2_ck \rightarrow$ reaction represents the amount of H_2 excreted by *C. kluyveri*. Reaction $\rightarrow H_2_e$ represents the uptake of H_2 in *C. autoethanogenum*. Reaction $\rightarrow AC_c$, represents the uptake of acetate by *C. autoethanogenum* in simulations where acetate acts as additional substrate. This serves to distinguish the fluxes between acetate feed rate ($\rightarrow AC_c$), acetate production rate ($AC_e \rightarrow$) and acetate consumed by *C. kluyveri* ($AC_e \rightarrow AC_ck$). These are special cases since H_2 and acetate can be shared, metabolized and produced in co-culture conditions.

Previous studies have shown that *C. autoethanogenum* is able to grow on CO, CO/ H_2 producing ethanol and acetate as the main fermentation products [211]. Acetate and ethanol can further be taken up by *C. kluyveri* producing H_2 , butyrate and hexanoate. H_2 produced by *C. kluyveri* appears to be further metabolized by *C. autoethanogenum* [64, 68]. Furthermore, the presence of aldehyde ferredoxin oxidoreductase and Ethanol:NAD⁺ oxidoreductase enzymes in *C. autoethanogenum* allows

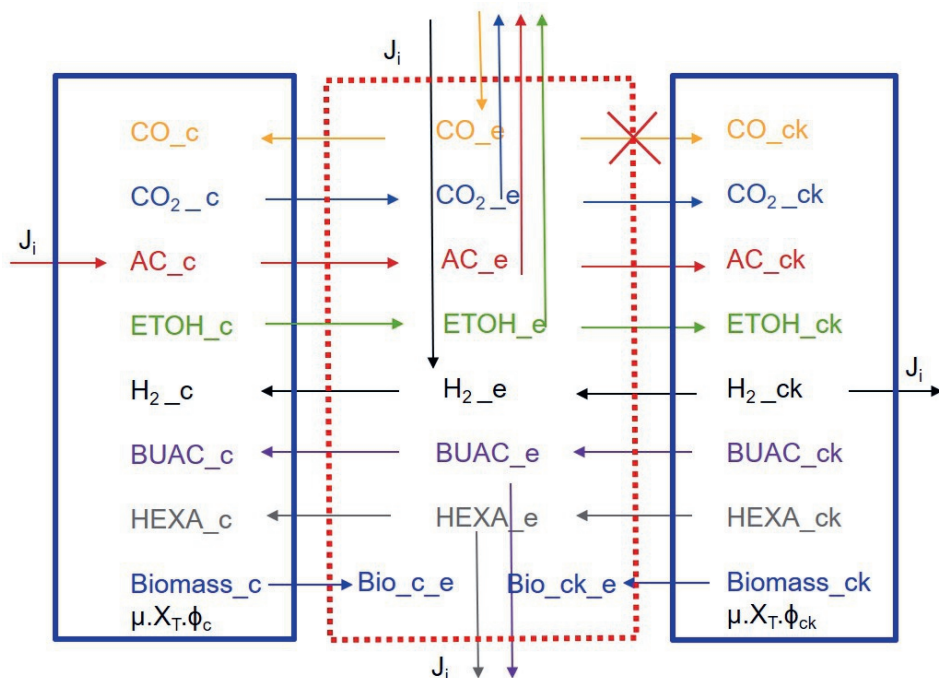


Figure 3.1: Dependencies applied to the multi-species model to describe possible interactions. Metabolites on the left belong to *C. autoethanogenum*'s compartment and on the right, to *C. kluyveri*'s compartment. Metabolites in the middle correspond to the extracellular compartment. Arrows between metabolites indicate transport reactions of that metabolite from one species' compartment to the extracellular compartment or the other way around. Arrows affecting single metabolites indicate uptake or production of that metabolite. CO: carbon monoxide; H_2 : Hydrogen; AC: acetate; ETOH: ethanol; BUAC: butyrate; HEXA: hexanoate; J_i : environmental fluxes of reaction i ; μ : growth rate; X_T : community biomass; ϕ_i : species abundance, with i equals c or ck for *C. autoethanogenum* or *C. kluyveri*, respectively.

for a potential two step conversion of butyrate and hexanoate, via the respective aldehyde, to butanol and hexanol respectively. *C. kluyveri* is not able to utilize CO and its metabolism can be inhibited by this compound [64]. However, providing co-cultivation with *C. autoethanogenum*, dissolved CO concentration can be kept low. Naturally, dissolved CO will be dependent on the gas-liquid mass transfer and the CO uptake rate of *C. autoethanogenum*. Because kLa values for CO-water are relatively low in stirred tanks [241], these systems are often not kinetically limited and

low dissolved CO concentrations are expected in the culture broth. This low dissolved CO concentration will leave *C. kluyveri* metabolism unaffected [64]. In the model this is indicated by preventing flux through the reaction $CO_e \rightarrow CO_{ck}$ as it is shown in Fig. 3.1.

Microscopy observation of the co-culture led to the estimation of a ratio of 10 cells of *C. autoethanogenum* per 1 cell of *C. kluyveri*. Analyses of transcriptome samples obtained by RNAseq of the community [68], were done to identify the fraction of RNA arising from each community member. The estimated relative abundances yielded between 90-95% of *C. autoethanogenum* and 5-10% of *C. kluyveri*. Differences in cell size and volume were considered as *C. kluyveri* cells have approximately 36 more volume than *C. autoethanogenum* [211, 233, 234]. The estimated volumes were used to estimate dry weight of each cell species, resulting the cell dry mass of *C. kluyveri*, 22 times more than *C. autoethanogenum*. Finally, the cell ratio (10:1) was taken into account resulting in a biomass ratio of 68.5% *C. kluyveri* and 31.5% *C. autoethanogenum*. This cell ratio was observed in CO and CO/H₂ conditions and it was assumed to be constant in the model simulations.

3.4.3 Multi-species GEM accurately predicts experimental results

The initial mono-culture experiments only involved *C. autoethanogenum* [68]. Fig. 3.2, shows the steady-state production rates of the fermentation products expressed in mmol L⁻¹ h⁻¹. Experiments were run on CO/H₂ and CO/AC (acetate) as initial substrates. Acetate production rate ('EX_AC_e') refers to the sum of the acetate feed rate not consumed by *C. autoethanogenum* and the one directly produced by *C. autoethanogenum*. Fig. 3.2 shows that the model predictions match relatively well the experimental results for *C. autoethanogenum*. Accordingly, the model predicts correctly that ethanol production increases at higher H₂ feed rates and gradually with the addition of acetate. However, the model predicts slightly higher production rates for acetate in conditions with higher amounts of acetate in the background.

The co-culture experiments were run under same conditions as the mono-culture experiments. Fig. 3.3, represents steady-state production rates of fermentation products expressed in mmol L⁻¹ h⁻¹ by the co-culture. It shows the comparison between experimental results collected in co-culture experiments [68] and the results obtained via the multi-species model. Acetate production rate ('EX_AC_e') refers to the sum of the acetate in the feed, the acetate directly produced by *C. autoethanogenum*, minus the acetate consumed by *C. kluyveri* (reaction id Rckl835). Ethanol production rate ('EX_ETOH_e') refers to the ethanol produced by *C. autoethanogenum* minus the ethanol consumed by *C. kluyveri* (reaction id Rckl837). The model correctly predicts production of medium-chain fatty acids upon introduction of *C. kluyveri*. Similarly to the mono-culture simulations, there is a slight mismatch be-

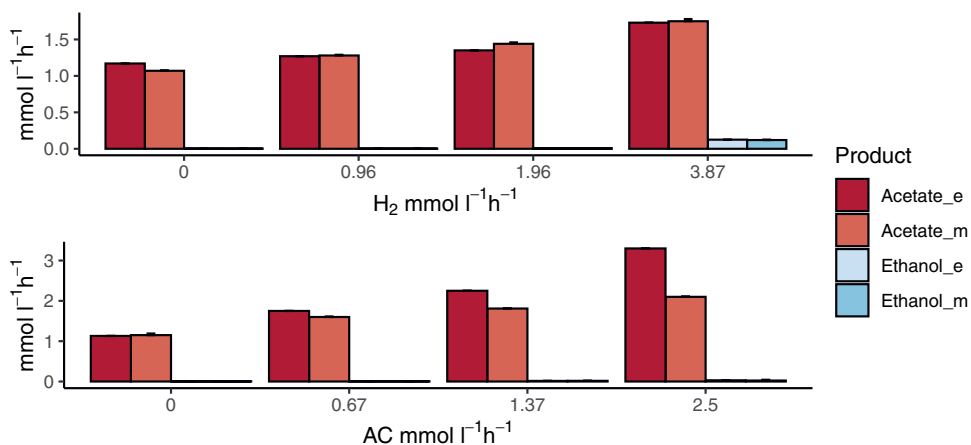


Figure 3.2: Comparison of experimental (_e) and model (_m) results of the steady-state production rates of fermentation products in *C. autoethanogenum* in mono-culture under CO/H₂ and CO/AC (acetate) conditions. X axis represents the H₂ and acetate feed rate, respectively. Y axis represents the steady-state production rates of acetate and the secondary y axis represents the steady-state production rate of ethanol. In CO/H₂ conditions, CO feed rate= 4.8 mmol L⁻¹ h⁻¹; growth rate=0.021 h⁻¹ and working volume= 1 l. In CO/AC conditions, CO feed rate= 6.4 mmol L⁻¹ h⁻¹; growth rate=0.028 h⁻¹ and working volume= 0.75 l. Substrates feed rates and production rates are expressed in mmol L⁻¹ h⁻¹.

tween predicted and observed acetate production. The model correctly predicts the increase of medium-chain fatty-acids when more H₂ or acetate is added. When H₂ feed rate is equal to 5.3 mmol L⁻¹ h⁻¹, butanol is also produced (0.075 mmol L⁻¹ h⁻¹). Also, ethanol accumulation is low in most co-culture conditions, suggesting most of it is metabolized by *C. kluyveri*. The steady-state production rates of acetate increases with increasing acetate uptake (see Fig. 3.2 and 3.3), but the amount of acetate expressively produced by *C. autoethanogenum* decreases with increasing acetate uptake, since the addition of acetate leads to more acetate converted to ethanol [68]. However, there is still a relative high level of acetate accumulated versus desired fatty acid products, which represents a loss of carbon into acetate that could be minimized if *C. kluyveri* could consume more acetate.

Assessing the distribution of metabolic fluxes with the multi-species model

After having shown that the model describes accurately the metabolic interactions between the two microbes, we used it to explore intracellular flux distributions that

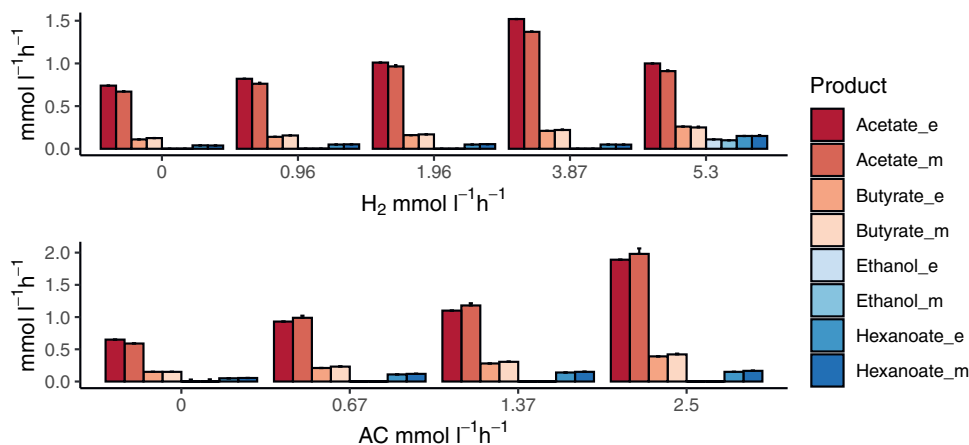


Figure 3.3: Comparison of the experimental ($_e$) and model ($_m$) results of the steady-state production rates of the fermentation products in co-culture under CO/H_2 and CO/AC (acetate) conditions. X axis represents the H_2 and acetate feed rate, respectively. Y axis represents the steady-state production rates of acetate and the secondary y axis represents the steady-state production rate of ethanol, butyrate and hexanoate by the co-culture. In CO/H_2 experiments, CO feed rate = $4.8 \text{ mmol L}^{-1} \text{ h}^{-1}$; growth rate = 0.021 h^{-1} and working volume = 1 l . In CO/AC conditions, CO feed rate = $6.4 \text{ mmol L}^{-1} \text{ h}^{-1}$; growth rate = 0.028 h^{-1} and working volume = 0.75 l . Feed rates of substrates and production rates are expressed in $\text{mmol L}^{-1} \text{ h}^{-1}$.

would be otherwise challenging to access. To study the metabolic fluxes in the co-culture, we used a sampling approach that produces, for each reaction in the combined model, a distribution of possible fluxes. Fig. 3.4 provides an overview of selected reactions in the system (indicated by R#). Fluxes for all reactions can be found in the supplementary material.

CO or CO and H_2 are converted via the Wood-Ljungdahl pathway in *C. autoethanogenum*. In this pathway, CO is converted to CO_2 via CO dehydrogenase, providing reducing equivalents to the cell. Released CO_2 is shuttled into the Wood-Ljungdahl pathway via the bifurcating formate dehydrogenase [242]. H_2 taken up by *C. autoethanogenum* is used for redox generation in NADP-dependent electron bifurcating hydrogenase (Hyt) reaction (R3) and in formate hydrogen lyase reaction (R2 in Fig. 3.4) to produce formate. The flux through these two reactions increases with increasing H_2 supply. Part of the formate is excreted and part is further metabolized to acetyl-CoA (ACCOA) following the Wood-Ljungdahl pathway. Pyruvate is partly

produced from acetyl-CoA via the pyruvate synthase (R8 in Fig. 3.4) for assimilation. The majority of the acetyl-CoA is converted to acetate via acetyltransferase (R6) and acetate kinase, yielding ATP. Ethanol can be formed in two ways [50]: from the reduction of acetate to ethanol via aldehyde ferredoxin oxidoreductase (R7) and alcohol dehydrogenase, or via reduction of acetyl-CoA to acetaldehyde (ACAL) and ethanol. Acetate and ethanol are secreted to the medium where it is partly taken up by *C. kluyveri*. Ethanol production rate by *C. autoethanogenum* (reaction R10) and ethanol uptake by *C. kluyveri* (R15) indicate that most of ethanol is removed by *C. kluyveri* and proves the metabolic change to solventogenesis due to addition of *C. kluyveri*. This can be observed comparing to mono-culture results showed in Fig. 3.2, where the steady-state production of ethanol was lower than in co-cultivation with *C. kluyveri* (flux through R10). In *C. kluyveri* ethanol is oxidized to acetyl-CoA (ACCOA) and part of acetyl-CoA is converted to acetate via acetyltransferase and acetate kinase (R16). Acetyl-CoA initiates the reverse β -oxidation pathway (R16-R19) to produce butyrate via acetoacetyl-CoA (AACCOA), then 3-hydroxybutyryl-coa (3HBUTCOA), crotonyl-CoA (CROCOA) and butyryl-CoA (C40COA). C40COA, transfers the CoA group to acetate, producing butyrate and acetyl-CoA. Some of the butyrate can be elongated further to hexanoate by reaction of butyryl-CoA together with hexanoyl-CoA (C60COA)(R19). Acetyl-CoA is also assimilated by fixing CO₂ to pyruvate via pyruvate synthase (R20) in *C. kluyveri*.

Succinate is converted to Crotonyl-CoA (CROCOA), yielding an additional 2 acetate (see Fig. 3.4), involving the pathway via succinyl-CoA, succinate semialdehyde, 4-hydroxybutyrate, and 4-hydroxybutyryl-CoA [230]. The model indicates that part of the acetate pool in *C. kluyveri* comes from uptake of succinate produced by *C. autoethanogenum* (see R28), which could explain the slight mismatch observed in Fig. 3.3 between acetate predicted by the model compared to experimental results. The model predicts a low amount of ethanol being oxidized to acetate (R16), supporting activity of the succinate pathway.

The model predicts reduction of CO₂ production by *C. autoethanogenum* with increasing H₂ feed rate (Fig. 3.4B). This was also observed in the experimental measurements [68], where CO₂/CO ratio decreased linearly with increasing hydrogen uptake. According to model predictions, CO₂ production rate drops to 0.28 mmol L⁻¹ h⁻¹ when H₂ is supplied, as compared to 2.5 mmol L⁻¹ h⁻¹ that is produced when CO is the only carbon source (see supplementary material). It is observed that more H₂ is metabolized by *C. autoethanogenum* with increasing H₂ feed rate (as shown in Fig. 3.4B) similar to what was found in experimental results [68]. When more H₂ is fed to the reactor (see R25), more protons are released. In contrast, less protons are released when more acetate is fed. ATP synthase increases in both species (R12, R22) when more H₂ or acetate is fed to the reactor.

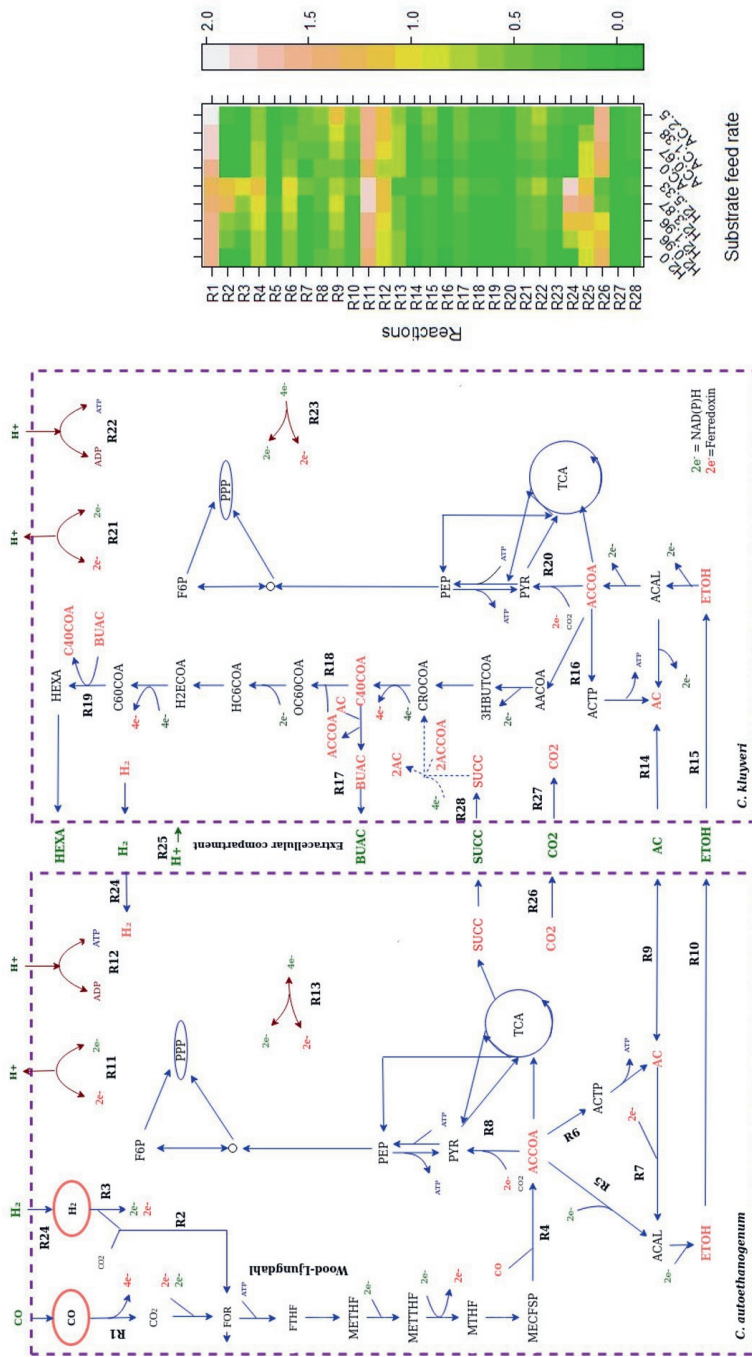


Figure 3.4: Schematic representation of the simulated metabolism of *C. autoethanogenum* and *C. kluyveri* under chemostat cultivation conditions. In CO/H₂ experiments, CO feed rate= 4.8 mmol L⁻¹ h⁻¹; growth rate=0.021 h⁻¹ and working volume= 1.1. In CO/AC conditions, CO feed rate= 6.4 mmol L⁻¹ h⁻¹; growth rate=0.028 h⁻¹ and working volume= 0.75 l. Blue arrows indicate the fluxes direction. Metabolites colored green are extracellular metabolites, partly exchanged between species and partly excreted or assimilated to/from the media. The heatmap on the right shows the fluxes of the R# reactions selected on the map for all conditions. Flux values are log transformed (log(Flux+1)) for a better visualization

3.4.4 Effect of the biomass ratio of *C. kluuyveri*-*C. autoethanogenum* on the metabolic profiles of the culture

The model enables detailed inspection of production and uptake profiles. Therefore we investigated the sharing of metabolites between both organisms. Analysis of intracellular fluxes in Fig. 3.4 suggests that succinate is produced by *C. autoethanogenum* and metabolized by *C. kluuyveri* producing part of the acetate and crotonyl-CoA pool needed for chain elongation and production of fatty-acids. Fig. 3.5, shows the

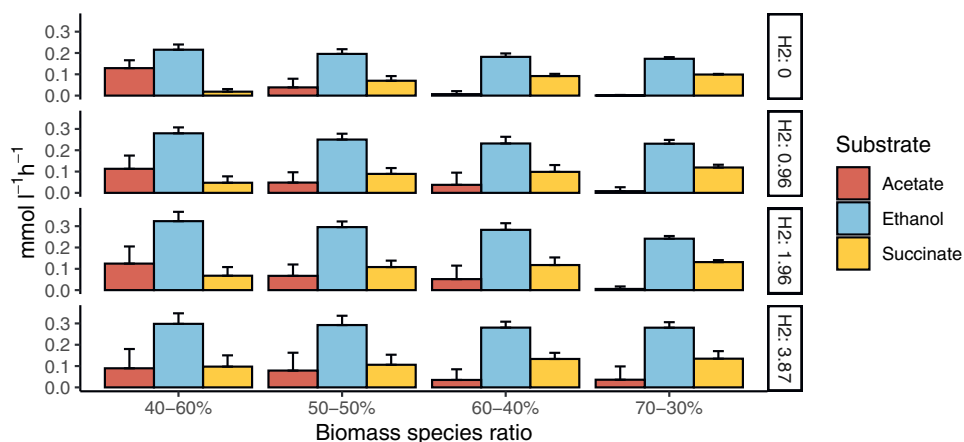


Figure 3.5: The effect of changing biomass species ratios on the uptake of acetate, ethanol and succinate by *C. kluuyveri* at different H₂ feed rates and fixed CO feed rate. CO= 4.8 mmol L⁻¹ h⁻¹ and growth rate=0.021 h⁻¹, respectively. *C. kluuyveri*-*C. autoethanogenum* biomass ratio are indicated on the x axis and y axis represents the fluxes of transport reactions from extracellular to *C. kluuyveri* compartment of acetate, ethanol and succinate.

different profiles depending on the biomass species ratio when we simulate chemostat cultivation experiments of *C. autoethanogenum* and *C. kluuyveri* growing on CO and H₂ as carbon and energy sources. Succinate, acetate and ethanol uptake by *C. kluuyveri* increases with more H₂ supply. Succinate uptake decreases when *C. kluuyveri* is less abundant in the co-culture. On the contrary, the amount of ethanol and acetate that is available to be metabolized by *C. kluuyveri* decreases along with the relative abundance of *C. autoethanogenum*.

To further investigate the role of succinate, similar simulations were performed but this time preventing the uptake of succinate by *C. kluuyveri* (Fig. 3.6). The model shows that, without succinate uptake, a biomass-species ratio of 70-30% and CO

as the only carbon source results in an infeasible situation. In addition, the fluxes through reactions related to non-growth associated maintenance (ATPM, ATPM_auto) decreased substantially when biomass ratios of 60-40%, 50-50% and 40-60% were considered. Thus, the *in silico* analyses show that a possible way to meet the experimentally observed constraints is through succinate uptake. Changes in the biomass ratio also affect acetate and ethanol exchange between the microbes. Acetate and ethanol uptake by *C. kluyveri* increases when more H₂ is fed to the system. Acetate/ethanol production ratios become higher when *C. kluyveri* is more abundant and decrease when there is more *C. autoethanogenum* in the co-culture. Based on these results, the species biomass ratio in co-cultivation is estimated to be between 60-40% and 70-30% (*C. kluyveri*-*C. autoethanogenum*).

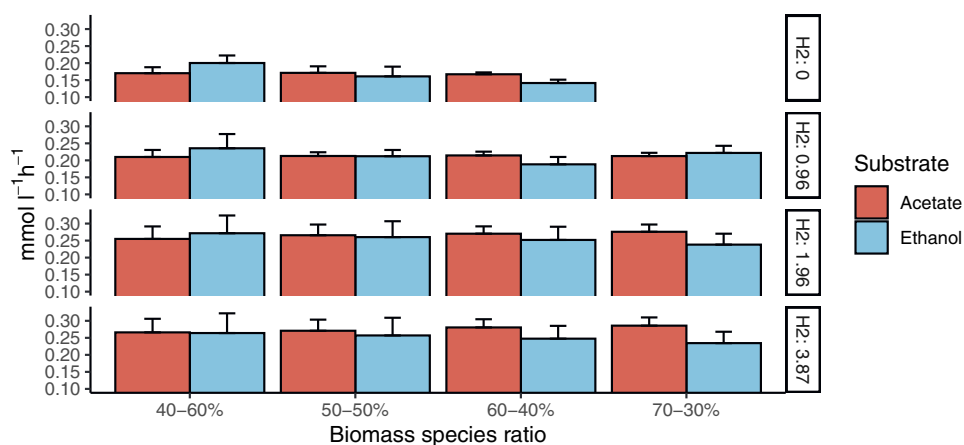


Figure 3.6: Effect of changing biomass species ratios on the uptake of acetate and ethanol by *C. kluyveri* at different H₂ feed rates without succinate uptake and fixed CO feed rate. CO= 4.8 mmol L⁻¹ h⁻¹ and growth rate=0.021 h⁻¹. *C. kluyveri*-*C. autoethanogenum* biomass ratio are indicated on the x axis and y axis represents the fluxes of transport reactions from extracellular to *C. kluyveri* compartment of acetate and ethanol.

3.4.5 Strategies to increase production of medium-chain fatty-acids

We used the experimentally-validated model to simulate alternative scenarios that have so far not been explored experimentally. Accordingly, we present here an analysis of possible strategies to increase medium-chain fatty acid production by the co-culture.

Addition of succinate

As a strategy to increase the production of desired products, we simulated how the addition of succinate as extra carbon source would affect the production of butyrate and hexanoate at different H₂ feed rates and fixed CO feed rate (4.8 mmol L⁻¹ h⁻¹). Fig. 3.7, shows the product profile for the species biomass ratio 70–30% (*C. kluyveri*-*C. autoethanogenum*), respectively. The increased carbon availability has been considered and used to normalize the results, so they are represented as mmol of product per total substrate (CO and succinate) per carbon. As already indicated in Fig.

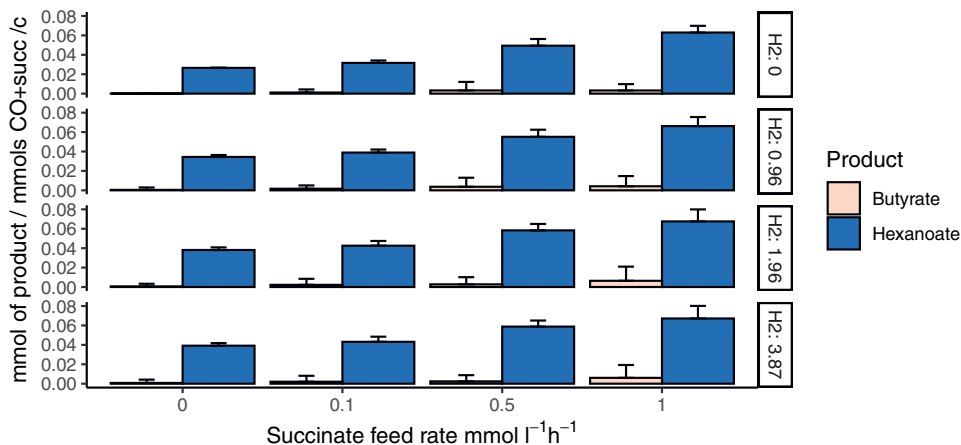


Figure 3.7: Effect of succinate addition on the production of butyrate and hexanoate under different H₂ feed rates when a biomass ratio of 70–30% is considered. X-axis represent succinate feed rate and y-axis represent mmol of butyrate or hexanoate normalized per mmols of total substrate per carbon.

3.3, and in contrast to experimental results, the model predicts more hexanoate than butyrate production even when succinate uptake is 0. The model predicts a yield of 0.026 mmol of hexanoate per mmol of CO. This means, that this co-culture has the capacity to produce three times more hexanoate than what it is currently being produced (0.009 mmol per mmol of CO) [68], reducing the gap respect to the maximum theoretical yield (0.056 mmol of hexanoate per mmol of CO) to 3%. Increased hexanoate production is observed next to an increase in CO₂ uptake by *C. kluyveri* and changes in H⁺ balance and ATP synthase.

Furthermore, succinate addition allows increased production of both fatty-acids. Hexanoate production can increase up to four times when succinate is added and

butyrate has potential to increase around five times with respect to the results obtained with no succinate addition. On the other hand, simulations show no relevant differences upon variations of H_2 feed rates.

Genetic intervention strategies

As a second strategy for co-culture optimization we have predicted and evaluated genetic interventions that could lead to higher medium-chain fatty-acid production.

The strain design algorithms OptKnock and RobustKnock [93, 237] were applied to identify candidate reactions to be knocked out. These were subsequently evaluated through dedicated simulations. Fig. 3.8 shows the effect of knocking out three

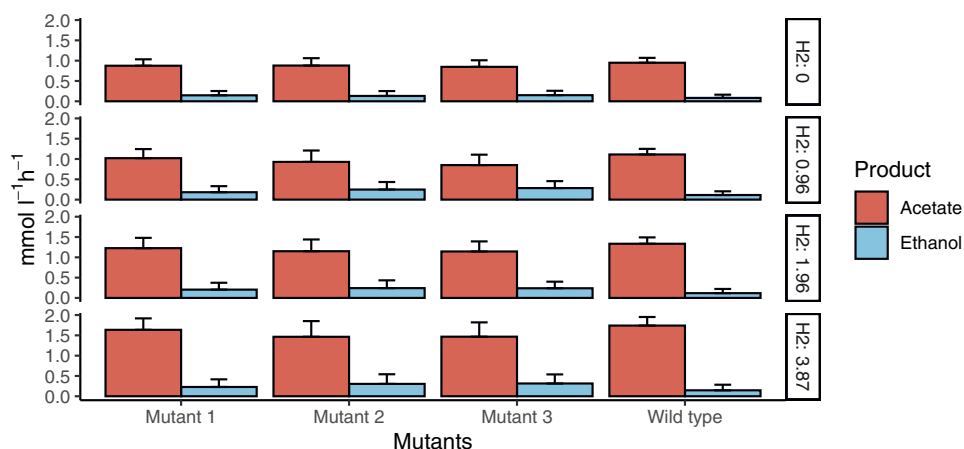


Figure 3.8: Effect of single reactions deletion on the production of ethanol in *C. autoethanogenum*. X axis represents the mutants applied on the GEM of *C. autoethanogenum* and y axis represents the production of acetate and ethanol. Mutant 1: Formate transport in via proton symport (rxn05559_c0). Mutant 2: acetaldehyde:NAD oxidoreductase (rxn00171_c0); Mutant 3: formate dehydrogenase (ferredoxin) (rxn00103_c0)

candidate reactions on the production of ethanol in *C. autoethanogenum*. The three reactions are located in the metabolism of *C. autoethanogenum*. Mutant 1 refers to the knock out of formate transport reaction via proton symport (FORt2, model id rxn05559_c0). Mutant 2 refers to the deletion of acetaldehyde:NAD⁺ oxidoreductase (ACALDx, model id rxn00171_c0). Mutant 3 refers to the knock out of formate dehydrogenase (ferredoxin) (FDH_{fer}, model id rxn00103_c0). The impact of removal of these reactions is compared to wild type *C. autoethanogenum*, correspond-

ing to the GEM without any modification. The deletion of each reaction results in increased ethanol production. Ethanol increases up to 83% with respect to the wild type in simulations with CO as the only carbon source. In conditions where H₂ acts as second substrate, ethanol production increases up to 150%. Acetate decreases up to 11% in simulations with only CO and decreases up to 30% in CO/H₂ simulations. Mutant 1 seems to have a higher ethanol yield when CO is the only carbon source compare to CO/H₂ conditions while mutant 2 and mutant 3 provide a higher effect on ethanol/acetate ratio in CO/H₂ simulations. As seen in Fig. 3.6, the production of ethanol by *C. autoethanogenum* and therefore, the uptake of ethanol by *C. kluyveri*, increases with increasing H₂ feed rate, resulting in an increased production of medium-chain fatty-acids. This suggests that these deletions in *C. autoethanogenum* can improve the production of medium-chain fatty-acids in this respective co-culture, since ethanol production can potentially be increased. Simulations of the effect of these mutations in mono-culture and co-culture are presented in the supplementary material.

3.5 Discussion

We present here a constraint-based model of the co-culture of *C. autoethanogenum* and *C. kluyveri* in the context of CO/syngas fermentation to produce medium-chain fatty-acids. A model with similar characteristics had already been used to simulate CO to butyrate conversion by bacterial co-culture systems [218]. Our model extends previous efforts, and is calibrated and tested with a battery of available experimental measurements. Modeling bacterial communities using flux balance analysis and GEM is complicated by the fact that special attention has to be paid to the biomass abundances of the microbial species in order to achieve balanced growth of the co-culture. Previous efforts used dynamic flux balance analysis to consider biomass growth [218]. Here, steady-state conditions were used of which additional data was available, allowing to overcome the challenge of estimating relative abundance of each species by combining microscopy observations and RNA seq in terms of cell numbers. These were subsequently converted to biomass ratios by considering the relationships between cellular dimensions, cell volume and biomass dry weight. This enabled the application of community flux balance analysis [221], which has been shown to accurately predict flux distributions and exchange fluxes between species and the community environment when analyzing stable communities in chemostat experiments. In this model it is assumed that the exchange of metabolites occurs indirectly using the culture medium as an intermediate. Recently, a direct exchange of electrons and metabolites due to direct cell-to-cell interactions have been observed in a co-culture of *C. ljungdahlii* and *C. acetobutylicum*

[243]. Further research on the latter co-culture also demonstrates a high exchange of proteins, showing persistence of cells with exchanged cellular components [244]. An extension of our model could include more detailed description of the mechanism of metabolite exchange. This could shed light on additional interactions that might take place such as a possible exchange of amino acids.

The presented co-culture model is versatile and can simulate the CO/syngas fermentation process leading to medium-chain fatty-acid production. The presented model describes both the behaviour of a *C. autoethanogenum* mono-culture thriving on syngas as well as the behaviour of a co-culture of *C. autoethanogenum* and *C. kluyveri*. The model accurately reproduces the steady-state production rates of fermentation products obtained in chemostat experiments, and predicts the shift of the metabolism of *C. autoethanogenum* towards solventogenesis in co-cultivation with *C. kluyveri* [68]. In addition, model predictions on production/consumption rates (see Fig. 3.4) agree reasonably with previous literature on CO/syngas fermentation [64, 68, 211, 230]. The product profile has shown the relative high level of carbon loss in acetate, compared to the desired elongated fatty-acids. This could be improved by in-line product removal, pH adjustments, an increase of CO pressure to obtain a higher conversion of acetate to ethanol or genetic engineering.

Analyses of metabolic fluxes in the model surprisingly suggested succinate production by *C. autoethanogenum* as an intermediate in the co-culture. Accumulation of succinate has not been experimentally observed in the calibration experiments [68], and is not described as major physiological end-product of *C. autoethanogenum* when grown on syngas [211]. However, its production by *C. autoethanogenum* in the presence of *C. kluyveri* could take place as it has been reported to be an overflow product of acetogenic metabolism [245]. Here, succinate could be produced to overcome the temporal overflow of C/electrons, potentially in conditions where too much reduction equivalents are provided. Succinate is described as a possible substrate for *C. kluyveri* [230]. Presence of succinate could slow down consumption of ethanol/acetate by *C. kluyveri*. This would also affect co-culture compositions by limiting *C. kluyveri* abundances. The suggested exchange of succinate, can explain the slight mismatch observed in the acetate production simulated compared to the laboratory results. Mono-culture results of *C. autoethanogenum* however, do not show succinate production. Thus, this difference can be derived from the biomass drop observed with increasing acetate feed rate affecting the ATP maintenance requirements [68] and redox balance.

Model simulations have shown that omitting succinate uptake resulted in unfeasible growth conditions when grown on only CO (see Fig. 3.6, ratio 70-30%). This dependency is additionally shown in the case with both CO and H₂, where ATPM decreased substantially to sustain growth. An alternative explanation for this dependency could be related to *C. autoethanogenum* cell size assumptions, being po-

tentially bigger than the average size, since it was reported to have considerable variations [211]. Therefore, the co-culture might operate in ratios where the biomass of *C. autoethanogenum* is more abundant, with relative values between 60-40% and 70-30%, leading to possible changes in the relative species abundance among different conditions.

As the model closely predicted obtained experimental values, it can be used to design potential strategies for improved production. Here, we explored a series of strategies to optimize the production of hexanoate. The first strategy relied on the role of succinate, as the model predicts it increases the pool of acetate and crotonyl-CoA, a precursor of the desired fatty-acids, in *C. kluyveri* (see Fig. 3.4). The flux through the reverse β -oxidation pathway increases up to four times when succinate is added (see supplementary material). The increase of crotonyl-CoA results in a higher butyryl-CoA pool. The presence of more butyryl-CoA initiates the chain-elongation process to produce hexanoyl-CoA in the same way as butyryl-CoA is formed (see Fig. 3.4). According to the model, most of butyrate formed from butyryl-CoA reacts with hexanoyl-CoA producing hexanoate. This results in an increase in hexanoate production up to three times (see Fig. 3.7). Moreover, an increase in ethanol uptake by *C. kluyveri* and a decrease in acetate production by *C. autoethanogenum* and subsequent uptake by *C. kluyveri* appears to cause an additional boost in hexanoate production. According to the model, addition of succinate raises hexanoate production up to 0.067 mmol per carbon of fed substrate (CO and succinate) and would possibly lead to a further increased production of MCFA and alcohols in conditions with higher H_2 influx ($> 5 \text{ mmol L}^{-1} \text{ h}^{-1}$), as it has been previously observed. Furthermore, it has already been proven that succinate leads to an increase of MCFA in *C. kluyveri* [239], so its addition in co-culture experiments could potentially confirm model results.

The second strategy aims to increase hexanoate by increasing ethanol production by *C. autoethanogenum*. An increasing ratio of ethanol/acetate ratio has been shown to result in increased hexanoate production in *C. kluyveri* [233, 246]. In cases where butyrate and hexanoate are not constrained (see Fig. 3.7), the predicted ethanol/acetate ratio (around 6:4) is higher than when butyrate is more prominent (see Fig. 3.6). The model thus confirms previous experimental results and highlights the potential of an increased ethanol/acetate ratio in stimulating the production of hexanoate. It should be bear in mind that model predictions are based on optimality principles and assumptions. The model suggests that increased ethanol production leads to increased medium-chain fatty-acids (see supplementary material).

C. autoethanogenum is known to increase production of ethanol under acidic or redox overloading conditions [56, 68, 247]. Additionally, partial inactivation of the adhE cluster or knock out of one of the AOR genes has been shown to result in increased ethanol production in *C. autoethanogenum* [50]. Using the GEM herein

developed for *C. autoethanogenum* we predicted that the individual knock-out of one of the following three reactions could increase the production of ethanol: acetaldehyde oxidoreductase (ACALDx), formate transport (FORt2), and the bifurcating formate dehydrogenase (ferredoxin) (FDH_fer) (see Fig. 3.8). The acetaldehyde oxidoreductase reaction (ACALDx, id rxn00171_c0) is associated with several isoenzymes encoded by genes: CAETHG-RS16140, CAETHG-RS08865, CAETHG-RS08810, CAETHG-RS18400 and CAETHG-RS18395. The same isoforms are associated to aldehyde ferredoxin oxidoreductase reaction (CODH-ACS) (leq000004) and two of them (CAETHG-RS18400 and CAETHG-RS18395) are also involved in ethanol oxidoreductase (ALCDx) (rxn00543_c0) reaction. The affinity of each isoenzyme to each reaction has to be studied in order to fully eliminate acetaldehyde oxidoreductase activity. An acetaldehyde oxidoreductase (ACALDx) mutant has previously been shown to indeed have increased ethanol production up to 180% [50], making the deletion of this reaction seems a promising application to increase fatty-acids production in the co-culture system. The knock out of formate-related reactions in *C. autoethanogenum* is not described previously, but model simulations done here, suggest that they contribute to ethanol production. Formate transport in via proton symport (FORt2, model id rxn05559_c0) is catalyzed by an enzyme encoded by only one gene -CAETHG-1601, which allows relatively easy removal of this activity. The model predicts that inactivation of this reaction forces more flux through the Wood-Ljungdahl pathway, increasing the amount of acetyl-CoA. Due to the increase in acetyl-CoA pool, the fluxes through aldehyde ferredoxin oxidoreductase and acetaldehyde oxidoreductase are increased, thus producing more ethanol. As third option the model suggests to knock out the formate dehydrogenase (ferredoxin) (FDH_fer, model id rxn00103_c0) activity. This reaction has three associated isoenzymes encoded by genes: CAETHG-RS00400, CAETHG-RS13720 and CAETHG-RS14690. The inactivation of this reaction forces the production of formate mostly via formate hydrogen-lyase from H₂ (FHL, rxn08518_c0). In mono-culture conditions where there is no H₂ supply, H₂ is produced via an NADP-dependent electron-bifurcating hydrogenase reaction (Hyt) (model id leq000001). This functionality of Hyt seems to occur in situations where redox mediators get too reduced [242]. The model shows a higher conversion of CO converted to CO₂ via CO dehydrogenase (CODH4, model id rxn07189_c0) which forces more flux through Wood-Ljungdahl pathway, producing more acetyl-CoA. Also, more CO₂ is fixed producing pyruvate via pyruvate synthase (rxn05938_c0) which is shuttled back via pyruvate formate lyase (rxn00157_Cc0) to produce more acetyl-CoA and formate. The extra pool of acetyl-CoA forces more flux through aldehyde ferredoxin oxidoreductase and acetaldehyde oxidoreductase which leads to more ethanol.

When the reactions of fatty-acids production are not constrained, the model always predicts more hexanoate as compared to butyrate production measured in the

actual chemostat experiments [68]. A potential reason for this is the pH of the co-culture and related toxicity effects of medium-chain fatty acids. Hexanoate production in *C. kluyveri* has been reported to be better at higher pH [248]. Thus, potentially the pH of 6.2 in the co-culture limits its production in the actual experiments. In addition to toxicity effects, the function of membrane proteins such as ATP synthase, electron transport chains or transporters can be affected by the change of proton motive force at different pH [249]. This is reflected by the observation that model predictions show differences in ATP synthase and proton balance under different butyrate/hexanoate production conditions (see supplementary material and Fig. 3.4). However, the acid stress response is difficult to simulate in GEMs, which possibly results in the differences observed between the model prediction and experimental results. In addition it has been observed oscillations in gas uptake rates and extracellular byproducts synchronized with biomass levels in *C. autoethanogenum* [250]. This could lead to thermodynamic changes affecting the reversibility of reactions and thus, the product range. An extensive thermodynamic and metabolic flux analysis study even extending the component contribution method [251] could have helped to better identified those changes.

We observe an increase of CO₂ uptake by *C. kluyveri* in cases where hexanoate is more abundant (see Fig. 3.4 and supplementary material) compared to simulations of experimental conditions, where butyrate is more abundant (see Fig. 3.4). CO₂ is essential for growth and C1 intermediate production in *C. kluyveri* [224, 225, 252, 253]. In line with model predictions, CO₂ is converted to formate via a cyclic mechanism [225]. CO₂ is first fixed via pyruvate synthase (model id Rckl119) producing pyruvate that is further converted to formate via formate lyase (model id PFL), for assimilatory purposes. Formate is then assimilated via the tetrahydrofolate pathway to, subsequently, be transformed to various amino acids needed for growth [224, 225, 252, 253]. Model predictions show that part of the CO₂ is also metabolized following phosphoenolpyruvate carboxylase reaction (PPC), where CO₂ is fixed together with phosphoenolpyruvate (pep) producing oxaloacetate (oaa). Oaa produces aspartate via aspartate aminotransferase (Rckl310). Aspartate is a precursor in the synthesis of threonine involving aspartate kinase (Rckl334), aspartate semialdehyde oxidoreductase (Rckl323), homoserine kinase (Rckl335) and threonine synthase (Rckl336). Then, threonine produces acetaldehyde and glycine via threonine aldolase (Rckl341). Acetaldehyde is converted to acetyl-CoA following aldehyde alcohol dehydrogenase (ADH) reaction. So, the increase in CO₂ assimilation could lead to more acetyl-CoA and thus, more fatty-acids. Around 30-40% of CO₂ is also converted to carbonic acid. Carbonic acid produces oxaloacetate via pyruvate carboxylase (Rckl014), which follows the aforementioned route to acetyl-CoA. Simulations made with higher CO₂ uptake rates than the ones predicted when hexanoate is more abundant (>0.75 mmol L⁻¹ h⁻¹) however, did not lead to higher

production rates of hexanoate or butyrate. This suggest that *C. kluyveri* metabolizes CO₂ up to a maximum value. In fact, this is supported by the observed correlation between growth and the maximum CO₂ fixed by *C. kluyveri* [253]. The use of lower hydraulic retention time and high pressure bioreactors, could possibly increase the uptake of CO₂, close to its maximum capacity.

The maximum hexanoate predicted by the multi-species GEM is reached when succinate is added into the system in combination with CO and H₂ (see Fig. 3.7). Table 3.1, shows a comparison of electron yields for the hexanoate production pre-

Table 3.1: Comparison of electron yield obtained for hexanoate production between predicted results by the multi-species GEM and other co-culture/mixed culture. Electron yield is expressed by the amount of electrons going to hexanoate per total amount of electrons entering the system.

	Substrates ^a	Hexanoate ^b	Electron yield ^c
<i>C. ljundahlii</i> & <i>C. kluyveri</i> [254]	CO=31.9 H ₂ = 79.1	0.48	0.07
Mixed culture [63]	CO=0.58	0.011	0.32
<i>C. autoethanogenum</i> & <i>C. kluyveri</i> [68]	CO=4.8 ^d H ₂ =5.3	0.15	0.26
<i>C. autoethanogenum</i> & <i>C. kluyveri</i> [68]	CO=6.5 ^c AC=2.5	0.15	0.15
Multi-species GEM (this study)	CO=4.8 H ₂ =3.87 SUCC=1	0.59	0.6

^aVolumetric consumption rate mmol L⁻¹ h⁻¹

^bVolumetric production rate mmol L⁻¹ h⁻¹

^chexanoate e⁻/total e⁻ in ; CO= 2 e⁻ per mol, H₂ = 2 e⁻ per mol; AC(acetate)= 8 e⁻ per mol; SUCC (succinate)= 14 e⁻ per mol and hexanoate = 32 e⁻ per mol

^d Assuming 90% gas consumption

dicted in this study compared to hexanoate production in other studies with similar culture systems [63, 68, 254].

Electron yield is calculated based on the amount of electrons going to hexanoate per the total amount of electrons going into the system as carbon and energy sources. Co-cultures of *C. autoethanogenum* and *C. kluyveri* yielded more hexanoate growing on CO/H₂ or CO and acetate compared to a co-culture of *C. ljundahlii* and *C. kluyveri*, potentially as in the latter relatively more alcohols and C8 acids were produced as well. A mixed culture enriched in *Acinetobacter*, *Alcaligenes*, and *Rhodobacteraceae* growing solely on CO [63], increased the electron yield with respect to pre-

viously mentioned co-cultures up to 0.32. However, the addition of succinate in co-cultivation of *C. autoethanogenum* and *C. kluyveri* grown on CO and H₂ (this study), is here predicted to increase the yield of hexanoate up to 0.6, reflecting the potential of this approach to produce medium-chain fatty-acids.

3.6 Conclusions

The generation of the multi-species GEM of *C. autoethanogenum* and *C. kluyveri* has provided insights into the fermentation of CO/syngas to medium-chain fatty acids by this co-culture. The prediction of intracellular flux distribution in this consortium enabled to uncover the potential importance of succinate uptake via *C. kluyveri* to produce butyrate, and suggested an effect of the biomass species ratio on the substrate profile of *C. kluyveri*. Simulations indicated that succinate addition might result in a substantial increase in hexanoate yield from syngas. In addition, the model of *C. autoethanogenum* shows that the deletion of reactions FORt2 or ACALDx or FDH_fer in *C. autoethanogenum* potentially increase ethanol production, suggesting a potential increase in hexanoate production when these deletions were to be applied in co-culture experiments. Altogether, our model-driven approach has set a good basis for the systematic design of strategies to modulate and optimize the production of valuable chemicals from syngas.

Declaration of competing interest

The authors declare that they have no known competing financial interests or personal relationships that could have influenced the work reported in this paper.

Acknowledgements

The research leading to these results has received funding from the Netherlands Science Foundation (NWO) under the Programme ‘Closed Cycles’ (Project nr. AL-WGK.2016.029) and the Netherlands Ministry of Education, Culture and Science under the Gravitation Grant nr. 024.002.002.

Author contributions

Sara Benito-Vaquerizo: Conceptualization, Methodology, Software, Formal analysis, Investigation, Writing-Original draft preparation. Martijn Diender: Formal analysis,

Investigation, Writing - Review & Editing. Ivette Parera Olm: Formal analysis, Investigation, Writing - Review & Editing. Peter J. Schaap: Conceptualization, Writing - Review & Editing. Vitor A.P. Martins dos Santos: Funding acquisition, Supervision, Writing- Reviewing & Editing. Diana Z. Sousa: Project administration, Funding acquisition, Conceptualization, Writing- Reviewing & Editing. Maria Suarez-Diez: Supervision, Conceptualization, Methodology, Visualization, Writing- Reviewing & Editing.

Chapter 4

Genome-scale metabolic modelling enables deciphering ethanol metabolism via the acrylate pathway in the propionate-producer *Anaerotignum neopropionicum*

4

Sara Benito-Vaquerizo*, Ivette Parera Olm*, This de Vroet, Peter J. Schaap, Diana Z. Sousa, Vitor Martins dos Santos, Maria Suarez-Diez
Published in: Microb. Cell Factories. 21, 116 (2022).

doi.org/10.1186/s12934-022-01841-1

* Contributed equally

4.1 Abstract

Microbial production of propionate from diluted streams of ethanol (e.g., deriving from syngas fermentation) is a sustainable alternative to the petrochemical production route. Yet, few ethanol-fermenting propionigenic bacteria are known, and understanding of their metabolism is limited. *Anaerotignum neopropionicum* is a propionate-producing bacterium that uses the acrylate pathway to ferment ethanol and CO₂ to propionate and acetate. In this work, we used computational and experimental methods to study the metabolism of *A. neopropionicum* and, in particular, the pathway for conversion of ethanol into propionate.

Our work describes iANEO_SB607, the first genome-scale metabolic model (GEM) of *A. neopropionicum*. The model was built combining the use of automatic tools with an extensive manual curation process, and it was validated with experimental data from this and published studies. The model predicted growth of *A. neopropionicum* on ethanol, lactate, sugars and amino acids, matching observed phenotypes. In addition, the model was used to implement a dynamic flux balance analysis (dFBA) approach that accurately predicted the fermentation profile of *A. neopropionicum* during batch growth on ethanol. A systematic analysis of the metabolism of *A. neopropionicum* combined with model simulations shed light into the mechanism of ethanol fermentation via the acrylate pathway, and revealed the presence of the electron-transferring complexes NADH-dependent reduced ferredoxin:NADP⁺ oxidoreductase (Nfn) and acryloyl-CoA reductase-EtfAB, identified for the first time in this bacterium.

The realisation of the GEM iANEO_SB607 is a stepping stone towards the understanding of the metabolism of the propionate-producer *A. neopropionicum*. With it, we have gained insight into the functioning of the acrylate pathway and energetic aspects of the cell, with focus on the fermentation of ethanol. Overall, this study provides a basis to further exploit the potential of propionigenic bacteria as microbial cell factories.

4.2 Background

Propionic acid is a naturally-occurring carboxylic acid produced by propionigenic bacteria as end-product of their anaerobic metabolism. It is an important intermediate in anaerobic fermentative processes such as those occurring in the human gut, anaerobic digesters and cheese production. It is also an essential platform chemical in the manufacture of cellulose-derived plastics, cosmetics and pharmaceuticals and, due to its antimicrobial properties, it can be used as food preservative [255, 256]. At present, industrial production of propionic acid is based on petrochemical processes, but efforts are being made to develop sustainable production platforms based on the use of propionigenic bacteria as biocatalysts [255, 256]. Microbial production of propionic acid has been researched for over 150 years, however industrial implementation is still limited mainly due to low productivities, which render such processes economically noncompetitive [255–257]. So far, most approaches have considered strains of the genus *Propionibacterium* - well-studied due to their involvement in cheese production [256] -, and have focused on the use of sugars as feedstock. However, the chemical industry is increasingly required to rely on the use of non-conventional, inexpensive raw materials to minimize its carbon footprint [258]. Ethanol, a low-priced common end-product of many fermentations, is re-

garded as one of such feedstocks [258, 259]. Moreover, ethanol can be synthesised from CO, CO₂ and H₂ (syngas) by acetogenic bacteria. Syngas-to-ethanol fermentation technology has been deployed at large scale, and recent advances are expected to accelerate its development in the years to come [260–262].

Anaerotignum neopropionicum, formerly *Clostridium neopropionicum* [263], was the first representative of the ethanol-fermenting, propionate-producing bacteria. It was isolated in 1982 from an anaerobic digester treating wastewater from vegetable cannery [264]. The ability of converting ethanol to propionate is shared with only three other microbial species: the closest relative *Anaerotignum propionicum* [265] (formerly, *Clostridium propionicum* [263]), the sulphate-reducing bacterium *Desulfobulbus propionicus* [266, 267], and *Pelobacter propionicus* [268]. In these four microorganisms, ethanol oxidation to propionate occurs in the presence of CO₂ with concomitant production of acetate, according to the theoretical Eq. (4.1). This ability of propionigenic bacteria could be exploited to upgrade dilute ethanol streams from beer production or syngas fermentation, among others. For example, Moreira et al. showed that co-cultures of acetogens and ethanol-consuming propionigenic bacteria can convert syngas into propionate [269]. In their study, the acetogen *Acetobacterium wieringae* was co-cultivated with *A. neopropionicum*; *A. wieringae* converted CO to ethanol, which was used by *A. neopropionicum* to produce propionate.



$$\Delta G^{\circ} = -124\text{kJ}$$

Two main pathways have been described for the fermentative production of propionic acid in bacteria: the methylmalonyl-CoA (also termed succinate pathway or Wood-Werkman cycle) and the acrylate pathway [255, 270]. Most of the known propionigenic bacteria, including strains of the genera *Propionibacterium* and *Cutibacterium*, use the methylmalonyl-CoA pathway for growth. The acrylate pathway is mostly found within members of the phylum Firmicutes [270]. Sugars and lactate are common substrates for these pathways. Ethanol fermenters *D. propionicus* and *P. propionicus* use the methylmalonyl-CoA pathway [267, 268], whereas *A. neopropionicum* and *A. propionicum* use the acrylate pathway [271].

To fully exploit the potential of microorganisms for biotechnological applications, it is fundamental to understand their metabolism and cellular processes. Genome-scale metabolic models (GEMs) and their analysis with CONstraint-Based Reconstruction and Analysis (COBRA) methods [272] have become indispensable tools in this regard [72, 214]. Flux balance analysis (FBA) is often used as the mathematical approach to explore the intracellular fluxes of GEMs under steady-state conditions (e.g., in chemostat cultivations) [86]. FBA can be extended to dynamic

FBA (dFBA), which simulates the time-step evolution of individual steady-states that take place in time-varying processes, such as batch and fed-batch cultures [89]. A wide range of GEMs have been successfully implemented to unravel novel metabolic features of microorganisms, guide experimental design or improve bioprocess operation in mono- and co-cultivation. For instance, the reconstruction of the first GEM of *Clostridium ljungdahlii* (iHN637) demonstrated the essential role of flavin-based electron bifurcation in energy conservation during autotrophic growth [273]. FBA enabled the estimation of intracellular metabolic fluxes in the GEM of the acetogen *Clostridium autoethanogenum* (iCLAU786), helping to understand the effects of CO supplementation on CO₂/H₂-growing cultures [274]. A multi-species GEM was recently developed that described a syngas-fermenting co-culture composed of *C. autoethanogenum* and *Clostridium kluyveri*; the model provided valuable insight into the microbial interactions between the two microorganisms and predicted strategies for enhanced production of the end products butyrate and hexanoate [51].

Many propionigenic bacteria have been sequenced to date [275–280], including the ethanol fermenters *D. propionicus* [281], *P. propionicus* [282], *A. propionicum* [278] and *A. neopropionicum* [280]. This has enabled the reconstruction of GEMs of some of these species. All GEMs of propionigenic bacteria published to date concern strains that harbour the methylmalonyl-CoA pathway. One of these works described the reconstruction of five *Propionibacterium freudenreichii* species using pangenome guided metabolic analysis [283]. Navone et. al used the *Propionibacterium* subsp. *shermanii* and the pan-*Propionibacterium* GEMs to guide genetic engineering strategies for increased propionic acid production [284]. Sun et. al developed a constrained-based GEM of *P. propionicus* and validated fermentative growth of this strain on ethanol [285].

Here we describe iANEO_SB607, the first GEM of *A. neopropionicum* and the first to model the acrylate pathway in a propionigenic microorganism. The model was reconstructed using automatic tools followed by an extensive manual curation, which led us to the identification of electron-transferring enzymes involved in the acrylate pathway, cofactor regeneration and energy conservation. In addition, a physiological characterisation of *A. neopropionicum* in batch cultures was performed to validate and complement the reconstruction of the model. FBA was used to assess growth phenotypes on several carbon sources, and dFBA was applied to simulate batch growth of *A. neopropionicum* on ethanol, and ethanol plus acetate. The combination of in-depth modelling and experimentation has enabled us to examine in detail the metabolism of ethanol fermentation in this bacterium and to address pre-existing ambiguities.

4.3 Materials and methods

4.3.1 Reconstruction of the GEM iANEO_SB607

The genome-scale metabolic network of *A. neopropionicum* was reconstructed in four main steps. First, the genome sequence of *A. neopropionicum* DSM 3847^T (GCA_001571775.1) [280] was retrieved from the European Nucleotide Archive in FASTA format and was annotated using RAST [81]. An additional re-annotation was carried out using eggNOG-mapper [286]. The annotation file can be found in the public Gitlab repository:

https://gitlab.com/wurssb/Modelling/Anaerotignum_neopropionicum. The second step was the generation of the draft model using ModelSEED [77]. For this, the RAST annotation file was imported into ModelSEED and a Gram-positive template was chosen to reproduce growth on rich medium. The draft model was downloaded in table format and SBML format. The third step consisted on the manual curation and refinement of the draft model. Every reaction entry was analysed individually and modifications were made on the table format file. Specifically, (i) unbalanced reactions were corrected based on charged formulas with the corresponding addition/deletion of H⁺ or H₂O molecules; (ii) reaction direction was adjusted using eQuilibrator [223]. Reactions were considered reversible if the change in Gibbs free energy was between -30 and 30 kJ mol⁻¹ at standard conditions for reactants/products, pH 7.3 and ionic strength 0.1 M. In cases where eQuilibrator did not retrieve information for a specific reaction, reaction direction was adjusted based on information from MetaCyc [287] and BIGG [288] databases. (iii) EC numbers were corrected or inserted for every reaction based on information from KEGG [289] and MetaCyc [287]. (iv) The original genes in Patric format [290] were replaced by the locus tag format ('CLNEO_XXXXX') found in Uniprot [291] and BRENDA [292] databases. The re-annotation file was used to identify potential gene(s) associated to reactions that lacked a gene in the original RAST annotation. (v) The final step consisted of gap-filling, where reactions were added or removed to reproduce known or observed phenotypes. Gap-filling was done combining a computational and a manual approach: an automatic gap-filling process was run using the KBase pipeline[78], while the manual curation was based on experimental data obtained in this study and published. The final model, iANEO_SB607, can be found in the git repository in Table format, json and SBML L3V1 [227] standardization. Furthermore, the different versions together with a Memote and FROG report (<https://www.ebi.ac.uk/biomodels/curation/fbc>) were combined in an OMEX archive file [293] deposited in BioModels [294] and assigned the identifier MODEL2201310001.

Generation of the biomass synthesis reaction and sensitivity analysis

The biomass reaction of *A. neopropionicum* was adapted from the biomass reactions of *Clostridium beijerinckii* (GEM iCM925 [295]) and *C. autoethanogenum* (GEM iCLAU786 [219]). The composition of the main building blocks was maintained but, based on the protocol of Thiele and Palsson [296], protons were stoichiometrically added to the hydrolysis part of the biomass synthesis reaction. Protons were also added to the reactions of DNA, RNA, proteins, teichoic acids and peptidoglycans synthesis in line with the ATP associated to polymerization. The DNA composition was determined based on the GC content of the genome of *A. neopropionicum* and it was adjusted in the reaction associated to the biosynthesis of DNA. The fatty acids composition was adjusted based on reported experimental data for *A. neopropionicum* [263].

A sensitivity analysis was performed by modifying the content of proteins, phospholipids (plipids) and cell wall components, considering cell wall components as the sum of teichoic acid, peptidoglycans and carbohydrates composition. The rest of components - DNA, RNA and trace- were kept fixed, as together they only represent 10% of the biomass. The composition of proteins and plipids were randomly selected within +/- 10% of their original value. In this way, the total cell wall components composition was calculated following equation 4.2.

$$\text{Cell wall components} = 1 - \text{protein} - \text{plipids} - (\text{DNA} + \text{RNA} + \text{trace}) \quad (4.2)$$

Consecutively, the value of each cell component, was distributed within teichoic acid, peptidoglycans and carbohydrates following the same proportion as they had in the original biomass synthesis reaction. For each randomly selected value, a new biomass synthesis reaction was obtained. This new biomass synthesis reaction was maximised as the objective function using FBA in COBRApy [235] maintaining fixed ethanol and CO₂ uptake rates. We repeated this process 1000 times, so that we obtained 1000 different biomass synthesis reactions. The composition of the cell wall components, proteins and phospholipids was stored for each biomass synthesis reaction, together with the growth rate, and acetate and propionate production rate. The obtained growth rate, acetate and propionate production rate were normalised with respect the original values and were plotted against each biomass building block (Additional file 1, Fig. S4.1) Additionally, we also studied the effect of varying GAM on the growth rate. In this analysis, the original fractions of the biomass components shown in equation 4.2 were maintained, and we randomly selected different GAM values within +/- 20% of the original value. We repeated this process 1000 times and calculated the growth rate for each GAM value. The obtained growth rate was normalised with respect the original growth rate and was plotted against GAM (Additional file 1, Fig. S4.2; git repository).

4.3.2 Model simulations at steady-state

The model was qualitatively validated by assessing growth capabilities and product profile on several carbon sources in steady-state. Model simulations were done using COBRAPy, version 0.24.0 [235], and Python 3.6.9. The maximum empirical ethanol uptake rate across cultivations was 30 to 40 mmol gDW⁻¹ h⁻¹ (see Quantitative assessment of iANEO_SB607 through dFBA). Based on this, the lower bound of the substrate uptake rate per time point was constrained to 30 mmol gDW⁻¹ h⁻¹ to assess growth on a single carbon source, and to 30 mmol gDW⁻¹ h⁻¹ in total to assess growth on more than one carbon source, unless specified otherwise. The biomass synthesis reaction was used as the objective function. Growth was considered when the growth rate was higher than 0.0001 h⁻¹. To better explore the solution space, the fluxes compatible with the applied constraints were sampled using the sample function with the 'achr' method in the flux_analysis submodule of COBRAPy [236]. The lower bound of the biomass synthesis reaction was constrained to be at least 99% of the maximum growth rate calculated by FBA. Presented results are the average and standard deviation based on 5000 iterations generated at each condition.

4.3.3 Dynamic flux balance analysis simulations

The reconstructed GEM iANEO_SB607 was subjected to dFBA to simulate batch growth of *A. neopropionicum* on ethanol and ethanol plus acetate. Model simulations were done using COBRAPy, version 0.24.0 [235], IBM ILOG CPLEX 128, and Python 3.6.9 (see git repository). The maximum uptake rate, maximum growth rate and initial substrate and biomass concentration obtained from batch cultivations, were used as model inputs. To constrain the feasible flux space, ethanol uptake was specified to follow a Michaelis-Menten-like kinetics (Eq. 4.3) with parameters $q_{S_i, \max}$ and $K_{m,i}$:

$$q_{S_i} = \frac{q_{S_i, \max} S_i}{K_{m,i} + S_i} \quad (4.3)$$

where q_{S_i} is the uptake rate of substrate i (mmol gDW⁻¹ h⁻¹); $q_{S_i, \max}$ is the maximum uptake rate of substrate i (mmol gDW⁻¹ h⁻¹); $K_{m,i}$ is the Michaelis-Menten constant (mM) for substrate i and S_i is the concentration of substrate i (mM). $K_{m,i}$ was determined based on experimental data and model fitting (Additional file 1, Table S4.1). $q_{S_i, \max}$ was calculated from experimental data of batch fermentations. Concentrations of substrates, products and biomass over time were determined as follows. First, the V_{S_i} was calculated using Eq. 4.3 for each given time step and the defined initial concentrations. Then, FBA was applied under those constraints

to compute the fluxes at maximum growth rate. After that, the following ordinary differential equations (ODE) were solved:

$$\frac{dX_i}{dt} = \mu_i X_i \quad (4.4)$$

$$\frac{dS_i}{dt} = q_{S_i} X_i \quad (4.5)$$

$$\frac{dP_j}{dt} = q_{P_j} X_i \quad (4.6)$$

where X_i is the biomass concentration (g L^{-1}); μ is the specific growth rate (h^{-1}); S_i is the concentration of substrate i (mM); q_{S_i} is the uptake rate of substrate i ($\text{mmol gDW}^{-1} \text{h}^{-1}$); q_{P_j} is the production rate of product j ($\text{mmol gDW}^{-1} \text{h}^{-1}$), and P_j is the concentration of product j (mM). Equations 4.4, 4.5 and 4.6 were used to calculate X , S_i and P_j . S_i is used as input to calculate the next state following equation 4.3. The objective function was changed to maximise the ATP generation (“rxn00062_c0”) once the model became infeasible due to the low concentration of ethanol. For each time step, the concentration of biomass, substrate and products was computed and the calculated values were stored and plotted.

4.3.4 Experimental batch fermentation data

Cultivation conditions

A. neopropionicum DSM 3847^T was obtained from the German Collection of Microorganisms and Cell Cultures (DSMZ, Braunschweig, Germany). Batch fermentations were done in 117 mL serum bottles containing 50 mL medium with the following composition (per litre): 0.9 g NH_4Cl , 0.3 g NaCl , 0.8 g KCl , 0.2 g KH_2PO_4 , 0.4 g K_2HPO_4 , 0.2 $\text{MgSO}_4 \times 7 \text{H}_2\text{O}$, 0.04 $\text{CaCl}_2 \times 2 \text{H}_2\text{O}$, 3.36 g NaHCO_3 , 10 mL trace element solution from DSM medium 318, 1 mL vitamin solution, 0.5 g yeast extract, 0.3 g $\text{Na}_2\text{S} \times x \text{H}_2\text{O}$ ($x=9-11$) as reducing agent and 0.5 mg resazurin as redox indicator. The vitamin solution contained (per liter): 0.5 g pyridoxine, 0.2 g thiamine, 0.2 g nicotinic acid, 0.1 g p-aminobenzoate, 0.1 g riboflavin, 0.1 g pantothenic acid, 0.1 g cobalamin, 0.05 g folic acid, 0.05 g thioctic acid and 0.02 g biotin. The headspace of the bottles was filled with a gas mixture of N_2/CO_2 (80:20 % v/v; 170 kPa). To test growth in the presence of H_2 , the headspace of bottles was filled instead with a gas mixture of $\text{H}_2/\text{CO}_2/\text{N}_2$ (10:20:70 and 80:20:0 % v/v; 170 kPa). Growth was assessed on the following substrates: ethanol, lactate, glucose and xylose, at an initial concentration of 25 mM. Where indicated, acetate (10 and 25 mM) was added to ethanol-fed cultures. The pH of the medium was 7.1 - 7.2. Cultures were incubated at 30°C statically.

Analytical techniques

Liquid and headspace samples were taken periodically over the course of batch fermentations and analysed for biomass, substrate and product concentrations. Biomass growth was measured by optical density at 600 nm (OD_{600}). Biomass concentration ($\text{mg}_{\text{CDW}} \text{L}^{-1}$) was estimated from OD_{600} measurements using the correlation: $\text{mg}_{\text{CDW}} \text{L}^{-1} = (OD_{600} - 0.016)/0.0032$, which was experimentally determined from *A. neopropionicum* cultures grown on ethanol. Concentrations of soluble compounds in the supernatant of liquid samples were determined using high-pressure liquid chromatography (HPLC) (LC-2030C Plus, Shimadzu, USA). The HPLC was equipped with a Shodex SH1821 column operated at 65°C. A solution of 0.1 N H_2SO_4 was used as mobile phase, at a flowrate of 1 mL/min. Detection was done via a refractive index detector. Concentrations below 0.2 mM could not be accurately quantified and are considered traces. Concentrations of gases in headspace samples were determined via gas chromatography (GC) (Compact GC 4.0, Global Analyser Solutions, The Netherlands). To analyse H_2 , a Molsieve 5A column operated at 140°C coupled to a Carboxen 1010 column was used. CO_2 was analysed in a RT-Q-BOND column at 60°C.

4.4 Results

4.4.1 Reconstruction of iANEO_SB607, the first GEM of *A. neopropionicum*

A draft model of the metabolism of *A. neopropionicum* was developed by automatic reconstruction using the publicly available genome sequence of the microorganism (DDBJ/EMBL/GenBank accession number: LRVM00000000; [280]). The draft model comprised 491 genes, 855 metabolites and 907 reactions. This preliminary model predicted growth only on rich medium supplemented with amino acids and biomass precursors, and it did not predict the production of propionate and acetate. We performed an extensive manual curation process that resulted in the deletion, modification or addition of reactions, metabolites and genes (see git repository). The final model, iANEO_SB607, comprises 607 genes, 815 metabolites and 932 reactions (Table 4.1). This is the first GEM of the propionigenic bacterium *A. neopropionicum*.

Two compartments are recognised in the model: the intracellular compartment (id: 'c0') and the extracellular compartment (id: 'e0'). Metabolites are assigned to either one of the compartments. Reactions are classified as metabolic reactions, transport reactions and exchange reactions. Metabolic reactions describe the biochemical conversion of metabolites within the intracellular compartment. Transport reactions

Table 4.1: Composition of iANEO_SB607

Features	Amount
Genes	607
Metabolites	815
Intracellular metabolites	742
Extracellular metabolites	73
Reactions	932
Metabolic reactions	771
Transport reactions	88
Exchange reactions	73
Reactions associated with genes	733
Reactions non-associated with genes	199

describe the transport of metabolites across the intracellular and extracellular compartments. Exchange reactions simulate the excretion of metabolites outside the cell or the uptake of metabolites into the cell. Reactions are distributed within cell subsystems (Fig. 4.1), except exchange reactions. The model also includes reactions involved in the production of acetate, propionate, butyrate, propanol, isobutyrate and isovalerate. Approximately 80 % of reactions could be associated to genes present in the genome of *A. neopropionicum*. The remaining 20% of reactions are not associated with genes. Half of these reactions are mostly exchange reactions and diffusion transport reactions. The other half are spontaneous reactions or gap-filled reactions describing, in a summarised manner, the biosynthesis of biomass building blocks (e.g., lipids, carbohydrates).

4.4.2 Sensitivity analysis of the biomass synthesis reaction

The constructed biomass synthesis reaction (BIOMASS_Aneopro_w_GAM) accounts for the production of DNA, RNA, proteins, peptidoglycans, phospholipids, teichoic acids and trace, and it is normalised to 1 gram per mmol. It also includes the growth-associated ATP maintenance (GAM) as an hydrolysis reaction, and the non-growth associated ATP maintenance (NGAM) as a reaction of ATP phosphohydrolase (rxn00062_c0). GAM was assumed to be 40 mmol ATP/gDW, as in the GEM of *C. acetobutylicum* [297]. The lower bound of this reaction was constrained to a rate of 8.4 mmol ATP $\text{g}_{\text{DW}}^{-1} \text{h}^{-1}$, an estimation based on the models of *C. beijerinckii* [295] and *C. autoethanogenum* [219].

Since the biomass synthesis reaction of *A. neopropionicum* was developed based

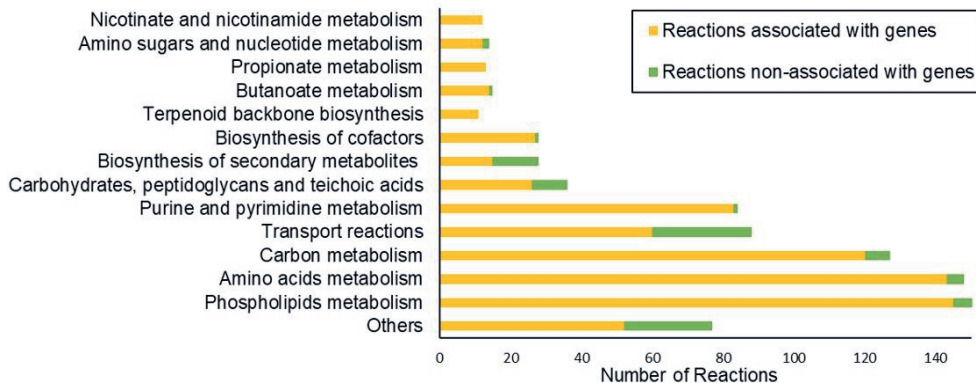


Figure 4.1: Distribution of the reactions of the iANEO_SB607 model within cellular subsystems

on these two other species, we performed a sensitivity analysis to test its robustness. The analysis showed the effect of modifying the proportion of the main biomass components from the biomass synthesis reaction on model predictions (i.e., growth and production rates). In all scenarios tested, growth and production rates remained virtually unaffected (Additional file 1, Fig. S4.1). The largest deviation of the growth rate, acetate and propionate production rates were $\pm 0.0005 \text{ h}^{-1}$, $\pm 0.005 \text{ mmol g}_{\text{DW}}^{-1} \text{ h}^{-1}$ and $\pm 0.0025 \text{ mmol g}_{\text{DW}}^{-1} \text{ h}^{-1}$, respectively, which are negligible as they only represent 3, 0.025 and 0.025 %, respectively. The effect of varying other biomass components -DNA, RNA and trace- was also considered negligible given that they represent a minor fraction of the biomass (10%). The growth rate was slightly more affected when GAM was changed. The largest deviation was $\pm 0.00175 \text{ h}^{-1}$, which corresponds to 10.8 % difference compared to the original growth rate. The biomass synthesis reaction was therefore considered a reliable representation of the biomass composition of *A. neopropionicum*.

4.4.3 Quality of the GEM iANEO_SB607

The quality of the iANEO_SB607 model was evaluated using the SBML validator [298] and the test suite Memote [299]. Additionally, we have run a FROG analysis to verify the reproducibility of the model. The GEM was correctly defined in SBML format, level 3, version 1. The GEM obtained an overall Memote score of 72 %. All metabolites, reactions and genes were fully annotated. The annotation per database of reactions and metabolites scored 83 %, however the annotation per database of

genes scored a much lower value, 33 %. Reactions are mass and charge balanced, except for reactions associated to the synthesis of biomass precursors. The model does not have infeasible cycles and all metabolites are connected. However, the model is only partly consistent (55 % scoring); this is due to the creation of metabolites to account for biomass precursors. These metabolites (e.g., RNA) lack a defined formula or a correct charge and, thus, their associated reactions are considered stoichiometrically inconsistent, decreasing the global consistency score. Memote identifies 102 metabolites that can only be consumed or produced, resulting in 422 blocked reactions in the model under the restrictive constraints. When the model does not have constraints, FVA analysis finds 354 blocked reactions, which is in line with the average % of blocked reactions in GEMs (20-40%) [300].

4.4.4 Qualitative assessment of iANEO_SB607 through analysis of growth phenotypes

The iANEO_SB607 model was qualitatively validated by assessing growth of *A. neopropionicum* on several carbon sources and contrasting the results with experimental data. Model predictions matched most of the growth phenotypes observed in cultivation experiments from this and previous studies (Table 4.2; full data is available in the git repository and Additional file 1, Table S4.2).

The model predicts growth of *A. neopropionicum* on ethanol. Growth on xylose and on glucose is also predicted by the model and supported by experimental evidence, with exception of one study, which reported no growth of *A. neopropionicum* on glucose [263]. According to a previous work, *A. neopropionicum* can also grow on D-lactate, but not on L-lactate [271]. In our batch cultivations with DL-lactate as substrate, we repeatedly observed that only ≈ 50 % of the substrate was used. The purity of the L- enantiomer in the racemic mixture solution was, according to the manufacturer, 27 - 33 %. This indicates that D-lactate is indeed used by *A. neopropionicum*, but it does not exclude the possibility that L-lactate is also metabolised. Yet, since the latter could not be confirmed, the model considers only the utilisation of D-lactate. The model predicts growth on pyruvate as well as on one pyruvate-derived amino acid, alanine. Serine also supports growth of *A. neopropionicum*, as predicted by the model and observed in cultivation experiments. The model indicates that branched-chain amino acids (valine, leucine and isoleucine) as well as TCA-derived amino acids (lysine and proline), with exception of threonine, are not utilised.

Further model validation was performed by assessing the product profile on a number of substrates from which sufficient experimental data was available, specifically: ethanol, lactate, glucose, xylose, L-threonine, L-serine, L-alanine, ethanol plus acetate, ethanol plus L-serine and ethanol plus L-alanine. For all the substrates tested, the model predicted mixed secretion of propionate and acetate, in accor-

Table 4.2: Growth phenotypes of *A. neopropionicum* on different substrates, predicted by the iANEO_SB607 model and observed in experiments from this and previous studies. +, Positive; -, negative; w, weakly positive; ND, no available data.

Substrates	iANEO_SB607	This study (exp.)	[271]	[263]	[269]
Ethanol	+	+	+	+	+
Ethanol & Acetate	+	+	+	ND	ND
Ethanol & Alanine	+ ^a	ND	ND	ND	+
Ethanol & Serine	+ ^b	ND	ND	ND	+
Pyruvate	+	ND	+	+	ND
D-Lactate	+	+	+	w ^c	ND
D-Glucose	+	+	+	-	ND
Xylose	+	+	+	+	ND
L-Threonine	+	ND	+	+	ND
L-serine	+	ND	+	+	ND
L-Alanine	+	ND	+	+	ND
D-Alanine	+	ND	+	ND	ND
L-Valine	-	ND	-	w	ND
L-Leucine	-	ND	ND	w	ND
L-Isoleucine	-	ND	ND	w	ND
Lysine	-	ND	-	ND	ND
L-Proline	-	ND	-	-	ND

^aL-Alanine

^bL-Serine

^c(L-D)-Lactate

dance with experimental evidence (Fig. 4.2; full data is available in the git repository and Additional file 1, Table S4.2). Model analysis shows that secretion of product mixture is a requisite for energy generation and redox cofactor regeneration. The involved pathways and their stoichiometry are described in following sections.

Butyrate, propanol, lactate, isobutyrate and isovalerate are also predicted by the model as fermentation products in all cases, albeit in different proportions. Butyrate appears as a minor product in all the simulations and cultivation experiments, except for in the fermentation of L-threonine; in this case, the model predicts butyrate as a major end product, as previously reported [263]. According to model simulations and in agreement with our experimental data, lactate, an intermediate of the acrylate pathway, and propanol are produced in minor amounts. In batch cultivations carried out in this study, isobutyrate and isovalerate were detected as traces



Figure 4.2: Product profile of the fermentation of different substrates by *A. neopropionicum*, predicted by the GEM iANEO_SB607 and observed in experiments from this and previous studies. P: Propionate; A: acetate; B: butyrate; Poh: propanol; L: lactate; iB: isobutyrate and iV: isovalerate. White spaces indicate the product is not reported produced. Grey areas indicate no available data.

with ethanol (plus acetate), glucose or xylose as substrates, but not with lactate. The model predicted both products to be produced as traces with these substrates. Model simulations predicted enhanced production of isobutyrate and isovalerate with ethanol plus L-valine and ethanol plus L-leucine as substrates, respectively (not shown), as observed in one study [263]. The model also predicted the production of isovalerate when L-alanine or L-serine are co-substrates with ethanol, which is in agreement with observations from a recent work [269].

H₂ was not detected as product in any of the fermentations of *A. neopropionicum* carried out in this study (with substrates: ethanol (plus acetate), lactate, glucose, xylose). In addition, H₂ was not utilised nor affected the growth or the product profile of *A. neopropionicum* cultures growing on ethanol (Additional file 1, Fig. S4.3). Previous works reported the same observations [271, 301]. A ferredoxin hydrogenase is annotated in the genome of *A. neopropionicum* (CLNEO_18070; EC 1.12.7.2; model id: 'rxn05759_c0'); yet, given the collected evidence, this reaction was blocked in the model.

4.4.5 Quantitative assessment of iANEO_SB607 through dFBA

The iANEO_SB607 model of *A. neopropionicum* was evaluated quantitatively by simulating the dynamics of batch fermentation using dFBA. Three conditions were considered, with regard to the substrates present: 25 mM ethanol, 25 mM ethanol plus 10 mM acetate, and 25 mM ethanol plus 25 mM acetate. To constrain the model, we used empirical data of ethanol consumption, product formation and cell growth from cultivation experiments. The fermentation profiles obtained by dFBA were contrasted with the experimental data of batch incubations. Across cultivations, car-

bon balance was 85 - 96 %, not completely closed likely due to the difficulty to accurately quantify CO₂ and to slight evaporation of ethanol in the bottles, as reported by others [302].

For the condition with only ethanol (and CO₂) as substrate, the time-course data obtained through dFBA accurately reproduced the fermentation profile, with only small deviations (Fig. 4.3). Exponential growth of *A. neopropionicum* began after a relatively short lag phase of ≈ 13 hours. During the exponential phase, ethanol was uptaken (together with CO₂; not shown) at an empirical maximum consumption rate ($q_{S,max}$) of 36.2 ± 5.5 mmol ethanol $g_{DW}^{-1} h^{-1}$. Modeled ethanol consumption fitted the experimental data with a small margin of error. Propionate and acetate were produced simultaneously during the exponential phase, at empirical maximum production rates ($q_{P,max}$ and $q_{A,max}$) of 12.0 ± 0.1 mmol propionate $g_{DW}^{-1} h^{-1}$ and 8.6 ± 0.5 mmol acetate $g_{DW}^{-1} h^{-1}$, respectively. The production profile of propionate was well predicted by dFBA, estimating a final propionate concentration (10.9 mM) close to the experimental value (9.5 mM). However, dFBA predicted a final concentration of acetate (11.5 mM) moderately higher than experimentally observed (8.6 mM). The empirical maximum specific growth rate of *A. neopropionicum* (μ_{max}) was $0.082 \pm 0.006 h^{-1}$ (duplication time = 8.4 h), which was used to constrain the model. In incubations, the biomass concentration peaked ($44.7 \pm 1.3 mg_{DW} L^{-1}$) at ≈ 47 hours, and decreased afterwards. The simulation predicted a slightly deviated pattern of biomass formation during the exponential phase, and it did not predict the observed drop in the stationary phase. Yet, the predicted maximum biomass concentration ($44 mg_{DW} L^{-1}$) matched the empirical value. Propanol (1.3 mM) and butyrate (1 mM) were detected as minor products in batch incubations; the evolution of both products was predicted correctly by the dFBA simulations. Traces of isobutyrate and isovalerate were also detected and predicted by dFBA (not shown).

To further evaluate the ability of *A. neopropionicum* to upgrade dilute ethanol streams from syngas fermentation, we considered a scenario with ethanol and acetate as co-substrates. Acetate is produced by acetogens as a major product of autotrophic metabolism, and it is therefore found in variable proportions in syngas fermentation effluent. *A. neopropionicum* can utilise acetate in the presence of propanol [264] or ethanol [271] as electron donors. To investigate the effect of acetate as co-substrate on ethanol-fermenting cultures of *A. neopropionicum*, incubations were set up with ethanol (25 mM) and acetate (10 and 25 mM) as substrates, and dFBA was used to simulate the dynamics of these fermentations. dFBA reproduced with high accuracy the fermentation profile of incubations containing ethanol plus 10 mM acetate (Fig. 4.4). In this condition, the observed μ_{max} was $0.098 \pm 0.005 h^{-1}$ (duplication time = 7.1 h); 19 % higher than in the incubations without acetate. However, less biomass was formed in comparison; the maximum biomass concentration was $41.1 \pm 0.8 mg_{DW} L^{-1}$ ($\approx 9\%$ lower), which was also predicted by dFBA. The presence

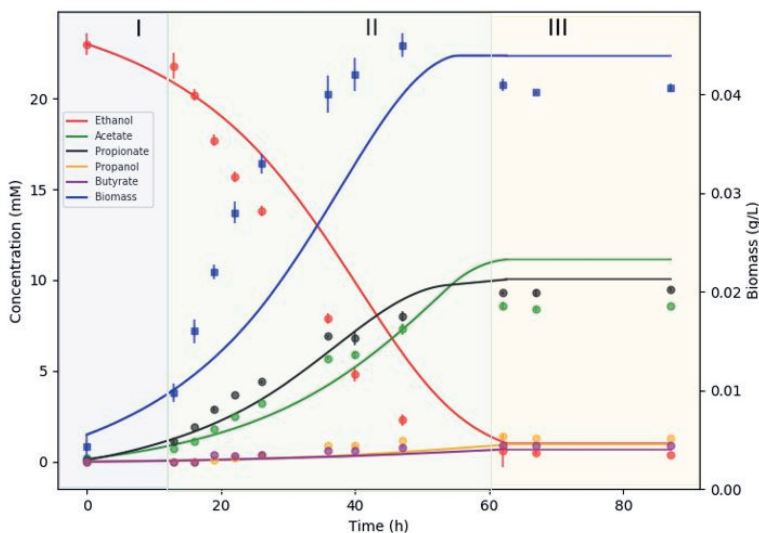


Figure 4.3: Fermentation of ethanol (25 mM) by *A. neopropionicum* in batch cultivation. Dots indicate experimental data and solid lines indicate the result of dFBA. Background colours distinguish fermentation phases: lag (blue), exponential (green) and stationary (orange).

of 10 mM acetate also affected the consumption and production rates; ethanol consumption was faster than in the absence of acetate; the $q_{S,max}$ was 43.3 ± 4.3 mmol ethanol $g_{DW}^{-1} h^{-1}$, a 20 % increase. The $q_{A,max}$ in this condition dropped to 3.1 ± 0.6 mmol acetate $g_{DW}^{-1} h^{-1}$. The biggest difference was in the $q_{P,max}$, which was 16.4 ± 0.8 mmol propionate $g_{DW}^{-1} h^{-1}$, a 37 % increase compared to the condition without acetate. The final propionate concentration was also slightly higher, 11.3 mM (vs. 9.5 mM). Here, again, the simulation predicted a similar propionate concentration to the observed value (12.2 mM), and a higher final acetate concentration (18.3 mM) than observed (16.7 mM). The incubations containing 25 mM acetate at the start followed a different trend than the incubations with 10 mM acetate (fermentation profile not shown). In batch bottles, the biomass concentration reached a similar value to that obtained in the condition with 10 mM acetate, but the μ_{max} , $q_{P,max}$ and $q_{A,max}$ were similar to the condition without acetate (data not shown). The final propionate concentration was 12.5 mM, the highest of the three conditions tested.

The presence of acetate had an effect on the utilisation of ethanol by *A. neopropionicum*, which is reflected in the fermentation yields. The biomass yield ($Y_{X/S}$) was

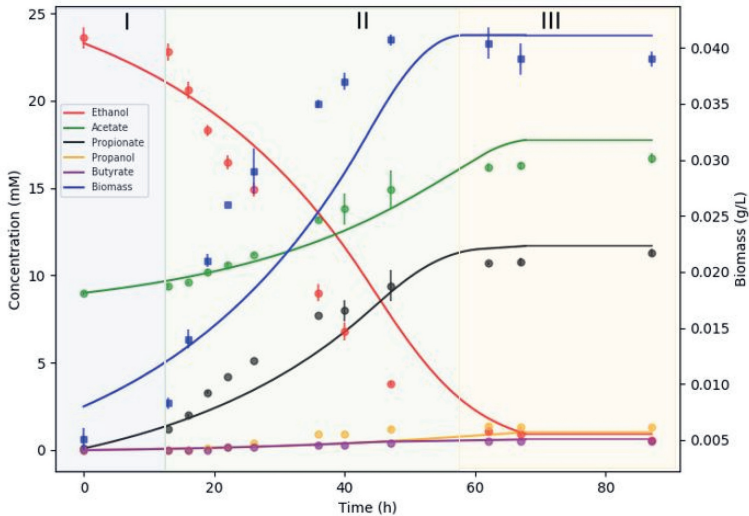


Figure 4.4: Fermentation of ethanol (25 mM) and acetate (10 mM) by *A. neopropionicum* in batch cultivation. Dots indicate experimental data and solid lines indicate the result of dFBA. Background colours distinguish fermentation phases: lag (blue), exponential (green) and stationary (orange).

slightly lower in the presence of both 10 and 25 mM acetate ($1.4 \text{ g}_{\text{DW}} \text{ mol ethanol}^{-1}$ vs. $1.6 \text{ g}_{\text{DW}} \text{ mol ethanol}^{-1}$ when no acetate was present). With acetate present at the start of incubations, more ethanol was invested in propionate production, as indicated by the propionate yields ($Y_{\text{P/S}}$, mol mol^{-1}), which were 0.33, 0.38 and 0.42 for the conditions with no acetate, 10 mM acetate and 25 mM acetate, respectively. The production of acetate followed the inverse trend; acetate yields ($Y_{\text{A/S}}$, mol mol^{-1}) were 0.29, 0.18 and 0.06 for the conditions with no acetate, 10 mM acetate and 25 mM acetate, respectively. Similarly, lower yields were obtained for propanol and butyrate when acetate was present (data now shown).

4.4.6 Ethanol fermentation via the acrylate pathway

The reconstructed iANEO_SB607 model describes the metabolism of ethanol fermentation and propionate production via the acrylate pathway in *A. neopropionicum* (Fig. 4.5). Model simulations provided new insights into the enzymatic reactions involved in propionate formation, cofactor regeneration and the energy metabolism

of the cell.

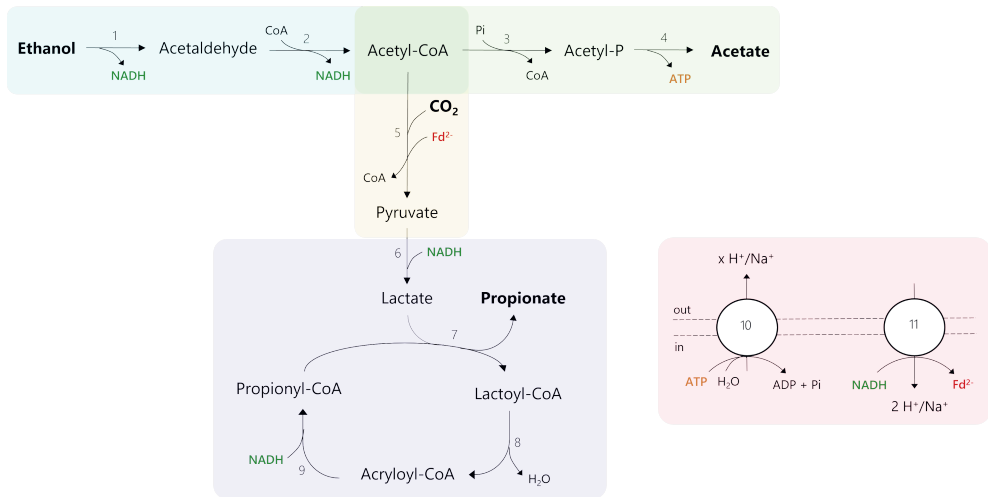


Figure 4.5: Proposed metabolism of ethanol fermentation to propionate via the acrylate pathway in *A. neopropionicum*. Coloured areas designate the following modules: ethanol oxidation (blue), acetate production (green), pyruvate synthesis (yellow), lactate production and acrylate pathway (purple), redox cofactor regeneration and ATPase (red). Numbers in reactions correspond to the following enzymes and reaction ids in the model: 1,2, aldehyde-alcohol dehydrogenase (rxn00543_c0 and rxn00171_c0); 3, phosphate acetyltransferase (rxn00173_c0); 4, acetate kinase (rxn00225_c0); 5, pyruvate:ferredoxin oxidoreductase (PFOR; rxn05938_c0); 6, NAD-dependent D-lactate dehydrogenase (rxn00500_c0); 7, propionate-CoA:lactoyl-CoA transferase (rxn01056_c0); 8, lactoyl-CoA dehydratase (rxn02123_c0); 9, acryloyl-CoA reductase (rxn40050_c0); 10, ATPase (rxn10042_c0); 11, Rnf complex (Rnf_c0).

Ethanol is oxidised to acetyl-CoA via acetaldehyde through alcohol and acetaldehyde dehydrogenases. The genome of *A. neopropionicum* harbours a bifunctional NAD⁺-dependent alcohol-aldehyde dehydrogenase (AdhE; CLNEO_13930) that can catalyse this two-step conversion. According to our model, two other alcohol dehydrogenases, encoded by *adh* (CLNEO_16910) and *adhB* (CLNEO_00480), could also drive the oxidation of ethanol to acetaldehyde. Initially, the model also predicted this reaction to be catalysed by NAD(P)H-dependent butanol dehydrogenase (BdhA), encoded by *bdhA* (CLNEO_09740; rxn00536_c0). However, the well-characterised BdhA of *C. acetobutylicum*, which shares 60.7 % identity with that of *A. neopropionicum*, is known to contribute primarily to butanol production and it is the alcohol dehydrogenase least involved in ethanol metabolism [303]. Thus, we

reasoned that BdhA would likely not be involved in ethanol oxidation in *A. neopropionicum* and excluded this reaction from model simulations.

Acetyl-CoA is partly used in the reductive reactions of the metabolism and partly invested in the formation of acetate, an energy-generating step. Acetate is synthesised via phosphate acetyltransferase (Pta; CLNEO_28570) and acetate kinase (Ack; CLNEO_28580), yielding ATP via substrate-level phosphorylation (SLP). In the reductive path, acetyl-CoA is converted to pyruvate through the CO₂-fixating reaction catalysed by pyruvate:ferredoxin oxidoreductase (PFOR; CLNEO_15240 or CLNEO_19010 or CLNEO_17780 or CLNEO_03040 or CLNEO_04330 or CLNEO_24550). This conversion requires reduced ferredoxin (Fd²⁻) as electron carrier. Our hypothesis, supported by model predictions, is that Fd²⁻ is produced in the Na⁺-translocating ferredoxin:NAD⁺ oxidoreductase (Rnf) complex. The Rnf complex is a membrane-bound respiratory enzyme involved in energy conservation in anaerobic microorganisms [304]. During growth on high-energy substrates, it catalyses the exergonic reduction of NAD⁺ with electrons from Fd²⁻ coupled to the translocation of two cations (H⁺ or Na⁺) across the membrane. The electrochemical potential established by the Rnf complex can then be used by a membrane-bound ATP synthase for energy generation. The Rnf complex can also operate in the reverse direction to produce Fd²⁻ at the expense of ATP [305]. The genome of *A. neopropionicum* harbours a complete *rnf* cluster, composed of the genes *rnfA* (CLNEO_01390), *rnfB* (CLNEO_01400), *rnfC* (CLNEO_01350), *rnfD* (CLNEO_01360), *rnfE* (CLNEO_01380) and *rnfG* (CLNEO_01370). With ethanol as substrate, our assumption is that the Rnf complex of *A. neopropionicum* operates in reverse, generating Fd²⁻. The endergonic reduction of ferredoxin (E_o' = - 500 to - 420 mV) with NADH (E_o' = - 320 mV) is driven by reverse electron transport across the membrane which, in turn, is an energy-driven process. A membrane-bound V-type ATPase is present in the genome of *A. neopropionicum*, encoded by the genes *atpA/ntpA* (CLNEO_280), *atpB/ntpB* (CLNEO_290), *ntpC*, (CLNEO_260), *atpD/ntpD* (CLNEO_23400), *atpE* (CLNEO_250), *ntpG* (CLNEO_270), *ntpK* (CLNEO_240) and *ntpI* (CLNEO_23330). We theorise that ATP is hydrolysed in the ATPase to create a proton- or sodium-motive-force that is used by the Rnf complex to catalyse the reduction of ferredoxin. The production of Fd²⁻ is an energy costly process, the implications of which are addressed later in this section.

Pyruvate produced by the PFOR is subsequently reduced to lactate with NADH via D-lactate dehydrogenase (CLNEO_28010). We assumed NADPH is not used as electron carrier in this reaction, since lactate dehydrogenases have a strict specificity for NAD⁺/NADH [306, 307]. Lactate then enters the acrylate pathway, a cyclic chain of reactions involving the intermediates lactoyl-CoA, acryloyl-CoA and propionyl-CoA. The characteristic enzyme of this pathway is propionate-CoA:lactoyl-CoA transferase (Pct, EC 2.8.3.1), which exchanges the CoA moiety between propionyl-CoA

and lactate, generating lactoyl-CoA and propionate as end product [308, 309]. Our first annotation of the genome of *A. neopropionicum* did not include Pct. However, an acetate CoA-transferase was present, encoded by the gene *ydiF* (CLNEO_17700), that shared 96 % identity with the purified and well characterised Pct of *A. propionicum* [309]. Thus, we deduced that *ydiF* encodes for Pct in *A. neopropionicum* and included this reaction in the model. Lactoyl-CoA dehydratase (CLNEO_17710 and CLNEO_17720) catalyses the dehydration of lactoyl-CoA to acryloyl-CoA, which is subsequently reduced to propionyl-CoA by acryloyl-CoA reductase. Our genome annotation revealed that the acryloyl reductase of *A. neopropionicum* forms an enzymatic complex with an electron-transferring flavoprotein (EtfAB). The complex, hereafter named acryloyl-CoA reductase-EtfAB (Acr-EtfAB), is also present and has been well characterised in *A. propionicum* [310]. Three gene clusters predicted to encode for acryloyl-CoA reductase (*acrC*) or EtfAB (*acrA,acrB*) were found in the genome: (i) CLNEO_21740 (*acrC*), CLNEO_21750 (*acrB_1*) and CLNEO_21760 (*acrA*); (ii) CLNEO_26130 (*acdA_1*) and CLNEO_26120 (*acrB_2*); and (iii) CLNEO_29850 (*acdA_2*) and CLNEO_29840 (*acrB_3*). The *acdA_1* and *acdA_2* genes encode for acyl-CoA dehydrogenases that share low identity (46 and 54 %, respectively) with the acryloyl-CoA reductase encoded by *acrC*; thus, we assumed that the former two enzymes are not responsible for acryloyl-CoA reductase activity. The first cluster is the only complete one, composed of acryloyl-CoA reductase (*acrC*) and the A (*acrA*) and B (*acrB_1*) subunits of EtfAB. The proteins encoded by these three genes share an identity of 92.9 %, 89.7 % and 89.1 %, respectively, with their homologues from the Acr-EtfAB complex of *A. propionicum*. The Acr-EtfAB of *A. propionicum* is a non-bifurcating soluble enzyme that catalyses the irreversible reduction of acryloyl-CoA to propionyl-CoA with NADH via electron transfer to a flavin moiety and appears not to be involved in energy conservation [310, 311]. Given their high similarity, we deduced the same features apply to the Acr-EtfAB of *A. neopropionicum*. To our knowledge, this is the first time that the Acr-EtfAB complex is identified in this microorganism.

According to the theoretical stoichiometry, the fermentation of ethanol yields propionate and acetate in a 2:1 ratio (Eq. 4.1). However, this ratio is not observed in cultures of *A. neopropionicum*; rather, ethanol fermentation resulted in a $\approx 1.2:1$ propionate to acetate ratio (Fig. 4.3 and Additional file 1, Table S4.2). We reasoned that the theoretical ratio cannot be achieved in *A. neopropionicum* due to energetic constraints of the cell, specifically, due to the requirement of Fd^{2-} . Model simulations were performed to confirm this. The oxidation of three moles of ethanol generates six moles of NADH and three moles of acetyl-CoA. To fit the theoretical 2:1 propionate to acetate ratio, two moles of acetyl-CoA would have to be used in the reductive part of the metabolism, and one mole of acetyl-CoA should be invested in acetate, with the concomitant production of one mole of ATP (via SLP).

The synthesis of two moles of pyruvate from acetyl-CoA would require two moles of Fd^{2-} , which is produced at the RnF complex at the expense of ATP. However, the hydrolysis of one mole of ATP ($\Delta G^o = -32 \text{ kJ mol}^{-1}$; [312]) could drive the reduction with NADH of no more than ≈ 1.3 moles of ferredoxin ($\Delta G^o = -25 \text{ kJ mol}^{-1}$; [313]). Moreover, two other issues arise: i) even if this one mole of ATP would solely be invested in the reduction of ferredoxin, this would leave no net ATP for growth, and ii) such a scenario would result in excess reducing equivalents from ethanol oxidation that could not be recycled in the production of propionate. Our model predictions confirmed this inconsistencies and are in agreement with the hypothesis that the propionate to acetate 2:1 ratio cannot be achieved in *A. neopropionicum* during the fermentation of ethanol. Instead, cells must invest more than one mole of acetyl-CoA in acetate production to obtain net ATP to support growth. This leaves less than two moles of acetyl-CoA available for propionate production and, overall, a propionate to acetate ratio lower than the theoretical 2:1. The actual propionate to acetate ratio (close to 1.2:1, based on the fermentation balance) depends on how much Fd^{2-} can be produced per hydrolysed ATP, which in turn depends not only on the Gibbs free energies of ATP hydrolysis and ferredoxin reduction with NADH under physiological conditions but also on the coupling ratio of the ATPase (number of cations translocated per ATP hydrolysed). While the Rnf complex can be assumed to translocate two cations per ferredoxin reduced/oxidised, the coupling ratio of the ATPase remains unknown for *A. neopropionicum*. Our model fitted with a coupling ratio of the ATPase of 3 to 3.5 H^+/Na^+ translocated per ATP.

4.4.7 Propanol and butyrate production pathways

A. neopropionicum produces propanol and butyrate as minor products of the fermentation of several substrates (Fig. 4.2). Propanol is formed from propionyl-CoA via propionaldehyde in a two-step reductive conversion catalysed by AdhE (Fig. 4.6). Reduction of propionaldehyde could also be catalysed by NAD^+ -dependent alcohol dehydrogenases *adh* (CLNEO_16910) and *adhB* (CLNEO_00480).

Butyrate production in *A. neopropionicum* takes place via the acetyl-CoA pathway (Fig. 4.6). In this pathway, acetyl-CoA is first converted to butyryl-CoA, which eventually yields butyrate. Most enzymes of the pathway were either present in the genome, were assigned during the re-annotation or were identified through protein sequence alignment. Only one enzyme was not found: acetoacetyl-CoA thiolase (EC 2.3.1.9), which catalyses the condensation of two molecules of acetyl-CoA to form acetoacetyl-CoA. However, since the rest of genes of the pathway were identified (see Additional file 2), we added this reaction to the model during the gap-filling process. A key enzyme of this pathway is the butyryl-CoA dehydrogenase/electron-transferring flavoprotein complex (Bcd-EtfAB). Bcd-EtfAB is an electron-bifurcating

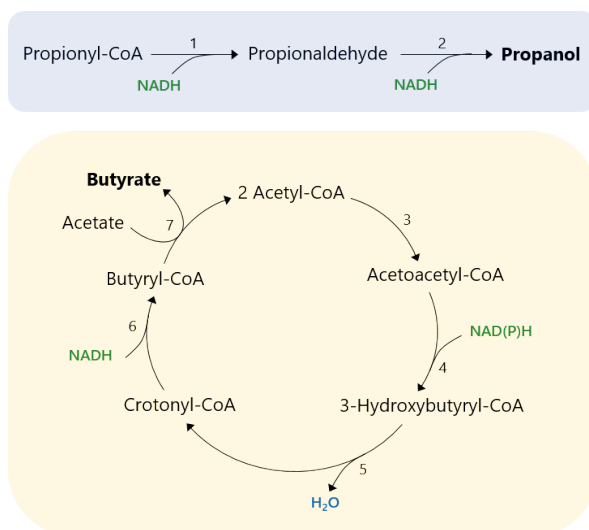


Figure 4.6: Putative pathways for the production of propanol (blue) and butyrate (orange) in *A. neopropionicum*. Numbers in reactions correspond to the following enzymes as annotated in the genome, and reaction ids in the model: 1 and 2, aldehyde-alcohol dehydrogenase (rxn09944_c0 and rxn01710_c0); 3, acetoacetyl-CoA thiolase (rxn00178_c0); 4, 3-oxoacyl reductase (rxn03861_c0); 5, 3-hydroxyacyl dehydratase (rxn03874_c0); 6, acryloyl-CoA reductase-EtfAB (rxn00868_c0) or acyl-CoA dehydrogenase-EtfAB; 7, propionate-CoA:lactoyl-CoA transferase (rxn00875_c0).

enzyme that couples the reduction of crotonyl-CoA to butyryl-CoA ($E_0' = -10$ mV) by NADH to the endergonic reduction of Fd by NADH [304]. Our model predicts that, in *A. neopropionicum*, reduction of crotonyl-CoA could be catalysed by the Acr-EtfAB complex or by either of the two acyl-CoA dehydrogenases that cluster with subunits of the EtfAB complex (*acdA_1-acrB_2* and *acdA_2-acrB_3*). Among the three, the acyl-CoA dehydrogenase encoded by *acdA_2* showed the highest identity with the butyryl-CoA dehydrogenases (Bcd) of *C. acetobutylicum* and of *C. kluyveri* (64 and 63 %, respectively). It remains a question whether, in *A. neopropionicum*, the latter two complexes could be involved in the reduction of ferredoxin.

Two distinct routes have been described for the last step of the pathway, the conversion of butyryl-CoA to butyrate. The first route, identified in *C. acetobutylicum* [314], involves phosphate butyryltransferase (Ptb; EC 2.3.1.19) and butyrate kinase (Buk; EC 2.7.2.7) and yields ATP via SLP. The second route relies on butyryl-CoA:acetate CoA-transferase (But; EC 2.8.3.8). Co-occurrence of both pathways is

rare among butyrate producers [315]. The genome of *A. neopropionicum* does not encode for Ptb nor Buk, yet our annotation initially assigned these activities to phosphate acetyltransferase (Pta) and acetate kinase (Ack). The Ack of *A. neopropionicum* is significantly similar to the well-characterised Buk (71 % identity) of *C. acetobutylicum*. We have considered this similarity to arise from the fact that the two enzymes belong to the same family, yet it has been established that they do not have the same function, since differences in the substrate binding site ultimately determine substrate specificity [316–318]. Thus, we assumed that Pta and Ack are not involved in butyrate production in *A. neopropionicum*. Instead, we hypothesise that butyrate production in *A. neopropionicum* takes place via butyryl-CoA:acetate CoA-transferase activity. Our model predicts that the propionate-CoA:lactoyl-CoA transferase (Pct) encoded by the gene *ydiF* catalyses this reaction. The Pct of *A. propionicum* exhibits broad substrate specificity for monocarboxylic acids, including butyrate, supporting the model prediction [309].

4.4.8 Identification of the NADH-dependent reduced ferredoxin: NADP⁺ oxidoreductase (Nfn)

During the genome re-annotation and manual curation process, we identified the enzyme NADH-dependent reduced ferredoxin:NADP⁺ oxidoreductase (Nfn). Nfn is an iron-sulfur flavoprotein complex with electron-confurcating/bifurcating activity that reversibly catalyses the endergonic reduction of NADP⁺ by NADH coupled with the exergonic reduction of NADP⁺ by Fd²⁻ [319]. Nfn is composed of two subunits, NfnA and NfnB, whose coding genes were both found in the genome of *A. neopropionicum* under the locus tags CLNEO_00270 and CLNEO_00280, respectively. In the initial automatic annotation, these two genes were assigned to ferredoxin:NADP⁺ oxidoreductase and glutamate synthase, respectively. It has been reported that NfnA/B share sequence similarities with these two enzymes [319]. Upon manual inspection, we observed that the protein complex showed a significant identity (60 - 66 %) with the Nfn complexes of *C. kluyveri* [320] and of *C. autoethanogenum* [321], which lead us to the re-assignment of the two proteins as NfnA and NfnB.

We used modelling to look into the role of the Nfn complex in the metabolism of *A. neopropionicum* during growth on ethanol. The model shows that the Nfn generates NADPH from NADH and Fd²⁻ for NADPH-dependent reactions of the cell. For instance, NADPH is required during butyrate production in the reduction of acetoacetyl-CoA to 3-hydroxybutyryl-CoA, a reaction catalysed by a NADPH-dependent 3-oxoacyl reductase. NADPH is also required in the biosynthesis of amino acids and biomass precursors. In our model, the Nfn complex does not function in the reverse direction, the production of Fd²⁻, during growth on ethanol; this

would require NADPH, and ethanol oxidation is assumed to occur only via NAD⁺-dependent reactions.

4.4.9 Fermentation of other carbon sources: the case of lactate

Besides ethanol, *A. neopropionicum* can grow on lactate, sugars and some pyruvate-derived amino acids (Table 4.2). The fermentation of these carbon sources proceeds with key differences compared to the fermentation of ethanol. To illustrate this with an example, we used the model to describe the case of lactate fermentation, since lactate is a typical substrate of propionate-producing bacteria and, in particular, of species that use the acrylate pathway [270, 308].

Lactate is metabolised in both oxidative and reductive reactions. In the oxidative branch, lactate is oxidised to pyruvate via lactate dehydrogenase, generating NADH. PFOR then catalyses the decarboxylation of pyruvate to acetyl-CoA and CO₂, a reaction that generates Fd²⁻. The PFOR reaction is reversible; here, it functions in the opposite direction to what occurs with ethanol as substrate. This enables the utilisation of lactate, sugars and pyruvate-derived amino acids. This implies that, contrary to the fermentation of ethanol, the oxidation of these substrates generates directly Fd²⁻, which can contribute to energy conservation. Acetyl-CoA is used for acetate production via Pta and Ack, yielding ATP via SLP. In the reductive branch, lactate is converted to propionate via the reactions of the acrylate pathway. In this conversion, NADH is needed for the reduction of acryloyl-CoA to propionyl-CoA, but the amount of NADH obtained in the oxidation of lactate is insufficient. Our model predicts that additional NADH is produced in the Rnf complex. Opposite to the scenario with ethanol as substrate, here the Rnf catalyses the exergonic reduction of NAD⁺ with electrons from Fd²⁻. This reaction is coupled to the translocation of two cations across the membrane, generating an ion-motive force that can be used by the ATPase to produce ATP. Thus, in the fermentation of carbon sources other than ethanol, ATP is generated both by SLP via acetate production and by chemiosmosis driven by the oxidation of Fd²⁻.

4.5 Discussion

In this study we have presented iANEO_SB607, the first GEM of the propionate-producer *A. neopropionicum*. The overall Memote score of 72 % indicates the high quality of the model. The low score of gene annotation per database (33 %) was expected, since there were almost no available annotations of the genome of *A. neopropionicum* in public databases recognised by Memote. A limitation of the GEM is the lack of an organism-specific biomass composition and GAM/NGAM measurements.

Our sensitivity analysis showed a maximum deviation of 10.8 % of the growth rate when varying the composition of biomass components or the GAM. NGAM has a more limited impact on growth rate predictions, given that it does not directly relate to the biomass synthesis reaction, still dedicated measurements of these parameters could further improve the predictive power of the model. Here, our focus has been on gaining insight into the metabolism of ethanol fermentation to propionate, which in this bacterium occurs via the acrylate pathway.

We have also addressed an important issue regarding the energetic metabolism of *A. neopropionicum*. During growth on ethanol, Fd^{2-} is required to reduce acetyl-CoA to pyruvate. In the earliest description of the metabolism of *A. neopropionicum*, authors suggested that the oxidation of acetaldehyde proceeded with ferredoxin as electron carrier, thus fulfilling this demand [271]. However, at the present time it is acknowledged that aldehyde dehydrogenases are NAD(P)-dependent enzymes [322], which invalidates that theory. Theoretically, the Acr-EtfAB complex could drive the reduction of Fd ($E_o' = -500$ to -420 mV) with NADH ($E_o' = -320$ mV) via electron bifurcation, given the high reduction potential of the acryloyl-CoA/propionyl-CoA pair ($E_o' = +70$ mV). Yet, this complex appears not to be involved in the reduction of ferredoxin [310], most likely to prevent transient accumulation of the very reactive intermediate acryloyl-CoA [323, 324]. Instead, our model predicted that Fd^{2-} is produced in the Rnf complex, as previously reported for other anaerobes during growth on low-energy substrates [305]. The Rnf complex had been previously present in the close relative *A. propionicum* [278]. Here, through the re-annotation and a thorough manual curation process, we identified all its subunits (*rnfA-E*, *rnfG*) and via modelling we verified its involvement in the metabolism of the cell.

Our annotation of the genome of *A. neopropionicum* revealed the presence of another key enzyme of the metabolism of anaerobes: the Nfn complex. Our model showed that the Nfn generates NADPH for NADPH-dependent reactions of the metabolism, which is essential during growth on ethanol. Further investigation is needed to define the instances in which the Nfn operates in the reverse direction, bifurcating electrons from NADPH to produce Fd^{2-} and NADH. The directionality and role of Nfn will depend on the cofactor requirements of the cell.

Butyrate and propanol are produced by *A. neopropionicum* as minor products during the fermentation of several substrates (Fig. 4.2), probably as a means to dispose of excess reducing equivalents generated during substrate oxidation. Our model showed that propanol is produced from propionyl-CoA with propionaldehyde as intermediate via NAD^+ -dependent reactions, as Tholozan et al. suggested [271]. The butyrate production pathway had not been described yet in this microorganism and further research is needed to confirm whether Pct is indeed involved in this pathway as observed *in vitro* in *A. propionicum* [309] and *E. coli* K-12 [325].

Another aspect of the metabolism that we aimed to clarify was the ability of *A. neopropionicum* to produce and consume H_2 . In our batch cultivations on different substrates, H_2 was not produced nor consumed, as previously reported [271]. Our results also confirm that neither the product profile nor the growth of ethanol-growing cultures of *A. neopropionicum* are affected by the presence of H_2 (Additional file 1, Figure S3). This is an advantageous trait when considering this strain for its application in syngas-fermenting co-cultures, since syngas contains H_2 . Interestingly, H_2 tolerance is manifested differently in functionally-related strains. While *P. propionicus* and *D. propionicus* both use the methylmalonyl pathway to metabolise ethanol, the first is not affected by the presence of H_2 while the second is strongly inhibited by it [268].

The GEM iANEO_SB607 accurately reproduced observed growth phenotypes on typical substrates (ethanol, sugars, lactate and amino acids). For glucose and xylose, model predictions agree with our batch incubations that *A. neopropionicum* can utilize these sugars (Additional Table S4.2). These analyses solve contradictions in literature most likely attributable to differences in media compositions across studies [263, 265, 271, 326]. Our results also indicate that D-lactate, and not L-lactate, support growth of *A. neopropionicum*, as previously observed [271]. Yet, the latter authors reported lactate dehydrogenase activity in cell-free extracts with D-, L- and DL-lactate, and hypothesised the presence of a lactate racemase which is absent in our annotated genome. However, *A. neopropionicum* has both L- and D-lactate dehydrogenases, so it cannot be excluded that L-lactate is also metabolised, perhaps at a much slower rate [327].

dfBA simulations showed good agreement with the dynamics of ethanol (and ethanol plus acetate) fermentation by *A. neopropionicum* in batch cultivation (Fig. 4.3 and Fig. 4.4). With ethanol as substrate, the theoretical 2:1 molar ratio of propionate to acetate (Eq. 4.1) was not achieved; instead, this ratio was $\approx 1.2:1$ (Fig. 4.3 and Additional file 1, Table S4.2), matching previous observations [263, 271]. The model helped clarify this aspect. During growth on ethanol, ATP is solely produced via SLP. Net ATP generation required to sustain growth and to drive ferredoxin reduction needed by PFOR appear as the main cause of the observed propionate to acetate ratio of 1.2:1. In addition, cells might favour acetate over propionate synthesis to prevent accumulation of acryloyl-CoA [308]. Finally, propanol production at the end of the fermentation, likely to halt further acidification of the environment, also contributes to decrease the propionate to acetate ratio.

Interestingly, we observed that a low acetate concentration (< 25 mM) or low acetate:ethanol ratio (< 1) at the start boosted the growth rate and propionate production rate of *A. neopropionicum* during growth on ethanol. However, despite higher rates, final biomass concentrations in batch cultivations were slightly lower in the presence of acetate (10 or 25 mM). Our model showed increase flux through ac-

etate:CoA ligase (*acs*; EC 6.2.1.1) in the presence of acetate (10 mM). This reaction assimilates acetate consuming ATP, which would explain the lower biomass concentrations observed. Model predictions showed that, in this scenario, more acetyl-CoA is converted to pyruvate through PFOR, which is another energy-consuming step. We also observed a higher flux through butanoyl-CoA:acetate CoA-transferase (catalysed by Pct). Batch cultivation experiments did not show a noticeable increase in butyrate concentration when acetate was present, rather lower. Therefore, we hypothesise that, *in vivo*, most acetate consumed is assimilated via acetate:CoA ligase, as our model predicts, or via reverse direction of PTAr and ACKr, instead of Pct. This deviation to the model is likely due to the fact that biomass synthesis was set as maximization objective in dFBA which would be achieved by a higher flux of acetate towards butyrate instead of assimilating it, saving ATP.

Overall, this work shows the advantages of using a model-driven approach to gain insight into the metabolism of microorganisms. The new findings fill in knowledge gaps and unravel key metabolic features of *A. neopropionicum*. As a result, this study means a step forward to further exploit this species as a cell factory for propionate production in mono-culture or in co-cultivation from sustainable feedstocks, e.g., syngas, as recently stated by Moreira et al. [269]. Additionally, *A. neopropionicum* can act as an intermediate species to extend the range of products from propionate to longer odd-chain carboxylic acids.

4.6 Conclusions

In this study, we have constructed iANEO_SB607, the first GEM of *A. neopropionicum*. Combining experimental data with a manual curation of the annotated genome and a comprehensive network reconstruction, we have gained insight into the central carbon and energetic metabolism of this microorganism. The model predicted the metabolic capabilities of *A. neopropionicum* with high accuracy, which allowed us to investigate with detail the enzymatic routes involved in the fermentation of ethanol to propionate. Our analysis showed that *A. neopropionicum* produces propionate via propionate-CoA:lactoyl-CoA transferase, the characteristic enzyme of the acrylate pathway. Our *in silico* analysis revealed, for the first time in this microorganism, the presence of the electron-bifurcating Nfn complex. This model provides the basis to explore the capabilities of *A. neopropionicum* as microbial platform for the production of propionate from dilute ethanol as substrate. While beyond the scope of this study, the construction of this model signifies a step closer towards the development of multi-species models that describe syngas-fermenting co-cultures comprised of acetogens with ethanol-consuming propionigenic bacteria. Follow-up studies that integrate, e.g., omics analyses with data from steady-state fermentations

should help improve this GEM.

Availability of data and materials

The supplementary information and the data generated during the current study are available in the following repository: https://gitlab.com/wurssb/Modelling/Anaerotignum_neopropionicum.

Author's contributions

SBV and IPO conceived and designed the study, and drafted the manuscript. SBV constructed the model and performed model predictions and data analysis. IPO performed the experiments and data analysis. TV contributed to model construction. MSD and PS conceived, designed and supervised the research. DS and VMdS acquired project funding, conceived and supervised the research. All authors reviewed and edited the study. All authors read and approved the final manuscript.

Acknowledgements

We thank Bart Nijssse for his valuable contribution on the re-annotation of *A.neopropionicum*'s genome. We thank Martijn Diender for the discussions and useful comments on the article, and we finally thank Rik van Rosmalen and Wasin Poncheewin for their contributions on the quantitative analysis.

Competing interests

The authors declare that they have no known competing financial interests or personal relationships that could have influenced the work reported in this paper.

Funding

This work was financially supported by the Netherlands Science Foundation (NWO) under the Programme 'Closed Cycles' (Project nr. ALWGK.2016.029) and the Netherlands Ministry of Education, Culture and Science under the Gravitation Grant nr. 024.002.002.

Additional Files

Additional File 1

Additional file 1 contains additional figures and tables and it is shown here.

Additional File 2

Additional file 2 contains a table of homologous genes found in the acrylate pathway and butyrate production pathway and it can be found in the online publication.

Supplementary information

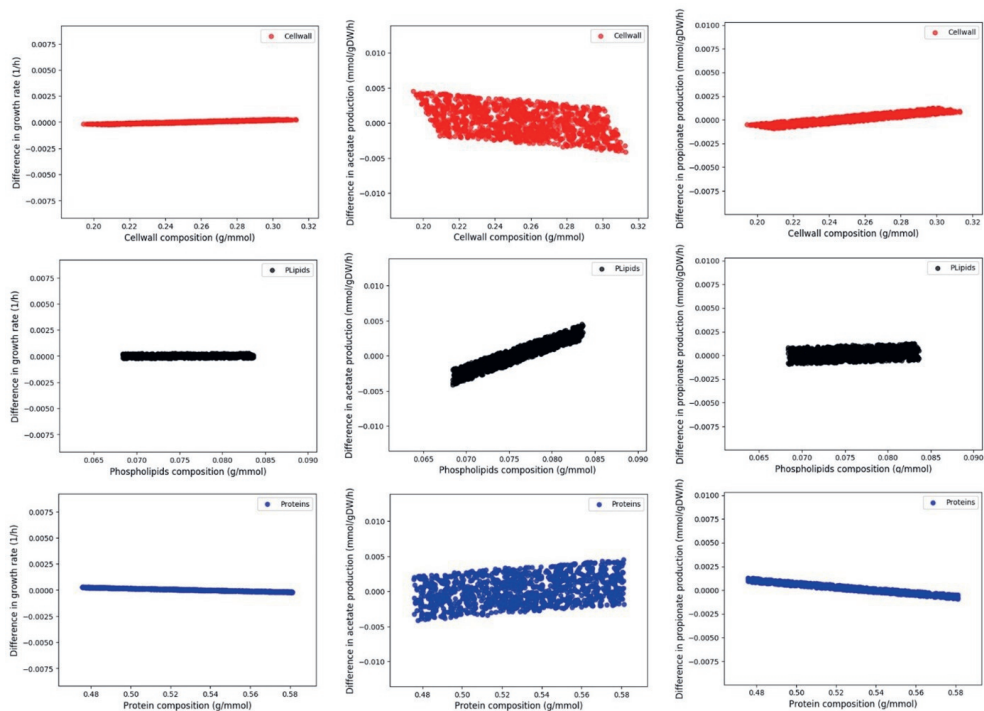


Figure S4.1: Sensitivity analysis of the biomass reaction. Effect of varying the composition of main biomass building blocks on the growth rate and product formation. Growth rate and product formation are represented as the difference between the values obtained when the new biomass reaction is defined as objective function and the values obtained when the original biomass synthesis reaction is defined as objective function.

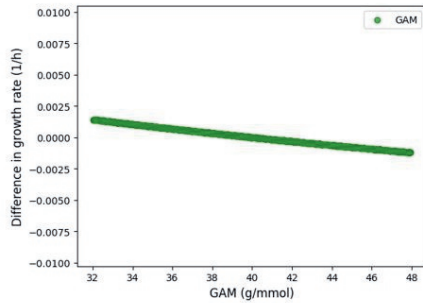


Figure S4.2: Effect of varying the growth-associated maintenance (GAM) of the biomass composition on the growth rate. The effect is represented as the difference between the values obtained when the new biomass reaction is defined as objective function and the values obtained when the original biomass synthesis reaction is defined as objective function.

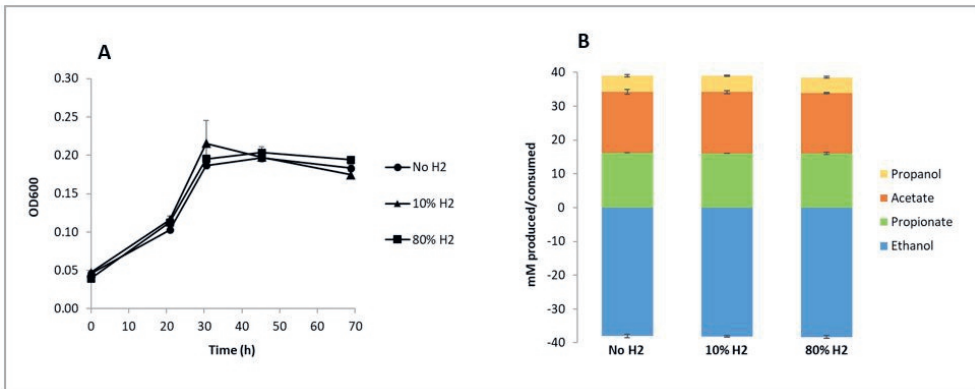


Figure S4.3: Effect of H₂ on ethanol-growing cultures of *Anaerotignum neopropionicum*. A) Cell growth profiles, determined by optical density at 600 nm (OD₆₀₀). B) End products and ethanol consumed at the end of batch fermentations. Error bars indicate the standard deviation of biological triplicates.

Table S4.1: Parameters used to simulate batch fermentations through dFBA. Column ‘Source’ indicates whether the parameter was constrained based on the experimental value (considering standard deviation error) or by model fitting.

Parameter	Symbol	Value	Units	Source
Ethanol fermentation (Fig. 3)				
Initial biomass concentration	X_0	0.0055	g L^{-1}	Exp. Value
Initial Ethanol concentration	$S_{\text{eth},0}$	23	mM	Exp. Value
Initial Acetate concentration	$S_{\text{ac},0}$	0.15	mM	Exp. Value
Initial propionate concentration	$S_{\text{prop},0}$	0.09	mM	Exp. Value
Initial butyrate concentration	$S_{\text{but},0}$	0	mM	Exp. Value
Initial propanol concentration	$S_{\text{ppoh},0}$	0	mM	Exp. Value
Maximum growth rate	μ_{max}	0.082	h^{-1}	Exp. Value
Michaelis-Menten constant for ethanol	$K_{\text{m,etoh}}$	11	mM	Fitting (~ exp. value)
Maximum ethanol uptake	$Q_{\text{etoh,max}}$	36.5	mM	Exp. Value
Ethanol + acetate fermentation (Fig. 4)				
Initial biomass concentration	X_0	0.008	g L^{-1}	Fitting (~ exp. value)
Initial Ethanol concentration	$S_{\text{eth},0}$	23.3	mM	Exp. Value
Initial Acetate concentration	$S_{\text{ac},0}$	9	mM	Exp. Value
Initial propionate concentration	$S_{\text{prop},0}$	0.1	mM	Exp. Value
Initial butyrate concentration	$S_{\text{but},0}$	0	mM	Exp. Value
Initial propanol concentration	$S_{\text{ppoh},0}$	0	mM	Exp. Value
Maximum growth rate	μ_{max}	0.098	h^{-1}	Exp. Value
Michaelis-Menten constant for ethanol	$K_{\text{m,etoh}}$	14	mM	Fitting (~ exp. value)
Maximum ethanol uptake	$Q_{\text{etoh,max}}$	43.6	mM	Exp. Value

Table S4.2: Fermentation balance of batch cultures of *A. neopropionicum* cultivated on different substrates. Note that CO₂, present in the headspace of bottles, is consumed but not included in this table. iBut: isobutyrate; iVal: isovalerate. Traces are concentrations < 0.2 mM. The hyphen symbol indicates undetected products. ND indicates not determined.

Substrate ^a	Substrate consumed (mM)	Products (mM)						
		Propionate	Acetate	Propanol	Butyrate	Lactate	iBut	iVal
Ethanol	22.5 ± 0.6	9.5 ± 0.1	8.6 ± 0.0	1.3 ± 0.0	0.9 ± 0.0	-	traces	traces
Ethanol + Acetate ^b	23.0 ± 0.5	11.3 ± 0.2	16.7 ± 0.3	1.2 ± 0.1	0.5 ± 0.0	-	traces	traces
Ethanol + Acetate ^c	23.0 ± 0.3	12.5 ± 0.2	28.7 ± 0.4	0.8 ± 0.1	0.3 ± 0.0	-	traces	traces
DL-Lactate	13.5 ± 1.2	8.7 ± 0.5	6.2 ± 0.4	-	-	ND	-	-
Glucose	13.1 ± 1.4	11.3 ± 0.2	8.7 ± 0.1	traces	1.4 ± 0.0	0.9 ± 0.0	traces	traces
Xylose	18.5 ± 0.9	15.0 ± 0.7	11.0 ± 0.3	traces	1.1 ± 0.1	2.9 ± 0.2	traces	traces

^a Except for acetate, all substrates were added at a concentration of 25 mM.

^b Concentration of acetate was 10 mM. The concentration of substrate consumed corresponds to ethanol.

^c Concentration of acetate was 25 mM. The concentration of substrate consumed corresponds to ethanol.

Chapter 5

Model-driven evaluation of the feasibility of Clostridia communities to produce even and odd-chain fatty-acids from syngas

Sara Benito-Vaquerizo*, Ivette Parera Olm*, Vitor Martins dos Santos, Diana Z. Sousa, Maria Suarez-Diez

* Contributed equally

5

5.1 Abstract

The valorization of biomass-derived C1 feedstocks through microbial conversion is gaining momentum. An example is the gasification of biomass into syngas (CO, H₂ and CO₂) and further conversion to medium-chain fatty acids and alcohols. Acetogens can uptake syngas converting it into acetate and ethanol, mainly. However, energy barriers limit the production of longer molecules by acetogens. Co-cultivation of acetogenic species with species that can grow on the acetogen products, has been shown to produce longer molecules, and thus, expand the product range. *Anaerotignum neopropionicum* and *Clostridium kluyveri* are two microbes that can grow on acetogen products. *A. neopropionicum* grows on ethanol and CO₂ producing acetate and propionate, whereas *C. kluyveri* grows on acetate and ethanol producing butyrate and caproate. Furthermore, *C. kluyveri* can grow on propionate and acetate producing odd-chain fatty-acids. Considering their metabolic capabilities, we used community metabolic modeling to explore the feasibility of a synthetic

tri-culture combining the acetogen *Acetobacterium wieringae* strain JM, the propionate producer *A. neopropionicum* and the chain elongator *C. kluyveri* for the fermentation of syngas. First, we built a genome-scale metabolic model of *A. wieringae* iAWJM_SB617, and validated it with experimental data obtained from this and published studies. This allowed the subsequent construction of both, the co-culture model formed by *A. wieringae* JM and *C. kluyveri*, and the final community with all three species. Model predictions suggested a range of conditions under which these communities were feasible, and how the product range changed from even to odd-chain fatty acids by the incorporation of *A. neopropionicum* into the community. Additional operating conditions, such as the addition of H₂, were proposed that doubled the production of medium-chain fatty-acids reducing acetate accumulation.

5.2 Introduction

The use of microbial gas fermentation for the production of high-value chemicals is emerging as a promising technology to reduce carbon emissions. These technologies can convert syngas (a mixture of CO, CO₂ and H₂) coming from the gasification of wastes and biomass, or directly from gaseous side-streams from industrial factories converting them into biofuels. In fact, the production of ethanol [262], acetone and isopropanol [59] from the fermentation of waste-derived carbon is now at industrial scale, or at industrial pilot scale.

Acetogens are gas fermenting microbes that can naturally grow on one-carbon molecules (C1), such as C1 gases (e.g CO, CO₂ + H₂), formate, and methanol via the CO₂-fixating Wood-Ljungdahl pathway (WLP) [328]. Acetogenic gas fermentation is hampered by the low solubility of gases and thermodynamic constraints, which limits the range of products to small molecules such as acetate, ethanol, lactate or 2,3-butanediol (2,3-BDO). Nevertheless, genetic engineering of acetogenic strains has made possible the production of around 50 products of molecules of up to 6 carbons (such as caproate, hexanol, aromatic compounds, or terpenes.) [262].

Over the pass decades, the use of synthetic microbial communities has brought attention as an additional strategy to overcome the energy limitations linked to gas fermentation [329]. Synthetic microbial communities can lead to a wider range of products than with pure acetogenic cultures due to their co-cultivation with microbes that can use the products of syngas fermentation (i.e., ethanol, acetate, CO₂) to make products of longer carbon chain and higher value. This has been proven, for instance, by the co-cultivation on each of the following acetogens: *Clostridium autoethanogenum*, *Clostridium ljungdahlii*, *Clostridium aceticum* with *Clostridium kluyveri* [65, 68, 330]. *C. kluyveri* is a strict anaerobe that uptakes the gas fermentation prod-

ucts (acetate and ethanol) and produces the medium-chain fatty acids (MCFA) butyrate and caproate via chain-elongation. Alternatively, one could choose an alternative species that can shift the range of products to molecules of different chain lengths. This was demonstrated by the co-cultivation of two acetogens: *Acetobacterium wieringae* strain JM and *Acetobacterium wieringae* DSM 1911^T with two propionigenic species: *Pelobacter propionicus* and *Anaerotignum neopropionicum* [269], which can ferment ethanol and CO₂ producing propionate via the acrylate pathway [82]. Furthermore, *A. neopropionicum* was recently used to drive production of longer odd-chain fatty-acids from ethanol and CO₂ through its co-cultivation with *C. kluyveri* [331]. *C. kluyveri* can ferment ethanol and propionate producing valerate (C5), pentanoate (C7), and thus, shifting again the product range.

The establishment of the latter communities suggests a modular approach to shift the product range from the fermentation of C1 gases from even- to odd-chain fatty-acids. Such an approach would entail the incorporation of a propionate producing species to a community formed by an acetogen and a species performing chain-elongation. Among the acetogens, *Acetobacterium wieringae* strain JM has been cultivated in a pH range (\approx 6.8-7.2) [332, 333] similar to *C. kluyveri*'s optimal pH for chain elongation (6.5-7.5) [334], and the pH reported for the cultivation of *A. neopropionicum* (\approx 7) [82]. Thus, *A. wieringae* JM seems to be a good candidate for establishing a community with *A. neopropionicum* and *C. kluyveri*.

Establishing such community is laborious and difficult, as a large range of operating conditions needs to be explored. An effective way to explore both the feasibility of such community and the product profile is to use computational approaches that can mimic these metabolic processes. This can be achieved through the use of genome-scale constrained-based metabolic models (GEMs). GEMs are mathematical representations of the genome-encoded metabolic potential of an organism. Constraint-based approaches can be used to explore GEMs, unravel new metabolic functions and to predict growth and production under specified conditions [56, 74, 82]. GEMs of single organisms have been combined using dedicated computational approaches [51, 70, 99] and used to drive experimental designs in microbial communities.

In this study, we followed a modeling framework to study the feasibility of a tri-culture for the production of odd-chain fatty acids from syngas. For that, we first built the GEM of the acetogen *A. wieringae* JM, iAWJM_SB617. Then, we constructed the community GEM with the new GEM of *A. wieringae* JM, the recent developed GEM of *A. neopropionicum* [82] and the existing GEM of *C. kluyveri* [220]. Consecutively, we assessed the feasibility of both, the co-culture of *A. wieringae* and *C. kluyveri*, and the tri-culture of *A. wieringae*, *A. neopropionicum* and *C. kluyveri* to produce even and odd-chain fatty acids on CO, respectively. Community Flux Balance Analysis (FBA) was used to explore the feasibility on a wide range of biomass

species ratios and growth rates. cFBA with Flux sampling was following used to explore the range of products where the co-culture and the tri-culture were feasible at a fix growth rate, both on CO and CO/H₂, suggesting potential designs for the optimization of MCFAs.

5.3 Materials and methods

Reconstruction of the GEM iAWJM_SB617

The genome-scale metabolic network of *A. wieringae* JM, iAWJM_SB617, was reconstructed using the GEM of the acetogen *C. autoethanogenum*, iCLAU786, as scaffold [219] and adapted according to the genomic information of *A. wieringae* JM. An orthology based approach was followed. First, the genome sequence of *A. wieringae* JM (GCA_008107585.1) and the reference annotation were retrieved (in GFF format) from the National Center for Biotechnology Information (NCBI) under accession number VSLA00000000 [332]. Then, the genome of *A. wieringae* JM was functionally annotated using eggNOG-mapper 2.1.7 [286], and structurally annotated using the reference annotation, and can be found in the public GitLab repository: https://gitlab.com/wurssb/Modelling/triculture_aw_an_ck/-/tree/master/. The genome sequence of *C. autoethanogenum* DSM 10061 (GCA_001484725.1) was retrieved (in FASTA format) from NCBI [335]. Ortholog genes between both species were identified using OrthoFinder 2.5.4. [336]. The scaffold model of *C. autoethanogenum* was adapted to *A. wieringae* JM. Model reactions with a gene-protein-reaction (GPR) association related to genes with predicted ortholog(s) in *A. wieringae* were kept. A new GPR was associated to those reactions by replacing the *C. autoethanogenum* locus tag of the form 'CAETGH_RSXXXXX' by the corresponding *A. wieringae* protein ID 'TYCXXXXX'. Reactions for which no homologous genes were identified were further inspected. Enzyme Commission (EC) number describing these reactions were retrieved from the template model and gene(s) associated to these EC numbers in *A. wieringae* were retrieved either from the genome annotation file or from PATRIC [290] or UniProt [291] database. Reactions without an annotated EC number in the template model were searched by their ModelSEED [77], KEGG [289], MetaCyc [287], or BIGG [288] identifier in the corresponding databases. From the databases -ModelSEED, KEGG, MetaCyc, BIGG-, the EC numbers were obtained and then used to retrieve the genes from either the genome annotation file, or PATRIC or UniProt. The stoichiometry and mass balances of the reactions was also verified in the previously cited databases. Finally, the draft model was transformed into SBML (xml) using python and COBRApy [235].

Consecutively, we maximized growth on CO and CO₂/H₂ using FBA in CO-

BRAPy [235] for both conditions. We fixed the CO uptake to $30 \text{ mmol g}_{\text{CDW}}^{-1} \text{ h}^{-1}$ and CO_2 and H_2 to 20 and $40 \text{ mmol g}_{\text{CDW}}^{-1} \text{ h}^{-1}$, respectively. Then, we removed one by one the reactions with non-associated GPR (orphan reactions), except extracellular and transport reactions, and checked whether the growth rate and the production of acetate were affected from their original values in the two conditions. To eliminate the reactions, we used the function `single_reaction_deletionReactions` in COBRAPy. Reactions that predicted the same growth rate and acetate production rate in both CO and CO_2/H_2 were removed from the model as they were considered not essential and they were not found in *A. wieringae*. The biomass reaction was kept as the one in the GEM of *C. autoethanogenum*. Metabolites only involved in the removed reactions, were also removed.

Additionally, the model was amended with reactions and metabolites whose related proteins were annotated in the genome of *A. wieringae* and reported to be present in others *Acetobacterium* species [337], but not in *Clostridium*. The GEM of *Acetobacterium woodii* ('CNA_AW') was used as additional support since it is a close related species [338]. Reactions were added by keeping the same information and namespace of the scaffold model using ModelSEED. Once new reactions were added, the previous procedure was repeated to identify possible non-essential orphan reactions. The final model version in xml was translated into SBML Level 3 Version 1 using KBase [78]. The model was validated using MEMOTE [299] and SBML Validator [298]. The GEM, iAWJM_SB617, can be found in the git repository in Table format, json and SBML L3V1 [227] standardization together with a MEMOTE report.

5.3.1 Qualitative validation of the GEM iAWJM_617

The model was qualitatively validated by assessing growth on carbon sources reported to support growth in other *A. wieringae* strains [337]. Model simulations were done using FBA in COBRAPy version 0.24.0 [235], and Python 3.9. For each assessed carbon source, the lower bound of the substrate uptake rate per time point was constrained to $-30 \text{ mmol g}_{\text{CDW}}^{-1} \text{ h}^{-1}$ to assess growth on a single carbon source, and to $-30 \text{ mmol g}_{\text{CDW}}^{-1} \text{ h}^{-1}$ in total to assess growth on more than one carbon source, unless specified otherwise. The biomass synthesis reaction was used as the objective function. Growth was considered when the growth rate was higher than 0.0001 h^{-1} .

5.3.2 Quantitative validation of the GEM iAWJM_617 with mono-culture experiments of *A. wieringae* JM

The GEM was quantitatively validated by comparing the production rate of acetate and ethanol predicted by the model with the production rate measured in duplicate continuous bioreactors of *A. wieringae* JM growing on CO. The hydraulic reten-

tion time (HRT) of the reactor was used to determine the growth rate of the culture ($1/\text{HRT}$). Fluxes were expressed as environmental fluxes instead of as specific fluxes following [221]. The biomass reaction was constrained with the growth rate multiplied by the average measured biomass in the reactor. The lower bound of the CO uptake rate reaction was constrained to -3.5 mmol h^{-1} , and the upper bound to 1 mmol h^{-1} . The NGAM value of the ATP maintenance reaction ('rxn00062_aw') was adjusted based on the CO consumed in the experiments and used to constrain the lower bound of this reaction. The solution space and the set of fluxes compatible with the measured constraints was sampled using the *sample* function in the flux_analysis submodule COBRapy. The results shown are the average and standard deviation of 10000 iterations.

5.3.3 Simulations with the GEM of *A. wieringae* JM

We simulated the effect of H_2 as additional energy source on the production of acetate and ethanol with the GEM of *A. wieringae*. The lower bound of the CO uptake reaction was constrained to -3.5 mmol h^{-1} , and the upper bound to -3 mmol h^{-1} . H_2 uptake rates were varied from 0 to 7 mmol h^2 . The growth rate was constrained to 0.021 h^{-1} and the total biomass was fixed to 0.32 g. The solution space and the set of fluxes compatible with the measured constraints were sampled using the *sample* function in the flux_analysis submodule of COBRapy. Presented results show the average and standard deviation based on 5000 iterations generated at each condition (gitrepository).

5.3.4 Construction of a co-culture model of *A. wieringae* + *C. kluyveri* and a tri-culture model of *A. wieringae* + *A. neopropionicum* + *C. kluyveri*

The tri-culture model of *A. wieringae*, *A. neopropionicum* and *C. kluyveri* was generated by combination of single species models: iAWJM_617 (introduced here), iA-NEO_607 [82], and iCKL708 [220], respectively, and following the same approach reported in our previous studies [51, 70]. In brief, every single species is associated to an internal compartment: 'Cytosol_AW', 'Cytosol_AN' and 'Cytosol_CK', with 'aw', 'an' and 'ck' as their respective identifiers (id). In addition, there is an extracellular compartment common for the three species whose identifier is 'e'. Intracellular metabolites were formed by the id of the metabolite and the corresponding compartment id (e.g acetate_aw) and extracellular metabolites were formed by their metabolite id followed by '_e'. Metabolites that were defined as extracellular ('_e') in each single species model, were also defined in the common extracellular compartment of the tri-culture model. Extracellular metabolites present in more than

one species were modified to follow the same naming system (namespace) in the three species. Similarly extracellular reactions were also adapted. Extracellular reactions present in single models, were also present in the tri-culture model. Again, repeated reactions were unified to be unique in the tri-culture model. Each species has its own biomass synthesis reaction represented by the following id: 'Biomass_aw', 'Biomass_an' and 'Biomass_ck'. Additionally, one extra reaction was created representing the community biomass ('EX_Biomass_e') formed by the combination of the three biomass contributions represented by metabolites 'cpd11416_aw', 'cpd11416_an' and 'Biomass_ck'. Finally, the tri-culture model was transformed into SBML level 3 version 1 (git repository).

The co-culture model of *A. wieringae* and *C. kluyveri* was not created *per se*. Instead, we blocked flux through all the reactions associated to *A. neopropionicum* in the tri-culture model.

5.3.5 Co-culture and tri-culture modeling framework

The co-culture and tri-culture model simulations were run using a steady-state approach that considers balanced growth of microbial species resembling Community FBA (cFBA) [221] and was implemented in our previous work [51, 70]. Species relative abundance was taken into account by the incorporation of the species ratio (relative abundance) and total biomass in the respective biomass synthesis reaction. Following this new notation, specific fluxes ($\text{mmol g}_{\text{CDW}}^{-1} \text{h}^{-1}$) were substituted by environmental fluxes (mmol h^{-1}), taking into account the biomass of each species (g L^{-1}) and the total working volume of the reactor (L).

5.3.6 Co-culture and tri-culture model simulations

We assessed the feasibility of the co-culture and the tri-culture on CO in a wide range of biomass species ratio combinations and growth rates. The biomass of the community was estimated based on the biomass measured in mono-culture experiments of *A. wieringae* (0.32 g). We studied growth rates from 0.005 to 0.05 h^{-1} , and (biomass) species ratio between 0.1 and 0.9 for each species for the co-culture model and from 0.1 to 0.8 for the tri-culture model. For each community biomass, we assessed growth with all the growth rates and species ratio combinations on CO. The biomass of each species was calculated based on the indicated species ratio and the community biomass. The biomass of each species was multiplied by the indicated growth rate, and the value was used to constrain the flux through the biomass synthesis reaction of each species. Species growth rates were set to be equal and equal to the community growth rate. The lower bound of the CO uptake reaction was constrained to -3.5 mmol h^{-1} , and the upper bound to -1 mmol h^{-1} , based on

the total CO inflow rate measured in mono-culture experiments of *A. wieringae*. We defined the community biomass reaction ('EX_Biomass_e') as the objective function for maximization and we performed FBA to assess the feasibility of each condition. Subsequently, we explored the metabolic profile of the fermentation of CO at a fix growth rate (0.02 h^{-1}) and the biomass species ratios that led to feasible solutions, both in the co-culture and the tri-culture. The solution space and the set of fluxes compatible with the measured constraints were sampled using the *sample* function in the flux_analysis submodule of COBRAPy. Presented results show the average and standard deviation based on 5000 iterations generated at each condition (git repository).

We also simulated the effect of H_2 as additional energy source on the production of MCFA. For that, we selected a specific biomass species ratio and growth rate, and calculated the fluxes at several H_2 uptake rates. We selected a 6-to-4 ratio (*A. wieringae*/*C. kluyveri*) and 0.02 h^{-1} for the co-culture model, and 4/3/3 ratio (*A. wieringae*/*A. neopropionicum*/*C. kluyveri*) and 0.02 h^{-1} for the tri-culture model. The total biomass was again fixed to 0.32 g. The lower bound of the CO uptake reaction was constrained to -3.5 mmol h^{-1} , and the upper bound to -3 mmol h^{-1} . H_2 uptake rates were varied from 2 to 5 mmol h^{-1} . The fluxes were computed using flux sampling with 5000 iterations as in the previous simulations.

The materials and methods related to the cultivation of *A. wieringae* strain JM, the bioreactor setup and operation, and the analytical techniques are described in the supplementary material.

5.4 Results

5.4.1 Reconstruction and characteristics of the GEM of *A. wieringae* JM, iAWJM_617

The GEM of *A. wieringae* JM was constructed based on the annotation of the genome sequence of this microorganism (GCA_008107585.1) [332], and using the GEM of *C. autoethanogenum*, iCLAU786, as scaffold [219]. The biomass synthesis reaction ('bio2') was kept the same as the biomass reaction in the GEM of *C. autoethanogenum*. OrthoFinder was used to retrieve orthologue genes between the two species; 2047 genes of *C. autoethanogenum* were identified as orthologues to *A. wieringae* JM. Part of these genes were present in the GEM of *C. autoethanogenum* and were replaced by the orthologous genes of *A. wieringae* JM. A total of 175 reactions did not have orthologous genes. After a thorough manual curation, we identified genes for 99 additional reactions. In order to decide whether to keep reactions with non-associated genes (orphan), we removed each of these reactions and assessed the variation in

growth and acetate production with CO and CO₂ + H₂ as substrates. This analysis identified 72 reactions that were considered non-essential, at least for the assumed conditions and, thus, were removed from the model. Lastly, we corrected the stoichiometry of 11 reactions and amended the model with 29 reactions, whose genes were found to be present in the genome of *A. wieringae* JM. These reactions belong to energy generation and the degradation of 1,3-propanediol (1,2-PDO), 2,3-BDO, glycine betaine, caffeate and alanine. The model contains pathways associated to acetogenic metabolism (i.e., the WLP) and the production of acetate, ethanol, lactate and 2,3-BDO; central carbon metabolism; energy generation; biosynthesis of amino acids, lipids, carbohydrates and the rest of biomass components.

Table 5.1: Composition of iAWJM_SB617

Features	Number
Genes	617
Metabolites	1065
Intracellular metabolites	915
Extracellular metabolites	152
Reactions	1081
Conversion reactions	832
Transport reactions	159
Exchange reactions	76
Reactions associated with genes	775
Reactions non-associated with genes	306

The final GEM, iAWJM_SB617, consists of 617 genes, 1065 metabolites and 1081 reactions (Table 5.1). Three types of reactions can be distinguished; conversion, transport and exchange reactions. Metabolites are transported through transport reactions from the intracellular compartment (id:'aw') to the extracellular compartment (id:'e'), and viceversa. Exchange reactions represent the uptake or production of metabolites, into and outside the cell. 72 % of reactions are associated with genes. Reactions non-associated with genes correspond mostly to: i) transport reactions that, depending on the type, do are enzyme-independent (e.g., diffusion reactions); and ii) exchange reactions that are artificial representations and, thus, without enzymes.

The final model was correctly defined in SBML, level 3 and version 1, and obtained a score of 73 % in MEMOTE. The annotation of metabolites and reactions

received a very high score ($\approx 82\%$). However, the annotation of genes scored only 33% , since neither KBase nor MEMOTE recognized the protein IDs (TYCXXXXX) or locus tags (FXB42_XXXXX) associated to *A. wieringae* JM. The lowest score obtained was for consistency (56%), due to the lack of stoichiometry introduced into the model for the use of artificial metabolites to represent biomass building blocks (e.g., protein, DNA, RNA). The model can be found in SBML, JSON and Table formats together with a MEMOTE report in the git repository.

5.4.2 Qualitative validation of the GEM iAWJM_SB617 by assessment of growth phenotypes

The GEM iAWJM_SB617 was qualitatively validated by assessing growth on several carbon sources and comparing the model output with experimental data generated in this study and from literature [332] [337], on both *A. wieringae* JM and the type strain. We evaluated growth on C1 feedstocks (CO, CO₂ + H₂, formate and methanol), ethanol, 1,2-PDO, glycerol, lactate, alanine, fructose and glucose (Fig. 5.1).

	CO	CO ₂ /H ₂	Formate	Methanol	Ethanol	1,2-propanediol	Glycerol	Lactate	Alanine	Fructose	Glucose
iAWIE_SB615				ND							
<i>A. wieringae</i> JM					ND			ND			
<i>A. wieringae</i> DSM 1911 ^T	*					ND					

* Plus 1mM formate

Figure 5.1: Growth phenotypes of *A. wieringae* JM predicted by the constructed GEM in this study (iAWJM_SB617) and reported in experimental studies (this work and [332]). For comparison, growth phenotypes reported in literature for the type strain, *A. wieringae* DSM 1911^T [337], are also included. Green: growth; grey: no growth; ND: no data available.

A. wieringae JM has been reported to grow on all the C1 feedstocks tested [332]. The model predicted these phenotypes except for growth on methanol, which could not be assessed due to incompleteness of the methanol assimilation pathway in the annotation and databases. The type strain of *A. wieringae* can grow on CO but only in the presence of formate [332], similarly to the close relative *A. woodii*, which also uses CO with formate or H₂+CO₂ as co-substrates ([339]). In contrast to its close relatives, *A. wieringae* strain JM grows on CO as sole substrate [332], which our model

predicted. The model predicted growth with the rest of substrates tested, including 1,2-PDO and the amino acid alanine, which both had not been tested before on the JM strain but are predicted substrates of the genus *Acetobacterium* [337]. The two strains of *A. wieringae* (type and JM) can grow on fructose. The same does not hold true for glucose: while the type strain has been reported unable to ferment this sugar [340], our model predicted that the strain JM can grow on glucose, as corroborated by cultivation experiments [332].

5.4.3 Product profile from the fermentation of CO and CO/H₂ by *A. wieringae* JM

To quantitatively validate the model of *A. wieringae* JM, we simulated the fermentation of CO and compared the results with experimental data from bioreactor experiments under steady-state conditions (HRT = 48 h). For model simulations, the growth rate was fixed as determined by the HRT (growth rate = dilution rate (D) = 1/HRT). The validation also served to adjust the non-growth associated with biomass term (NGAM) into the ATP maintenance reaction ('rxn00062_aw') in the GEM; model fitting led to a NGAM of 1.5 mmol g_{CDW}⁻¹ h⁻¹ (0.48 mmol h⁻¹).

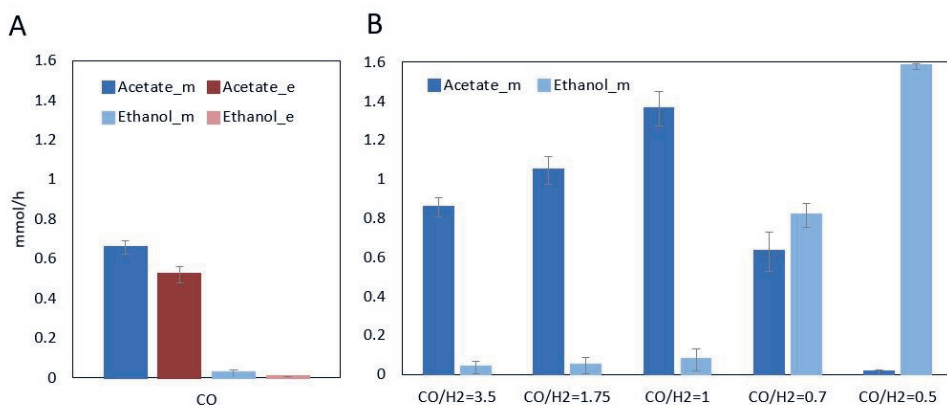


Figure 5.2: A: Steady-state production rates of acetate and ethanol by *A. wieringae* JM growing on CO as predicted by the model ('_m') and observed in bioreactors ('_e') (two biological replicates). B: Effect of CO/H₂ uptake ratios on steady-state production rates of acetate and ethanol in *A. wieringae* JM, as predicted by model simulations. A growth rate of 0.021 h⁻¹ (HRT = 48 h) and a biomass of 0.32 g were assumed, based on experimental values. The maximum uptake rate of CO was set to 3.5 mmol h⁻¹, and the minimum to 3 mmol h⁻¹ in all scenarios. Model predictions show the average and standard deviation of 5000 samples.

Acetate and ethanol production rates obtained by the model simulations fitted the experimental values with high approximation (Fig. 5.2A). In the bioreactor experiments under steady-state, *A. wieringae* JM consumed ≈ 3.3 mmol CO h⁻¹, producing mostly acetate (≈ 0.52 mmol h⁻¹) and traces of ethanol (< 0.01 mmol h⁻¹). The steady-state biomass concentration was 0.8 g L⁻¹. The slightly higher production rates of acetate (0.66 mmol h⁻¹) and ethanol (0.02 mmol h⁻¹) resulting from the simulation can be linked to a higher predicted CO uptake rate (3.5 mmol h⁻¹) than observed.

Besides CO, *A. wieringae* JM can use H₂ as electron donor, and both gases are commonly found in varying proportions in syngas streams. Here, we carried out simulations with the model to predict the effect of different CO/H₂ uptake ratios (3.5 - 0.5) on the production of acetate and ethanol under steady-state conditions. For that, the CO uptake rate, the HRT and the total biomass were assumed as in the bioreactor experiment with CO. The predicted production rates of acetate and ethanol are shown in Fig. 5.2B. With CO as sole substrate, virtually only acetate was produced, and ethanol was produced at a very low rate, as specified above. The acetate production rate increased moderately with the addition of H₂ up to a CO/H₂ uptake ratio of 1, where it reached the highest value (1.36 mmol h⁻¹). Ethanol production rates remained low (< 0.1 mmol h⁻¹) in this range of CO/H₂ ratios (≥ 1). By contrast, when CO/H₂ ratios were < 1 , that is, when the uptake rate of H₂ was higher than that of CO, solventogenesis was significantly boosted. With a CO/H₂ ratio of 0.5, acetate production was negligible compared to an ethanol production rate of 1.56 mmol h₋₁, the highest obtained in the simulations.

5.4.4 Model of a co-culture of *A. wieringae* JM and *C. kluyveri*

Before constructing the tri-culture, we evaluated the feasibility of a co-culture of *A. wieringae* JM with *C. kluyveri*, simpler in structure and similar to other modelled co-cultures [51]. The co-culture model resulted in a total of 2032 reactions and 1804 metabolites (git repository). With it, we assessed the feasibility of a co-culture of *A. wieringae* JM and *C. kluyveri* converting CO to medium-chain fatty acids in a range of biomass species ratios (relative abundances) and growth rates.

Simulations predicted feasible solutions in a wide range of species ratios with growth rates ≤ 0.015 h⁻¹ (Fig. 5.3A). At 0.02 h⁻¹, the co-culture was only feasible with species ratios between 4/6 and 6/4 (*A. wieringae* JM/*C. kluyveri*). At growth rates higher than 0.03 h⁻¹, the co-culture was feasible only when both species were equally abundant.

In view of these results, we explored the range of product profiles predicted by the co-culture model for a fixed growth rate of 0.02 h⁻¹ at the biomass species ratios that led to feasible solutions (4/6, 5/5 and 6/4). Model predicted mainly production

of caproate ($\approx 0.18 \text{ mmol h}^{-1}$) (Fig. 5.3B) followed by butyrate in the three scenarios. Longer-chain products (e.g., octanoate) were not predicted. The predicted production rate of acetate was $0.13 - 0.14 \text{ mmol h}^{-1}$ in all scenarios. This represents the acetate produced only by *A. wieringae* JM. In our model, the acetate transport reaction was constrained to acetate consumption (by *C. kluyveri*). However, *C. kluyveri* also produces acetate, specifically $1/6^{\text{th}}$ of the ethanol that it consumes, according to theoretical stoichiometry [230]. Thus, the actual accumulation of acetate is expected to be higher than in model predictions. Ethanol production by *A. wieringae* JM was $\approx 0.33 \text{ mmol h}^{-1}$ in the three scenarios, and it was almost fully consumed by *C. kluyveri*. Traces of formate, lactate and 2,3-BDO were also produced by the acetogen according to the model.

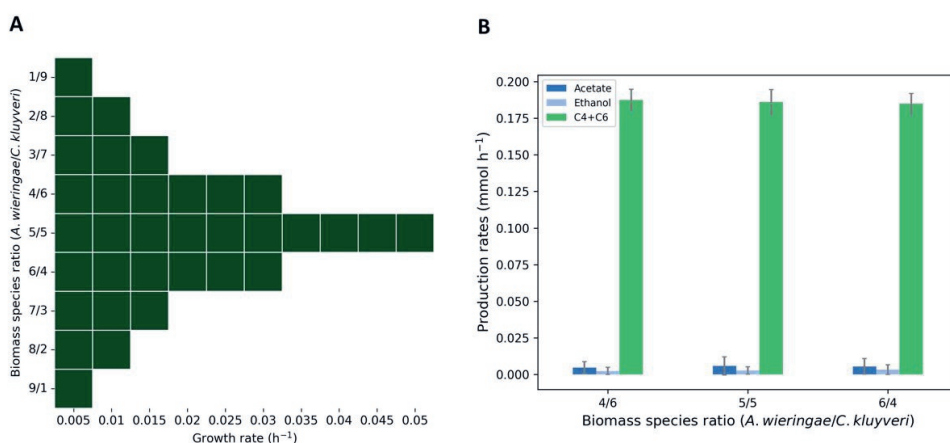


Figure 5.3: A: Predicted feasible solution space of the co-culture of *A. wieringae* JM and *C. kluyveri* fed on CO. Green squares indicate the conditions when the co-culture is feasible. The maximum uptake rate of CO was set to 3.5 mmol h^{-1} , and the minimum to 1 mmol h^{-1} . The total biomass was 0.32 g . B: Production rates of the main fermentation products from CO predicted for the co-culture model of *A. wieringae* JM and *C. kluyveri*. C4+C6: Butyrate and caproate. The growth rate was fixed to 0.02 h^{-1} , the total biomass was fixed to 0.32 g , and the CO uptake rate was constrained between 3 and 3.5 mmol h^{-1} .

The co-culture model was used to explore the fluxes through the metabolic pathways involved in the fermentation of CO to MCFA (butyrate and caproate). An overview of the metabolic pathways is given below within the description of the tri-culture model (Section 5.4.5) and a representation of it can be consulted in Fig. S5.1.

5.4.5 Tri-culture model of *A. wieringae* JM, *A. neopropionicum* and *C. kluyveri*

The model of the tri-culture was constructed by combining the GEMs of *A. wieringae* JM (this study), *A. neopropionicum* [82] and *C. kluyveri* [51]. The resulting model was composed of 2893 reactions and 2547 metabolites.

The model was used to assess the feasibility of the tri-culture in a wide range of biomass species ratios and growth rates during growth on CO. With a low growth rate (0.005 h^{-1}), the tri-culture was feasible at all biomass species ratios tested (Fig. 5.4). With growth rates higher than 0.005 h^{-1} , very low or high abundance of any of the species resulted in infeasibility of the tri-culture. A wider range of feasible solutions was found when *A. wieringae* JM dominated the community (e.g., 40 - 50% abundance) and *C. kluyveri*'s presence was between 30% - 40%, or the other way around. At growth rates higher than 0.03 h^{-1} , no combinations were found that would result in a feasible tri-culture.

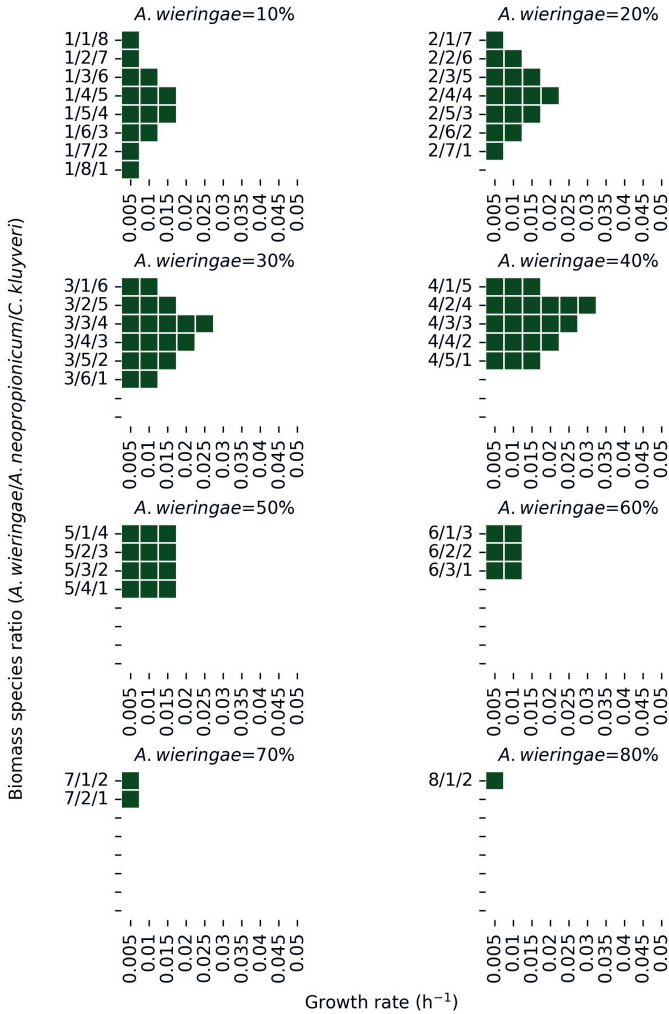


Figure 5.4: Predicted feasible solution space of the *A. wieringae* JM-*A. neopropionicum*-*C. kluyveri* tri-culture fed on CO, with 0.32 g total biomass. Each panel presents a fix *A. wieringae* JM abundance. CO uptake rate was set between 1 and 3.5 mmol h⁻¹.

Next, we explored the production rates predicted by the tri-culture model for growth on CO at a rate of 0.02 h⁻¹ at the biomass species ratios that resulted in

feasible solutions (2/4/4, 3/3/4, 3/4/3, 4/2/4, 4/4/2). The tri-culture produced a mixture of odd- and even-chain carboxylic acids (up to C7), with acetate being a main product in the majority of scenarios (5.5). The highest production rate of odd-chain MCFAS (valerate and heptanoate) was predicted for a rather balanced biomass species ratio of 3/3/4 (*A. wieringae* JM/*A. neopropionicum*/*C. kluyveri*). In all scenarios, the production rate of valerate (0.07 - 0.14 mmol h⁻¹) was higher than the production of heptanoate, except for a the species ratio 4/2/4, in which the heptanoate production rate has higher than that of valerate (0.09 vs 0.032 mmol h⁻¹, respectively). As expected, even-chain MCFAs were most abundant when the presence of *A. neopropionicum* was low ($\approx 20\%$), that is, with a species ratio of 4/2/4. The production rate of caproate was higher than that of butyrate (0.03 vs. 0.01 mmol h⁻¹, respectively). Still, in the latter scenario, odd-chain MCFAs together accounted for the majority of products.

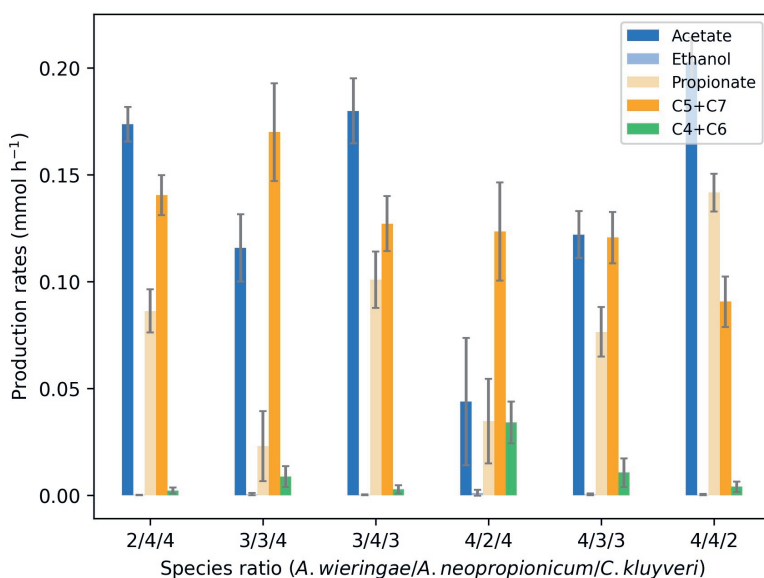


Figure 5.5: Production rates of the main fermentation products from CO by the *A. wieringae* JM-*A. neopropionicum*-*C. kluyveri* tri-culture, predicted by the community model for different species ratios. C5+C7: valerate and heptanoate; C4+C6: butyrate and caproate. The growth rate was fixed to 0.02 h⁻¹, the total biomass was fixed to 0.32 g, and the CO uptake rate was constrained between 3 and 3.5 mmol h⁻¹

Propionate (produced solely by *A. neopropionicum*) was produced the fastest ($\approx 0.14 \text{ mmol h}^{-1}$) when the presence of *A. neopropionicum* was dominant in the community (40%; species ratios of 2/4/4, 3/4/3 and 4/4/2) (5.5). As for acetate, its production rate was the highest when *A. wieringae* JM and *A. neopropionicum* were most dominant (40% each). In turn, consumption of acetate by *C. kluyveri* was higher when *A. neopropionicum*'s abundance was 20-30%. The rate of acetate production by *A. wieringae* JM was $< 0.01 \text{ mmol h}^{-1}$, and by *A. neopropionicum* it was $0.17\text{-}0.25 \text{ mmol h}^{-1}$ in all scenarios. Ethanol production (by *A. wieringae* JM) was higher (0.17 mmol h^{-1}) when the presence of *A. neopropionicum* was low (20%). However, ethanol was almost fully consumed by *A. neopropionicum* and *C. kluyveri*.

Metabolic fluxes predicted by the tri-culture model of *A. wieringae* JM, *A. neopropionicum* and *C. kluyveri* during CO fermentation

The tri-culture model was used to explore the fluxes through the key metabolic pathways involved in the fermentation of CO to MCFAs. The model combines the three central carbon metabolism pathways of the three interacting microorganisms: the WLP (*A. wieringae* JM), the acrylate pathway (AcrP) (*A. neopropionicum*) and the reverse β -oxidation pathway (r- β -ox; *C. kluyveri*). A schematic representation of the relevant pathways and interactions taking place in the tri-culture is shown in 5.6.

A. wieringae JM oxidizes CO to CO₂ via the activity of carbon monoxide dehydrogenase (CODH), which generates reduced ferredoxin as electron carrier. Fixation of CO₂ with electrons derived from CO takes place in the WLP, which ultimately yields acetyl-CoA via CODH/acetyl-CoA synthase. In the annotated genome of *A. wieringae* JM, four subunits were identified to be involved with CODH activity (TYC 86630, TYC87912, TYC87913, TYC87914; genes *textitcooS*, *cooS1*, *cooC* and *cdhC*, respectively) and three other subunits with acetyl-CoA synthase activity (TYC87909, TYC87910, TYC87911; *acsD*, *acsC* and *acsE*, respectively). Some of these genes were also identified by [332]. In addition, *C. kluyveri* produces H₂ that is partly consumed by *A. wieringae* JM as additional electron donor. According to the model, H₂ is metabolized via the complex hydrogen-dependent carbon dioxide reductase (HDCR), yielding formate that enters the methyl branch of the WLP. Our annotation data indicates that the HDCR would comprise the following two subunits: a formate dehydrogenase (TYC86388; *fdh*) and a Fe-hydrogenase (TYC85752; *hydA*), however further analyses would be needed to confirm this. Acetyl-CoA is converted to acetate, coupled to the production of ATP via substrate-level phosphorylation. Ethanol can be produced from acetyl-CoA via a bifunctional alcohol-aldehyde dehydrogenase, or via acetate involving acetaldehyde:ferredoxin oxidoreductase (AOR) (TYC88292 or TYC84206). As is the case in acetogens, additional energy is obtained through the coupling of a Na⁺-translocating ferredoxin:NAD⁺ oxidoreductase (Rnf) complex and

a membrane-bound ATP synthase, producing ATP driven by the oxidation of ferredoxin. The genome of *A. wieringae* JM contains two distinct Rnf clusters (TYC84275-80; *rnfB, rnfA, rnfE, rnfG, rnfD, rnfC* and TYC88316-21; *rnfC, rnfD, rnfG, rnfF, rnfA, rnfB*). The model predicted the production of 2,3-BDO by *A. wieringae* JM. 2,3-BDO was derived from pyruvate via the activities of acetolactate synthetase (Acs), acetolactate decarboxylase (Alcd) and 2,3-BDO dehydrogenase (Bdh).

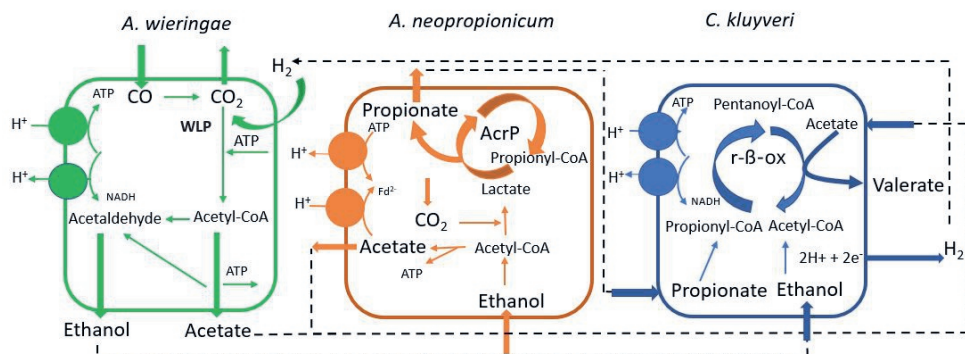


Figure 5.6: Schematic representation of the fermentation of CO by the *A. wieringae* JM-*A. neopropionicum*-*C. kluyveri* tri-culture. WLP: Wood-Ljungdahl pathway; AcrP: acrylate pathway; r- β -ox: reverse β -oxidation pathway. Arrows indicate the direction of the flux. Ticker arrows show production or consumption of the indicated metabolites in the specified species. For simplicity, additional interactions predicted by the model (see main text) are not shown here.

The model showed that part of the CO₂ and ethanol produced by the acetogen were consumed by *A. neopropionicum*. Ethanol is oxidized to acetyl-CoA via bifunctional alcohol-aldehyde dehydrogenase. Part of the acetyl-CoA is then used for acetate production coupled to the formation of ATP, and the rest is carboxylated to pyruvate via pyruvate:ferredoxin oxidoreductase (PFOR). Pyruvate is then reduced to lactate, which enters the acrylate pathway, which we described elsewhere [82] (AcrP in Fig. 5.6). *A. neopropionicum* also produces lower amounts of propanol, butyrate, lactate, isobutyrate and isovalerate (not shown in the figure). Besides CO₂ and ethanol, the model indicated that 2,3-BDO (produced by *A. wieringae* JM) was also consumed by *A. neopropionicum*, which had not been reported before. In the model, consumption of 2,3-BDO takes place via the enzymes Bdh, Alcd and Acs.

C. kluyveri also takes up part of the ethanol, CO₂ and acetate produced by the acetogen, as well as the propionate, acetate and traces of propanol produced by *A. neopropionicum*. The uptake of propionate and ethanol results in the production of

odd-chain MCFAs by *C. kluyveri*. Ethanol oxidized to acetyl-CoA, which is used for chain elongation together with propionyl-CoA (derived from propionate), ultimately yielding valerate via the reverse β -oxidation pathway (r- β -ox in Fig. 5.6). In turn, valerate can be cycled through the r- β -ox pathway, producing heptanoate. Acetate is also used for chain elongation, generating butyrate and caproate. According to the model, traces of propanol produced by *A. neopropionicum* were also consumed by *C. kluyveri*.

The tri-culture model predicted transport of amino acids between species. For instance, *A. wieringae* JM produces traces of alanine which are consumed by *A. neopropionicum* (see git repository). While not explored in this study, we hypothesized that traces of secondary alcohols (e.g., butanol, pentanol) could be produced by assimilation and reduction of the respective MCFAs by *A. wieringae* JM, as observed in other acetogens [64].

5.4.6 Modeling the effect of H₂ on the production of MCFAs by the co-culture and the tri-culture

Similarly to what was done for the mono-culture of *A. wieringae* JM, here we did simulations to study the effect of different CO/H₂ uptake ratios on the production of MCFAs by both, the co-culture of *A. wieringae* JM and *C. kluyveri* and the tri-culture with the addition of *A. neopropionicum*. For these simulations, we chose to study a ratio of 6/4 (*A. wieringae* JM/*C. kluyveri*) and a ratio of 4/3/3 (*A. wieringae* JM/*A. neopropionicum*/*C. kluyveri*) for the co-culture and the tri-culture, respectively. This ratio was chosen based on the feasibility study of the tri-culture (Fig. 5.4), since conditions with higher presence of *A. wieringae* led to a wide range of feasible solutions, and the total biomass of *A. wieringae* obtained in mono-culture experiments was high. Three CO/H₂ uptake ratios were tested: 1.75, 1 and 0.7 (Fig. 5.7).

With H₂, the production of even-chain MCFAs in the co-culture increased up to 0.46 mmol h⁻¹ with a CO/H₂ ratio of 0.7 (Fig. 5.7A). Likely, this is driven by a higher ethanol production by the acetogen (up to 1 mmol h⁻¹; not shown), that is in turn, almost fully consumed by *C. kluyveri*. Acetate production by *A. wieringae* JM also increased with addition of H₂ (up to 0.37 mmol h⁻¹; not shown), but was further consumed by *C. kluyveri*. A CO/H₂ ratio < 0.7 led to infeasible solutions, since almost no acetate was produced, and *C. kluyveri* requires acetate for chain elongation.

In the tri-culture with H₂ supplementation, production of odd-chain MCFAs reached 0.35 mmol h⁻¹ (Fig. 5.7B). The addition of H₂ gradually increased the production of even chain MCFAs (up to a CO/H₂ < 1). With H₂, ethanol production (by the acetogen) increased (up to 0.78 mmol h⁻¹) and, thus, more ethanol was available for its conversion to propionate and odd-chain MCFAs. Acetate production by

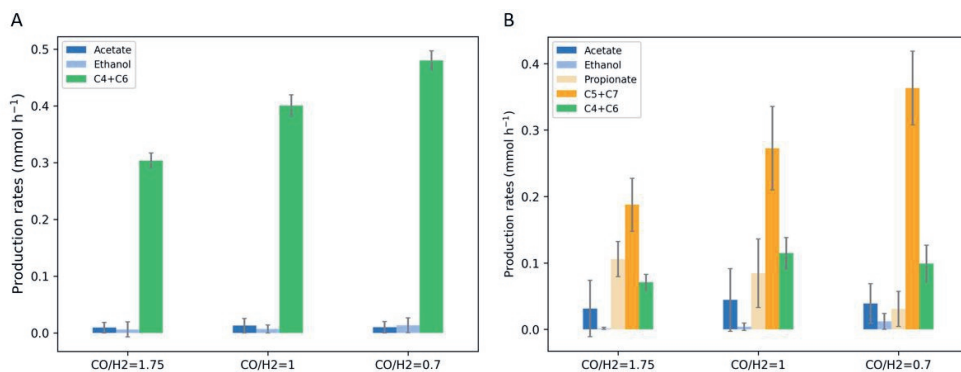


Figure 5.7: Effect of different CO/H₂ uptake ratios on the production of MCFAs by the co-culture of *A. wieringae* JM and *C. kluyveri* (A) and by the tri-culture of *A. wieringae* JM, *A. neopropionicum* and *C. kluyveri* (B). The biomass species ratio of the co-culture was fixed to 6/4 (*A. wieringae* JM/*C. kluyveri*). The biomass species ratio of the tri-culture was fixed to 4/3/3 (*A. wieringae* JM/*A. neopropionicum*/*C. kluyveri*). The growth rate was fixed to 0.02 h⁻¹, the total biomass was fixed to 0.32 g, and the CO uptake rate was constrained between 3 to 3.5 mmol h⁻¹

A. wieringae JM and *A. neopropionicum* increased up to 0.34 mmol h⁻¹ at a CO/H₂ = 1. Propionate production decreased with addition of H₂; more propionate was consumed (by *C. kluyveri*) in this case (up to 0.36 mmol h⁻¹).

The production of CO₂ decreased with increased H₂ uptake up to values < 0.1 mmol h⁻¹, both in the co-culture and the tri-culture.

5.5 Discussion

In this study, we have used a systematic computational approach to assess the feasibility of two synthetic microbial co-cultures converting CO to even- and odd-chain MCFAs (C4 - C7). The two co-cultures had in common the presence of the acetogen *A. wieringae* JM, for which we have constructed the first GEM. One co-culture was composed of *A. wieringae* JM with the chain-elongator *C. kluyveri*, and the other comprised the same two species with the addition of the propionigenic bacterium *A. neopropionicum* (tri-culture). Model simulations have also allowed us to study the effect of H₂ addition on the final product spectrum of the co-cultures.

Our reconstructed GEM of *A. wieringae* JM, iAWJM_SB617, scored sufficiently high in the MEMOTE report (73%) and predicted well the reported phenotypes of

this strain for the fermentation of C1 feedstocks and other substrates (Fig. 5.1). In addition, the simulations with the model for the fermentation of CO fitted well the experimental values obtained in bioreactors under steady-state conditions (Fig. 5.2A), supporting the validity of the GEM. The model was reconstructed based on the available model of *C. autoethanogenum* [219], a well-studied acetogen, and taking into consideration genomic information of *A. wieringae* JM. To refine the model, we used the GEM of *A. woodii* [338], the only one that was available of an *Acetobacterium* species. The reason we did not use the latter model as scaffold to reconstruct the GEM of *A. wieringae* JM is that it is a core model with reduced genomic information, and therefore was not that suitable for the reconstruction of a full model (as it was the case here).

The re-annotation of the genome of *A. wieringae* JM contributed to the identification of key enzymes of the central carbon and energetic metabolism of this strain, such as the CODHs, the different subunits of the Rnf complex, or the AOR, involved in ethanol production, supporting the previous annotation by Arantes et. al [332]. In addition, our analysis expanded the understanding of the physiology of this novel acetogen and of the *Acetobacterium* genus. *A. wieringae* JM was isolated from a syngas-converting enrichment culture [332], which might explain why this strain evolved to be able to utilise CO as sole substrate (as our model corroborated), as opposed to the type strain [332]. How this change occurred, though, was unclear. It was hypothesized that the hydrogen-dependent carbon dioxide reductase (HDCR) complex, present in both *A. wieringae* type strain and *A. woodii*, was sensitive to high CO concentrations and, therefore, would make formate a requirement during growth in the presence of CO by these two strains [332, 339]. However, as Arantes et. al [332] hinted and was corroborated by our re-annotation, *A. wieringae* JM presumably also contains an HDCR complex, composed of a formate dehydrogenase (TYC86388; *fdh*) and an Fe-hydrogenase (TYC85752; *hydA*). A similar case is that of the acetogen *Thermoanaerobacter kivui*, which also employs the HDCR complex and, after an adaptation period, was able to grow exclusively on CO [341]. CO inhibition of the HDCR complex has been shown to be fully reversible [342]. Thus, it is possible that prolonged exposure to CO (i.e., via enrichment or adaptive laboratory evolution) reverses CO inhibition in the HDCR, enabling acetogens that use this formate dehydrogenase to grow on CO in the absence of formate.

The community model of *A. wieringae* JM - *C. kluyveri* was used to explore the effect of different growth rates and species abundances on the viability of the co-culture and the production of MCFAs from CO under steady-state conditions. Since the biomass of *A. wieringae* JM in mono-culture experiments was high (Section 5.4.3), we hypothesized that the presence of this strain would be dominant (60 - 65%) in a viable co-culture. The model predicted the co-culture to be viable with growth rates up to 0.03 h^{-1} (HRT $\approx 33 \text{ h}$). While mono-culture simulations with *A. wieringae* JM

led to mostly acetate, there was a clear shift to solventogenesis upon the addition of *C. kluyveri* to the model (Fig. 5.2A). This metabolic shift was also reported in a co-culture of *C. autoethanogenum* and *C. kluyveri* [68]. The authors stated that it was mainly thermodynamics driving the shift from acetate to ethanol production, which might be also the case here. Cross-feeding of H₂ between *C. kluyveri* and the acetogen might also contribute to increase ethanol production, although H₂ production should be sufficiently high for this to be noticeable. Indeed, our simulations showed that H₂ supplementation promoted solventogenesis in *A. wieringae* JM (Fig. 5.2). In turn, in co-culture with *C. kluyveri*, H₂ supplementation yielded a higher MCFAs production, specifically when decreasing the CO/H₂ ratio from 1.75 to 0.7 (Fig. 5.7A). A similar phenomenon was observed empirically in a co-culture of *C. autoethanogenum* and *C. kluyveri*, although in that study the CO/H₂ ratios tested were higher than 1 [68], which in our simulations lead to mostly acetate production by the acetogen (Fig. 5.2B).

The co-culture model predicted a higher production of caproate than butyrate. This is expected to be the case for *C. kluyveri* growing at neutral pH and with high ethanol/acetate ratios [330, 343], which was the case here (ethanol/acetate ratios higher than 1). That said, acetate production is expected to be slightly higher than what was predicted by the model, since, according to stoichiometry of chain elongation, 1/6th of ethanol is converted to acetate by *C. kluyveri* [230]. In the model, this reaction only indicates consumption of acetate. Besides, *A. wieringae* JM produces mostly acetate at neutral pH (Fig. 5.1), and it should be experimentally confirmed how much more ethanol is produced with addition of *C. kluyveri* and H₂, to favour caproate production rather than butyrate.

In this study we also studied the viability of a tri-culture of *A. wieringae* JM, *A. neopropionicum* and *C. kluyveri* converting CO to odd- and even-chain MCFAs. The tri-culture was predicted not to be feasible at growth rates higher than 0.03 h⁻¹. The range of feasibility was enlarged when *A. wieringae* JM was dominant in the community, which fitted with observations of high biomass obtained in mono-culture experiments. However, with abundances higher than 50% of *A. wieringae* JM, the tri-culture was only feasible at growth rates lower than 0.02 h⁻¹. *C. kluyveri* was dominant in a co-culture with *C. autoethanogenum* at pH 6 - 6.2 [51]. Hence, one could argue that *C. kluyveri*'s presence in co-cultivation with *A. wieringae* JM and *A. neopropionicum* could also be noticeable (30 to 40%), since the pH range of the three species is within the optimal pH for chain elongation [334].

The addition of *A. neopropionicum* to the co-culture shifted the product range from fully even- to a mix of even- and odd-chain MCFAs, the latter (valerate and heptanoate) being favoured in the conditions we tested. The production of odd-chain products increased with supplementation of H₂ as energy source, as the availability of ethanol increased. *A. neopropionicum* produced more propionate (and ac-

etate) that was consumed by *C. kluyveri*, therefore increasing the production of odd-chain MCFAs. With $\text{CO}/\text{H}_2 < 1$, acetate production decreased slightly and, consequently, the production of even-chain MCFAs also did. Mono-culture simulations with *A. wieringae* JM also showed decreased acetate production with higher H_2 presence (Fig. 5.3B). Interestingly, the model reported cross-feeding of 2,3-BDO between *A. wieringae* JM and *A. neopropionicum*, which had not been observed in a study of this co-culture [269]. It is possible that the tri-culture model required additional ATP to be established and to meet the constraints, and that the production of alternative products resolved ATP availability [74, 344]. For instance, *A. woodii* obtains 1.6 ATP per 2,3-BDO on CO, and *C. autoethanogenum* between 1.3-1.9 ATP per 2,3-BDO, which is slightly higher than the net ATP per acetate produced (1 - 1.5/ATP per acetate) [54].

Accumulation of acetate was very noticeable from the fermentation of CO by the tri-culture, which limits the product yield of MCFA. While acetate production by *A. wieringae* JM was decreased in the presence of *C. kluyveri*, the incorporation of *A. neopropionicum* increased the production of acetate in the community, since it produces it as one of the main products from ethanol next to propionate [82, 271]. Here, *A. wieringae* JM was cultivated at pH 7, which led to production of mostly acetate. However, lower pH favours ethanol production in acetogens [345]. Thus, a good strategy could be reducing the pH up to values still optimal for chain elongation (up to 6.5) [334]. While completely blocking acetate production in *A. neopropionicum* would lead to no growth on ethanol, the addition of threonine could decrease the production of acetate by *A. neopropionicum*, as it was previously reported [82, 263]. *A. neopropionicum* produces mostly propionate and butyrate during growth on threonine. In that scenario, butyrate could be in turn used by *C. kluyveri* and/or taken up by *A. wieringae* JM resulting in butanol production. On the other hand, one could use an alternative acetogen that produces more ethanol under the same conditions. For instance, *Clostridium aceticum* was shown to shift to solventogenesis at pH close to neutral (≈ 6.9) [330]. Another alternative to boost solventogenesis would be to supplement with H_2 , (i.e., to feed syngas) as model predictions showed that CO/H_2 ratios lower than 1 led to a decrease in acetate production in favour of ethanol production, both in mono-culture of *A. wieringae* JM (Fig. 5.2B) and in co-cultivation (Fig. 5.7).

In this work, metabolic modeling was shown to be a powerful tool to gain understanding into the feasibility and characteristics of synthetic co-cultures, evaluating community designs for the production of even or odd-chain MCFAs, and suggesting operational strategies for their optimization. Community models were constructed and assessed following a modular approach, where microbes were removed/added from/to the community targeting products of different chain lengths (even/odd). Furthermore, following this strategy, each of these microbes could be replaced by

another one of the like or by other type of microbes targeting alternative products. Follow-up experimental studies should be carried out to support model predictions.

Availability of data and materials

The supplementary information and the data generated during the current study are available in the following repository:

https://gitlab.com/wurssb/Modelling/triculture_aw_an_ck/-/tree/master/.

Declaration of competing interest

The authors declare that they have no known competing financial interests or personal relationships that could have influenced the work reported in this paper.

Funding

The research leading to these results has received funding from the Netherlands Science Foundation (NWO) under the Programme ‘Closed Cycles’ (Project nr. AL-WGK.2016.029) and the Netherlands Ministry of Education, Culture and Science under the Gravitation Grant nr. 024.002.002.

Acknowledgements

We thank Bart Nijssse for his valuable contribution on the annotation of the genome of *A. wieringae* JM and the orthology based approach.

Author Contributions

SBV and IPO conceived and designed the study. SBV and IPO drafted the manuscript. SBV constructed the models and performed model predictions and data analysis. IPO performed the experiments and respective data analysis. MSD conceived, designed and supervised the research. DS and VMdS acquired project funding, conceived and supervised the research. All authors reviewed and edited the study. All authors read and approved the final manuscript.

Supplementary information

Cultivation of *A. wieringae* strain JM

A. wieringae strain JM is an isolate from our own culture collection [332]. *A. wieringae* JM was cultivated anaerobically in defined medium containing (per litre): 1 g NH₄Cl, 0.7 g NaCl, 2.8 g KH₂PO₄, 1.3 g Na₂HPO₄, 0.2 g MgSO₄ × 7H₂O, 0.04 g CaCl₂ × 2H₂O, 10 mL trace element solution from DSMZ medium 318, 0.5 g yeast extract, 0.75 g L-cysteine-HCl as reducing agent and 0.5 mg resazurin as redox indicator. Vitamins were added to a final composition of (per litre): 0.5 mg pyridoxine, 0.2 mg thiamine, 0.2 mg nicotinic acid, 0.1 mg p-aminobenzoic acid, 0.1 mg D-Ca-pantothenate, 0.1 mg cobalamin, 0.1 mg riboflavin, 0.05 mg folic acid, 0.05 mg lipoic acid and 0.02 mg biotin. The pH of the medium was adjusted to 7. Pre-cultures for bioreactor experiments were set up in anaerobic bottles of 120 mL filled with 50 mL medium and with CO in the headspace (100 % v/v; 170 kPa) as substrate. Bottles were incubated at 30°C.

Bioreactor setup and operation

A. wieringae JM was cultivated in duplicate chemostat bioreactors under CO limitation. Two 0.55 L bioreactors vessel (BioXplorer 400P®, H.E.L Group, Borehamwood, United Kingdom) with a working volume of 0.4 L were operated anaerobically in continuous mode. The composition of the medium was as described above with the addition of 0.005 % (v/v) Antifoam 204. The reactor was equipped with pH, redox and temperature sensors. The system was operated at 30° C and pH 7, the latter controlled by the addition of 3 M KOH. Mass flow controllers regulated the inflow of N₂ and CO separately. Start-up of the reactor operation was done as follows: the autoclaved reactor vessel, containing only mineral medium, trace elements and resazurin, was connected to the system and flushed with N₂ (5 L h⁻¹) for ≈ 3 hours to establish anaerobic conditions. Next, the gas inflow was switched to CO/N₂ (70:30 v/v) at a total gas flowrate of 4 mL min⁻¹ (0.01 vvm). The following supplements were added aseptically to the vessel from anaerobic, sterile stock solutions: yeast extract, vitamins and L-cysteine-HCl. When the redox potential dropped below -300 mV, the reactor was inoculated with 5 % (v/v) of an exponentially-growing pure culture of *A. wieringae* JM. Agitation was set at 350 rpm for the initial batch phase, which lasted 3.8 days, and afterwards it was progressively increased to 700 rpm for continuous operation. Fresh medium was continuously supplied aseptically from a 20-L tank via a peristaltic pump (Masterflex, Germany). The medium tank was flushed with N₂ thorough the whole operation to ensure anaerobic conditions. The medium inflow pump was adjusted to give an hydraulic retention time (HRT) of 48h

(dilution rate, $D = 0.021 \text{ h}^{-1}$). Liquid samples were routinely taken for analyses of ethanol and carboxylic acids, cell density and cell dry weight (CDW). Gas samples of the headspace were taken for determination of gas composition. Gas and liquid outflow rates were regularly measured during operation.

Analytical techniques

Gaseous compounds (CO , CO_2 , H_2) were analysed in a gas chromatograph (Compact GC 4.0, Global Analyser Solutions, The Netherlands) equipped with two channels and a thermal conductivity detector (TCD). CO and H_2 were detected using a Molsieve 5A column operated at 100°C and coupled to a Carboxen 1010 pre-column. Determination of CO_2 was done in a Rt-Q-BOND column operated at 60°C . In both channels, argon was used as carrier gas. Concentrations of soluble compounds in liquid samples were determined by high-performance liquid chromatography (HPLC; LC-2030C, Shimadzu, Japan). The apparatus was equipped with a Shodex SH1821 column operating at 55°C . $0.01 \text{ N H}_2\text{SO}_4$ was used as eluent and the flow rate set at 1 mL min^{-1} . Amounts detected in a concentration $< 0.3 \text{ mM}$ could not be accurately quantified and are considered traces. The Chromeleon™ data analysis software (Thermo Fisher Scientific), version 7.2.9, was used for both GC and HPLC peak analysis. Microbial growth was estimated based on the measurement of optical density at 600 nm (OD600) using a spectrophotometer (UV-1800, Shimadzu, Japan). CDW was determined by gravimetric analysis: pellets from a known culture volume ($\sim 50 \text{ mL}$) were washed twice in deionized water, resuspended and transferred into pre-weighed aluminium trays. These were dried overnight at 103°C and weighed again the day after.

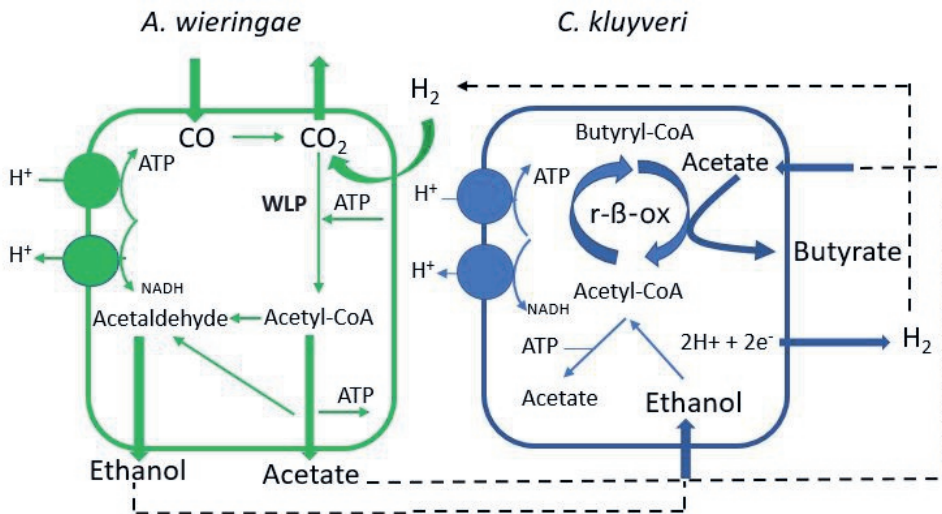


Figure S5.1: Schematic representation of the fermentation of CO by *A. wieringae* and *C. kluyveri*. WLP: Wood–Ljungdahl pathway; r-β-ox: Reverse β-oxidation pathway. Arrows indicate the direction of the flux. Ticker arrows shows production or consumption of the indicated metabolites. Additionally, part of CO₂ produced by *A. wieringae* is consumed by *C. kluyveri*.

Chapter 6

Model-driven approach for the production of butyrate from CO₂/H₂ by a novel co-culture of *C. autoethanogenum* and *C. beijerinckii*

Sara Benito-Vaquerizo*, Niels Nouse*, Peter J. Schaap, Jeroen Hugenholtz, Stanley Brul, Vitor Ana M. López-Contreras, Martins dos Santos, Maria Suarez-Diez
Published in: Front. Microbiol. 13 (2022).

doi.org/10.3389/fmicb.2022.1064013

* Contributed equally

6.1 Abstract

One-carbon (C1) compounds are promising feedstocks for the sustainable production of commodity chemicals. CO₂ is a particularly advantageous C1-feedstock since it is an unwanted industrial off-gas that can be converted into valuable products while reducing its atmospheric levels. Acetogens are microorganisms that can grow on CO₂/H₂ gas mixtures and syngas converting these substrates into ethanol and acetate. Co-cultivation of acetogens with other microbial species that can further process such products, can expand the variety of products to, for example, medium chain fatty acids (MCFA) and longer chain alcohols. Solventogens are microorganisms known to produce MCFA and alcohols via the acetone-butanol-ethanol (ABE) fermentation in which acetate is a key metabolite. Thus, co-cultivation of an ace-

togen and a solventogen in a consortium provides a potential platform to produce valuable chemicals from CO₂.

In this study, metabolic modelling was implemented to design a new co-culture of an acetogen and a solventogen to produce butyrate from CO₂/H₂ mixtures. The model-driven approach suggested the ability of the studied solventogenic species to grow on lactate/glycerol with acetate as co-substrate. This ability was confirmed experimentally by cultivation of *Clostridium beijerinckii* on these substrates in batch serum bottles and subsequently in pH-controlled bioreactors.

Community modelling also suggested that a novel microbial consortium consisting of the acetogen *Clostridium autoethanogenum*, and the solventogen *C. beijerinckii* would be feasible and stable. On the basis of this prediction, a co-culture was experimentally established. *C. autoethanogenum* grew on CO₂/H₂ producing acetate and traces of ethanol. Acetate was in turn, consumed by *C. beijerinckii* together with lactate, producing butyrate.

These results show that community modelling of metabolism is a valuable tool to guide the design of microbial consortia for the tailored production of chemicals from renewable resources.

6.2 Introduction

The energy crisis and the effects of climate change have emphasised the need to accelerate the transition towards a circular bio-based economy [346]. Current circular approaches focus on the application of microbial conversion to convert low-value carbon feedstocks, such as biomass waste streams, into commodity chemicals [347]. Recalcitrant lignocellulosic biomass can be pretreated and hydrolysed into sugars [348] or gasified to produce synthesis gas (syngas), a one-carbon (C1) feedstock consisting of a mixture of CO, CO₂ and H₂ [349]. In addition, C1-rich industrial waste gases from steel and thermal power plants can be directly used as microbial feedstocks [350]. In this regard, CO₂ is an advantageous one-carbon feedstock (C1) since it can be obtained from natural and industrial sources, and can be converted into valuable products reducing the release of contaminant gases to the environment.

Acetogens are strict anaerobes that can grow on CO₂/H₂ and syngas as their sole carbon source using the Wood-Ljungdahl metabolic pathway [131, 328]. Acetogenic fermentation of C1 gases leads mainly to the production of acetate and ethanol, as well as, 2,3-butanediol or lactate [56, 351], and the production of ethanol has been commercialised recently [49, 352]. Acetogens that grow autotrophically on these slightly soluble gases are energy limited and produce a constrained product spectrum and low product titres. This can be overcome by exploring alternative strategies, such as mixotrophic growth or co-cultivation [353].

Solventogenic Clostridia have been widely applied to ferment sugars into mixtures of the solvents acetone, butanol and ethanol (ABE) [354] or in some cases isopropanol, butanol, ethanol (IBE) [355]. These fermentations consist of an acidogenic phase followed by a solventogenic phase. During acidogenesis, solventogens produce carboxylic acids (mainly acetate and butyrate), and CO₂ and H₂. Accumulation of carboxylic acids and the concomitant lowering of the pH trigger solventogenesis during which solventogens reduce the carboxylic acids into solvents [356].

Cross-feeding strategies have been used to establish synthetic microbial communities that produce a wider product range [64, 68, 269, 357]. Therefore, co-cultivation of an acetogen and a solventogen has the potential to overcome the drawbacks associated to acetogens by increasing the product spectrum. Charubin and Papoutsakis [69] recently established a co-culture of the solventogen *Clostridium acetobutylicum* and the acetogen *Clostridium ljungdahlii*. In this setup, glucose was metabolised by *C. acetobutylicum* to butanol, ethanol, acetone, acetoin, CO₂ and H₂. Subsequently, CO₂ and H₂ were fixed, and acetone and acetoin were reduced to isopropanol and 2,3-butanediol, respectively, by *C. ljungdahlii*.

Acetate is one of the most abundant products in acetogens [358], and while solventogenic strains cannot grow on acetate as sole carbon source, they can re-assimilate acetate and convert it into carboxylic acids such as butyrate, or solvents when glucose is used as co-substrate [359–361]. Therefore, in a co-culture of acetogens/solventogens on CO₂/H₂, butyrate could be produced as main product. Butyrate is a valuable product as it is used in many commercial applications, as a solvent, cosmetic, food, animal feed or as a precursor of pharmaceuticals [362, 363].

In this study, we followed a model-driven approach to find an alternative route for production of butyrate. We produced butyrate from CO₂ using a co-culture of two strains, one acetogen producing acetate from CO₂/H₂, and one solventogenic strain that co-metabolised acetate with an alternative carbon source into butyrate. To select the solventogenic strain, we systematically assessed growth on several carbon sources using the genome-scale metabolic models (GEMs) of *C. acetobutylicum* and *Clostridium beijerinckii*. The most promising carbon sources were experimentally tested and validated. On the basis thereof, we constructed a community model of *C. autoethanogenum* and *C. beijerinckii*, and qualitatively assessed the fermentation of CO₂/H₂ and the new carbon source through scenario simulations. Model predictions guided the experimental work and led to the successful establishment of this new co-culture.

6.3 Materials and Methods

6.3.1 GEM availability and curation

The GEM of *C. autoethanogenum* DSM 10061, iCLAU786 [219] was downloaded in sbml and table format and used without modification.

The GEM of *C. acetobutylicum* ATCC 824, iCac802 [364] was downloaded in sbml and table format, and modified as follows: Two reactions were defined as reversible: ATP:3-phospho-D-glycerate 1-phosphotransferase (with model identifier R0239), and Hydrogenase (R1563). Formate dehydrogenase (R1562) was removed since it was not found in the genome of *C. acetobutylicum*. Three new reactions were added in the model: Pyruvate transport (pyrt), Pyruvate exchange (EX_PYR_e), and glycerol kinase (R0426), the latter reaction was found to be present in the genome of *C. acetobutylicum* (EC 2.7.1.30; locus tag: CAC1321). Finally, we replaced the ethanol transport reaction (R1708), expressed as a proton (H⁺) symport reaction, by a diffusion transport reaction. The modified version of the model (iCac803) is available at: https://gitlab.com/wurssb/Modelling/coculture_cacb.

The GEM of *C. beijerinckii* NCIMB 8052, iCM925 [295] was downloaded in sbml and table format and modified as follows: Ferredoxin-NAD⁺ reductase (FDXNRx) and ferredoxin-NADP⁺ reductase (FDXNRy) reactions were removed, and Na⁺-translocating ferredoxin:NAD⁺ oxidoreductase (Rnf) complex and electron-bifurcating, ferredoxin-dependent transhydrogenase (Nfn) complex, were added to the model. Transport of hydrogen reaction (Habc) was replaced by the ATPase reaction (ATPase). The EC number and genes of (S)-3-Hydroxybutanoyl-CoA:NADP⁺ oxidoreductase reaction (HACD1y) were modified and the EC numbers of butyryl-CoA dehydrogenase (ACOAD1) and 3-hydroxybutyryl-CoA dehydrogenase (HACD1x) as well. Finally, the reduced ferredoxin:dinitrogen oxidoreductase (ATP-hydrolysing) reaction (DNOR) was stoichiometrically balanced. The updated version of the model (iCM943) is available in the git repository.

6.3.2 *In-silico* carbon source screening in *C. acetobutylicum* and *C. beijerinckii*

We systematically assessed growth capabilities on the updated versions of the GEMs of *C. acetobutylicum* and *C. beijerinckii* on a wide range of carbon sources. Model simulations were done using COBRAPy, version 0.15.4 [235], and Python 3.9. Growth capabilities were assessed using Flux Balance Analysis (FBA). The biomass synthesis reaction (termed 'Biomass' or 'biomass' in the respective *C. acetobutylicum* and *C. beijerinckii* models), was defined as the objective function for maximisation. Growth was considered when the growth rate was higher than 0.0001 h⁻¹. For each assessed

carbon source, the maximum uptake (corresponding to minus the lower bound of the associated exchange reaction denoted 'EX_xx') was constrained to $20 \text{ mmol g}_{\text{DW}}^{-1} \text{ h}^{-1}$, and the minimum uptake (corresponding to minus the upper bound of the associated exchange reaction) was constrained to $0.1 \text{ mmol g}_{\text{DW}}^{-1} \text{ h}^{-1}$. In addition, uptake of small metabolites and ions was allowed by setting the lower bound of the corresponding exchange reaction to -1000 as described in the corresponding script in the git repository.

6.3.3 Co-culture GEM reconstruction

A compartmentalised co-culture model of *C. autoethanogenum* and *C. beijerinckii* was obtained by combining single species models iCLAU786 [219] and iCM943 [295], following a previous approach [51]. In this approach, each species is considered a single compartment. The compartment associated with *C. autoethanogenum* was defined as 'cytosol_ca' and the compartment associated with *C. beijerinckii* was defined as 'cytosol'. Intracellular metabolites were assigned to their respective compartment and the flag '_ca' was added to the identifier of metabolites belonging to 'cytosol_ca' to distinguish them from the *C. beijerinckii* metabolites. In addition, the combined model included an extracellular compartment, defined as 'extracellular', common to both species. Metabolites in this compartment are either secreted, metabolised or exchanged by both species, and separated from metabolites present in the cellular compartments by adding the '_e' flag to the identifier. All extracellular metabolites follow the same naming system (namespace) for both species. Therefore, the same namespace was applied to metabolites secreted by both species. All metabolites present in both intracellular compartments and the extracellular compartment can be exchanged between species if favoured by the directionality. Interchanged metabolites are assumed to be first transported into the extracellular compartment, before taken up by the other species using the corresponding exchange reaction. The co-culture GEM contains one biomass synthesis reaction per species, termed 'biomass_auto' and 'biomass_beije' for *C. autoethanogenum* and *C. beijerinckii*, respectively. Additionally, the model contains a community biomass synthesis reaction ('Community_biomass'), which incorporates the biomass of *C. autoethanogenum* and *C. beijerinckii* in the form of metabolite 'biomass_ca' and metabolite 'biomass', respectively. The combined model incorporates a transport reaction of butyrate ('BU-*Tex_au*') from the extracellular compartment to the intracellular compartment of *C. autoethanogenum*, and the reaction to produce butyraldehyde from butyrate ('but-tobuta') in *C. autoethanogenum*. In addition, we incorporated the transport reaction of acetone ('ACETONE_ca') from the extracellular compartment to the intracellular compartment of *C. autoethanogenum*; an alcohol dehydrogenase to convert acetone into isopropanol ('ISOBIO'); a transport reaction of isopropanol from the intracel-

lular compartment of *C. autoethanogenum* to the extracellular compartment ('ISO-PRO_ca'), and an exchange reaction of isopropanol ('EX_IPRO_e').

The final three-compartment co-culture model was translated into SBML level 3 version 1 (see git repository).

6.3.4 Co-culture modelling framework

Co-culture model simulations were carried out using a previously described modelling framework [51], similar to SteadyCom [365], and based on Community FBA (cFBA) [221]. Specific fluxes ($\text{mmol g}_{\text{DW}}^{-1} \text{h}^{-1}$) were substituted by environmental fluxes ($\text{mmol L}^{-1} \text{h}^{-1}$), and thus, the biomass synthesis reaction of each species was changed accordingly accounting for the growth rate and biomass of each species ($\text{g}_{\text{DW}} \text{L}^{-1} \text{h}^{-1}$). The relative contribution of each species to the community biomass was calculated from the total biomass of the community and the species ratio.

6.3.5 Co-culture model simulations

In this study, we simulated hypothetical scenarios varying biomass species ratios, growth rates, and substrates environmental fluxes to explore the feasible solution space of the co-culture. We selected a community biomass of $0.22 \text{ g}_{\text{DW}} \text{L}^{-1}$ based on the average value measured for a similar co-culture of *C. autoethanogenum* and *Clostridium kluyveri* on syngas [68]. The biomass of each species was calculated based on the indicated species ratio and the community biomass. The biomass of each species was multiplied by the indicated growth rate, and the value was used to constrain the flux through the biomass synthesis reaction of each species. We assessed conditions with *C. autoethanogenum* - *C. beijerinckii* ratios ranging from 0.1-0.9 to 0.9-0.1, and growth rates from 0.005 to 0.1 h^{-1} . For this exploratory analysis, we assumed equal growth rates for each species and steady-state. For each condition, we fixed the uptake rate of CO_2 and H_2 to $5 \text{ mmol L}^{-1} \text{h}^{-1}$ or to $2.5 \text{ mmol L}^{-1} \text{h}^{-1}$, covering values found in literature for a similar co-culture [68]. The maximum lactate uptake rate was constrained to 2.5 or $5 \text{ mmol L}^{-1} \text{h}^{-1}$ and a minimum uptake rate of $0.1 \text{ mmol L}^{-1} \text{h}^{-1}$ was imposed. We defined the community biomass reaction ('Community_biomass') as the objective function and we performed FBA to assess the feasibility of each condition. For a selected number of feasible conditions, the solution space and the set of fluxes compatible with the measured constraints were sampled using the *sample* function in the flux_analysis submodule of COBRAPy. Presented results show the average and standard deviation based on 5000 iterations generated at each condition (git repository).

6.3.6 Bacterial strains

The laboratory strains *C. beijerinckii* NCIMB 8052 and *C. acetobutylicum* ATCC 824 were stored as spore suspensions in 20% glycerol at -20 °C. Spores of *C. beijerinckii* and *C. acetobutylicum* were heat-activated for 1 min at 95 °C and 10 min at 70 °C, respectively, before inoculation. *C. autoethanogenum* DSM 10061 was kindly provided by Professor Diana Z. Sousa from the Laboratory of Microbiology, Wageningen University and Research, Wageningen, the Netherlands, and was stored as vegetative cells suspended in 25% glycerol buffered with phosphate and reduced with Ti(III)citrate under anoxic conditions at -80 °C.

6.3.7 Experimental carbon source screening of *C. acetobutylicum* and *C. beijerinckii*

Cultures were prepared in serum bottles containing CM2 medium consisting of the following components: 2.5 g L⁻¹ yeast extract (Duchefa Biochemie), 1.0 g L⁻¹ KH₂PO₄ (Fischer Scientific), 0.61 g L⁻¹ K₂HPO₄ (Sigma-Aldrich), 1 g L⁻¹ MgSO₄·7H₂O (Roth), 2.9 g L⁻¹ ammonium acetate (USB), 0.10 g L⁻¹ 4-aminobenzoic acid (Duchefa Biochemie), 6.6 mg L⁻¹ Fe(II)SO₄·7H₂O (Sigma-Aldrich), and 0.5 mg L⁻¹ Na-resazurin (Sigma-Aldrich). Acetic acid (Sigma-Aldrich), L-lactic acid (~90%, Merck), ethanol (Merck) and glycerol (Sigma-Aldrich) were added to final concentrations of 40 mM. pH was set to pH 6.1-6.2 with KOH and/or HCl. Media were made anoxic with N₂(g) and autoclaved. D-Glucose was made anoxic and autoclaved separately and added to a final concentration of 40 mM. Media were inoculated with 4% (v/v) culture made from heat-activated spore suspension grown overnight at 37 °C in CM2 medium supplemented with 40 g L⁻¹ D-glucose (Duchefa Biochemie). Cultures were incubated at 37 °C and sampled at t₀ and after 4 d. Cell density was measured as optical density at 600 nm (OD₆₀₀), extracellular metabolites were analysed with high-performance liquid chromatography (HPLC) as described in section 6.3.9, and pH was measured. Acetate co-assimilation was determined by calculating the fraction of the total converted carbon coming from consumed acetate.

6.3.8 Cultivation experiments in pH-controlled bioreactors

pH-controlled bioreactor experiments were performed in a working volume of 2 L in Infors HT Labfors 5 bioreactors (Infors HT, Switzerland). The stirrer, set at 150 rpm, consisted of at equidistance from top to bottom a pitch-blade and two Rushton impellers. Temperature was controlled at 37 °C and pH at pH 5.5 ± 0.1 using 3 M KOH and 2 M H₃PO₄. Foaming was controlled with Antifoam 204 (Sigma-Aldrich). 2.9 g L⁻¹ ammonium acetate in the CM2 medium was replaced by 2.5 g L⁻¹

ammonium sulfate (Merck). 0.75 g L^{-1} anoxic and sterilized L-cysteine HCl·H₂O (Merck) was added after autoclaving.

In pH-controlled batch fermentations of *C. beijerinckii* growing on different concentrations of acetate and lactate, the adapted CM2 medium was supplemented with acetic acid and L-lactic acid prior to autoclaving. 10 mL min^{-1} N₂(g) was flushed across the head space to keep anoxic conditions. Reactors were inoculated with 1% (v/v) *C. beijerinckii* culture growing overnight at 37 °C in CM2 medium supplemented with 20 g L^{-1} D-glucose and 0.75 g L^{-1} L-cysteine HCl·H₂O. Cultures were sampled at regular time intervals for analysis of cell density, extracellular metabolites, and morphology with phase-contrast microscopy. The overall stoichiometry was calculated by scaling the difference of the concentrations of the main extracellular metabolites between t_0 and t_{end} to the difference in the measured lactate concentration.

In pH-controlled fed-batch co-cultivation experiments of *C. autoethanogenum* and *C. beijerinckii*, reactors were equipped with sinter spargers to flush 40 mL min^{-1} H₂(g) and 10 mL min^{-1} CO₂(g) through the medium. At t_0 , reactors were inoculated with <1% (v/v) *C. autoethanogenum* culture growing at 37 °C in CM2 medium supplemented with 10 g L^{-1} D-fructose (VWR Chemicals) and 0.75 g L^{-1} L-cysteine HCl·H₂O. After establishment of growth and acetate production by *C. autoethanogenum*, reactors were inoculated with <1% (v/v) *C. beijerinckii* culture growing overnight at 37 °C in CM2 medium supplemented with 20 g L^{-1} D-glucose and 0.75 g L^{-1} L-cysteine HCl·H₂O. Furthermore, the continuous L-lactic acid feed was started. Cultures were sampled at regular time intervals for analysis of cell density, extracellular metabolites, and morphology with phase-contrast microscopy. Theoretical acetate production from CO₂ was calculated for each time point after the start of the L-lactic acid feed as follows: The amount of lactate converted was calculated from the difference in the amount of lactate fed and calculated amount of lactate remaining in the reactor. The conversion of lactate via pyruvate yields the intermediate metabolite acetyl-CoA and CO₂ in a 1:1 ratio. The fraction of the amount of carbon from lactate available for the formation of products was subtracted from the amount of carbon present in the produced (iso)butyrate to obtain a theoretical amount of carbon coming from a difference source than lactate, i.e., from converted acetate. This theoretical amount of converted acetate was added to the calculated amount of acetate in the reactor to get a theoretical amount of acetate produced from CO₂. Subsequently, the stoichiometry for the production of (iso)butyrate from lactate and acetate was calculated by scaling the difference of (iso)butyrate produced, theoretical acetate converted, and lactate converted between t_0 and the selected time points to lactate converted.

6.3.9 Analysis of extracellular metabolites

Concentrations of acetate, acetone, butanol, (iso)butyrate, ethanol, fructose, glycerol, glucose, and lactate were analysed with HPLC. Supernatant was mixed with an equal volume of 1 M H₂SO₄ with 30 mM 4-methylpentanoic or 100 mM pentanoic acid as internal standard. This was filtered through a 0.2 μm regenerated cellulose filter followed by analysis on a Waters HPLC system with a Shodex KC-811 column at 65 °C, 1 mL/min 3 mM H₂SO₄ mobile phase, and a refractive index and UV detector.

6.4 Results

Fig. 6.1 shows the steps for the model-driven approach followed to establish a novel co-culture of *C. autoethanogenum* and *C. beijerinckii* for the production of butyrate from CO₂/H₂. GEMs of solventogens were used to evaluate candidate species and possible carbon sources. After the experimental validation of the model predictions, the co-culture was successfully established.

6.4.1 Updated GEMs of *C. autoethanogenum*, *C. acetobutylicum* and *C. beijerinckii*

The GEM of *C. autoethanogenum*, iCLAU786 was used as the original version [219] with no modification. The updated version of the GEM of *C. acetobutylicum*, iCac803 [364], had 1254 reactions, 1465 reactions and 803 genes, and the GEM of *C. beijerinckii*, iCM943 [295], had 881 metabolites, 941 reactions and 943 genes.

Regarding the GEM of *C. beijerinckii*, we included the Na⁺-translocating ferredoxin:NAD⁺ oxidoreductase (Rnf) complex (EC 7.2.1.2) in the model of *C. beijerinckii*. Rnf is formed by the following gene cluster: *rnfC*, *rnfD*, *rnfG*, *rnfE*, *rnfA*, *rnfB*, (locus_tag: Cbei_2449, Cbei_2450, Cbei_2451, Cbei_2452, Cbei_2453 and Cbei_2454, respectively). Additionally, we have identified an electron-bifurcating, ferredoxin-dependent transhydrogenase (Nfn) complex that catalyses NADH-dependent reduced Ferredoxin:NADP⁺ oxidoreductase activity in *C. beijerinckii*. The Nfn complex has two subunits: NAD(P)-binding subunit, and a glutamate synthase subunit. These two subunits showed 56% to 79% identity with the Nfn subunits of *C. kluyveri*, *C. autoethanogenum*, *C. difficile* [366], and of the recently annotated *Anaerotignum neo-propionicum* [82], forming two possible complexes: (Cbei_2182 and Cbei_2183) or (Cbei_0661 and Cbei_0662). To our knowledge, this is the first time the Nfn complex is reported in *C. beijerinckii* NCIMB 8052. Ferredoxin NAD⁺ reductase (EC 1.18.1.3) is not found in the genome of *C. beijerinckii*, and the ferredoxin NADP⁺ reductase

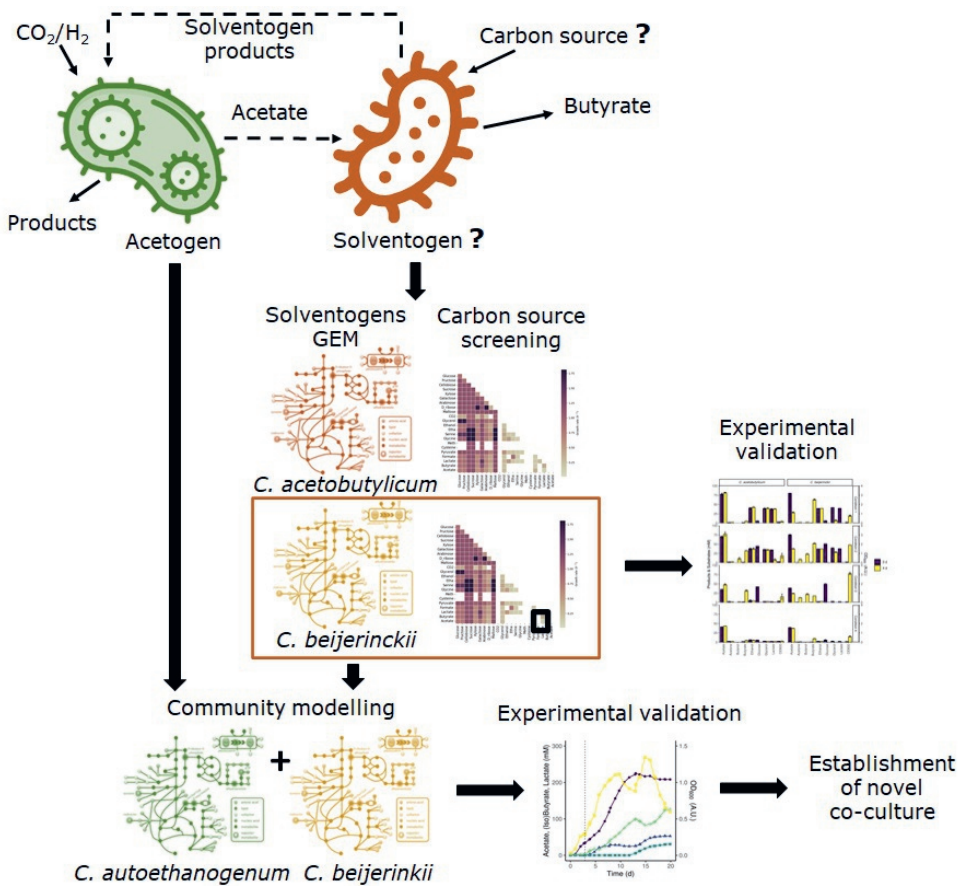


Figure 6.1: Overview of the followed methodology to establish a co-culture of an acetogen and a solventogen to produce butyrate from CO_2/H_2 . We used genome-scale metabolic models of two solventogens to assess growth on several carbon sources and to find the alternative carbon source that sustained growth on the solventogen with acetate. The predicted carbon sources were experimentally validated and growth was confirmed in one of the solventogens. After that, we assessed the feasibility of the co-culture of the acetogen *C. autoethanogenum* and the selected solventogen using community modelling, and finally, the co-culture was experimentally established.

(EC 1.18.1.2) showed lower percentage identity to the FNR of *C. acetobutylicum*, and thus, we hypothesised that the former FNR corresponds to the NADP-binding sub-

unit of the Nfn complex.

6.4.2 *In-silico* carbon source screening of *C. acetobutylicum* and *C. beijerinckii*

We explored growth on 25 carbon sources individually and pairs of these carbon sources with one another in the model of *C. acetobutylicum* (Fig. 6.2). Growth was

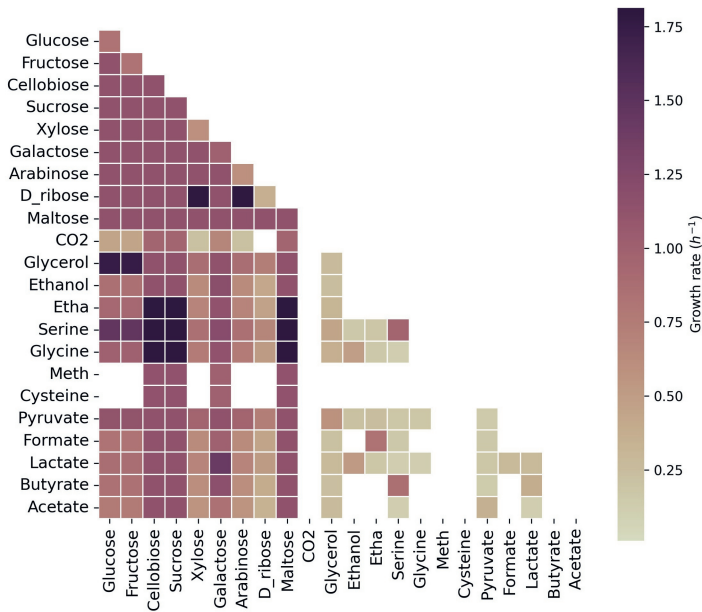


Figure 6.2: Growth capabilities predicted for *C. acetobutylicum*. The color scale shows growth rates in h^{-1} . Squares on the diagonal correspond to single carbon sources. Squares below the diagonal correspond to the combination of the carbon source presented on the x-axis with the carbon source presented on the y-axis. Non-colored squares show that no growth was predicted for the specified carbon source(s). Meth: Methionine; Etha: Ethanolamine. The maximum uptake rate for each carbon source was set to $20 \text{ mmol g}_{\text{DW}}^{-1} \text{ h}^{-1}$ and the minimum to $0.1 \text{ mmol g}_{\text{DW}}^{-1} \text{ h}^{-1}$.

predicted on sugars, glycerol, lactate, serine and pyruvate as single carbon sources, reaching the highest growth rates on cellobiose, sucrose and maltose. As expected,

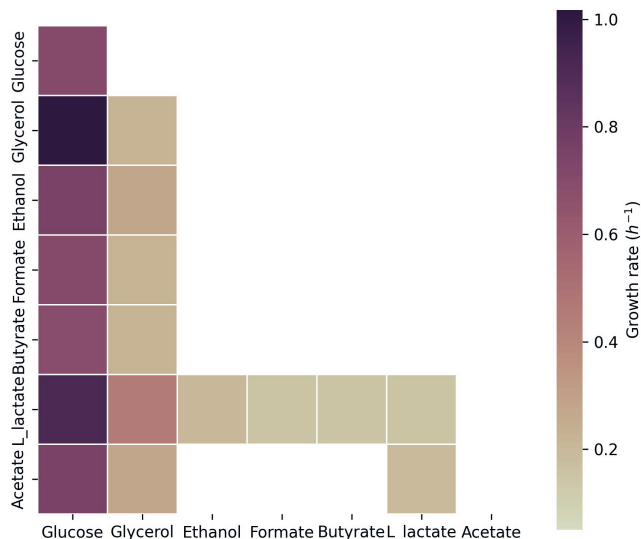


Figure 6.3: Growth capabilities predicted for *C. beijerinckii*. The color scale shows growth rates in h^{-1} . Squares on the diagonal correspond to single carbon sources. Squares below the diagonal correspond to the combination of the carbon source presented on the x-axis with the carbon source presented on the y-axis. Non-colored squares show that no growth was predicted for the specified carbon source(s). The maximum uptake rate for each carbon source was set to $20 \text{ mmol g}_{\text{DW}}^{-1} \text{ h}^{-1}$ and the minimum to $0.1 \text{ mmol g}_{\text{DW}}^{-1} \text{ h}^{-1}$.

acetate did not sustain growth as the sole carbon source and neither was sustained on acetone, succinate, acetoin (not shown here). Pairwise combinations of most carbon sources that led to growth as single carbon source, also led to growth in combination with an alternative carbon source. However, L-methionine, L-cysteine and CO_2 did not show growth in combination with carbon sources that sustained growth alone since the model was forced to uptake a minimum amount of each carbon source, leading in some cases, to infeasible solutions. The highest growth rates were obtained with cellobiose, sucrose or maltose in combination with serine, glycine or ethanolamine; the combination of glucose or fructose with glycerol, and xylose, or arabinose with ribose. Interestingly, acetate, in combination with lactate or glycerol, could sustain

growth in *C. acetobutylicum*, as previously described for other solventogens [367, 368].

Additionally, we assessed growth on glucose, glycerol, ethanol, formate, butyrate, lactate and acetate in the model of *C. beijerinckii* (Fig. 6.3). As observed for *C. acetobutylicum*, *C. beijerinckii* only sustained growth on glucose, glycerol and lactate as single carbon sources. Pairwise combinations of the latter carbon sources sustained growth in combination with the rest of carbon sources. The highest growth rates were obtained with glucose in combination with glycerol or lactate. Here, acetate with lactate or glycerol also sustained growth, being the growth rate higher with addition of acetate in both scenarios.

6.4.3 Growth of *C. acetobutylicum* and *C. beijerinckii* on lactate and acetate

The substrate space provided by the model was used in an initial screening to assess growth and co-assimilation of acetate on various carbon sources by the solventogens *C. acetobutylicum* and *C. beijerinckii* (Fig. 6.4). On all assessed carbon sources *C. beijerinckii* grew to higher cell densities after 4 days than *C. acetobutylicum*, which is known to produce autolysins towards the end of the exponential growth phase [369]. As predicted by the models (Fig. 6.2 and Fig. 6.3), neither strain grew on acetate alone (Fig. 6.4; Condition 4), as both strains only converted the residual metabolites from the inoculum, i.e., glucose. This showed the need for an additional carbon source to co-assimilate acetate. Contrary to the model predictions (Fig. 6.2), *C. acetobutylicum* did not grow on acetate with lactate, glycerol and ethanol as co-substrates under the tested conditions. However, the model predictions for *C. beijerinckii* (Fig. 6.3) were confirmed, and acetate was co-assimilated using all lactate and part of the glycerol into butyrate (Fig. 6.4; Condition 1). Both solventogens further reduced butyrate to butanol with the addition of glucose (Fig. 6.4; Condition 2). The fraction of carbon coming from acetate in the products produced by *C. beijerinckii* was not improved by the addition of glucose to the medium, and was highest in the medium containing only acetate, ethanol, glycerol and lactate (Fig. 6.4; Condition 1-3, Table S1).

Growth of *C. beijerinckii* on lactate and acetate was further explored in a bioreactor at a controlled pH of 5.5 (Fig.S1). This pH is close to the optimal pH of *C. autoethanogenum* [211], and acid re-assimilation and ABE production in *C. beijerinckii* [359, 370]. Butyrate was the most abundant product and the stoichiometry was as follows: consumption of one mol lactate and 0.4-0.5 mol acetate produced 0.6-0.7 mol butyrate. This was similar to the stoichiometry reported for *Clostridium saccharobutylicum* NCP 262, previously known as *Clostridium acetobutylicum* P262 [371], growing on lactate and acetate [367].

The screening of the solventogens *C. acetobutylicum* and *C. beijerinckii* on various carbon sources showed that the combination of *C. beijerinckii* and lactate was most promising for the re-assimilation of acetate produced from CO₂/H₂ by *C. autoethanogenum* in a future co-culture.

6.4.4 Fermentation of lactate and acetate by *C. beijerinckii*

In *C. beijerinckii*, lactate is oxidised to pyruvate via NAD-independent L-lactate dehydrogenase (EC 1.1.1.27) encoded by the following isoenzymes: Cbei_4072, Cbei_4903 or Cbei_2789 (Fig. 6.5). Pyruvate is decarboxylated to acetyl-CoA via pyruvate:

ferredoxin oxidoreductase (PFOR; EC 1.2.7.10, encoded by Cbei_1853, Cbei_4318 or Cbei_1458), generating reduced ferredoxin and CO₂. Model predictions showed that reduced ferredoxin is partly spent to produce H₂ and oxidised ferredoxin via ferredoxin hydrogenase (EC 1.12.7.2, Cbei_0327, Cbei_4000 or Cbei_3796), and partly spent to regenerate oxidised ferredoxin and NADH via the Rnf complex (EC 7.2.1.2, Cbei_2449-55), translocating Na⁺/H⁺ [372]. The Rnf complex is coupled to an ATPase (EC 7.1.2.2) encoded by the cluster Cbei_0412 to Cbei_0419, that pumps in Na⁺/H⁺ for energy generation. Model predictions suggested that acetate is converted into acetyl phosphate (acetyl-P) investing ATP by acetate kinase (EC 2.7.2.1, Cbei_1165), and acetyl-P is converted into acetyl-CoA via phosphate acetyltransferase (EC 2.3.1.8, Cbei_3402 or Cbei_1164). As previously mentioned, *C. beijerinckii* produces butyrate via acetyl-CoA [373]. First, two acetyl-CoA molecules are converted into one acetoacetyl-CoA by acetoacetyl-CoA thiolase (EC 2.3.1.9, Cbei_0411 or Cbei_3630). Acetoacetyl-CoA is reduced to 3-hydroxybutyryl-CoA via (S)-3-Hydroxybutanoyl-CoA:NAD⁺ oxidoreductase (EC 1.1.1.157, Cbei_0325) or via NAD(P)-dependent acetoacetyl-CoA reductase (EC 1.1.1.36, Cbei_5834). Then, 3-hydroxybutyryl-CoA is converted into crotonyl-CoA by 3-hydroxybutyryl-CoA dehydratase (EC 4.2.1.55, Cbei_2034 or Cbei_4544). Crotonyl-CoA is reduced via the butyryl-CoA dehydrogenase/electron-transferring flavoprotein complex (Bcd-EtfAB) producing reduced ferredoxin. Two complete clusters were identified in the genome: Cbei_0322 (Bcd), Cbei_0323 (EtfB) and Cbei_0324 (EtfA) or Cbei_2035 (Bcd), Cbei_2036 (EtfB) and Cbei_2037 (EtfA). An acyl-CoA dehydrogenase (Acd) showed 79.4% similarity with the Bcd subunit of *C. acetobutylicum* ATCC 824. Butyrate can be produced from butyryl-CoA via two routes in *C. beijerinckii*. The first route is a linear pathway in which butyryl-CoA is first converted into butyryl phosphate via butanoyl-CoA:phosphate butanoyltransferase (Ptb; EC 2.3.1.19, Cbei_0203). Butyryl phosphate is then converted into butyrate producing ATP via butyrate kinase (Buk; EC 2.7.2.7, Cbei_0204). The second route is catalysed by a butyryl-CoA-acetoacetate CoA-transferase (EC 2.8.3.9, Cbei_2654 or Cbei_2653 or Cbei_3834 or

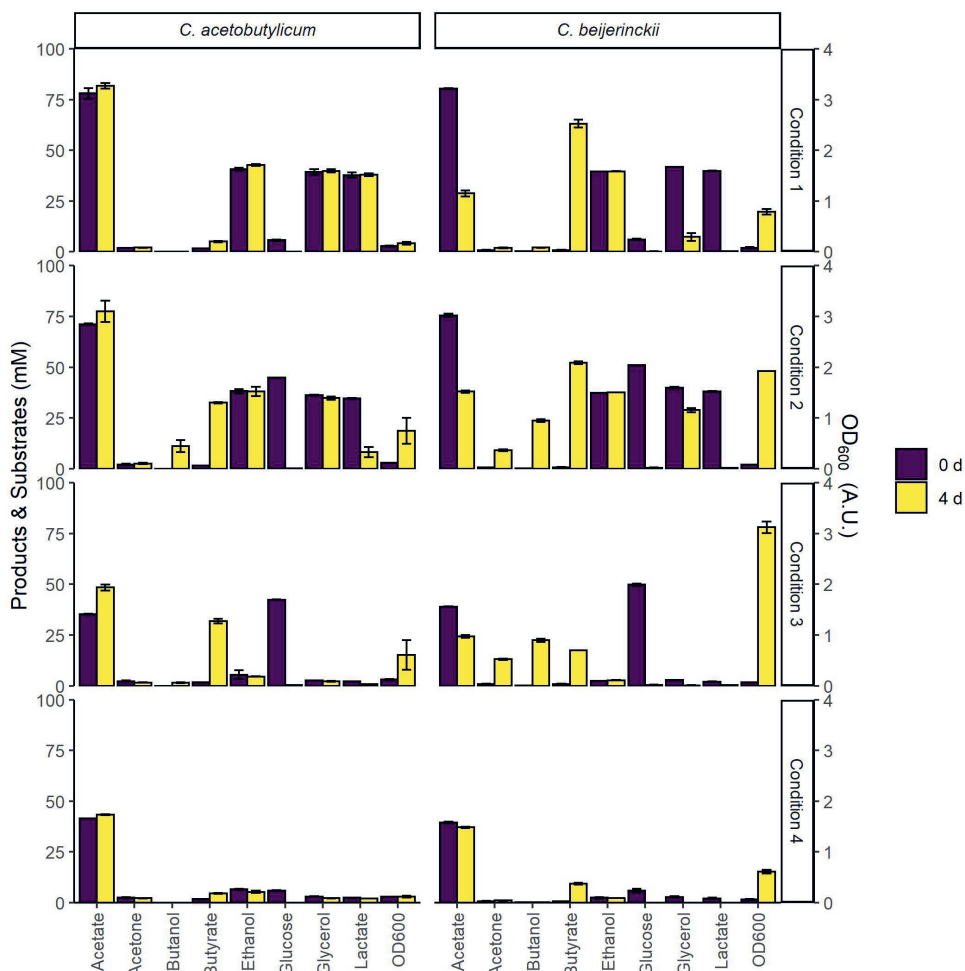


Figure 6.4: Initial screening of *C. beijerinckii* and *C. acetobutylicum* for growth on various combinations of carbon sources. The bars indicate substrate and product concentrations, and cell density at the time of inoculation and after 4 days. CM2 medium, containing 38 mM acetate, was supplemented with 40 mM of each of the various carbon sources as follows: **Condition 1**: acetic acid, ethanol, glycerol, and L-lactic acid; **Condition 2**: acetic acid, ethanol, glycerol, L-lactic acid and glucose; **Condition 3**: glucose. **Condition 4**: none. Error bars show standard deviations between two cultures inoculated with the same inoculum.

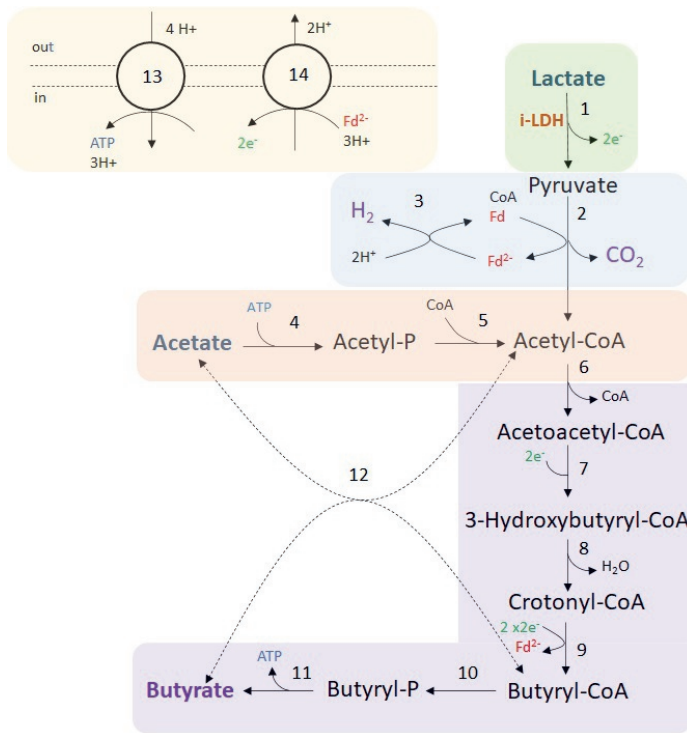


Figure 6.5: Fermentation of lactate and acetate by *C. beijerinckii*. Coloured areas correspond to the following modules: lactate oxidation (green); H_2 , CO_2 , and acetyl-CoA production (blue); acetate consumption (red); butyrate production (purple); and redox cofactor regeneration, and ATPase (yellow). Numbers in reactions correspond to the following enzymes and reaction identifiers in the model: 1, NAD-independent L-lactate dehydrogenase (LDH_L); 2, pyruvate:ferredoxin oxidoreductase (POR4); 3, Ferredoxin hydrogenase (FDXNH); 4, acetate kinase (ACK); 5, phosphate acetyltransferase (PTA); 6, Acetoacetyl-CoA thiolase (ACACT1); 7, (S)-3-Hydroxybutanoyl-CoA:NAD⁺ oxidoreductase or NAD(P)-dependent acetoacetyl-CoA reductase (HACD1x or HACD1y); 8, 3-hydroxybutyryl-CoA dehydratase (3HBCD); 9, Butyryl-CoA dehydrogenase/electron-transferring flavoprotein complex (Bcd-EtfAB) (ACOAD1); 10, Butanoyl-CoA:phosphate butanoyltransferase (BCOPBT); 11, Butyrate kinase (BUTK); 12, Butyryl-CoA-acetoacetate CoA-transferase (COAT2); 13, ATPase (ATPase); 14, Na⁺-translocating ferredoxin:NAD⁺ oxidoreductase complex (Rnf). Dashed lines (reaction 12) indicate that the reaction might not be the main pathway.

Cbei_3833 or Cbei_4614 or Cbei_4612), where the CoA moiety of butyryl-CoA is

transferred to acetate producing acetyl-CoA and butyrate. However, model predictions showed that butyrate is mostly produced generating ATP via Ptb and Buk.

6.4.5 Community model simulations of *C. autoethanogenum* and *C. beijerinckii* for the fermentation of CO₂/H₂ and lactate

The GEM of the co-culture consisted of 2005 metabolites, 2107 reactions and 1659 genes. Community model simulations supported the co-existence of the co-culture of *C. autoethanogenum* and *C. beijerinckii* for the fermentation of CO₂/H₂ and lactate in a wide range of growth rate and species ratio combinations. Fig. 6.6 shows the feasible solution space for multiple combinations of species ratios, growth rates, CO₂, H₂ and lactate feeds. When the maximum uptake rate of lactate is 2.5 mmol L⁻¹ h⁻¹ (Fig. 6.6; green figures), the feasibility of the co-culture becomes more limited. In these conditions, the co-culture is only feasible at low growth rates (< 0.02 h⁻¹) for all species ratios, and feasible at higher growth rates (up to 0.07 h⁻¹) when *C. autoethanogenum* and *C. beijerinckii* are similarly present in the community for CO₂/H₂ feed ratio of 0.5. The co-culture is infeasible in all conditions when the CO₂/H₂ feed ratio is 2, and only feasible when the presence of *C. autoethanogenum* is low and the CO₂/H₂ feed ratio is 1. The range of feasible solutions becomes wider when the lactate feed rate is 5 mmol L⁻¹ h⁻¹. When *C. autoethanogenum* and *C. beijerinckii* are equally present in the community, the co-culture can be established with all explored growth rates, except when the CO₂/H₂ feed ratio is 2, that is only feasible up to 0.04 h⁻¹. Again, only at lower growth rates (< 0.02 h⁻¹), the co-culture is feasible for all tested species ratios.

Fig. 6.7 shows the steady-state consumption and production rates observed in co-culture compared to the consumption and production rates associated to *C. autoethanogenum* or *C. beijerinckii*. Part of the acetate produced by *C. autoethanogenum* is taken up by *C. beijerinckii* since the steady-state production rates in the co-culture are lower than the production rates of *C. autoethanogenum*. The fermentation of acetate and lactate leads to the production of butyrate in *C. beijerinckii*. A small amount of butyrate is reassimilated by *C. autoethanogenum* and by *C. beijerinckii* and converted into butanol (not shown). Furthermore, ethanol is being produced in smaller amounts by *C. autoethanogenum* and *C. beijerinckii*. Model predictions also showed an exchange of CO₂ and H₂ from *C. beijerinckii* to *C. autoethanogenum*. *C. beijerinckii* produces CO₂ and H₂ that are taken up by *C. autoethanogenum*, since the flux through *C. autoethanogenum* is higher than the flux through the exchange reaction in the co-culture. Model predictions suggested that acetate consumption by *C. beijerinckii* varied depending on the lactate feed rate, being lower when the lactate feed rate was higher than 2.5 mmol L⁻¹ h⁻¹ (≈ 5 mmol L⁻¹ h⁻¹). A higher lactate feed rate also led to more CO₂ and H₂ produced by *C. beijerinckii*, and thus, to more gases

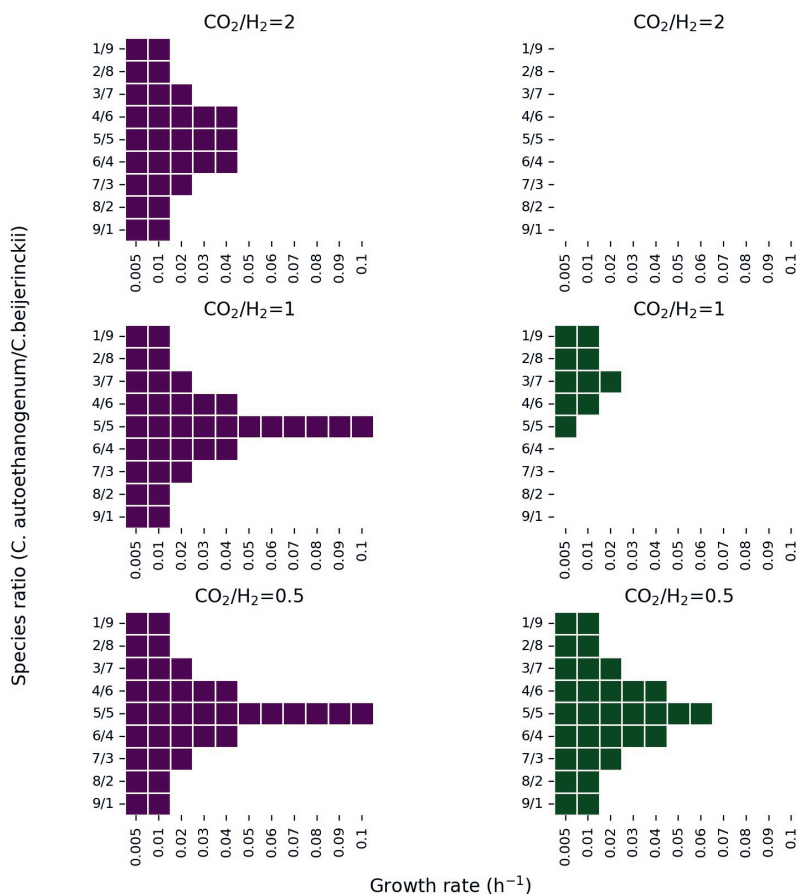


Figure 6.6: Feasible solution space of the co-culture of *C. autoethanogenum* and *C. beijerinckii* for several species ratio and growth rate combinations under different CO_2 , H_2 and lactate feed rates. The y-axis shows the biomass species ratio of *C. autoethanogenum*/*C. beijerinckii* and the x-axis shows the growth rate in h^{-1} . Colored areas indicate feasible solutions predicted by the model. Figures in purple and green show results when the lactate feed rate is set to a maximum of $5 \text{ mmol L}^{-1} \text{h}^{-1}$, and $2.5 \text{ mmol L}^{-1} \text{h}^{-1}$, respectively. Predictions shown on the first row were obtained with a CO_2 and H_2 feed rate of 5, and $2.5 \text{ mmol L}^{-1} \text{h}^{-1}$, respectively. Predictions shown on the second row were obtained with a CO_2 and H_2 feed rate of $5 \text{ mmol L}^{-1} \text{h}^{-1}$, and on the third row, with a CO_2 and H_2 feed rate of 2.5, and $5 \text{ mmol L}^{-1} \text{h}^{-1}$, respectively.

being recirculated and consumed by *C. autoethanogenum* producing more acetate (git repository).

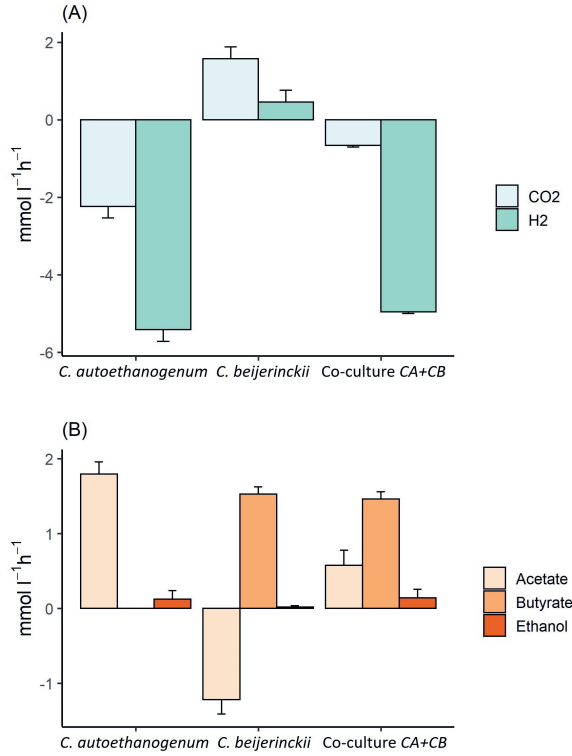


Figure 6.7: Steady-state production and consumption rates of the main substrates and products predicted by the community model of *C. autoethanogenum* and *C. beijerinckii*. The x-axis shows the species associated to the illustrated fluxes. The y-axis shows uptake (negative) or production (positive) fluxes in $\text{mmol L}^{-1} \text{h}^{-1}$. (A) shows CO_2 and H_2 production or consumption rates, and (B) shows the production or uptake of acetate, butyrate and ethanol. Modelled uptake and production rates are shown for *C. autoethanogenum*, *C. beijerinckii* and for the co-culture of *C. autoethanogenum* and *C. beijerinckii* (Co-culture CA+CB), respectively. Growth rate was set to 0.02 h^{-1} ; biomass species ratio was set to 1:1; maximum and minimum lactate uptake rate was set to 2.5 and $0.1 \text{ mmol L}^{-1} \text{h}^{-1}$, and the maximum and minimum uptake of CO_2 and H_2 were set to 5 and $0.5 \text{ mmol L}^{-1} \text{h}^{-1}$, respectively

Furthermore, we observed traces of formate, 2,3-butanediol, acetone, isopropanol and butanol (see git repository).

6.4.6 Fed-batch fermentation of CO₂/H₂ and lactate by the novel co-culture of *C. autoethanogenum* and *C. beijerinckii*

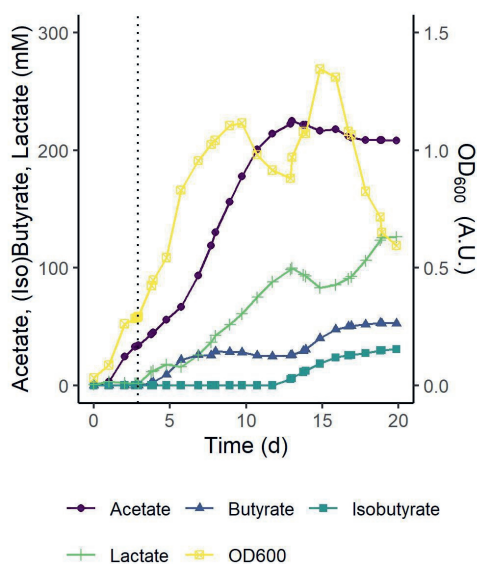


Figure 6.8: pH-controlled fed-batch fermentation of the *C. autoethanogenum* - *C. beijerinckii* co-culture on 1:4 CO₂/H₂ with an L-lactic acid feed. Concentrations of the main substrates, products and cell density are shown. At t_0 cultures were inoculated with *C. autoethanogenum*. The dotted black line marks inoculation with *C. beijerinckii* and the start of the L-lactic acid feed. L-lactic acid was fed at a rate of 3 mL d⁻¹ till 19 d. Traces of ethanol (3 d - 8 d, max. 4.6 mM at 7 d and 13d - 20 d, max. 5.6 mM at 20 d), butanol (14 d - 20 d, max. 3.1 mM at 20 d) and glucose from the *C. beijerinckii* inoculum (<1 mM at 3 d) were detected. pH was controlled at pH 5.5 ± 0.1. Results of a single biological replicate are shown here and the results of a second independent biological replicate are shown in Fig.S2.

Production of butyrate from CO₂/H₂ and the co-substrate lactate by the modelled co-culture of *C. autoethanogenum* and *C. beijerinckii* was experimentally verified with two biologically independent pH-controlled fed-batch fermentations (Fig. 6.8, and Fig.S2). Both fermentations showed similar trends in biomass production

and metabolites profiles. Below, the results are described for the fermentation shown in Fig. 6.8. Initially, *C. autoethanogenum* was grown solely on a continuous CO₂/H₂ feed, and after 3 d, the OD₆₀₀ had reached a value of 0.29 and the acetate concentration a value of 34 mM. This acetate concentration was considered sufficient to support *C. beijerinckii*. *C. beijerinckii* was added and the L-lactic acid feed was started. The rate of the L-lactic acid feed was set lower than the rate of acetate production from CO₂/H₂ by *C. autoethanogenum* to prevent complete depletion of acetate. Upon inoculation with *C. beijerinckii* and the start of the L-lactic acid feed, a continued growth phase was observed till 10 d in which butyrate was produced up to 28 mM.

A theoretical acetate production from CO₂ was calculated from which the corresponding stoichiometry for butyrate production at each time point was calculated (Fig.S2). Between 4 d and 7 d, during butyrate production in the first growth phase, for each mol of consumed lactate, 0.2-1 mol acetate was reassimilated, and 0.5-0.6 mol butyrate was produced.

The drop in cell density observed between 10 d and 13 d could be explained by the accumulation of biomass observed at the reactor wall above the fermentation medium from 6 d onward (data not shown). No production of butyrate was observed in this period and microscope observations showed that the consortium consisted almost entirely of vegetative cells (data not shown). These cells could not be assigned to either species as the morphologies of *C. autoethanogenum* and *C. beijerinckii* could not be clearly distinguished. As a result, the species ratio in the co-culture was not determined experimentally. In future studies, the species ratio could be obtained from transcriptomic [51], amplicon [374] or qPCR data [69].

After this adaptation period, a second growth phase was observed between 13 d and 15 d coinciding with a larger fraction of sporulating cells in the culture and the co-production of butyrate and isobutyrate to final concentrations of 53 mM and 31 mM, respectively. While measured in both replicates (Fig. 6.8 and Fig.S2), the production of isobutyrate by the consortium was not predicted by the models, and will be further investigated in a follow-up research. The calculated stoichiometry indicated a shift towards the conversion of lactate during this second growth and production phase (Fig.S2).

6.4.7 Analysis of substrate consumption and product formation by the co-culture model

C. autoethanogenum takes-up CO₂ and H₂ through the Wood-Ljungdahl pathway, where H₂ is used as an electron donor for CO₂ reduction to acetyl-CoA (Fig. 6.9). Acetyl-CoA is mainly converted into acetate producing ATP, and ethanol. In addition, traces of 2,3-butanediol, formate and lactate were predicted by the model (not shown here). Part of the acetate was in turn taken-up by *C. beijerinckii* together with

the external lactate feed, following the metabolism described in section 6.4.3. Ethanol was produced by *C. autoethanogenum* and by *C. beijerinckii*, as observed in the experiments. Model simulations suggested the production of butyrate, CO₂ and H₂ by *C. beijerinckii*, and traces of acetone and butanol. We observed that most of the CO₂ and H₂ produced by *C. beijerinckii* was metabolised by *C. autoethanogenum* (Fig. 6.7). Furthermore, we observed traces of isopropanol formed from the conversion of the assimilated acetone by *C. autoethanogenum* through an alcohol dehydrogenase. The community model suggested that butanol was produced by *C. beijerinckii* and by *C. autoethanogenum* (Fig. 6.9). As Diender et al. already observed [64], butyrate could be exchanged between *C. beijerinckii* and *C. autoethanogenum*, and converted into butanol by an alcohol dehydrogenase and the aldehyde ferredoxin oxidoreductase.

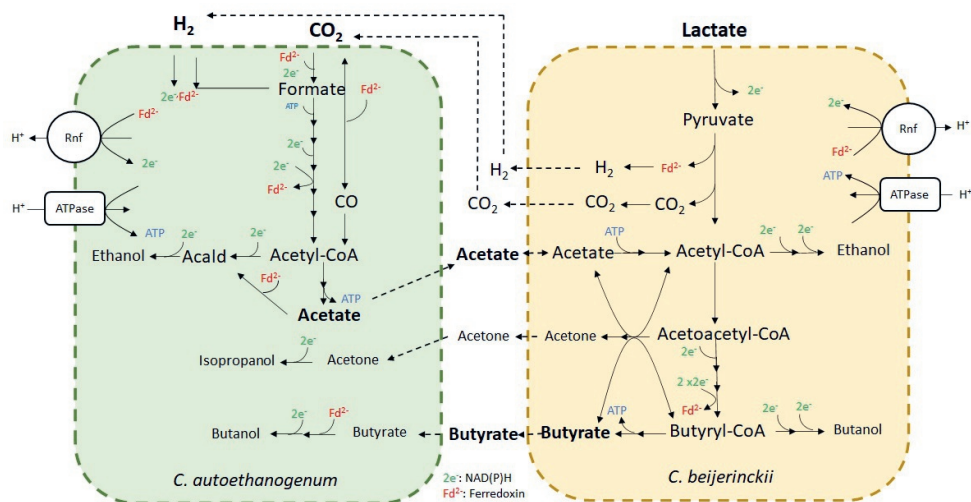


Figure 6.9: Fermentation of CO₂/H₂ and lactate by the novel co-culture of *C. autoethanogenum* and *C. beijerinckii*. Metabolites in bold indicate substrates and main products. Metabolites in smaller letter size indicate minor products. Arrows indicate the flux direction. Dashed lines display transport reactions of metabolites from the extracellular compartment to the intracellular compartment of the indicated microbe, and *vice versa*

In addition, the model predicts traces of formate and lactate produced by *C. autoethanogenum* being assimilated by *C. beijerinckii* (not shown here).

Fig.S3 represents the metabolic profile of the novel co-culture with glucose, instead of lactate, as additional carbon source. As observed in Fig. 6.4, the addition

of glucose would lead to an increase of ABE production by *C. beijerinckii*, since there are more reducing equivalents when glucose is converted to pyruvate. Acetate would still be the main product in *C. autoethanogenum* and ethanol would be produced in minor amounts. Part of the acetate could be metabolised by *C. beijerinckii*, but also produced together with butyrate during the acidogenic phase. Once the pH drops enough, the acids could be partly reassimilated during solventogenesis to produce solvents. Acetone and butyrate could be partly taken up by *C. autoethanogenum* producing isopropanol and more butanol. Possibly, part of the CO₂ and H₂ produced by *C. beijerinckii* would be consumed by *C. autoethanogenum* as described for the co-culture growing on lactate.

6.5 Discussion

GEMs are mathematical representations of the metabolism and have been successfully employed to gain insights into metabolic capabilities of single species [72, 82, 219, 295, 364], and to elucidate possible strategies to optimise the performance of microorganism(s) in mono- and co-cultivation [51, 107, 375, 376]. In this study, the use of constrained-based modelling has been key to design an alternative way to produce butyrate from CO₂/H₂ and lactate. We have proven the capacity of *C. beijerinckii* NCIMB 8052 to grow on lactate and acetate as the sole carbon and energy source. Moved by the need to upcycle sustainable feedstocks, we have used this new found capacity of *C. beijerinckii* to established a novel synthetic co-culture of *C. autoethanogenum* and *C. beijerinckii* for the fermentation of CO₂/H₂ and lactate into butyrate.

The use of lactate as alternative carbon source by *C. beijerinckii* as co-substrate with acetate creates new possibilities for the production of butyrate. Acetate is the most abundant product of gas fermentation, and therefore, has an essential role in the establishment of the co-culture. Lactate is a minor fermentation product of acetogens grown on syngas or CO₂/H₂ [56, 377], but a major fermentation product of acetogens grown on sugars [378]. Acetogens could be engineered towards autotrophic lactate production from CO₂/H₂ [379] or syngas, thereby facilitating butyrate production in co-cultivation with *C. beijerinckii* without the need of adding an additional carbon source. Alternatively, lactate can be obtained from other sources, such as side-streams from the dairy industry [380], spoiled agri-food products [381], ensiled agricultural biomass [382], and fermented grass [383].

C. beijerinckii has wide physiological versatility, which makes this microbe an ideal candidate to produce butyrate in a co-culture. However, butyrate production could also be achieved by the co-cultivation of an acetogen with a butyrate producing species, such as *Clostridium butyricum*, whose ability to grow on lactate and acetate

was also proved recently [384].

Additionally, the use of the newly established co-culture could increase carbon recycling and electron transport, since model predictions indicated that CO₂ and H₂ produced by *C. beijerinckii* were almost fully reassimilated by *C. autoethanogenum* (Fig. 6.7), which reduces the carbon footprint. Incorporation of an organism able to produce H₂ needed for CO₂ assimilation is interesting to consider for future approaches. Besides solventogenic Clostridia, other anaerobic bacterial species have been described that produce H₂ from the fermentation of sugars at high yields [385]. This opens up new alternatives for more efficient co-cultures without the need of external H₂.

Model predictions showed slow growth on lactate and acetate by *C. acetobutylicum*. However, this was not confirmed by experiments in which lactate was not consumed, and acetate was produced rather than consumed (Fig. 6.4; condition 1). Diez-Gonzalez et al. [367] showed growth on lactate and acetate in the solventogenic *C. saccharobutylicum* NCP 262. They analysed extracts of cells grown on lactate and acetate and observed NAD-dependent lactate dehydrogenase (d-LDH) as well as NAD-independent lactate dehydrogenase (i-LDH) activity. d-LDH regulated the conversion of pyruvate to lactate and required fructose-1,6-biphosphate to be active [367, 386]. i-LDH regulated the conversion of lactate to pyruvate (Fig. 6.5) and had double the activity over d-LDH. In addition, i-LDH activity decreased fourfold when glucose was added to cultures growing on lactate and acetate. However, lactate was only converted by *C. acetobutylicum* ATCC 824 when glucose was added (Fig. 6.4; Condition 2) suggesting that i-LDH from *C. acetobutylicum* ATCC 824 is activated by glucose. Interestingly, the LDH of *C. beijerinckii* NCIMB 8052 and *C. acetobutylicum* ATCC 824 showed 87.7% and 57% similarity with the LDH of *C. saccharobutylicum* NCP 262, respectively. [371] showed that *C. saccharobutylicum* NCP 262 is more similar to *C. beijerinckii* NCIMB 8052 than to *C. acetobutylicum* ATCC 824. Therefore, we hypothesise that *C. beijerinckii* has an i-LDH activity comparable to *C. saccharobutylicum*, whereas i-LDH activity in *C. acetobutylicum* ATCC 824 is regulated differently.

Model predictions showed a high production of butyrate, acetate, and traces of ethanol, acetone, butanol, isopropanol, 2,3-butanediol, and formate. Fed-batch experiments also showed butyrate and acetate as major fermentations products, and ethanol and butanol as minor fermentation products. Charubin et al. [69] observed production of 2,3-butanediol from the assimilation by *C. ljungdahlii* of the acetoin produced by *C. acetobutylicum*. However, acetolactate decarboxylase was only annotated in the genome of *C. autoethanogenum* and not in the genome of *C. beijerinckii* [387], and thus, acetoin could not be produced by the solventogen. Lactate degradation results in less NAD(P)H available, and therefore, the production of solvents is lower compared to the standard ABE fermentation on sugars [69, 388]. In con-

trast, the co-culture in our study has a relatively high butyrate production (up to 53 mM). Furthermore, mono-culture experiments on lactate and acetate in our study produced higher concentrations of butyrate (up to 42 mM) than the reported co-assimilation of glycerol and acetate by *C. beijerinckii* (≈ 20 mM) [368], and than the co-assimilation of lactate and acetate by *C. saccharobutylicum* [367] (≈ 20 mM).

Model predictions indicated that *C. beijerinckii* could grow on lactate as the sole carbon and energy source, as was recently observed [389]. However, the growth rate was improved by the addition of acetate (Fig. 6.3), as was previously shown [367]. The addition of acetate favours lactate uptake, since the acetyl-CoA pool increases with addition of acetate as co-substrate, and thus, more acetyl-CoA would be converted into butyrate producing more ATP. Co-culture fed-batch experiments showed, however, accumulation of acetate in the fermentation broth. This showed that not all acetate produced by *C. autoethanogenum* was consumed by *C. beijerinckii*, as indicated by the model, and possibly that some acetate could also be produced by *C. beijerinckii*.

We should note that the deployed modelling approach predicts steady-state production or consumption rates, and thus, we cannot compare the results quantitatively with bioreactor data, which consist of concentrations over time. Instead, our study should be seen as an exploratory study assessing the feasibility of the co-culture. Future optimization of this co-culture could integrate current experimental data and relative abundance of species into dynamic modelling approaches to gain better insights into the concentration profiles over time. These results show that community modelling of metabolism is a valuable tool to guide the design of microbial consortia for the tailored production of important chemicals from renewable resources. It thereby expands the space of options to possibly accelerate the transition to a biobased economy.

6.6 Conclusion

Genome-scale metabolic modelling helped identifying the ability of *C. beijerinckii* to co-metabolise acetate and lactate for the production of butyrate. This ability was experimentally verified in batch serum bottles and pH-controlled batch bioreactor fermentations. A community model of *C. autoethanogenum* and *C. beijerinckii* was then constructed to assess the feasibility of the co-culture to produce butyrate from CO_2/H_2 and lactate. Community modelling predicted the feasibility of the co-culture in several conditions and the interactions between species, especially, the exchange of acetate. Following model predictions, the co-culture of *C. autoethanogenum* and *C. beijerinckii* was established in pH-controlled fed-batch fermentations. The main products were acetate, butyrate and the newly identified metabolite,

isobutyrate. Our study shows the strength of a model-driven approach to explore the high metabolic flexibility of clostridial species for the production of chemicals from renewable sources.

Abbreviations

ABE: Acetone, Butanol and Ethanol; C1-feedstock: One-Carbon Feedstock; cFBA: Community Flux Balance Analysis; FBA: Flux Balance Analysis; GEM: Genome-Scale Metabolic Model; HPLC: High-Performance Liquid Chromatography; IBE: Iso-propanol, Butanol and Ethanol; LDH: Lactate Dehydrogenase; MCFA: Medium-Chain Fatty Acid; OD: Optical Density; Syngas: Synthesis Gas.

Conflict of Interest Statement

VMds has interests in LifeGlimmer and JH has interests in NoPalm Ingredients BV. The authors declare that they have no known competing financial interests or personal relationships that could have influenced the work reported in this paper.

Author Contributions

SBV and NN conceived and designed the study, and drafted the manuscript. SBV constructed the models and performed model simulations and data analysis. NN performed the experiments and data analysis. MSD, AMLC, JH, SB, PJ and VMdS conceived, designed and supervised the research. MSD, VMdS, JH and AMLC acquired project funding. All authors reviewed and edited the study. All authors read and approved the content of the submitted version.

Funding

The research leading to these results has received funding from the Netherlands Science Foundation (NWO) under the programme 'Closed Cycles' (Project nr. AL-WGK.2016.029) and the Netherlands Ministry of Education, Culture and Science under the Gravitation Grant nr. 024.002.002. AMLC received funding from the European Union's Horizon 2020 research and innovation programme under Grant Agreement no. 761042 (BIOCON-CO2).

Acknowledgments

We thank Dr. Truus de Vrije and Hetty van der Wal for their help with the experiments and Professor Diana Z. Sousa for the fruitful discussions.

Data Availability Statement

The data generated for this study can be found in the following git repository:
https://gitlab.com/wurssb/Modelling/coculture_cacb.

Supplementary information

Table S6.1: Consumption/production of metabolites and co-assimilation of acetate by *C. acetobutylicum* and *C. beijerinckii* growing on various carbon sources. CM2 medium, containing 38 mM acetate, was supplemented with 40 mM of each of the various carbon sources as follows: **Condition 1:** acetic acid, ethanol, glycerol, and L-lactic acid; **Condition 2:** acetic acid, ethanol, glycerol, L-lactic acid and glucose; **Condition 3:** glucose. **Condition 4:** none. Negative and positive values show conversion and production, respectively. Acetate co-assimilation is shown as the percentage of carbon converted coming from acetate (C from acetate). NA: Not available.

Condition	<i>C. acetobutylicum</i>				<i>C. beijerinckii</i>			
	1	2	3	4	1	2	3	4
Difference (mM)								
Acetate	4	6	13	2	-52	-38	-15	-2
Acetone	0	0	-1	0	1	8	12	0
Butanol	0	11	2	0	2	23	22	0
Butyrate	3	31	30	3	62	51	17	9
Ethanol	2	0	-1	-1	0	0	0	0
Glucose	-6	-45	-42	-6	-6	-51	-49	-6
Glycerol	1	-1	0	-1	-34	-11	-3	-3
Lactate	0	-26	-1	0	-39	-37	-2	-2
C from Acetate (%)	NA	NA	NA	NA	29	14	9	7

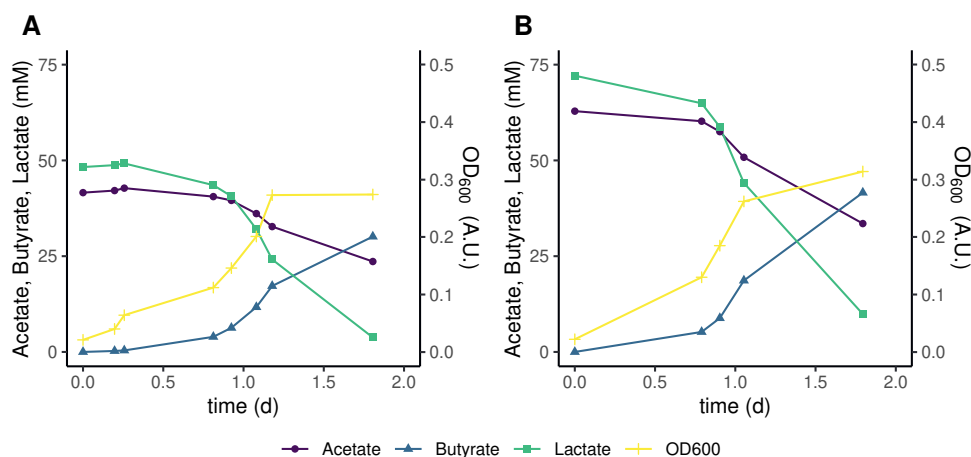


Figure S6.1: pH-controlled batch fermentations of *C. beijerinckii* growing on L-lactic acid and acetic acid at a 1:1 ratio at pH 5.5 ± 0.1 . Concentrations of the main substrates, products and cell density are shown for two biologically independent replicates with different starting concentrations. Traces of ethanol and butanol (<1 mM), and glucose from the inoculum (1 mM) were detected in both conditions. Overall reaction stoichiometries for lactate, acetate and butyrate were -1, -0.40 and 0.68 for (A), and -1, -0.47 and 0.67 for (B), respectively.

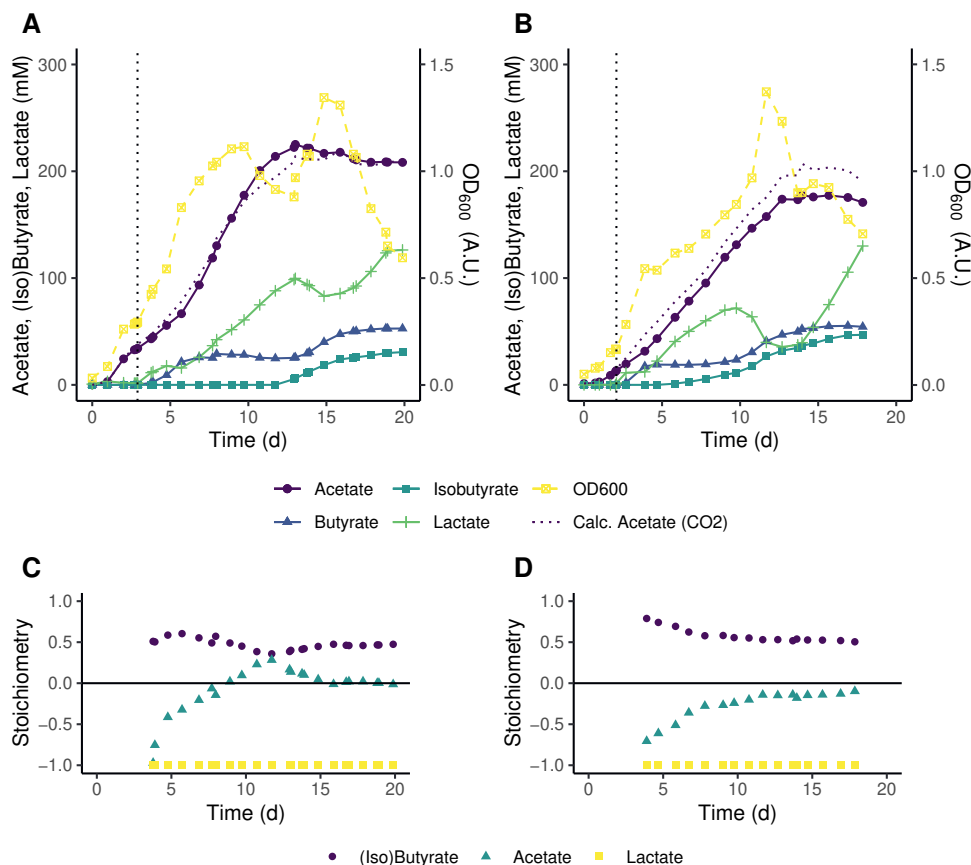


Figure S6.2: pH-controlled fed-batch fermentations of *C. autoethanogenum* - *C. beijerinckii* co-culture on 1:4 CO₂/H₂ with L-lactic acid feed at pH 5.5 ± 0.1. Concentrations of the main substrates, products and cell density are shown for two biologically independent replicates in (A) and (B) and corresponding stoichiometries in (C) and (D), respectively. At t₀ cultures were inoculated with *C. autoethanogenum*. The dotted black line in (A) and (B) marks inoculation with *C. beijerinckii* and the start of the L-lactic acid feed. In (A) L-lactic acid was fed at a rate of 3 ml d⁻¹ till 19 d and in (B) at a rate of 3 ml d⁻¹ till 14 d and 6 ml d⁻¹ from 14 d till 18 d. A theoretical acetate concentration produced from CO₂ was calculated (Calc. Acetate (CO₂)). In (A) traces of ethanol (3 d - 8 d, max. 4.6 mM at 7 d and 13 d - 20 d, max. 5.6 mM at 20 d), butanol (14 d - 20 d, max. 3.1 mM at 20 d) and glucose from the *C. beijerinckii* inoculum (<1 mM at 3 d) were detected. In (B) traces of ethanol (1 d - 18 d, max. 5.1 mM at 15 d) and butanol (3 d - 18 d, max. 6.3 mM at 17 d) were detected.

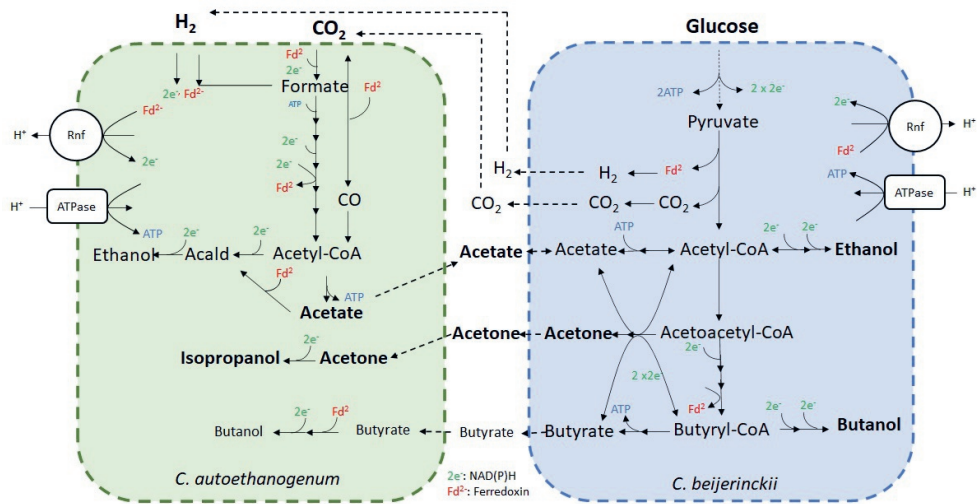


Figure S6.3: Hypothetical fermentation of CO_2/H_2 and glucose by *C. autoethanogenum* and *C. beijerinckii*. Metabolites in bold indicate substrates and main products. Metabolites in smaller letter size indicate minor products. Arrows indicate the flux direction. Dashed lines indicate transport reactions of metabolites from extracellular compartment to intracellular compartment of the indicated microbe, and viceversa.

Chapter 7

A structured evaluation of genome-scale constraint-based modeling tools for microbial consortia

William T. Scott Jr.*, **Sara Benito-Vaquerizo***, Johannes Zimmerman, Djordje Bajić, Almut Heinken, Maria Suarez-Diez, Peter J. Schaap
Available in bioRxiv and Submitted for publication (2023).

doi.org/10.1101/2023.02.08.527721

* Contributed equally

7.1 Abstract

Harnessing the power of microbial consortia is integral to a diverse range of sectors, from healthcare to biotechnology to environmental remediation. To fully realize this potential, it is critical to understand the mechanisms behind the interactions that structure microbial consortia and determine their functions. Constraint-based reconstruction and analysis (COBRA) approaches, employing genome-scale metabolic models (GEMs), have emerged as the state-of-the-art tool to simulate the behavior of microbial communities from their constituent genomes. In the last decade, many tools have been developed that use COBRA approaches to simulate multi-species consortia, under either steady-state, dynamic, or spatiotemporally varying scenarios. Yet, these tools have not been systematically evaluated regarding their software quality, most suitable application, and predictive power. Hence, it is uncertain which tools users should apply to their system and what are the most urgent directions that developers should take in the future to improve existing capacities.

This study conducted a systematic evaluation of COBRA-based tools for microbial communities using datasets from two-member communities as test cases. First, we performed a qualitative assessment in which we evaluated 24 published tools based on a list of FAIR (Findability, Accessibility, Interoperability, and Reusability) features essential for software quality. Next, we quantitatively tested the predictions in a subset of 14 of these tools against experimental data from three different case studies: a) syngas fermentation by *C. autoethanogenum* and *C. kluyveri* for the static tools, b) glucose/xylose fermentation with engineered *E. coli* and *S. cerevisiae* for the dynamic tools, and c) a Petri dish of *E. coli* and *S. enterica* for tools incorporating spatiotemporal variation. Our results show varying performance levels of the best qualitatively assessed tools when examining the different categories of tools. The differences in the mathematical formulation of the approaches and their relation to the results were also discussed. Ultimately, we provide recommendations for refining future GEM microbial modeling tools.

7.2 Author summary

Constraint-based modeling employing genome-scale reconstructions of microbial species has become one of the most successful approaches for studying, analyzing, and engineering microbial consortia. Over the past decade, many constraint-based modeling tools have been published to examine an immense variety of microbial consortia spanning from the application areas of bioremediation to food and health biotechnology. However, new potential users lack an overview of the quality and performance of existing metabolic modeling tools that would guide their choice. To tackle this issue, we examined 24 tools for genome-scale metabolic modeling of microbial consortia. After an initial qualitative screening, we quantitatively evaluated 14 adequate tools against published experimental data that included different organisms and conditions. We conducted simulations and evaluated model features such as predictive accuracy, computational time, and tractability in capturing critical physiological properties. We found that, generally, more up-to-date, accessible, and documented tools were superior in many important aspects of model quality and performance. Although, in some cases, we observed tradeoffs in older, less elaborate tools that can be more accurate or flexible. This work has broad implications to help researchers navigate the most suitable tools, and suggests to developers opportunities for improvement of the currently existing capabilities for metabolic modeling of multi-species microbial consortia.

7.3 Introduction

The goods and services provided by microbial consortia have long been harnessed in biotechnology. Recent years have seen a soar in the use of multi-species microbial consortia beyond their traditional application in the production of food and beverages [390, 391]. For example, microbial consortia are increasingly applied in the production of commodity chemicals [70, 392], pharmaceuticals [108], or biofuels [393–395]; the valorization of waste and emissions [68, 396, 397], the improvement of sustainable agriculture systems [398–400], and applications in health [401] or bioremediation [109, 402, 403]. Besides the obvious advantage over established industrial processes in terms of sustainability, multi-species consortia offer a number of advantages compared to monocultures. These include the reduction of metabolic burden (a major issue) through division of labor [60, 404, 405], an enhanced substrate versatility, and an increased robustness to fluctuating environments [406, 407]. In consequence, synthetic ecology – the rational engineering of multi-species microbial consortia – is emerging as a new frontier in biotechnology and biomedicine. In order to advance this frontier, it is imperative to build predictive models that will allow us to design and control the composition and function of microbial communities [408, 409].

Constrained-based metabolic modeling (CBM) is a powerful computational approach that mechanistically predicts microbial metabolic traits from genomes. In the past decades, this method has proven invaluable as a guide for microbial experimental design and for elucidating metabolic engineering strategies [73, 93]. Because metabolic traits are also a central determinant of ecological interactions in microbes (e.g. competition for resources or metabolite sharing), CBM also holds great promise as a predictive and an engineering tool in synthetic ecology [70]. In a nutshell, CBM use genome-scale metabolic models (GEMs), a mathematical representation of the metabolic network encoded in an organism's genome, to simulate metabolic fluxes in a given environment [410]. In the case of single organisms, one of the most popular methods is Flux balance analysis (FBA) [86]. FBA optimizes a predefined objective function (e.g., biomass production) and assumes steady-state exponential growth (balanced growth). Dynamic-FBA (dFBA) –an extension of FBA– is applied to represent non-continuous operations, such as batch or fed-batch reactors, by incorporating differential equations that describe the rate of change of the extracellular fluxes and the mass balances of the reactor [89, 90]. dFBA assumes a quasi-stationary state where internal dynamics are supposed to be much faster than external changes of the medium [222]. Going a step further, another general methodology has been developed to model microbial systems in which the extracellular environment varies spatially and temporally [106, 411, 412]. This approach

is known as spatiotemporal FBA. A spatiotemporal FBA framework typically consists of partial differential equations (PDEs) conveyed in terms of time and spatial coordinates as independent variables [411]. The PDEs mainly characterize extracellular mass balance equations for biomass, metabolite, and potentially other chemical species concentrations. They account for the transport mechanisms that cause spatial disparities, including metabolite diffusion and liquid/gas phase convection. Some spatiotemporal FBA approaches choose to represent microbial biomass as individuals or agents (IBM) [413–415]. In contrast, others opt to represent microbial biomass at the population level (PLM) [106, 412].

With the continuous development of novel synthetic microbial consortia, considerable efforts have been made to extend CBM to microbial communities [98, 222, 416–418]. In the past decades, many tools have become available with the aim of studying microbial interactions in the gut microbiome [97, 100, 101] or simulating the growth of microbial consortia in continuous and non-continuous environments. The increasing availability of these tools makes the selection process difficult for the user [419]. A key feature when selecting a tool is to verify whether it follows the FAIR (Findable, Accessible, Interoperable, and Reusable) principles [420]. In particular, adhering to the software FAIR guiding principles is best as they assure quality research maintenance and reproducibility [421, 422]. As such, the findability of a tool is based on the capacity of the metadata and software to be easily found by both humans and computers. Accessibility pertains to the ease of knowledge available at which a software tool can be accessed, possibly including authentication and authorization. Interoperability refers to the ability to communicate with other software via exchanged data (or metadata). The reusability of tools is related to how well-described (by metadata) and appropriately structured the software is so that outputs/results can be replicated, combined, reinterpreted, reimplemented, and/or used in different settings. Many studies have reviewed the state of the art of steady-state, dynamic, or spatiotemporal tools and followed qualitative assessments [98, 222, 376, 416–418, 423–425]. However, no study has yet reviewed these tools quantitatively. Thus, a systematic evaluation of the latter element would be highly beneficial for the users and developers in the field. In this work, we have followed an extensive qualitative assessment to evaluate FAIR principles of available tools and a quantitative assessment to evaluate the performance of a subset of tools reproducing available experimental data of two-species communities. The following case studies were selected to quantitatively evaluate the tools: i) syngas fermentation by *Clostridium autoethanogenum* and *Clostridium kluyveri* for the static tools, b) xylose and glucose mixture fermentation with engineered *Escherichia coli* and *Saccharomyces cerevisiae* for the dynamic tools, and c) a Petri dish of *E. coli* and *Salmonella enterica* for the spatiotemporal tools. In particular, we tested tools that use CBM and GEMs; based on steady-state, dynamic, or spatiotemporal conditions and suit-

able to model synthetic microbial communities of two species. Ultimately, we made recommendations for the best modeling tools to use based on qualitative and quantitative performance outcomes and for the future development and improvement of the tools.

7.3.1 Overview of constrained-based modeling tools/approaches

Most of the community modeling tools available are based on steady-state, dynamic, and spatiotemporal conditions, describing continuous cultures, non-continuous cultures, and complex liquid and/or solid systems, for instance, a preferred environment of a Petri dish, respectively (Fig. 7.1). Steady-state approaches are suitable to describe growth in chemostats or continuous stir batch reactor (CSBR) systems. These tools require a single GEM of individual species and a community GEM, often generated by the tool. Extracellular metabolites and reactions of single species models must be defined by the user in the same namespace (unified identifier) upon constructing the community model. Most tools require the definition of medium composition, and some require either the relative abundance (microbial composition) or the growth rate of individual species. The community growth is often defined as the objective function, and/or the species growth. The objective function is maximized under the specified constraints by computing the metabolic fluxes, microbial composition, or species growth rate, thus allowing a solution where microbial interactions can be inferred.

Tools based on dynamic approaches are suitable to describe non-continuous systems, such as batch serum bottles, batch or fed-batch reactors as well as some continuous systems, e.g., temporal dynamics of recovery from a perturbation in a CSBR. GEMs of species in the community are provided separately as inputs. All the tools require the medium composition in the form of initial concentration and substrate uptake rates and the kinetic parameters as inputs. The kinetic parameters are normally based on Michaelis-Menten-like kinetics, and thus, Michaelis-Menten constant (K_m) and maximum uptake rate of substrates ($q_{S_i,m}$) are required parameters. After optimization of individual species' growth rate, we can obtain information on cross-feeding metabolites, concentration dynamics of substrates, products and biomass, and metabolic fluxes.

Finally, the spatiotemporal tools aim to describe 2D dimensional surface environments such as mimicking simple solid-state Petri dish environments. In addition to the required inputs described for dynamic tools, these tools need information on the diffusion parameters. The diffusion parameters consist of diffusion coefficients for biomass and metabolites. The main output in spatiotemporal models is the spatial distribution of extracellular metabolites, biomass of the different species, as well as growth and uptake rates, at any given time point. This information can be then




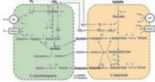





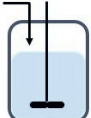


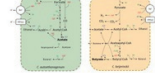
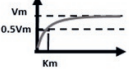
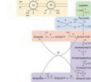






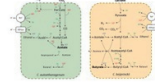
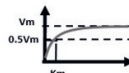



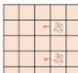
Environment	Inputs		Outputs	
Continuous culture  Steady-state	Medium composition  Microbial composition 	Community GEM  Growth rate 	Metabolic fluxes  Microbial composition 	Microbial interactions  Growth rate 
Non-continuous culture  Dynamic	Medium composition  Microbial composition 	GEMs  Kinetic parameters 	Metabolic fluxes  Concentration dynamics 	Microbial interactions  Biomass curves 
Petri dish  Spatiotemporal	Medium & microbial composition  Diffusion parameters 	GEMs  Kinetic parameters 	Metabolic fluxes  Concentration dynamics 	Microbial interactions  Spatial distribution 

Figure 7.1: Overview of steady-state, dynamic, and spatiotemporal tools to model microbial communities. The division among steady-state, dynamic, and spatiotemporal tools is not firm since dynamic tools can be used to describe steady-state systems. Likewise, spatiotemporal tools can be used to describe dynamic and steady-state systems. However, most tools were specifically designed to be used for the highest dimensional cases.

used to resolve space-dependent ecological interactions. For instance, we can observe how growth and competition for substrates occurs at the border of a colony, but not in the interior.

In this study, we evaluated a total of twenty-four tools/approaches based on steady-state (9) [97, 100–102, 221, 228, 338, 418, 426, 427], dynamic (8) [103–105,

428–432] and spatio-temporal (7) [106, 412–415, 433–435] methods according to their usability to model microbial communities using GEMs. A description of the tools/approaches is found in Supplementary_File1.

7.4 Results

Both a qualitative and a quantitative assessment were performed to evaluate the modeling tools and approaches. The assessment workflow began by first constructing a list of 16 essential features for quality constraint-based GEM modeling of microbial communities. Each tool was rated according to performance on these qualitative metrics ranging from 1 for inadequate (Red) to 5 for excellent (Blue). The qualitative features are strongly related to FAIR Guiding Principles for research software which include aspects such as software availability, user support, traceability, interoperability, etc [422]. These 16 features were evaluated from the perspective of a fairly experienced user of COBRA methods and tools. Some features can be subjective. Thus, a description of the criteria followed to evaluate each qualitative metric was described in an evaluation rubric (Supplementary File; S2 Table). More specifically, to evaluate the numerical stability and reproducibility of the tools, we relied on existing literature, tool architecture, and/or their performance in reproducing the available experimental studies chosen for the quantitative assessment. Not all features could be examined since some tools were not readily available, there was no tool developed for those approaches, or there was a lack of related information in the literature. These features were marked as ‘Not applicable’ (NA; grey square).

From the qualitative examination of the tools, a subset of tools/approaches were quantitatively evaluated for their potential to directly model microbial consortia under various conditions. For this subsequent evaluation, we needed data pertaining to substrate uptake rates, biomass composition and growth rates for static tools, substrate and product concentrations and biomass concentrations over time for dynamic tools, and media concentrations and spatial distribution of metabolites for spatiotemporal tools. However, these types of raw data are rarely available along with their metadata. Therefore, only a few suitable candidate datasets were applicable to the surveyed modeling scenarios. We selected three datasets (Diender et al.[329], Hanly and Henson [436], and Harcombe et al.[106]), one dataset for each category of modeling tools to use as case studies to validate the predictive capabilities of the tools. Every case study represents a consortium of two species. To have an unbiased comparison of the approaches, tools were not modified or augmented to revise their functionalities. Some tools were also available, but they were not quantitatively assessed since they were too specific to a particular application and not designed for general application.

In these evaluations, two main points were addressed: the quality of the tool for modeling microbial communities, and the predictability of the community behavior by the tool when presented with data from simple test cases.

Qualitative assessment - Static tools/approaches

Fig. 7.2 shows the evaluation of the described features in every tool/approach based on the rubric (S2 Table). Joint FBA was not assessed since it is the oldest approach and did not include important parameters such as the relative abundance of species. cFBA, RedCom, and NECom are methods, and therefore, some features were not evaluated (grey squares) since there is no tool developed specifically for those methods. The tools/approaches that best meet FAIR principles are MICOM, MMT, SteadyCom, and cFBA (see scores in S2 Figure). All tools/approaches are accessible for external use except CASINO and RedCom. OptCom is freely available for academic users upon request.

OptCom did not undergo updates throughout the years. SteadyCom is integrated as part of COBRA Toolbox [437] and has had some updates from the original publication. Small issues are fixed from time to time in SteadyCom. However, changes are not documented clearly. MMT and MICOM are routinely updated, and developers fix issues. Besides, all the modifications applied in every update of MICOM are described.

OptCom does not have community repository support, and developers only provide a contact person. SteadyCom and MMT offer good community support within COBRA Toolbox. MICOM has excellent user support since it has two channels available for discussions and support. cFBA only needs the installation of CBMPy [438]. SteadyCom and MMT are already available as part of the COBRA Toolbox, whose installation is fast and easy. MICOM is easy to install as it only needs a sentence of code and the installation of COBRAPy [235]. OptCom was run using the 'OptCom' function from MICOM, and thus, they were equally evaluated.

OptCom requires GAMS and BARON as solvers also accessed through GAMS. GAMS is not a free programming language, and therefore, its use is more limited. All the dependencies of cFBA and MICOM are freely accessible. SteadyCom, RedCom, MMT, and NECom are written in Matlab, which is not free, but licenses are inexpensive for a wide group of users. Besides, SteadyCom and MMT require COBRA Toolbox, and RedCom requires *CellnetAnalyzer* [439] that are both freely available. Required solvers are either integrated by default or freely accessible to a wide group of users. CASINO uses the RAVEN Toolbox, a free software suited for Matlab [440].

The developers of OptCom provide a book with tutorials to run the tool. Some tutorials are included in COBRA Toolbox that explains case studies used with SteadyCom. However, they merely explain some aspects of the software. MMT has ex-

Feature	Description	Static Tools/approaches								
		OptCom (2012)	cFBA (2013)	CASINO (2015)	SCom (2017)	RedCom (2019)	MICOM (2020)	NECom (2020)	MMT (2022)	
Software availability	Is readily and freely accessible to users	Good	Excellent	Inadequate	Excellent	Inadequate	Excellent	Excellent	Excellent	
Software maintenance	Developers and community specialists fix issues and routinely update tool	Inadequate	NA	NA	Satisfactory	NA	NA	NA	Excellent	
Traceability	Changes or any modifications are documented and detected for users	Inadequate	NA	NA	Satisfactory	NA	NA	NA	Satisfactory	
User support	Experts to answer user questions and community repository support	Satisfactory	NA	NA	Good	NA	NA	NA	Good	
Simple installation	The installation process is fast and easy.	NA*	Excellent	NA	Excellent	NA	Excellent	Good	Excellent	
Dependencies	Dependence on available software or packages	Satisfactory	Excellent	Satisfactory	Satisfactory	Satisfactory	Excellent	Satisfactory	Satisfactory	
Complete documentation	An up-to-date user manual is provided which explains all the aspects of the software	Satisfactory	NA	NA	Satisfactory	NA	Excellent	NA	Good	
User-friendly interface	The interface is straightforward, allowing non-specialized users to employ the tool	Satisfactory	Satisfactory	NA	Satisfactory	NA	Satisfactory	NA	Satisfactory	
Open-source	The source code is available to all users	Good	Excellent	Inadequate	Excellent	Inadequate	Excellent	Excellent	Excellent	
Reproducibility	Possible to get the same results over time	NA*	Satisfactory	NA	Satisfactory	NA	NA	NA	Excellent	
Numerical stability	Able to obtain consistent solutions without infeasibility or non-convergence issues	NA*	Excellent	NA	Satisfactory	NA	Excellent	NA	Satisfactory	
Scalability	The tool can be applied to more than two species and to other various systems	Satisfactory	Satisfactory	Excellent	Good	Good	Excellent	Satisfactory	Excellent	
Adherence to current standards	Meets SBML and other COBRA community level standards for model inputs & outputs	Inadequate	NA	Satisfactory	Satisfactory	NA	Satisfactory	NA	Good	
Interoperability	Able to be used and adjusted to standard GEM formats and with other formats	Inadequate	NA	**	Good	Good	Excellent	NA	Excellent	
Flexibility	Various parameters can be adjusted.	NA*	Satisfactory	NA	Satisfactory	**	Satisfactory	NA	Satisfactory	
Visualization of results	Is capable of producing ready, easy to understand visual outputs of model results	Inadequate	Inadequate	NA	Inadequate	NA	Excellent	Inadequate	Excellent	

Figure 7.2: Qualitative assessment of the static tools/approaches. The colored squares indicate the evaluation of the specified feature in every tool/approach. The color scale (upper right) goes from excellent (blue) to inadequate (red). When a feature does not apply to the specified tool/approach or the feature was not evaluated, it is indicated as NA (Not applicable; grey). The metrics contained in the figure were inspired by [419]. Colored squares with ‘*’ indicate features of OptCom evaluated using the OptCom function from MICOM. Colored squares with ‘**’ indicate that the evaluation is an assumption based on the given information. Scom: SteadyCom; MMT: Microbiome Modelling Toolbox. The tools/approaches are ordered by the year of the latest publication (e.g., MMT).

planatory tutorials and includes README files for each main function of the tool, but it is not completely maintained to have the latest functionality. MICOM contains an extensive user manual explaining all aspects of the tool, and it is up to date (at

the time of preparing this manuscript).

All the tools require certain expertise from the user to be run. OptCom is not considered a user-friendly tool as GAMS is used as the programming language, and it is not an extended programming language. cFBA, MMT, and MICOM require some knowledge of programming and constrained-based modeling by the user. SteadyCom is somehow constrained to the case studies of the original publication, and thus, extending their use to new cases, and GEMs requires more knowledge by the user.

Except for CASINO and RedCom where the source code is unavailable, the source code is accessible to all users. OptCom, MICOM, and MMT produce the same results over time. OptCom, cFBA, and MICOM produce consistent solutions without infeasibility or non-convergence issues. SteadyCom and MMT can lead, in some cases, to non-convergence solutions or infeasibilities.

NECom was applied to model a co-culture of two species. OptCom and cFBA have been used to model small microbial consortia (up to 3). CASINO, MMT, and MICOM can be used to model large communities (gut microbiota). SteadyCom and RedCom can be applied to model larger microbial communities than OptCom and cFBA (≈ 9).

OptCom toolbox used 'txt' files as input models that do not meet any community-level standard. cFBA, CASINO, SteadyCom, RedCom, MICOM, and NECom meet SBML or COBRA community-level standards for model input and output files. Based on the original publication, we hypothesize that CASINO meets the SBML standard for model input and output since the RAVEN Toolbox is employed [440]. MMT meets both SBML and COBRA community-level standards for model inputs and outputs models in COBRA format. RedCom meets COBRA community-level standards. OptCom cannot be adjusted to standard GEM formats. cFBA uses CBMPy, which reads the standard SBML format. MICOM is used with COBRAPy, which allows for different GEM formats. CASINO reads models imported in COBRA format. SteadyCom allows for the translation of GEM models from/to other formats. MMT allows for the import of SBML, XML, and COBRA models within the tool, and the user does not need to transform them before running the tool. NECom allows for the use of COBRA models.

Every tool/approach allows for adapting some parameters and constraints with more or less difficulty. MMT and MICOM provide a wide set of visualizations for different analyses. The rest of the tools do not produce visual outputs by default.

7.4.1 Quantitative assessment - Static tools/approaches

cFBA, SteadyCom, MICOM, and MMT scored higher than the other tools in the qualitative assessment (Figure in S1 Figure), and thus, they were also evaluated regard-

ing their performance in reproducing an experimental case study. OptCom was also assessed because it was available as an additional function in MICOM, and it is highly cited (Table in S1 Table). The case study consisted of syngas fermentation to medium-chain fatty acids by a co-culture of *C. autoethanogenum* and *C. kluyveri*. Syngas is a mixture of H_2 , CO and CO_2 . *C. autoethanogenum* can thrive on syngas by assimilating CO or CO_2 and H_2 and producing acetate and ethanol as byproducts. *C. kluyveri* does not grow on syngas. It needs acetate and ethanol to grow, and therefore, it depends on the direct cross-feeding of these metabolites by *C. autoethanogenum*. The study of Diender et al. [68] reported data on the steady-state consumption and production rates of CO, acetate, ethanol, butyrate, and caproate. The hydraulic retention time (HRT) of the reactor was fixed in the chemostat, suggesting that the species growth rates and the community growth rate were equal (Fig. 7.3A).

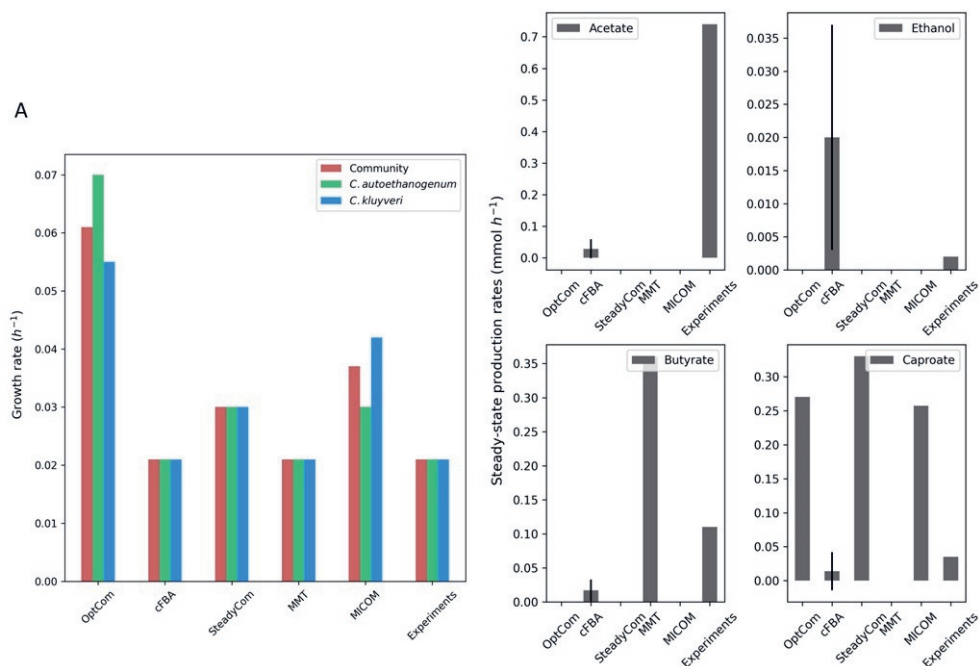


Figure 7.3: Comparison of tool predictions to experimental data from the study of Diender et al. [68]. (A) Community and species growth rate and (B) Steady-state production rates of the main fermentation products obtained in the fermentation of CO by *C. autoethanogenum* and *C. kluyveri* with the assessed tools. cFBA shows the average fluxes and standard deviation of the samples used with Flux sampling.

The latter assumption is also considered in cFBA, SteadyCom, and MMT, as illustrated in Fig. 7.3A. cFBA and MMT were run constraining the growth rates to the experimental values. SteadyCom allows for the definition of the species' growth rates and relative abundance. However, SteadyCom was not feasible in those conditions, and the unconstrained parameters resulted in higher growth rates than the experiments. OptCom and MICOM do not assume equal growth rates of species, and the predicted growth rates were also higher than the experiments. The use of additional constraints in OptCom and MICOM to enforce equal growth rates is possible and would result in a better fit, but tools have been run using the standard methodology.

In the study of Diender et al., almost all the ethanol produced by *C. autoethanogenum* on CO was fully consumed by *C. kluyveri*, whereas the acetate produced by *C. autoethanogenum* was only partly consumed by *C. kluyveri* (Fig. 7.3B) [51]. The fermentation of acetate and ethanol by *C. kluyveri* led to butyrate (≈ 0.11 mmol h^{-1}), caproate (≈ 0.035 h^{-1}), and H_2 (not showing here). Standard deviations for experimental values were not reported.

All tools predicted the exchange of acetate and ethanol between *C. autoethanogenum* and *C. kluyveri*, except MMT, which only predicted the exchange of ethanol (see fluxes in the online repository: <https://doi.org/10.5281/zenodo.7573135>). OptCom, SteadyCom, and MICOM predicted that the acetate produced by *C. autoethanogenum* was entirely consumed by *C. kluyveri* (see fluxes in the online repository: <https://doi.org/10.5281/zenodo.7573135>). However, cFBA predicted acetate production by the co-culture (Fig. 7.3B) and acetate consumption by *C. kluyveri*. Yet, acetate production was lower compared to the acetate measured in chemostat (≈ 0.73 mmol h^{-1}). MMT did not predict the production of acetate. Ethanol was difficult to detect in chemostat (<0.1 mM), as most of it was consumed by *C. kluyveri*. cFBA predicted more ethanol than in chemostat, and in OptCom, SteadyCom, MMT, and MICOM, ethanol was fully consumed by *C. kluyveri*. Butyrate production was only predicted by cFBA and MMT. Caproate production was over-estimated by all the tools except cFBA, which predicted a value comparable to the experiments, and MMT, which did not predict caproate production.

Following the procedure of the modeling study of the same co-culture [51], flux sampling was used to compute the fluxes with cFBA. While the agreement of experimental data with model predictions is less accurate here than in the previous computational study for the lack of constraints, the new adaptation of cFBA can reproduce the experimental data better than the other tools [68]. MICOM, SteadyCom, and OptCom could also reproduce the cross-feeding of acetate and ethanol, which is a key feature in this co-culture. MMT only reproduced the exchange of ethanol, being infeasible for the CO uptake rate reported in the experiments. The adjustment of the coupling factor ('c') or the use of mgPipe pipeline [97] in MMT

could lead to alternate outputs. Regardless, MMT was mainly designed to model the gut microbiome using AGORA models, and thus, it is more suitable to model large communities. The use of FVA as an alternative method to compute fluxes with the existing tools and approaches could also lead to additional information on cross-feeding metabolites.

7.4.2 Qualitative assessment - Dynamic tools

Fig. 7.4 shows the evaluation of the described features in every tool based on the evaluation rubric (S2 Table). From the qualitative assessment of all the dynamic tools, it was apparent that none were flawless (all features being good or excellent). There were, in fact, compromising aspects in many of the tools where tools were superior for some features while flawed for other features (see Fig. 7.4 and supplementary file). For instance, when examining their availability, it was determined that dyMMM, DAPHNE, MMODES, and surfinFBA were good or excellent. Still, the tools were considered merely satisfactory when evaluating their interoperability, flexibility, and reproducibility, except MMODES. In addition, tools such as dMMM, DFBALab, μ bialSim, and MMODES were easy to install and contained accessible and tractable dependencies, but did not score above satisfactory levels for the software being traceable (Fig. 7.4). Nevertheless, there was one tool, d-OptCom, that scored poorly compared with the other methods because the software was not readily available from the developers (available upon reasonable request). It was also constructed under an uncommonly utilized GAMS programming language.

Most of the tools received a good or excellent score for some features. For example, all the tools, except d-OptCom and DFBALab, are open source (contain source code available to all users). DFBALab also includes source code reachable to some users, but potential users first need to request the software to gain access as it is not available in the public domain for all users. All tools were deemed at least satisfactory regarding their reproducibility and potential to visualize outputs. Furthermore, all the tools other than d-OptCom and DAPHNE adhere to COBRA community standards [441] and contain a user-friendly interface, at least to a satisfactory degree. This means most methods consist of relatively simple and direct ways of designating inputs, such as adding GEMs, setting up media compositions, and defining model constraints and kinetic parameters. Also, tools that were built incorporating existing COBRA frameworks, such as COBRAPy or COBRA Toolbox, typically scored well for being user-friendly and following current standards because they assimilate the current community standards and acquire greater functionality from the existing infrastructure.

All the dynamic tools received at least a satisfactory score for their interoperability except MCM, which got a poor score. This is due to MCM having difficulties han-

Feature	Description	Dynamic Tools								
		dyMMM (2011)	DFBALab (2014)	dOptCom (2014)	MCM (2015)	DAPHNE (2019)	ubialSim (2020)	MMODES (2020)	surfinFBA (2020)	
Software availability	Is readily and freely accessible to users	Good	Poor	Inadequate	Satisfactory	Good	Excellent	Excellent	Good	
Software maintenance	Developers and community specialists fix issues and routinely update tool	Poor	Satisfactory	Inadequate	Satisfactory	Satisfactory	Poor	Satisfactory	Poor	
Traceability	Changes or any modifications are documented and detected for users	Satisfactory	Poor	Inadequate	Satisfactory	Satisfactory	Good	Satisfactory	Satisfactory	
User support	Experts to answer user questions and community repository support	Poor	Satisfactory	Satisfactory	Satisfactory	Poor	Satisfactory	Poor	Poor	
Simple installation	The installation process is fast and easy.	Excellent	Good	Poor	Satisfactory	Satisfactory	Good	Good	Satisfactory	
Dependencies	Dependence on available software or packages	Good	Satisfactory	Poor	Poor	Satisfactory	Good	Good	Good	
Complete documentation	An up-to-date user manual is provided which explains all the aspects of the software	Satisfactory	Good	Poor	Excellent	Satisfactory	Satisfactory	Satisfactory	Poor	
User-friendly interface	The interface is straightforward, allowing non-specialized users to employ the tool	Good	Good	Poor	Satisfactory	Poor	Satisfactory	Satisfactory	Satisfactory	
Open-source	The source code is available to all users	Good	Poor	Inadequate	Good	Good	Good	Excellent	Good	
Reproducibility	Possible to get the same results over time	Satisfactory	Satisfactory	Satisfactory	Satisfactory	Satisfactory	Good	Satisfactory	Satisfactory	
Numerical stability	Able to obtain consistent solutions without infeasibility or non-convergence issues	Good	Satisfactory	Poor	Good	Satisfactory	Excellent	Satisfactory	Satisfactory	
Scalability	The tool can be applied to more than two species and to other various systems	Poor	Good	Poor	Satisfactory	Poor	Good	Good	Good	
Adherence to current standards	Meets SBML and other COBRA community level standards for model inputs & outputs	Good	Good	Poor	Poor	Poor	Satisfactory	Good	Satisfactory	
Interoperability	Able to be used and adjusted to standard GEM formats and with other formats	Satisfactory	Satisfactory	Satisfactory	Poor	Good	Satisfactory	Satisfactory	Satisfactory	
Flexibility	Various parameters can be adjusted.	Satisfactory	Satisfactory	Poor	Poor	Poor	Good	Satisfactory	Satisfactory	
Visualization of results	Is capable of producing ready, easy to understand visual outputs of model results	Satisfactory	Satisfactory	Satisfactory	Good	Satisfactory	Good	Satisfactory	Satisfactory	

Figure 7.4: Qualitative assessment of the dynamic tools. Colored squares indicate the evaluation of the specified feature in every tool. The color scale (upper right) goes from excellent (blue) to inadequate (red). When a feature does not apply to the specified tool or the feature was not evaluated, it is indicated as NA (Not applicable; grey). The metrics contained in the figure were inspired by [419]. The tools are ordered by year of publication.

dling some GEMs, especially those of eukaryotes with multiple compartments. Also, MCM utilizes an in-house convention when processing GEMs; thus, issues could arise when needing to employ the GEM in another tool or database. It is best that GEMs adhere to SBML standards [442]. Most software except MCM and d-OptCom earned at least a satisfactory score for dependencies. MCM earned a relatively low score because of the reliance on a not up-to-date micog.py extension (Python 2.7) for

using GEMs. Overall, tools such as MMODES, μ bialSim, and dyMMM received superior scores because they are readily available, accessible, and inoperable compared to the other tools.

7.4.3 Quantitative assessment - Dynamic tools

A case study comprising a dataset published by Hanly and Henson [436] was used to validate and quantitatively evaluate the dynamic tools. The experimental setup consists of a bioreactor operating in batch mode with a co-culture of *E. coli* and *S. cerevisiae* designed to study the efficient aerobic consumption of glucose/xylose mixtures. Each microbe utilizes a specific substrate. *S. cerevisiae* only consumes glucose, whereas the engineered *E. coli* strain ZSC113 only consumes xylose. This was done to prevent diauxic growth shown in monoculture for *S. cerevisiae*. The individual biomasses of the two microbial species as well as the concentration dynamics of the substrates glucose and xylose, were studied. Moreover, ethanol concentration dynamics were also measured because *S. cerevisiae* produces it during fermentation, thus, inhibiting the growth of *S. cerevisiae* and *E. coli*.

Furthermore, tools that scored 50 or above when summing up the qualitative scores were deemed of sufficient quality for a further quantitative examination. These tools were DFBALab, dyMMM, μ bialSim, and MMODES. We evaluated each tool's capability of simulating the observed kinetics using the same inputs across the methods. The error distribution for the different methods was determined (see Methods Section for a description of the normalized error calculation). *S. cerevisiae* and *E. coli* biomass concentration increases (Fig. 7.5). DFBALab was the only tool to predict the biomass formation of *E. coli* somewhat accurately though the simulation differed substantially from hours 5 to 12.5, showing no growth while growth was observed (Fig. 7.5B). μ bialSim and MMODES predicted growth for *E. coli*, but the biomass formations were at least an order of magnitude below measured biomass levels (Fig. 7.5B). dyMMM predicted slight growth of *E. coli*. Overall, μ bialSim and DFBALab achieved the best predictions for *E. coli* based on the experimental data with R^2 values of 0.959 and 0.775, respectively. For the *S. cerevisiae* growth kinetics, the dyMMM tool most accurately simulated biomass formation (Fig. 7.5D). While DFBALab predicted growth for *S. cerevisiae*, the final biomass concentration was about 65% less than the experimental value (Fig. 7.5D). μ bialSim and MMODES simulated slight growth for *S. cerevisiae*. Overall, dyMMM and DFBALab achieved the best predictions for *S. cerevisiae* based on the experimental data with R^2 values of 0.900 and 0.682, respectively (for all R^2 values, see supplementary materials).

The measure and predicted kinetics for the consumption of glucose and xylose, as well as the formation of ethanol, are illustrated in Fig. 7.6. Both sugars' concentration decrease over time, where glucose is completely consumed around 7.6 h

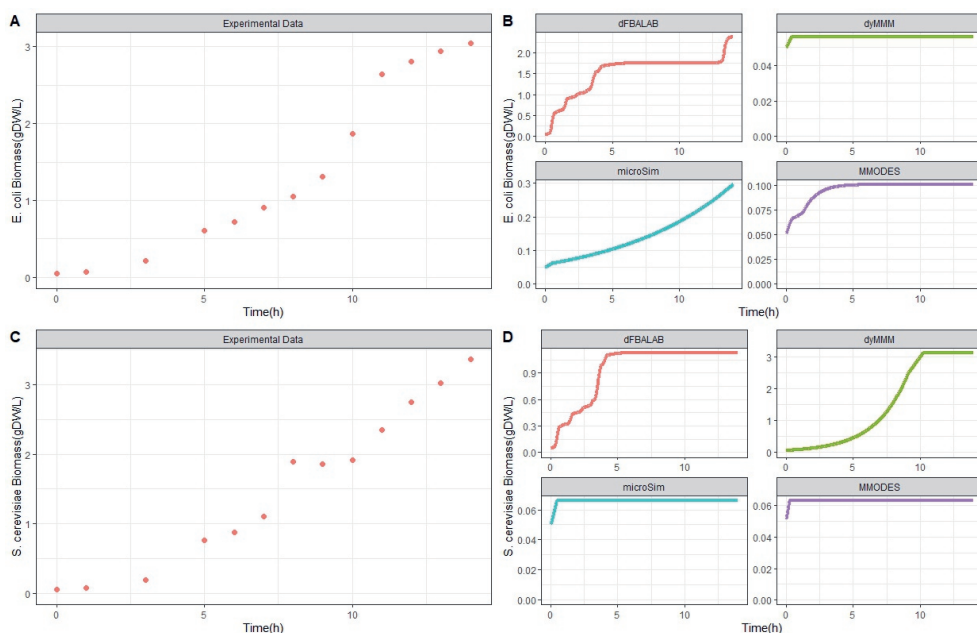


Figure 7.5: Quantitative assessment of the dynamic tools. Experimental biomass concentration profiles of *E. coli* and *S. cerevisiae* (Panel A and C, respectively). Comparison of tool predictions of biomass concentration profiles with data for *E. coli* and *S. cerevisiae* (Panel B and D, respectively) from the study of Hanly and Henson. [436]

while xylose remains in the medium longer and is used up entirely by around 13.2 h. This is due to a faster glucose uptake rate from *S. cerevisiae* compared to xylose's consumption rate by *E. coli*. There is a steady production of ethanol until the 7.5h duration. Then, there is a decrease in ethanol, perhaps because *S. cerevisiae* consumes ethanol under aerobic conditions. The co-culture featured a high increase in ethanol levels due to *S. cerevisiae* fermentation metabolism; ethanol is an inhibitor of *E. coli* growth. This ethanol inhibition from *S. cerevisiae* on *E. coli* growth was the only interspecies interaction identified in this experiment.

For the sugar substrates glucose and xylose, dyMMM and DFBalab simulated the kinetics most precisely according to the experimental values (Fig. 7.6A and Fig. 7.6B). However, DFBalab predicted rapid xylose consumption at the end of fermentation. MMODES simulated a linear glucose consumption with a final concentration of about 52 mM, while xylose consumption was not predicted. μ bialSim did not simulate glucose consumption, while xylose was consumed slightly with a final

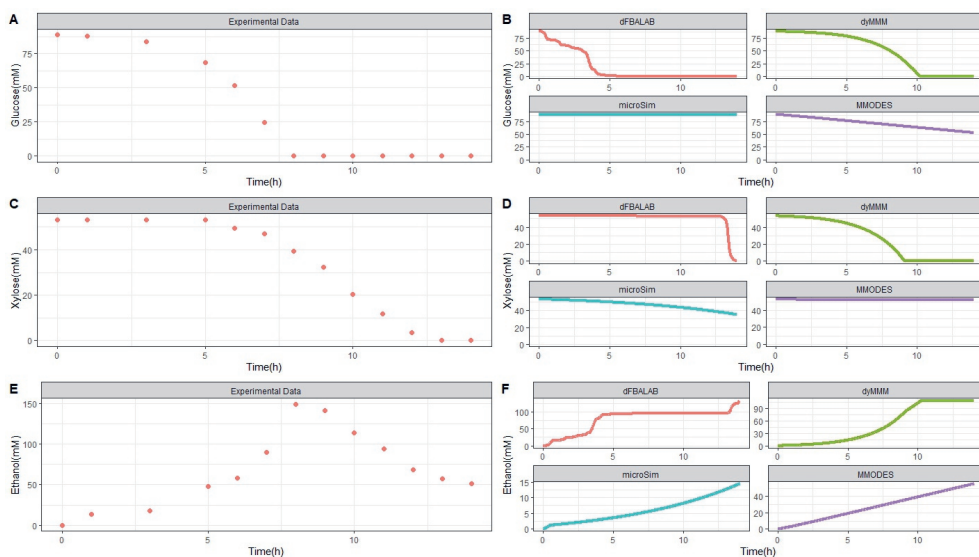


Figure 7.6: Quantitative assessment of the dynamic tools. Experimental extracellular metabolite concentration profiles of glucose, xylose, and ethanol (Panel A, C, and E, respectively). Comparison of tool predictions of biomass concentration profiles with data for glucose, xylose, and ethanol (Panel B, D, and F, respectively) from the study of Hanly and Henson. [436]

concentration of about 35 mM. All the tools simulated ethanol production. Nevertheless, none of the tools could accurately estimate the dynamics of ethanol production. This is because the diauxic shift from glucose to ethanol by *S. cerevisiae* cannot be modeled by simple optimization as done by FBA. dFBALab predicted the magnitude and kinetic characteristics most accurately, while µbialSim and MMODES gave an underestimation for the ethanol concentrations and reflected linear profiles (Fig. 7.6C). Overall, DFbALab achieved the best predictions for glucose, xylose, and ethanol kinetics based on the experimental data with R^2 values of 0.902, 0.978, and 0.440, respectively (for all R^2 values, see supplementary materials).

7.4.4 Qualitative assessment - Spatiotemporal tools

Fig. 7.7 shows the evaluation of the described features in every tool based on the evaluation rubric (S2 Table). From the qualitative assessment of all the spatiotemporal tools, none of the tools received a perfect score. Many tools were highly rated in many categories, while several were also deficient in many categories (see Fig. 7.7)

and supplementary files). For example, COMETS, BacArena, CROMICS received excellent scores for software availability and being open-source because these tools and their source codes are readily available via a GitHub repository or a maintained website, whereas MatNet received an adequate score because neither the tool nor its source code can be easily accessed online. When evaluating the software maintenance, user support, and ease of installation of the software, two tools stood out as excellent: COMETS and BacArena. In contrast, many of the tools, including IndiMeSH, MiMoSA, ACBM, and CROMICS were merely rated as being satisfactory to poor for software maintenance and user support (Fig. 7.7). However, except for MiMoSA, they were regarded as good for simple installation because of the accompanying instructions within the software download. Most of the tools received a good or excellent score for some features. For instance, for reproducibility, scalability, and visualization of results, all tools scored good to excellent, except ACBM and MatNet (for reproducibility), MiMoSA and MatNet (for scalability), and MiMoSA and MatNet (for visualization of results) (Fig. 7.7). ACBM did score well for reproducibility because slight changes in the same GEM files caused the tool to be invalid or inoperable. In general, IBM methods scored lower in terms of scalability because of the additional computational costs compared to PLM methods. Most of the tools contained some functionality for visualizing results or rendered outputs which were easy to use by other software tools. Many of the tools have at least a satisfactory level of traceability, reliance on available software, and documentation. Only ACBM scored poorly for traceability because changes to the software cannot be detected, whereas most other tools contain mechanisms to trace various versions, and updates are documented.

All the spatiotemporal tools received at least satisfactory scores except MatNet for their user-friendly interfaces and numerical stability (Fig. 7.7). These relative scores reflect how well the functionality, design, and incorporation of community-devised constraint-based modeling infrastructure into the methods. Also, some tools, such as COMETS and ACBM contain GUI options for novice users who may be less comfortable using command-line interfaces. Many of the tools were numerically stable, using examples implying users can start using the software assuming no infeasibilities occur under basic conditions. Overall, tools such as COMETS, BacArena, and CROMICS received superior scores because they are more readily available, up-to-date, open-source, and contain user-friendlier interfaces compared to the other tools.

7.4.5 Quantitative assessment - Spatiotemporal tools

A case study comprising a dataset published by Harcombe et al.[106] was used to validate and quantitatively evaluate the spatiotemporal tools. The experimental

Feature	Description	Spatiotemporal Tools						
		MatNet (2013)	COMETS (2021)	BacArena (2017)	IndiMeSH (2019)	MiMoSA (2019)	ACBM (2020)	CROMICS (2021)
Software availability	Is readily and freely accessible to users	Inadequate	Excellent	Excellent	Good	Good	Good	Excellent
Software maintenance	Developers and community specialists fix issues and routinely update tool	Inadequate	Excellent	Excellent	Satisfactory	Satisfactory	Poor	Satisfactory
Traceability	Changes or any modifications are documented and detected for users	Inadequate	Good	Good	Satisfactory	Good	Poor	Satisfactory
User support	Experts to answer user questions and community repository support	Inadequate	Excellent	Excellent	Satisfactory	Satisfactory	Satisfactory	Satisfactory
Simple installation	The installation process is fast and easy.	Poor	Excellent	Good	Good	Poor	Good	Good
Dependencies	Dependence on available software or packages	Poor	Good	Satisfactory	Satisfactory	Satisfactory	Satisfactory	Satisfactory
Complete documentation	An up-to-date user manual is provided which explains all the aspects of the software	Poor	Good	Excellent	Good	Satisfactory	Satisfactory	Satisfactory
User-friendly interface	The interface is straightforward, allowing non-specialized users to employ the tool	Poor	Excellent	Good	Satisfactory	Satisfactory	Good	Satisfactory
Open-source	The source code is available to all users	Inadequate	Excellent	Excellent	Excellent	Good	Poor	Excellent
Reproducibility	Possible to get the same results over time	Poor	Good	Good	Good	Satisfactory	Satisfactory	Good
Numerical stability	Able to obtain consistent solutions without infeasibility or non-convergence issues	Poor	Good	Excellent	Excellent	Satisfactory	Good	Good
Scalability	The tool can be applied to more than two species and to other various systems	Poor	Good	Satisfactory	Satisfactory	Satisfactory	Satisfactory	Satisfactory
Adherence to current standards	Meets SBML and other COBRA community level standards for model inputs & outputs	Satisfactory	Good	Good	Good	Satisfactory	Satisfactory	Good
Interoperability	Able to be used and adjusted to standard GEM formats and with other formats	Satisfactory	Good	Satisfactory	Poor	Poor	Poor	Good
Flexibility	Various parameters can be adjusted.	Poor	Good	Poor	Satisfactory	Poor	Poor	Satisfactory
Visualization of results	Is capable of producing ready, easy to understand visual outputs of model results	Poor	Excellent	Excellent	Good	Poor	Good	Good

Figure 7.7: Qualitative assessment of the spatiotemporal tools. Colored squares indicate the evaluation of the specified feature in every tool. The color scale (upper right) goes from excellent (blue) to inadequate (red). When a feature does not apply to the specified tool or the feature was not evaluated, it is indicated as NA (Not applicable; grey). The metrics contained in the figure were inspired by [419]. The tools are ordered by year of publication.

setup consists of a two-member consortium of two mutant strains of *E. coli* K-12 and *S. enterica* LT2 was designed to study the syntrophy between the two stains. *E. coli* K-12 is deficient in methionine production, so it relies on methionine production from *S. enterica* LT2. Conversely, *S. enterica* LT2 relies on the secretion of acetate by *E. coli* K-12 because *S. enterica* LT2 cannot uptake lactose under microaerobic conditions. This experiment created the optimal condition to observe a mutualistic relationship

where neither species can grow without the other being present. The two-species consortium was grown as a lawn on a Petri dish. Furthermore, experimentally, *E. coli* and *S. enterica* were grown overnight in permissive lactose Hypho minimal media (see Table S2 in [106] for more details) and then mixed at a ratio of 1:99 and 99:1. To examine the impact of time and space on the consortium, on LB, both *E. coli* and *S. enterica* can grow independently, and X-gal (5-bromo-4-chloro-3-indolyl-b-D-galactopyra- noside) was included in the plates so that blue *E. coli* colonies could be distinguished from white *S. enterica* colonies (see [106] for more details). The individual biomasses of the two microbial species were examined and measured over a 48-hour growth cycle by counting colonies. By the end of the cycle, the composition converged even when the inoculum frequencies varied by two orders of magnitude. Furthermore, the study also found a relationship concerning the spatial structure with the metabolite resources being allocated, which caused decreased growth between the species as they were moved further apart.

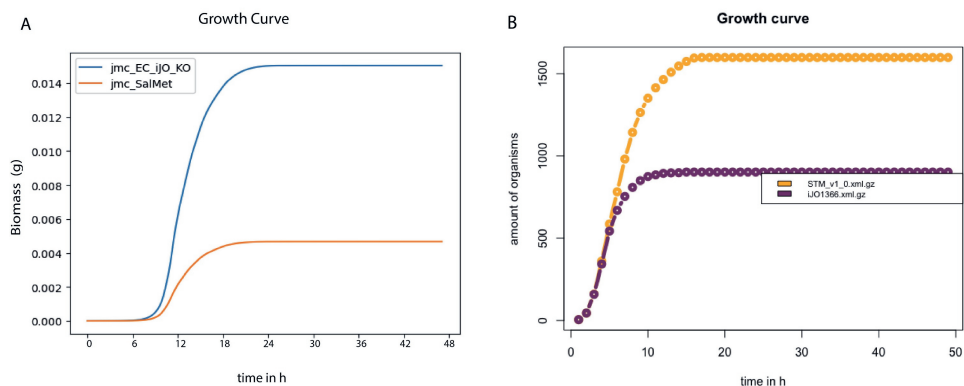


Figure 7.8: Quantitative assessment of the spatiotemporal tools. Relative abundance simulation profiles of *E. coli* and *S. enterica* from COMETS (Panel A) and BacArena (Panel B). Note biomasses used per individual organisms were 5×10^9 fg and 3×10^8 fg for *E. coli* and *S. enterica*, respectively. Experimental data used was from the study of Harcombe et al. [106]

From the qualitative assessment, there were four tools considered to be adequate for a further quantitative survey. Furthermore, from an enumeration of the qualitative scores, tools that scored overall 50 or above were deemed requisite quality (see supplementary material). These tools were COMETS, BacArena, IndiMeSH, and CROMICS. We evaluated each tool's capability of simulating the observed biomass dynamic as well as the spatial composition based on moving the species apart using similar inputs across the methods. The error distribution for the different methods

was determined (see Methods Section for a description of the normalized error calculation). Over the 48-hour cycle, the community composition of species converged regardless of whether the initial frequency was 1% or 99% of *E. coli*. COMETS predicted species ratios for the two initial frequency conditions (Fig. 7.8). COMETS predicted a composition of $79\% \pm 4\%$ *E. coli*, which is not significantly different from the experimental frequency of $78\% \pm 6\%$ (Fig. 7.9A). However, BacArena predicted a composition of 63.2% *E. coli* (Fig. 7.8B). The predictions of the community composition from IndiMeSH were determined not to be significantly different from both the experimental and COMETS simulation results (p-value of 0.66 and 0.33, respectively, two-tailed t-test) (see supplementary material). The CROMICS results showed that regardless of the initial frequency, the system converged in a species ratio of $76.3\% \pm 0.1\%$ for *E. coli* (see supplementary material).

The two-species consortium was used to examine the influence of spatial structure on resource allocation and growth within this mutualistic system. Here, we illustrate the evolution of the colony spatial distribution over time using a PBM (COMETS) and an IBM (BacArena) for their representations of biomass (Fig. 7.9). The COMETS simulation shows a rapid rise in the population density of *E. coli* and a shift in the location within the grid from *E. coli* from 9h to 48h (Fig. 7.9A). COMETS also predicted a moderate increase in population density in *S. enterica* as well as a slight shift in position from 9h to 48h (Fig. 7.9A). BacArena takes a different approach and models each organism individually on a two-dimensional grid to simulate a spatial environment. For BacArena, the colony evolved first around the initial microbial positions of *E. coli* and *S. enterica* where *E. coli* reaches a near-final individual amount $t = 9\text{h}$ (Fig. 7.9B). The simulated *S. enterica* colony continued to grow more abruptly, however, from $t = 9\text{h}$ to $t=48\text{h}$, filling up most of the remaining spatial elements (Fig. 7.9B).

As a simple test, we attempted to simulate conditions where the growth of the species should be affected by increasing distance between them. Consistent with what was observed experimentally[106], the simulations using COMETS, IndiMeSH, and CROMICS showed similar degrees of decreased growth as they were initiated further apart (see supplementary material for output data for all the tools). However, the BacArena tool could not capture any variation in spatiotemporal growth as observed during the experiment.

7.5 Discussion

This study provides a survey of the chronicled expansion of GEM modeling methods for microbial communities throughout the past decade and recommends the best GEM modeling tools based on qualitative and quantitative assessments. In par-

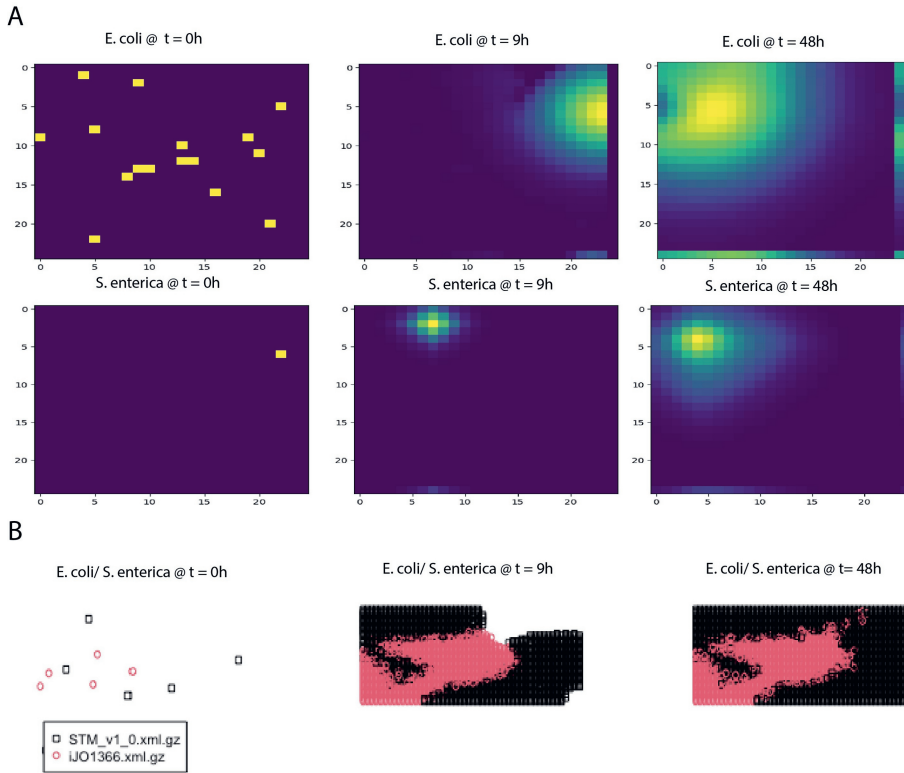


Figure 7.9: Quantitative assessment of the spatiotemporal tools. Colony spatial distribution over time simulation profiles of *E. coli* and *S. enterica* from COMETS (Panel A) and BacArena (Panel B). For Panel B, the red dots represent *E. coli* and the black dots represent *S. enterica*. Experimental data used was from the study of Harcombe et al. [106]

particular, we assessed tools that used CBM methods and their performance to model synthetic microbial communities of two species. This study also illustrates the challenges and brings forth issues and recommendations that should be considered when developing future tools, so that overall serviceability and performance can best facilitate potential users.

In general, GEM modeling tools fall into several categories for analyzing microbial communities. They have been used to identify interspecific interactions, which are embodied in tools such as SMETANA [443]. These tools can also contain extensive functionality, as illustrated in the Community Gap-Filling [444] tool for creating

draft GEMs from genome assemblies and performing gap filling and, based on the resolved metabolic gaps, can determine interspecies relationships. There are tools available such as CommModelPy [445], DOLMN [405], FLYCOP [446], and Community Opt-yield-FBA [447], which were developed to facilitate the synthetic designing of microbial consortia. However, this study focuses on static, dynamic, and spatiotemporal Flux-Balance-Analysis-based modeling tools used for simulating extracellular and intracellular metabolic phenotypes of microbial consortia. Furthermore, the scope of the work was limited to evaluating GEM modeling tools for microbial communities where the user needs to provide draft or curated GEMs as inputs and not tools that are used primarily to create the reconstructions. CommModelPy [445], DOLMN [405], and FLYCOP [446] likewise were omitted from this study's assessment because we believe they are outside its scope. For instance, the DOLMN tool is applicable for investigating the division of labor or interactions among different strains within the same species. Moreover, the FLYCOP pipeline employs the COMETS version 1 tool, which is already included in this study's assessment. Therefore, we feel that FLYCOP is more appropriate as an expansion tool to facilitate the *in-silico* design of synthetic microbial communities.

The criteria to qualitatively evaluate the tools was based on the FAIR principles that we consider, should be applied for data, operating procedures, tools, and models [420, 422]. Generally, tools that scored the highest in the qualitative assessment were shown to perform best in the quantitative assessment, highlighting the importance of following the FAIR principles. Tools that were less 'FAIR' could hardly be accessed nor used in this study. Thus, further information and access to the code would be required to quantitatively assess the performance of these tools and draw a conclusion. Nevertheless, a tool needs to be FAIR to be used, to contribute to the field, and thus, to shed light on the continuous challenges that can be, later on, tackled in new tools. In fact, this study observed the latter, since the continual publication of GEM modeling methods for microbial consortia over the past decade, has generally improved in performance over time. The first tools have served as a proof of concept and have established the basis for developing the new tools. However, there were a few exceptions of tools that had high scores in the qualitative assessment and performed worse than the average in the quantitative assessment.

In this study, the assessment was based on the modeling of two-species co-cultures, and therefore, the results could have varied when the tools were applied to larger communities, or to alternative systems. In addition, the limited availability of experimental data affected the selection of case studies, which might have an effect on the assessment of tools. By having more publicly available datasets, GEM modeling tools would be able to be more robustly evaluated on a quantitative level in terms of their scalability and numerical stability. In general, the performance of these tools would be enhanced if the quality of the GEMs or model architecture was

improved, and more constraints were applied to fit the experimental studies or to compute fluxes. However, we ran the tools without augmenting them and following the reported standards used to avoid an unbiased evaluation. The quantitative evaluations should be taken with a degree of awareness about their generality and projection to other types of systems. Furthermore, the quantitative evaluations here performed should be carefully considered as indications of tool performance rather than absolute measures of performance. They represent the behavior of the tools when confronted with specific datasets with defined biological characteristics. The syntrophic relationship established in the system used to test the static tools is different from the alleviation of toxicity observed in the dataset used for the dynamic tools. We can not rule out that tool performance is affected by the nature of the interactions.

The current status of the array of static, dynamic, and spatiotemporal tools for GEM modeling microbial consortia presents a substantial barrier to entry for researchers unfamiliar with specific requirements and idiosyncrasies that may arise within CBM frameworks. Tools should be user-friendly enough for a novice user who may be familiar with metabolic modeling concepts such as FBA and has some basic programming knowledge. We believe that user-friendliness is also linked to the quality of available documentation and the existence of community support. Therefore, we recommend keeping manuals and related repositories up to date and including dependencies amenable to changing computational environments or, alternatively, describing which packages are compatible. When the software is open/free, a possible solution could be to provide a container with the tool and the dependencies. All changes should be equally specified and updated in all places where the tool can be found unless specified otherwise. It is crucial that the tool is accessible to the users. Licenses are also important and should be provided because they allow tools to be incorporated in pipelines such as FLYCOP that build upon and extend the functionalities of COMETS to design microbial communities. We recommend the tools can read several GEM formats and namespaces without the need to translate the input models using other packages (e.g., COBRA Toolbox, COBRApy). The translation of these models often leads to a loss of information and a lack of key attributes that might generate errors when running the tools. The community models built by some static tools could keep the original bounds of the transport reactions of a single GEM to avoid the user the re-definition of the bounds once the community model is built. This would extend the use of these tools to cases with unspecified mediums/diets. Dynamic tools should allow the possibility of including inhibitory effects to better predict community behavior.

Tools oriented for modeling small and big communities should incorporate sufficient series of examples featuring a range of application scenarios from small to big communities. Tools could incorporate case studies with GEMs of non-model organ-

isms since many case studies are typically proven on communities of several *E. coli* species that use the same GEM. Other tools are meant to work with models retrieved from a specific database and defined namespace (e.g., AGORA [448]). The applicability of these tools to non-model organisms is critical for designing and optimizing synthetic communities. In the past decades, many synthetic communities have been established that do not depend on model organisms and have shown a high potential for producing commodity chemicals [64, 69, 70, 269, 449]. On the other hand, GEMs require accurate genome annotation and curation to properly account for interactions mediated through pathways, but there is still difficulty identifying these components in microbial genomes. Therefore, most GEM modeling efforts have been restricted in application to high-quality GEMs (*E. coli* and *S. cerevisiae*). To extend the applicability to alternative GEMs, the quality of GEMs of single species and communities should follow the community standards (e.g standard-GEM [450]) and, thus, be verified using test suites such as MEMOTE [299].

Some tools are based on approaches that use FBA and, therefore, are limited to the maximization of the community growth rate or species growth rate. In those cases, FBA favors growth over production, and cross-feeding metabolites might be overlooked (7.3B). Objective functions can be improved by using experimental data, or frameworks can be refined in dynamic tools to use a bi-level objective routine [451] or a multiphase, multiobjective approach [452]. Yet, these amendments may still not apply to all growth scenarios [453]. Flux sampling has been proven to be an effective tool to explore metabolism using GEM [88, 89, 454], and its use can mitigate the influence of the objective function. Flux sampling has also been successfully implemented to model microbial communities [51]. Therefore, we recommend integrating flux sampling methods in current and newly developed tools for modeling microbial communities in different environments, even though computational costs are high [455].

Future tools/approaches could consider using enzyme-constrained models to model microbial communities since they have shown great potential to better understand microbial phenotypes and phenomena such as overflow metabolism [89].

It is of the utmost importance that static tools/approaches incorporate the biomass composition of each species in their formulations beyond simply integrating the ratio by changing the stoichiometry of their biomass reaction. There is no clear consensus yet among static approaches on whether the species grow at balanced growth or whether the community and species growth rates differ. This challenges the selection of the objective function and the optimization approach of static tools. We believe that static tools best fit the simulation of continuous environments where the dilution rate is assumed to be constant, and thus, the community growth rate should be the same as single species [51]. Techniques that predict variable growth rates among microbes within a community should be incorporated into dynamic tools.

The drawback, nonetheless, is the inability to account for longitudinal community composition. An original method for alleviating this limitation is integrating ecological models within existing constraint-based frameworks. Some researchers have already begun employing COBRA methods and evolutionary game theory [456]. However, in the future, it would be beneficial to bolster more tools in this direction.

The results of this work suggest there is still much room for improving the overall quality of GEM modeling tools for microbial communities. Despite the immense number of proposed tools over the last decade, the availability, user-friendliness, and overall performance quality of the tools are disparate, and there is no perfect tool for all scenarios. In addition, although some of the tools were available and accessible to a moderately novice-level user, there were still some flaws in the quantitative predictions of those tools. However, we determined some tools were exceptional and should be preferred starting points for researchers or developers.

For instance, for static systems, cFBA is the approach that achieves the best outcome, but it largely requires manual adaptation. Moreover, it is not a tool, but merely a generalized approach or algorithm. However, self-contained tools, such as MICOM and SteadyCom, produce reasonable results. None of them outperform the others, so they can be considered as a starting point, and given the usability characteristics, we recommend MICOM. For dynamic systems, the choice is more difficult to discern, but given our results, we suggest dFBALab. MMODES is also a solid option, although discretion is advised when interpreting results from MMODES as predictions largely disagree with the measurements. Yet ethanol inhibition should be taken into account because the case we simulated contains ethanol inhibition. Therefore, an option or flexibility for augmenting a more complex Michaelis–Menten or Hill kinetic expression to reflect growth rate suppression at high ethanol concentrations would be desirable in a new tool. For spatiotemporal systems, we recommend either COMETS or BacArena because of their extensive development, accessible platforms, and documentation. COMETS performed better in simulating a simple co-culture experiment. However, BacArena is an individual-based method that can be beneficial when studying heterogeneous cell populations.

Through this qualitative and quantitative survey, we have presented and analyzed a broad overview of many GEM modeling tools for microbial consortia. These tools have been successfully applied in various types of systems of microbial communities. In addition, while these constraint-based tools have significantly transformed our understanding of communities by incorporating mechanistic details and highlighting metabolic interactions, there are still many opportunities for improving modeling frameworks by making software FAIR, user-friendly, and improving the accuracy of simulations of various types of systems. The work presented here can guide researchers in selecting the proper modeling tools and help developers build upon suitable modeling frameworks for new software tools.

7.6 Materials and Methods

An extensive literature review was executed to identify the state of the art of tools for modeling microbial communities in steady-state, dynamic, and spatiotemporal environments that used GEMs. Every tool was rigorously studied to follow a qualitative assessment. For that, we created an evaluation rubric that described each of the evaluation levels for every feature (S2 Table). All tools evaluated in this study are the most up-to-date versions as of December 15, 2022. In addition, we looked into studies that provided experimental data of synthetic microbial consortia of two species in every environment and assessed the performance of a set of each type of tool to reproduce them. The code used to produce our reported results can be downloaded from: <https://doi.org/10.5281/zenodo.7573135> and https://gitlab.com/wurssb/Modelling/modelingtools_microbial_consortia. The scripts can be used by other users as a guide to facilitate the evaluation and use of these tools.

7.6.1 Evaluation of static tools

The case study chosen to evaluate the static tools was the production of medium-chain fatty acids from the fermentation of CO by a co-culture of *C. autoethanogenum* and *C. kluyveri*. The GEM of *C. autoethanogenum*, iCLAU786 [219], and the GEM of *C. kluyveri*, ick1708 [220], were downloaded from their original publications in SBML (xml) format and used as the input files in every tool. Extracellular metabolites (defined in compartment ‘_e’) and exchange reactions (‘EX_XX’) common in both GEMs were modified to have the same namespace, as required to build the community model in all tools.

Experimental data was obtained from steady-state concentrations of fermentation products, total biomass, and hydraulic retention time (HRT) reported in the study of Diender et al. [68]. In particular, we simulated the condition defined in reactor run number three from the latter publication (Table 1 and Table 3; 116 mmol CO L⁻¹ d⁻¹ and 0 H₂). CO feed rate and steady-state concentrations of fermentation products were converted to mmol h⁻¹, and HRT (d) was converted to the growth rate (h⁻¹). The biomass species ratios were obtained from the computational study of the same co-culture [51], 0.4-0.6 *C. autoethanogenum*-*C. kluyveri*, respectively. CO feed rate was constrained to the experimental value in every tool unless stated otherwise. Additional constraints were applied and are specified per tool in the supplementary_File2 (S3 and S4 Tables). Predicted steady-state fluxes of acetate, ethanol, butyrate, and caproate, as well as the community growth rate, were compared to the experimental measurements.

Below, we describe the specific methods applied to run every tool. The links to access the tools repository can be found in S1 Table of the supplementary_File2.

OptCom

OptCom was run using the OptCom function found within the MICOM module called 'micom.optcom' instead of using the code from the original publication. Therefore, we first installed MICOM 0.32.2 using pip upon installation of Python 3.7 and COBRApy 0.24.0. 'OSQP' was installed by default with MICOM and was used as the solver. The community model was created using the 'Community' function. The function requires a 'taxonomy' table as an input parameter, which contains information about the species, models, and species relative abundance (biomass fraction). In addition, we included the mass as the input parameter (0.22 g). OptCom function was run with the generated community model as input, selecting 'original' as the strategy parameter and setting a min_growth of 0.01 h^{-1} for each species. The community growth rate was maximized simultaneously with all individual growth rates, and fluxes were computed. The input fluxes were provided as environmental fluxes in mmol h^{-1} , and thus, they had to be divided by the total community biomass (0.22 g) to simulate growth and multiplied by the total community biomass to output again environmental fluxes.

cFBA

cFBA was run using Python 3.7 and COBRApy 0.24.0 following the methodology implemented in a previous computational study, where a community model of the same two species was built [51]. 'GLPK' was used as the default solver installed with COBRApy. The community model was built manually, unifying the extracellular metabolites and extracellular reactions common between species in one single reaction or metabolite. We used the same community model without adding the extra reactions described in the latter publication. The species biomass reactions were constrained to the relative abundance multiplied by the growth rate (g h^{-1}), and the same as the community growth rate (0.021 h^{-1}). The solution space was computed using the 'sample' function in the flux_analysis submodule found in COBRApy. The results shown here are the average and standard deviation based on 10000 samples generated under the specified condition.

SteadyCom

MATLAB 2022b was installed using an academic license, and COBRA Toolbox version 3.33 was installed following the installation instructions specified in the GitHub

repository of COBRA Toolbox. SteadyCom was run using the 'SteadyCom' subroutine in COBRA Toolbox and 'GLPK', the LP solver installed when installing COBRA Toolbox. The community model was built using 'createMultipleSpeciesModel.' The names and IDs for metabolites and exchange reactions in the shared compartment of the community [u] were added into the community model as 'infoCom' and 'indCom' fields using 'createMultipleSpeciesModel.' The bounds of the reactions defined in the [u] compartment (e.g., 'autoIEX_MG[u]tr', 'EX_MG[u]') were imported from an excel file. SteadyCom was run using the built community model and the following options as input parameters: GRguess=0.5; algorithm=1; feasCrit=1 and BMweight=0.2. The community growth rate was maximized, and fluxes were computed.

Microbiome Modelling Toolbox (MMT)

MATLAB 2022b was installed using an academic license, and COBRA Toolbox version 3.33 was installed following the installation instructions specified in the GitHub repository of COBRA Toolbox. MMT 2.0 was run from COBRA Toolbox using 'GLPK', the LP solver installed when installing COBRA Toolbox. The community model was created using the 'joinModelsPairwiseFromList' function. The coupling factor 'c' and threshold 'u' was maintained at their default values, 400 and 0, respectively. The bounds of the reactions defined in the [u] compartment of the generated community model were imported and defined from an Excel file. The interactions and fluxes of the co-culture were next explored using the function called 'simulatePairwiseInteractions.' The species biomass reactions were constrained to the relative abundance multiplied by the growth rate (g h^{-1}). To run the latter function, the community model and the pairedModelInfo.mat file created by 'joinModelsPairwiseFromList' were used as the input parameters. Besides, 'saveSolutionsFlag' was selected to output the fluxes.

MICOM

MICOM was run using Python 3.7 and COBRAPy version 0.24.0. MICOM 0.32.2 was installed using pip as described in the GitHub repository of MICOM. 'OSQP' was installed by default with MICOM and was used as the solver. The community model was created using the 'Community' function following the procedure described to run OptCom. 'The cooperate tradeoff' algorithm was used with a fraction of 0.5 to simulate growth. The input fluxes were provided as environmental fluxes in mmol h^{-1} , and thus, they had to be divided by the total community biomass (0.22 g) to simulate growth, and multiplied by the total community biomass to output again environmental fluxes.

7.6.2 Evaluation of the dynamic tools

Similar to what was done by Hanly and coworkers [436], *S. cerevisiae* S288C (iND750) [457] and *E. coli* K-12 substr. MG1655's (iJR904) [458] GEMs, acquired from the BiGG database [459], were used to perform the model simulations with DyMMM, DFBAlab, MMODES, and μ bialSim. Furthermore, the *E. coli* model(iJR904) was modified by constraining flux bounds for glucose exchange and glucose kinase at zero to mathematically reflect the associated gene deletions. The simulations were based on an aerobic xylose co-culture of *S. cerevisiae* and the engineered *E. coli* strain ZSC113 fermentation experiment. In this experiment, glucose and xylose concentrations are expected to decrease over time, while the ethanol concentration is expected to increase. Simultaneously, *S. cerevisiae* and *E. coli* biomass concentrations are expected to increase over time. For all simulations, any constraints and parameters given in the original tools were modified according to the experimental values from the respective dataset from Hanly and coworkers [436]. Please see the supplementary_File2 (S6 and S7 Tables) for specific inputs. The simulated growth and metabolite concentration curves of *E. coli* and *S. cerevisiae*, as well as from glucose, xylose, and ethanol were compared to the experimental measurements.

The coefficient of determination, also known as R-squared (R^2) was calculated to quantitatively estimate the quality of the model fits and performance with the experimental data as in the work of Montgomery [460] for the dynamic and spatiotemporal cases.

The equation for R-squared is:

$$R^2 = 1 - \frac{SSE}{SST}$$

where: R^2 is the coefficient of determination, SSE is the sum of squared residuals, and SST is the total sum of squares, and $\frac{SSE}{SST}$ represents the ratio of the sum of squared residuals to the total sum of squares.

The equation for the sum of squared residuals:

$$SSE = \sum_{i=1}^n (y_i - \hat{y}_i)^2$$

where: SSE is the sum of squared residuals, y_i is the actual value of the dependent variable for the i^{th} observation, \hat{y}_i is the predicted value of the dependent variable for the i^{th} observation, and n is the number of observations.

The equation for the total sum of squares:

$$SST = \sum_{i=1}^n (y_i - \bar{y})^2$$

where: SST is the total sum of squares, y_i is the actual value of the dependent variable for the i^{th} observation, \bar{y} is the mean of the dependent variable, and n is the number of observations.

dyMMM

An implementation for this method is provided by the developers on sourceforge.net: <https://sourceforge.net/p/dyMMM/wiki/Home/>. This method requires a working installation of COBRA Toolbox [84] version 3.33 was used in this study with MATLAB 2022b. The provided formulation allows users to add initial concentrations of limiting or important substrates as well as products of interest. There is also a field to add initial biomass concentrations of microbes. We followed as instructed in the source code by the developers to add the proper inputs regarding initial concentration values of substrates and microbial biomasses, as well as GEMs, where needed. These inputs we added as presented in the supplementary table (S6 and S7 Tables).

DFBALab

An implementation for this method is provided by the developers via the website <https://yoric.mit.edu/software>. This method requires a working installation of IBM CPLEX (version 20.1.0 was used in this study with MATLAB 2022b) or Gurobi (we used Gurobi version 10.0). A similar example is supplied in the tutorial to the user as the case study used in this work. Although the original formulation of this method uses values directly from the literature [105], in the implementation, the values are not exactly as reported for our chosen case study. Therefore, the initial concentrations of glucose, xylose, and microbial biomasses were adapted (S6 and S7 Tables), and the time span of the simulation was modified from 10 to 14 hours.

µbialSim

An implementation for this method is supported via the website: <https://github.com/fcentler/microbialSim>. This method requires a working installation of COBRA Toolbox (version 3.33 was used in this study with MATLAB 2022b) or CellNetAnalyzer (version 2022.1 was used in this study). The provided example 2, based on a batch-culture growth of a binary syntrophic community, served as a starting point for employing our dynamic case study conditions. The reactor was defined according to initial substrate concentrations (see supplementary table). The GEMs (iJR904 and iND750) were loaded and adapted according to the COBRA Toolbox protocol within µbialSim. In addition, reaction indices for the non-growth associate maintenance (NGAM) and biomass reaction were provided. Exchange reactions were defined that link compounds in the reactor to cellular uptake and secretion. The models were parameterized according to the kinetic parameters provided in the literature (S6 and S7 Tables). The simulation duration and time step size chosen were 14 and 0.02 h, respectively. dFBA was selected as the solver type between the options ODE and dFBA. However, GPLK was used as the COBRA solver.

MMODES

An implementation for this method is supported via the website: <https://mmodes.readthedocs.io/en/latest/index.html>. MMODES was installed via pip (using Python 3.9 in this study as well as COBRAPy version 0.24.0). The example script and the documentation were used for instructions. First, the medium file was defined according to the medium composition given and initial conditions from the work of Hanly and Henson (see supplementary table). Next, the kinetic parameters were defined and set according to values used by Hanly and Henson (see supplementary table). Then, the GEMs (iJR904 and iND750) of the microbes, along with their respective initial biomasses and substrates they consume, were added to the model framework. The FBA optimization routine using the GPLK solver was selected. We chose a simulation time of 14 h with 0.02 h timesteps. Also, finite element analysis was used for the ordinary differential equation integrator.

7.6.3 Evaluation of the spatiotemporal tools

Similar to what was done by Harcombe et al. [106], simulations were performed using the GEMs for *E. coli* (iJO1366) [461] and *S. enterica* (iRR1083) [462]. We compared BacArena, IndiMeSH, and CROMICS, which were designed to study microbial communities using FBA and IBMs, with COMETS which was mainly designed to investigate the interrelationships of bacterial communities in space using FBA and PLMs. The goal was to compare the methods with one another for their potential in simulating trophic dependences of multispecies bacterial communities without making prior assumptions. Therefore, simulations mimicked the two-member consortium experiment studied in the original publication [106]. This consortium was composed of two mutant strains, *S. enterica* LT2 and *E. coli* K-12. *S. enterica* LT2 cannot metabolize and consume lactose, and *E. coli* K-12 cannot produce methionine. Hence, these two species participate in a mutualistic relationship because *S. enterica* relies on the secretion of acetate for a substrate by *E. coli* while *E. coli* needs *S. enterica* to produce methionine. Stoichiometric models of each species were modified to incorporate known genetic constraints according to the method of Harcombe and coworkers [106]. For instance, in the *E. coli* strain, the metB mutation was accounted for by constraining to zero the flux through the corresponding reaction (cystathionine γ -synthase). In *S. enterica*, methionine necessitated that we added a gain-of-function mutation in metA (homoserine transsuccinylase). This secretion was modeled as coupled to biomass where lactose is utilized by *E. coli*, so that as cells grew, they produced appropriate amino acid levels. A summary of boundary conditions, constraints, and parameters for all GEMs for spatiotemporal methods can be found in the Supplementary_File2 (S10 and S11 Tables).

COMETS

The *in silico* experiment was set up as reported in the work of Harcombe et al.[106] (for more detail, see experimental procedures in the original work). The developers provide an implementation for this method via the website: <https://www.runcomets.org/>. This method requires a working installation of Java and Gurobi (we used Java 20 in this study as well as Gurobi version 10.0). The Python version of the COMETS Toolbox (we used Python version 3.9 in this study as well as COMETS v0.4.1) was installed using the Anaconda distribution.

BacArena

The developers provide a tutorial to help implement this method via <https://bacarena.github.io/>. This method requires a working installation of R and Sybil (we used R version 4.2.2 in this study as well as Sybil version 2.2.0). Both GEMs of *E. coli* (iJO1366) and *S. enterica* (STM v1 multistrain) were retrieved from the BiGG database [459]. The *S. enterica* model was modified to ensure methionine production using the method of Harcombe et al.[106]. The biomass reaction was updated to include the production of 0.5 mmol gDW⁻¹ of excreted extracellular methionine, which was balanced by an equal amount of intracellular methionine consumed. The methionine transporter (METtex, METabcpp) were set to export only (upper bounds set to 0). The *E. coli* model was modified to block flux through the corresponding reaction, cystathionine γ -synthase (CYSTL). To model metabolic exchanges between the microbes and compare the results of BacArena with the other methods, we performed the simulations with our method using a setup similar to COMETS [106]. The simulations were carried out on a 50 times 50 grid environment for 48 hours. In the setups, a minimal medium stated in Harcombe et al.[106] was added to the environment with 1 mmol of lactose per grid position, oxygen, and several co-factors (calcium, chlorine, cobalt, potassium, iron, magnesium, ammonium, manganese, nickel, phosphate, zinc, and sulfate). To ensure the growth and mimic the preculture environment, an initial amount of 1.0 mmol methionine and acetate was added to each grid position. The amounts and biomasses of the initial species were also set according to initial frequencies used in Harcombe et al. [106]. The diffusion of metabolites was calibrated to the standard diffusion of glucose.

IndiMeSH

The developers provide an implementation for this method in the supporting materials of the original paper [415]. This method requires a working installation of MATLAB (we used MATLAB version 2022b in this study). The *in silico* experiment was performed to simulate microbial life on a two-dimensional surface in IndiMeSH,

a rectangular, saturated pore network (coordination number: 4) was created with the same topology as in the COMETS simulations (for details, see S1A Fig in the supplementary material of the original paper). Each pore has dimensions of 500x250x70 microns (LxWxH), as specified in the paper. Furthermore, we followed the setup as reported in the work of Borer et al. [415] (for details, see the Methods section in the original paper).

CROMICS

The developers provide an implementation for this method via a GitHub repository: <https://github.com/EPFL-LCSB/cromics>. This method requires a working installation of MATLAB and CPLEX solver (version 20.1.0 was used in this study with MATLAB 2022b). We used the setup detailed in the original paper [435], which mimics the setup of Harcombe and coworkers [106] for the two-species consortium of *S. enterica* and *E. coli* (for details, see the Methods section in the original paper [435]).

Supporting information

The code used to produce our reported results can be downloaded from: <https://doi.org/10.5281/zenodo.7573135> and https://gitlab.com/wurssb/Modelling/modelingtools_microbial_consortia. Additional information can be found in Supplementary_File1 and Supplementary_File2 of the gitlab repository.

Acknowledgments

P.J.S. and W.T.S.J. acknowledge the Dutch Research Council (NWO), and Wageningen University and Research for their financial contribution to the Unlock initiative (NWO: 184.035.007). This work was also supported by the Netherlands Science Foundation (NWO) under the Programme ‘Closed Cycles’ (Project nr. AL-WGK.2016.029) and the Netherlands Ministry of Education, Culture and Science under the Gravitation Grant nr. 024.002.002.

We thank Dr. William R. Harcombe and Dr. Jeremy Chacon from the Department of Biological Sciences at the University of Minnesota for assistance with the COMETS Toolbox for spatiotemporal modeling and interpretation of some experimental and model results. We thank Dr. Costas D. Maranas and Dr. Mohammad M. Islam from the Pennsylvania State University Department of Chemical Engineering for providing the d-OptCom tool and making suggestions for how to use the software.

We thank Dr. Louca Stilianos from the Institute of Ecology and Evolution at the University of Oregon for correspondence and assistance employing the Microbial Community Modeler (MCM) tool. We thank Dr. Christian Diener from the Gibbons Laboratory at the Institute of Systems Biology for assistance with MICOM.

Author Contributions

Authors' contributions: CRediT (Contribution Roles Taxonomy)- Conceptualization, W.T.S.J., S.B-V., M.S-D., and P.J.S.; Data Curation, W.T.S.J. and S.B-V.; Formal Analysis, W.T.S.J., S.B-V., and J.Z.; Funding Acquisition, M.S-D. and P.J.S.; Investigation, W.T.S.J. and S.B-V.; Methodology, W.T.S.J., S.B-V., and M.S-D.; Resources, P.J.S. and M.S-D.; Software, W.T.S.J., J.Z., D.B., and A.H.; Supervision, W.T.S.J., M.S-D., and P.J.S.; Validation, W.T.S.J. and S.B-V.; Visualization, W.T.S.J. and S.B-V.; Writing—original draft, W.T.S.J. and S.B-V.; Writing—review and editing, W.T.S.J., S.B-V., J.Z., D.B., A.H., M.S-D., and P.J.S. All authors have read and agreed to the published version of the manuscript.

Chapter 8

Discussion

The goal of this thesis was to explore, optimize and guide novel designs for the microbial upcycling of C1 feedstocks to added-value chemicals by means of genome-scale, constraint-based metabolic modeling methods. This underpins the aim to convert C1 compounds to a wide range of products/molecules (and chain lengths) by assembling different combinations of microbes in synthetic microbial communities. Thereby, this research contributes to the ultimate goal of society to become carbon neutral by closing the carbon cycle.

8.1 Investigation on the conversion of C1 feedstocks through synthetic microbial communities

First, the state-of-the-art of C1 conversion was investigated and a potential approach was selected for bioconversion of C1 feedstocks. In **chapter 2**, we contrast the energetic efficiency of converting different C1 substrates into biomass aerobically and anaerobically. Anaerobic conversion by acetogens leads to a higher energy efficiency than aerobic conversion, which gave rise to our subsequent studies with acetogens. However, acetogens grow at the edge of thermodynamics [54], as only 0.3 ATP are produced per each CO₂/ H₂ or 1.5 ATP per 1 CO converted [54]. The lack of additional energy and the low solubility of the gases limit the product range of acetogens to simple molecules: acetate, ethanol, low amounts of formate, 2,3-butanediol and lactate, or in few exceptions, butyrate, butanol, caproate and hexanol [353, 463]. The energetic barriers acetogens face can be partly overcome using miscible C1 substrates such as formate or methanol, as they showed superior energetic efficiency (**chapter 2**). However, the ATP yield reported in *Acetobacterium woodii* for formate conversion was 0.3 ATP per mol of acetate produced in absence of ethanol [464], as compared to 0.4 and 1 ATP mols per mol of acetate produced from CO₂/H₂ and CO, respectively [54]. On the other hand, co-utilization of formate or methanol with C1 gases (e.g., CO) warrants further investigation, since these compounds can act as electrons donors leading to increased ethanol production, as we have seen to be the

case with the addition of H₂ (**chapter 5**).

Through several studies in this thesis, I have demonstrated the potential of synthetic microbial communities as a means to expand the range of products obtained from acetogenic fermentation of C1 gases. Following a modular approach (Fig. 8.1), microbes were replaced or added to steer the product range from even- to odd-chain fatty acids. This is possible due to division of labour among community members [465], which allows them to perform complex tasks for mutual benefit that would be seldomly achieved in pure acetogenic cultures [353, 463].

As a proof of concept, the co-culture of *Clostridium autoethanogenum* and *Clostridium kluyveri* was first experimentally established for the fermentation of CO to medium-chain fatty acids (MCFAs) of even number of carbon and their respective alcohols [64, 68]. Here, the acetogenic products served as substrates for *C. kluyveri* to produce even-chain MCFAs. In this thesis, I extend the latter study by modeling the aforementioned co-culture using and expanding cFBA with sampling methods to further explore (intra)cellular fluxes (Fig. 8.1) (**chapter 3**). The study enlightened the effect of the species ratio on their metabolism, and suggested strategies to optimize the production of MCFAs.

Acetobacterium wieringae JM is an acetogen usually cultivated at pH close to neutral (6.8-7.2) [332, 333], similar to *C. kluyveri*'s optimal pH for chain elongation (6.5-7.5) [334]. Thus, in **chapter 5** we computationally assess the feasibility of an alternative co-culture where the acetogen *C. autoethanogenum* studied in co-cultivation with *C. kluyveri* is replaced by *A. wieringae* JM. Modeling of this community required the reconstruction of the model of *A. wieringae* JM (**chapter 5**) (Fig. 8.1). *A. neopropionicum* grows on ethanol and ethanol/acetate (**chapter 4**) in the presence of CO₂ producing propionate, and it also thrives at a pH range around neutrality (**chapter 4**). In co-cultivation, propionate can be taken up by *C. kluyveri* shifting the product spectrum from even- to odd-chain fatty acids [331]. Thus, I construct the model of *A. neopropionicum* (**chapter 4**) (Fig. 8.1), and assemble the models of these three microbes to assess the feasibility of the tri-culture for the production of odd-chain fatty acids from syngas (Fig. 8.1). In this study, metabolic modeling is used to further explore hypotheses and to drive experimental designs thereby reducing experimental efforts.

In **chapter 6**, I demonstrate the use of modeling to guide new experimental designs by assembling the model of *C. autoethanogenum* with two solventogenic species. Following a model-driven approach, we found that lactate and acetate were co-metabolized and sustained growth as well as butyrate and isobutyrate production by the solventogen *C. beijerinckii*. This demonstrated that the addition of a new carbon source can enable the establishment of a community and produce valuable products overcoming the limitations of acetogens as well. Furthermore, this study highlighted the importance of the biomass species ratios for the establishment of the

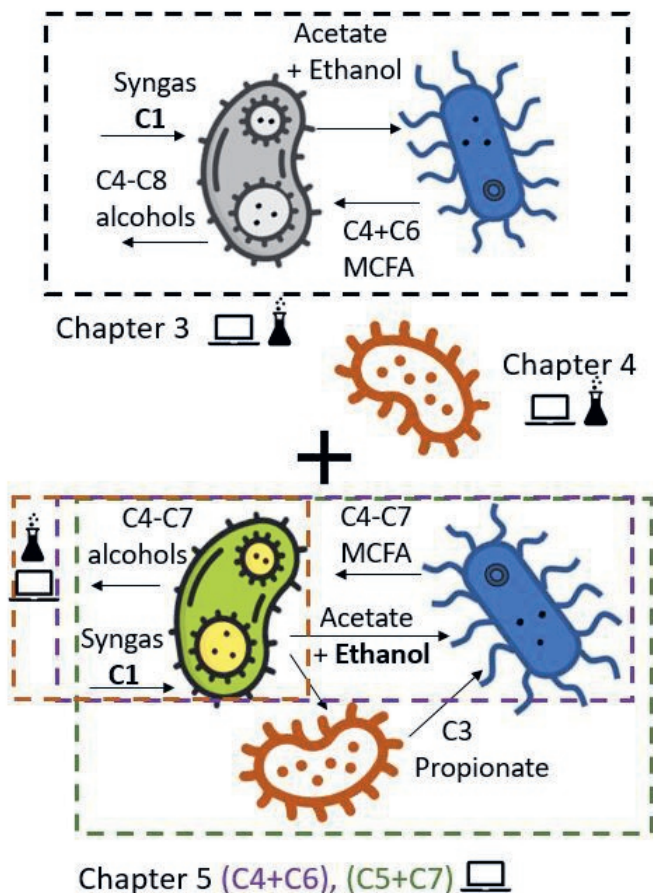


Figure 8.1: Modular approach followed throughout chapters 3-5 to shift production from even- to odd-chain fatty-acids by the incorporation of *A. neopropionicum* (orange microbe) in a CO-fermenting co-culture. Grey microbe: *C. autoethanogenum*; green microbe: *A. wieringae* JM; blue microbe: *C. kluyveri*. In the bottom part, squared areas indicate different communities or single microbes. Orange square: *A. wieringae* JM is modelled and characterized as single species. Purple square: production of even-chain MCFA. Green square: production of odd-chain MCFA. The computer and the flask symbols indicate whether the specified chapter describes computational and experimental approaches, respectively.

co-culture and their effect on cross-feeding metabolites.

Throughout this thesis I use cFBA upon manual construction of the community models by combining single species models. Even though this approach has been positively evaluated (**chapter 7**), it is laborious and difficult to implement. However, there are several tools that automatically construct community models and scale the fluxes to account for relative abundance, which facilitates initial reconstructions. Thus, I followed a systematic approach to evaluate those tools by ascertaining their strengths and limitations (**chapter 7**).

Thereby, through metabolic modeling, I have achieved the primary goals of this thesis of: a) assessing the feasibility of building synthetic microbial communities, b) getting insights into their combined and individual metabolisms, c) unraveling new metabolic capabilities, and d) guiding experimental designs and suggesting potential strategies for the optimization of MCFA for C1 conversion by synthetic microbial communities. However, during the realization of this thesis, I faced several challenges and identified the main limitations that hinder the potential of synthetic microbial communities as an additional solution for the conversion of C1 feedstocks. The following sections address some of these challenges and limitations, suggesting possible solutions to overcome them. Finally, I reflect on the future perspectives of C1 conversion by synthetic microbial communities.

8.2 Low ethanol availability hampers MCFAs production in CO-fermenting synthetic communities

Recurrent challenges found to limit the establishment of synthetic microbial communities were the accumulation of unwanted products (**chapter 3, chapter 5, chapter 6**), the selection of pH for cultivation, and substrate competition. Acetate was the main fermentation product obtained from syngas fermentation by the studied acetogens. Ethanol was also produced, but generally in lower amounts. *C. kluyveri* consumes 6 ethanol and 4 acetate to produce 5 butyrate and 2 H₂ [320]. Thus, ethanol:acetate ratios >1 promote chain elongation. Even though the addition of *C. kluyveri* shifted the acetogenic metabolism to solventogenesis (**chapter 3, chapter 5**) [68], acetate accumulation was still significant. Strategies are sought to increase ethanol production by acetogens. Ethanol production increases substantially at acidic pH (≈ 5) in *C. autoethanogenum* [345]. However, *C. kluyveri* grows optimally at a higher pH ($\approx 6.5-7.5$), therefore, in a co-culture of these two species, a trade-off exists between ethanol and MCFAs production [65].

In **chapter 5**, we replaced the acetogen *C. autoethanogenum* by the acetogen *A. wieringae* JM, since the latter grows optimally at pH neutral pH, closer to that of the

other two community members, *A. neopropionicum* and *C. kluyveri*. Cross-feeding of ethanol is again essential in this community. Both *A. neopropionicum* and *C. kluyveri* require ethanol for the production of propionate and for chain elongation, respectively. This substrate competition between the two members affected the feasibility of the community in some conditions, when ethanol production was not high enough to sustain growth of both species. While the acetogen produced mostly acetate in mono-culture, in co-cultivation with *A. neopropionicum* and *C. kluyveri*, acetate production decreased in favour of ethanol. However, ethanol availability was still low in some conditions, leading to increased accumulation of acetate and propionate, which ultimately limited the production of odd- and even-chain MCFAs (**chapter 5**). Thus, modeling was used to identify possible strategies to increase ethanol production. The supplementation of H₂ was shown to increase ethanol production by *A. wieringae* JM reducing the accumulation of acetate and propionate, and positively impacting the final product output (**chapter 3, chapter 5**).

Metabolic engineering strategies have also shown potential for increasing the production of ethanol in Clostridia (co)-cultures [50]. In **chapter 3**, metabolic modeling led to the suggestion of genetic modifications in *C. autoethanogenum* that could increase ethanol production up to 150%. Some of these strategies have been in fact demonstrated in previous studies [50, 345]. In **chapter 6**, we investigated endogenous lactate production as electron donor instead of ethanol to drive the production of MCFA [466]. Yet, the production of lactate from syngas was very low, and lactate had to be externally supplemented. Again, metabolic engineering strategies can tackle this issue as they have already been applied to increase lactate production in acetogens [379]. Alternatively, one could use an acetogen that shifts to solventogenesis at a higher pH, as it seems to be the case for *Clostridium aceticum*, in which ethanol production is triggered at pH 6.9 [330].

8.3 Determining biomass composition in microbial communities: a must-do

The amount of experimental data available determines to which extend community modeling tools can be implemented (**chapter 7**). In **chapter 3, chapter 5, and chapter 6** we saw how the relative contribution of each species to the biomass of the community affected the feasibility and product profile of the co-cultures. I believe that measurement and integration of relative biomass abundance data in community modeling tools is key for more accurate predictions. However, these measurements are often not available.

In **chapter 3**, we relied on microscopic observations of cells and RNAseq reads to

estimate the abundances to be considered in the overall biomass composition. Both measurements resulted in similar ratios for the conditions where data was collected. The measurements reflected microbial relative abundances, so these had to be complemented with estimates on bacterial weight to obtain the corresponding biomass species ratios. An estimate of the proportion of each strain was based on detailed microscopy observations, and information from literature was used to calculate the volume of each cell and derive the dry weight. The dry weight of each cell was estimated and the final biomass species ratio was retrieved based on the proportion observed under the microscope. This step was critical, since the proportion of cells observed was 10/1, and the biomass species ratio was 4/6 (*C. autoethanogenum*/*C. kluyveri*). Thus, determination of the composition of the community and the cell weight is key.

Since data reflecting variation of the species ratio under different conditions was not available, we made the assumption that the ratio remained constant. However, the operational and environmental conditions (e.g., pH, substrate availability, growth rates) do have an effect on the biomass formation of each species. In future studies, I recommend to obtain experimental data on biomass composition under a variety of conditions of interest, e.g., growth on CO and CO/H₂ and at different growth rates. In addition, the use of alternative methodologies to quantify cell populations, such as qPCR, flow cytometry, fluorescence microscopy [69, 467] or metagenomic analyses [468] should be considered. Tackling the effect of biomass composition in the absence of experimental data is a challenge for modelers and therefore, the predictability of models can be affected.

That being said, when cultivating a microbial community in bioreactors, the biomass species ratio is not a parameter that can be as easily imposed as operational parameters such as the dilution rate or the pH. In fact, the ratio is partly determined by the latter factors. However, the information from the modeling can help at least in tuning the process towards a specific ratio or avoiding another, or evaluating the capabilities/uncapabilities of the community at a given ratio. Besides, this insight could drive the development/implementation of techniques to establish certain ratios, such colloid biology [469, 470] or the use of hydrogels [471].

8.4 Modeling the impact of pH in microbial (community) behaviour

As we have observed, the pH has a crucial role on the stability, product spectrum and, thus, the potential of the synthetic microbial communities. However, metabolic models have only very rarely accounted for the role of pH thus far [472]. The

pH is defined as the negative \log_{10} of the proton concentration (H^+) expressed in mol L^{-1} . Microbes can endure changes of extracellular pH, and very often the extracellular pH is different than the intracellular pH. As a response to changes in the external pH, homeostasis mechanisms are triggered in the cell. Rather than maintaining a constant intracellular pH, maintaining a constant pH gradient across the cell membrane ($\Delta\text{pH} = \text{pH}_{\text{in}} - \text{pH}_{\text{out}}$) seems to be essential for growth of Clostridia [473].

The ΔpH is generated and maintained by the ATPase, which translocates protons and generates a transmembrane difference in electrical potential ($\Delta\psi$). The ΔpH and the $\Delta\psi$ determine the proton motive force (PMF), which drives ATP synthesis [473]. The PMF is maintained constant. This means that the ATPase is also involved in the de-acidification of the cytosol. In some solventogenic species, the ΔpH does not seem to be constant for acidic external pH (≈ 4.5), since the intracellular pH seems to not change once the pH drops from 5.5. In these circumstances, an additional mechanism to the ATPase might also be involved for extrusion of H^+ in deacidification of the cytosol [474].

The direct extrapolation of these mechanisms into metabolic models is difficult to achieve. In GEMs, the flux of H^+ is typically indicated by the artificial exchange reaction 'EX_H⁺_e', which directly depends on the production or consumption flux of metabolites in the form of extracellular reactions ('EX_XX_e') and the ATPase reaction. Consequently, varying the flux through the H^+ exchange reaction ('EX_H⁺_e'), might give us a correlation with the pH, as Sánchez-Clemente et al. showed [472]. Fig. 8.2 shows the effect of changing the flux of H^+ on the fermentation of CO by *C. autoethanogenum* (8.2A), and on the fermentation of acetate and ethanol by *C. kluyveri* (8.2B). The optimal pH of *C. autoethanogenum* is in the 5.8 - 6 range, being acetate the main product under this condition [211]. Thus, I hypothesize that the conditions reached within the green band would correspond to a situation where the extracellular pH is close to the optimal pH in *C. autoethanogenum* (Figure 8.2A). The production of acetate acidifies the medium. Consequently, acetate is re-assimilated and ethanol is produced. At this moment, pH is lower, which could indicate that the yellow band corresponds to situations where the pH is lower than the optimal. Allaart et al. showed how the pH affected the product profile in the fermentation of acetate and ethanol in *C. kluyveri* [343]. At pH 7 (\approx optimal pH), caproate production was higher than butyrate production, and at pH 5.5, butyrate production was higher than caproate for ethanol:acetate ratios > 1 . Extrapolating this information to the graph, the colored bands might represent conditions where the pH is close or lower than the optimal. I hypothesize that the maximum growth rate obtained using FBA, would likely indicate conditions close to the optimal pH, as it can be derived from the figure. However, we cannot directly relate H^+ flux and pH values, as the latter refer to concentrations.

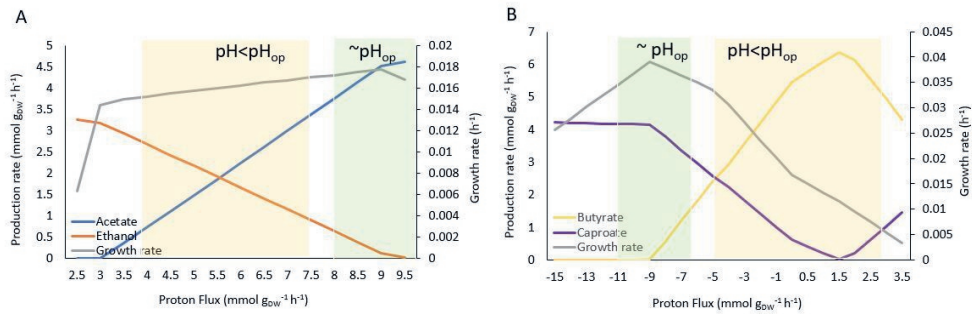


Figure 8.2: Effect of varying the flux of H^+ on the growth rate and product profile of *C. autoethanogenum* (A) and *C. kluyveri* (B) on CO and acetate + ethanol, respectively. CO uptake was fixed to $10 \text{ mmol g}_{\text{DW}}^{-1} \text{ h}^{-1}$ and uptake of acetate and ethanol to 5 and $8 \text{ mmol g}_{\text{DW}}^{-1} \text{ h}^{-1}$, respectively. For each possible value of the H^+ uptake or production rate (negative and positive values respectively), the growth rate was maximized using FBA.

This information suggests a range of H^+ flux in order to simulate steady-state conditions at a pH lower or similar to the optimal pH of each species. In continuous environments where the pH is controlled, one does not expect great variations in the intracellular pH, as the ΔpH is to be kept constant. Thus, one could correlate H^+ flux with pH using measured experimental uptake rates, growth rate and products rates at one specific pH as constraints in the model, and retrieve the compute H^+ flux.

Concentration of H^+ , on the other hand, could directly be investigated using dFBA. For instance, one could run batch experiments at different initial pH on CO with one of the acetogens here studied, and measure the pH change, CO uptake rate, concentration of substrates and products, production rates, initial and final biomass, and the maximum growth rate. Besides CO, H^+ concentration can be studied as a metabolite that is being consumed, so that we see the H^+ concentration at every pH over time. One could then retrieve a relation between the difference in concentration of H^+ from one pH to another which, in turn, is translated in the translocation of H^+ through the ATPase. I do not expect the models to precisely predict the impact of pH changes, as homeostasis requirements are introduced through the NGAM contributions in the models, which is a very general method. Still these adaptations would allow better predictions on a range of concentrations where the model better correlates with the experimental data.

Based on the previous investigation, communities of species cultivated at a pH different than their optimal pH will potentially lead to product profiles different to the ones obtained at optimal conditions with pure cultures (e.g., butyrate vs.

caproate production in **chapter 3**). The differences in product profile might impact the biomass of each species and, thus, the intracellular fluxes. These effects could be analyzed in a combined experimental and *in-silico* approach. One could extrapolate the H⁺ flux/concentration range derived from the previously described experiments at specific pH and use them as constraints for each of the species involved in the community. However, community models have a unique H⁺ exchange reaction. Thus, experiments should be run for the community following the same approach proposed for single species and derived the H⁺ flux/concentration of the community as a whole to constraint the model.

Alternatively, thermodynamic models (e.g., pyTFA, matTFA) could be used in combination with the previously described experimental approaches to inform on the energy metabolism in acetogens [475], where production of acetate and ethanol seems to be controlled by thermodynamics rather than by enzyme expression [68, 344]. Acidify-ME is another framework to study acid stress through ME-Models, but it is still limited to the explanation of some mechanisms (e.g protein stability) and it cannot be directly used yet to fully model the pH effect [249].

8.5 Modeling approaches to study synthetic microbial communities

When modeling microbial communities, it is important to use the right tool and approach for the environment being represented or the type of information that is sought. In this thesis, we used mainly static approaches to represent chemostat operations (**chapter 3**, **chapter 5**) and to evaluate co-culture feasibility (**chapter 6** and **chapter 5**). At industrial scale, continuous operations are often preferable for products that require a massive production (e.g, bulk chemicals), since they can be run for longer periods of time avoiding product toxicity. Production of MCFAs would likely follow the latter procedure, which emphasizes the need of model those operations. In **chapter 7**, we reviewed available static tools and their respective assumptions in regard of their objective function. Some static tools do not assume equal growth rates of the species in the community, and their objective function is often the community growth rate. Static tools are based on steady-state assumptions, which are assumed to be reached in continuous environments (e.g., chemostat cultivation). In a chemostat, the growth rate of cells is fixed and controlled via the dilution rate of the reactor. Thus, the growth rate of each species should be the same and equal to the community growth rate when the community is stable. In the latter situation and using methods that require the definition of an objective, one could choose the maximization of the community growth rate at the same time as the species growth rate

as a linear problem (e.g., SteadyCom) [228]. An alternative would be to maximize or optimize the production of a specific metabolite, or to use Flux sampling that does not require an objective function. Flux sampling gives information of the exchange of amino acids or other secondary metabolites that might be, in some cases, key to establish the community. In **chapter 7**, results proved the ability of Flux sampling to predict cross-feeding interactions, while some approaches that rely on FBA did not.

At industrial scale, the production of secondary metabolites or products with lower/seasonal demand (e.g pharmaceuticals) are produced in non-continuous operations. At laboratory scale, non-continuous operations (e.g batch, fed-batch) are used for instance in growth experiments and characterization of products at different conditions, etc. In this thesis, batch operations were used for the establishment of a novel synthetic community (**chapter 6**) and for the characterization of *A. neopropionicum* (**chapter 4**). In the latter examples, non-continuous operations were used to analyze the concentration of biomass, substrates, products and maximum growth of these species. To model cultivation in batch or fed-batch, dynamic approaches are required to follow the consumption and production of metabolites over time (**chapter 4**). These approaches require additional data, such as initial concentrations, maximum uptake rates, growth rates and kinetic parameters. This data is often not available, and more assumptions would need to be taken in detriment of trustworthy predictions. This was the case when modeling was used to drive the establishment of a novel co-culture of *C. autoethanogenum* and *C. beijerinckii* (**chapter 6**). Here, there was not data available and we used a static approach to study the co-culture feasibility.

8.6 Future perspectives of microbial C1 conversion to valuable products

Despite the drawbacks associated to the low solubility of gases, the production of over 50 products from gas fermentation has already been demonstrated [262]. One of the most successful examples is the production of ethanol at industrial scale by acetogenic Clostridia [49, 50, 59, 476]. Lanzatech has already deployed two industrial plants with an annual production of more than 90,000 metric tons of ethanol. Furthermore, they have recently reported the production of acetone and isopropanol by gas fermentation at industrial pilot scale with recombinant acetogenic strains [59]. The feasibility of Lanzatech's technology is a stepping stone towards the transition to a circular bio-based economy and opens new possibilities for alternative technologies that focus on the valorization of renewable C1 feedstocks through microbial conversion. Here, we highlighted the potential of synthetic microbial com-

munities to produce MCFAs and alcohols from syngas. MCFAs have great potential for their use in the production of animal feed, food, pharmaceuticals, cosmetics or antimicrobials [477]. Furthermore, their market size is expected to increase due to an expected growing demand of food, pharmaceuticals and cosmetics. The global butyric acid market was over 175 USD Million in 2020 and it is estimated to grow $\approx 13.2\%$ in the next seven years [478], while the global market for caproic acid was estimated at USD 176.7 Million in 2020 and it is projected to reach USD 283.6 Million by 2027 [479].

The production of MCFAs from waste-derived carbon by synthetic microbial conversion is not yet feasible at industrial scale. However, there is an interest for the recovery of these metabolites produced during the anaerobic digestion, due to their higher economic value than methane or biogas [480, 481]. The conversion of food-waste to biogas via anaerobic digestion processes in open-mixed cultures is at industrial scale [482], but it is estimated that only a tonne of food waste leads to biogas € 76 worth [483]. In fact, the production of MCFAs could become the main source of income in such process, and biogas production by bioaugmentation with acetoclastic methanogens could be regarded as a secondary process and a way to reduce acetate accumulation. As a rule of thumb, the production of MCFAs needs to exceed $1 \text{ g L}^{-1} \text{ h}^{-1}$ to be economically feasible [28], and many factors have an impact on productivity, such as feedstock use, reactor design, downstream processing, etc. An open-mixed culture produced $0.1 \text{ g L}^{-1} \text{ h}^{-1}$ of caproate from food waste [484], still an order of magnitude lower than the target. However, a co-culture of *C. kluyveri* and *C. saccharolyticum* already reported up to $\approx 0.9 \text{ g L}^{-1} \text{ h}^{-1}$ of caproate production during growth on sugars [485]. While microbial conversion of syngas to MCFAs at industrial scale is not there yet, the continuous efforts foresee an optimistic future. A few years ago, a continuous culture of *C. autoethanogenum* and *C. kluyveri* on syngas achieved a production of 1.1 and 0.8 g L^{-1} of butyrate and caproate, respectively. The co-culture of *C. autoethanogenum* and *C. beijerinckii* on CO_2/H_2 (**chapter 6**) led to 4.4 g L^{-1} of butyrate. Last year, a continuous culture of *C. aceticum* and *C. kluyveri* on syngas reached a production of 7.0 and 8.2 g L^{-1} of butyrate and caproate, respectively [330]. Despite this being a relatively new technology, production yields from syngas will likely reach competitive values in the coming years due to biotechnological advances. Continuous developments in metabolic engineering and synthetic biology strategies shall potentially increase production yields of MCFAs, as it has been demonstrated in pure cultures with acetogenic species [50, 59, 262, 486–488].

Furthermore, the use of electrodes has also shown potential as additional electron donor with ethanol to improve chain elongation [489]. The selection of the separation technique is also important. The use of in-line extraction or pertraction -reactor recirculation stream- might increase the productivity of MCFAs, since it avoids accumulation of the products and, thus, the reduction of activity due to

toxicity events [62, 477]. Sequential fermentation is envisioned as a promising approach for the conversion of C1 feedstocks to lipids, isopropanol, polyhydroxybutyrate [488], and could be coupled with synthetic co-cultivation for increased economical value. This could include aerobic fermentation of C1 feedstocks using natural or engineered strains (e.g., *E.coli*, *C. necator*) that can already convert these feedstocks using efficient routes as the reductive glycine pathway (rGly) [38]. Furthermore, the use of alternative technologies such as colloid biology [469, 470] or hydrogels [471] might allow the control of microbial compositions and, thus, the selection of the most optimal design for increasing production of MCFAs. The future development of gas fermentation through synthetic microbial communities needs to be coupled to computational approaches for generating testable hypotheses, driving designs, shading light into the metabolism and following DBTL cycles (Design, Build, Test, Learn). Bioprospecting should be considered as a tool to identify traits and new microbial platforms that could potentially outperform the species mentioned here or perform alternative tasks producing other valuable products.

In addition, techno-economical analysis are needed to ascertain the future of this technology and set the goals. Furthermore, governments can play an important role, through regulation and incentives, in nudging and fostering new technologies and economic models that better align to global sustainable development goals.

Summary

Human-induced climate change caused by the emission of contaminant gases has led to a global crisis affecting society and nature all over the world. Therefore, we urgently need solutions to mitigate these emissions and their effects. This requires a radical change on the way we manage our resources, produce and use our products, and treat our wastes. Gasification of biomass and waste into syngas and further microbial conversion of syngas or industrial off-gas to valuable chemicals is envisioned as a promising strategy. In this thesis, using metabolic modeling, I work on a circular approach to produce medium-chain fatty-acids (MCFAs) and alcohols from the upcycling of biomass-derived C1 feedstocks through synthetic microbial communities.

Synthetic microbial communities can expand the range of products obtained by pure cultures on syngas to molecules of longer and different chain lengths. Here, I have constructed metabolic models of single species and of communities to assess the feasibility and potential of these microbial communities for the production of even- and odd-chain fatty acids and alcohols from C1 gases. For that, I have used a battery of computational methods such as Flux balance analysis (FBA), Flux Sampling, community modeling (with FBA, Flux Sampling), model-reconstruction tools, and experimental data from continuous and non-continuous environments.

In chapter 2, we compared the energetic efficiency of the conversion of several C1 feedstocks by several pathways in both, aerobic and anaerobic conditions, being the latter the most efficiency way. Following these observations, we focused on the anaerobic conversion of C1 feedstocks and, in particular, of C1 gases. Acetogens are anaerobic microorganisms that can grow on C1 gases as the sole carbon and energy source. However, their energetic barriers limit their products to small molecules; mainly acetate and ethanol. Thus, the co-cultivation of an acetogen with a microorganism capable of chain elongation, which can grow on the products of acetogenic metabolism, extends the range of products of gas fermentation.

In chapter 3, chapter 4 and chapter 5, a modular approach was followed to establish microbial communities targeting molecules of different chain lengths (even-/odd-chain fatty acids) by the replacement or addition of microbes to the community. In chapter 3, using community modeling, I first modeled a previously established co-culture of the acetogen *Clostridium autoethanogenum* and the chain-elongator *Clostridium kluyveri* producing even-chain MCFAs from CO/syngas. In this study I used metabolic modeling to find possible strategies to increase the pro-

duction of MCFA, and lower the accumulation of acetate. Several genetic interventions for increasing ethanol production in detriment of acetate production by *C. autoethanogenum* could potentially increase the production of MCFA. Yet, the co-culture presented some limitations, such as the difference in optimal pH between community members, which limited the chain elongation activity in *C. kluyveri* and, thus, the production of the target products. A solution to this was the replacement of *C. autoethanogenum* by an acetogen whose optimal pH was similar to the one of the chain-elongating species. For this, we chose *Acetobacterium wieringae* strain JM, an isolate from our own culture collection. Thus, upon construction of the model of *A. wieringae* JM, I modeled the co-culture of *A. wieringae* JM and *C. kluyveri* to study the feasibility of such co-culture, and its potential to produce even-chain MCFAs (chapter 5).

The next target was the production of odd-chain fatty-acids from syngas. The combination of the construction of the model of *Anaerotignum neopropionicum* and the experimental observations in chapter 4, led to the identification of key metabolic features and increased understanding of this microbe. *A. neopropionicum* was shown to produce propionate from ethanol and ethanol/acetate in the presence of CO₂ through the acrylate pathway, the mechanism of which was clarified here. Thus, we hypothesized that the addition of *A. neopropionicum* to the previous co-culture of *A. wieringae* JM and *C. kluyveri* would potentially shift the product range from even- to odd-chain MCFAs due the presence of propionate. To assess the feasibility of this tri-culture, we used community modeling (chapter 5). Model predictions suggested the feasibility of the tri-culture and the partial shift of products from even- to odd-chain MCFAs (chapter 5). Furthermore, the model predicted that CO/H₂ ratios < 1 could increase ethanol production, in favour of MCFAs.

In chapter 6, I used a model-driven approach for the establishment of a co-culture of *C. autoethanogenum* and the solventogen *Clostridium beijerinckii* producing MCFAs from CO₂ and H₂. Here, I assessed the growth capabilities of two solventogenic species by using metabolic modeling to find a carbon source that could lead to growth together with acetate, since this is the main product produced by *C. autoethanogenum*. Model predictions suggested lactate as additional carbon source. Subsequent growth experiments with lactate and acetate as co-substrates led to growth of *C. beijerinckii* producing butyrate and traces of butanol. I then used community modeling to assess the feasibility of the co-culture, which was later established in fed-batch bioreactors. Furthermore, isobutyrate was a newly identified product in this co-culture.

Acknowledging the disparity in scope and capabilities of community modeling tools, I concluded the primary work of my thesis by reviewing and assessing the state of art of said tools (chapter 7). Together with my co-authors, I qualitatively evaluated twenty-four tools, and quantitatively tried fourteen of them and assessed

their capability to predict case studies of microbial communities of two species. Finally, we identified the strengths, challenges and limitations of these tools and gave a wide range of recommendations for future development of the field. In the general discussion (chapter 8), I discussed the challenges and limitations of using microbial communities for the upcycling of C1 feedstocks, both from the laboratory and computational perspectives. Furthermore, I discussed the future perspectives of this technology and I suggested strategies to overcome their limitations.

Resumen

El cambio climático, causado por la emisión de gases contaminantes debido a la actividad humana, ha provocado una crisis global que afecta tanto a la sociedad como a la naturaleza a nivel mundial. Por tanto, es necesario encontrar soluciones urgentes para mitigar las emisiones y minimizar sus efectos. En definitiva, se requiere un cambio radical en nuestra forma de gestionar nuestros recursos, utilizar y producir productos, así como en el tratamiento de nuestros desechos. La gasificación de biomasa y residuos en gas de síntesis (syngas), seguida de la conversión microbiana del syngas o de gases industriales en productos químicos valiosos, es una estrategia prometedora. En esta tesis, utilizamos modelos metabólicos de comunidades microbianas sintéticas para estudiar la producción de ácidos grasos de cadena media y alcoholes a partir de la conversión de gases de un carbono.

La conversión de syngas mediante el uso de comunidades microbianas sintéticas puede ampliar la gama de productos obtenidos por cultivos de una sola especie. Un ejemplo es la producción de ácidos grasos con cadenas más largas. En este proyecto, he construido modelos metabólicos de especies individuales y de comunidades para evaluar la viabilidad y el potencial de dichas comunidades para producir ácidos grasos y alcoholes de cadena par e impar a partir de gases de un carbono (CO , CO_2). Para ello, he utilizado una serie de métodos computacionales como Flux Balance Analysis (FBA), Flux Sampling, community modeling (con FBA y Flux Sampling), herramientas de construcción de modelos y datos experimentales de operaciones en continuo y discontinuo.

En el capítulo 2, comparamos la eficiencia energética de la conversión de varias materias primas de un carbono a través de varias rutas metabólicas tanto en condiciones aeróbicas como anaeróbicas, siendo esta última la forma más eficiente. Siguiendo estas observaciones, nos enfocamos en la conversión anaeróbica de compuestos de un carbono y, en particular, de gases como el CO y CO_2 . Los acetógenos son microorganismos anaeróbicos que pueden crecer utilizando gases de un carbono como única fuente de carbono y energía. Sin embargo, sus limitaciones energéticas reducen sus posibles productos a moléculas pequeñas, principalmente acetato y etanol. Por lo tanto, el co-cultivo de un acetógeno con un microorganismo capaz de crecer utilizando los productos generados por este microorganismo, puede ampliar la gama de productos en la fermentación de gases de un carbono.

En los capítulos 3, 4 y 5, seguimos un enfoque modular para establecer comunidades microbianas dirigidas a producir moléculas de diferentes longitudes de ca-

dena (ácidos grasos de cadena par/impar) mediante la sustitución o adición de microorganismos a la comunidad. En el capítulo 3, modelé una comunidad establecida previamente del acetógeno *Clostridium autoethanogenum* y el alargador de cadena *Clostridium kluyveri* que produce ácidos grasos de cadena par a partir de CO/syngas. En este estudio, utilicé el modelado metabólico para encontrar posibles estrategias para aumentar la producción de ácidos grasos de cadena par y reducir la acumulación de acetato. Observamos que varias intervenciones genéticas para aumentar la producción de etanol en detrimento de la producción de acetato por parte de *C. autoethanogenum* podrían aumentar potencialmente la producción de ácidos grasos en la comunidad. Sin embargo, la comunidad presentaba algunas limitaciones como la diferencia de pH óptimo entre los miembros de la comunidad, lo cual limitaba la actividad de alargamiento de cadena en *C. kluyveri* y, por lo tanto, la producción de ácidos grasos. Una solución fue la sustitución de *C. autoethanogenum* por un acetógeno cuyo pH óptimo fuera similar al de *C. kluyveri*. Para ello, elegimos la cepa JM de *Acetobacterium wieringae* de nuestra propia colección de cultivos. Así, tras la construcción del modelo de *A. wieringae* JM, modelé la comunidad de *A. wieringae* JM y *C. kluyveri* para ver si la comunidad se podía establecer y si podía producir ácidos grasos de cadena par (capítulo 5).

El siguiente objetivo fue la producción de ácidos grasos de cadena impar a partir de syngas. La combinación de la construcción del modelo de *Anaerotignum neopropionicum* y las observaciones experimentales en el capítulo 4 condujeron a la identificación de características metabólicas clave y a un mayor entendimiento de este microorganismo. Se demostró que *A. neopropionicum* produce propionato a partir de etanol y etanol/acetato en presencia de CO₂ a través de la vía del acrilato, cuyo mecanismo se aclaró en este trabajo. Por lo tanto, planteamos la hipótesis de que la adición de *A. neopropionicum* a la comunidad previa de *A. wieringae* JM y *C. kluyveri* podría potencialmente cambiar el rango de productos de ácidos grasos de cadena par, a ácidos grasos de cadena impar debido a la presencia de propionato. Para evaluar la viabilidad de la comunidad de tres especies utilizamos modelado de comunidades (capítulo 5). Las predicciones del modelo sugirieron la viabilidad de la nueva comunidad y el cambio parcial de productos de ácidos grasos de cadena par a cadena impar (capítulo 5). Además, el modelo predijo que con ratios de CO/H₂ < 1, la producción de etanol podría aumentar en favor de una mayor producción de ácidos grasos.

En el capítulo 6, el uso de modelos ayudó a establecer una comunidad compuesta por *C. autoethanogenum* y el solventógeno *Clostridium beijerinckii* para producir ácidos grasos a partir de CO₂/H₂. Se evaluaron las capacidades de crecimiento de dos especies solventogénicas utilizando modelado metabólico para encontrar una fuente de carbono que permitiera al solventógeno crecer con acetato, ya que este es el principal producto producido por *C. autoethanogenum*. Las predicciones del modelo su-

girieron el lactato como fuente adicional de carbono al acetato, lo cual se confirmó experimentalmente en *C. beijerinckii* junto con la producción de butirato y trazas de butanol. A continuación, se construyó un modelo de la comunidad de *C. autoethanogenum* y *C. beijerinckii* para estudiar la viabilidad de la comunidad y posteriormente, se estableció en biorreactores operados como batch. El crecimiento de la nueva comunidad en CO₂/H₂ y lactato condujo a la producción de butirato e isobutirato, un producto que no se había observado previamente en ninguna de las especies de la comunidad.

El alcance y capacidades de las herramientas de modelado de comunidades es muy diverso, por lo tanto, este trabajo de tesis concluyó con la evaluación del estado actual de dichas herramientas (capítulo 7). Junto con otros autores, evaluamos veinticuatro herramientas de forma cualitativa y catorce herramientas de forma cuantitativa comparando las predicciones de las herramientas con resultados de estudios experimentales de comunidades microbianas de dos especies. Finalmente, identificamos las fortalezas, desafíos y limitaciones de estas herramientas y propusimos una amplia gama de recomendaciones para el futuro desarrollo de este campo.

En la discusión general (capítulo 8), se han analizado los desafíos y las limitaciones de utilizar comunidades microbianas para la conversión de materias primas de un carbono, tanto desde la perspectiva de laboratorio como computacional. Además, se han evaluado las perspectivas futuras de esta tecnología sugiriendo estrategias para superar dichas limitaciones.

References

- [1] *World Population Prospects 2022: Summary of Results*. United Nations, Department of Economic and Social Affairs, Population Division, 2022.
- [2] Kaza, S. et al. *What a Waste 2.0: A Global Snapshot of Solid Waste Management to 2050*. Urban Development. Washington, DC: World Bank, 2018. ISBN: 978-1-4648-1329-0.
- [3] *International Energy Outlook 2021*. U.S. Energy Information Administration, 2021.
- [4] Lelieveld, J. et al. “Effects of fossil fuel and total anthropogenic emission removal on public health and climate”. In: *PNAS* 116 (15 2019), 7192–7197. DOI: 10.1073/PNAS.1819989116.
- [5] *CHAPTER XXVII ENVIRONMENT. 7.d Paris Agreement*. United Nations Treaty Collection, 2015.
- [6] *It’s time for a circular economy*. <https://ellenmacarthurfoundation.org>.
- [7] *A New Circular Economy Action Plan. For a cleaner and more competitive Europe*. European Commission, 2020.
- [8] *Climate Change 2014: Impacts, Adaptation, and Vulnerability. Part A: Global and Sectoral Aspects*. IPCC, 2014.
- [9] Nigam, P. S. and Singh, A. “Production of liquid biofuels from renewable resources”. In: *Prog. Energy Combust. Sci.* 37.1 (2011), 52–68. DOI: 10.1016/j.peccs.2010.01.003.
- [10] Coma, M. et al. “Organic waste as a sustainable feedstock for platform chemicals”. In: *Faraday Discuss.* 202 (0 2017), 175–195. DOI: 10.1039/C7FD00070G.
- [11] Horita, M. et al. “On-farm solid state simultaneous saccharification and fermentation of whole crop forage rice in wrapped round bale for ethanol production”. In: *Biotechnol. Biofuels* 8 (2015). DOI: 10.1186/s13068-014-0192-9.
- [12] Naik, S. et al. “Production of first and second generation biofuels: A comprehensive review”. In: *Renew. sustain. energy rev.* 14.2 (2010), 578–597. DOI: 10.1016/j.rser.2009.10.003.

- [13] Cotton, C. A. et al. “Renewable methanol and formate as microbial feedstocks”. In: *Curr. Opin. Biotechnol.* 62 (2020), 168–180. DOI: 10.1016/j.copbio.2019.10.002.
- [14] Hamelinck, C. N., Hooijdonk, G. van, and Faaij, A. P. “Ethanol from lignocellulosic biomass: techno-economic performance in short-, middle- and long-term”. In: *Biomass Bioenergy* 28.4 (2005), 384–410. DOI: 10.1016/j.biombioe.2004.09.002.
- [15] Jiang, W. et al. “Metabolic Engineering strategies to enable microbial utilization of C1 feedstocks”. In: *Nat. Chem. Biol.* 17 (8 2021), 845–855. DOI: 10.1038/s41589-021-00836-0.
- [16] Handler, R. M. et al. “Life Cycle Assessments of Ethanol Production via Gas Fermentation: Anticipated Greenhouse Gas Emissions for Cellulosic and Waste Gas Feedstocks”. In: *Ind. Eng. Chem.* 55 (12 2016), 3253–3261. DOI: 10.1021/ACS.IECR.5B03215.
- [17] *LanzaTech, Shougang open sustainable ethanol refinery in China*. <https://renewablesnow.com/news/lanzatech-shougang-open-sustainable-ethanol-refinery-in-china-615844/>.
- [18] Sanford, P. A. and Woolston, B. M. “Synthetic or natural? Metabolic Engineering for assimilation and valorization of methanol”. In: *Curr. Opin. Biotechnol.* 74 (2022), 171–179. DOI: 10.1016/j.copbio.2021.12.001.
- [19] Yishai, O. et al. “The formate bio-economy”. In: *Curr. Opin. Chem. Biol.* 35 (2016), 1–9. DOI: 10.1016/j.cbpa.2016.07.005.
- [20] Sokol, K. P. et al. “Photoreduction of CO₂ with a Formate Dehydrogenase Driven by Photosystem II Using a Semi-artificial Z-Scheme Architecture”. In: *J. Am. Chem. Soc.* 140.48 (2018), 16418–16422. DOI: 10.1021/jacs.8b10247.
- [21] Sorokin, A. et al. “Oxidation of methane and ethylene in water at ambient conditions”. In: *Catal. Today* 157 (2010), 149–154. DOI: 10.1016/j.cattod.2010.02.007.
- [22] Giuliano, A., Freda, C., and Catizzone, E. “Techno-Economic Assessment of Bio-Syngas Production for Methanol Synthesis: A Focus on the Water–Gas Shift and Carbon Capture Sections”. In: *Bioengineering* 7.3 (2020). DOI: 10.3390/bioengineering7030070.
- [23] Dalena, F. et al. *Chapter 1 - Methanol Production and Applications: An Overview*. Ed. by A. Basile and F. Dalena. Elsevier, 2018, 3–28. DOI: <https://doi.org/10.1016/B978-0-444-63903-5.00001-7>.
- [24] Hood, E. E. “Plant-based biofuels”. In: *F1000Research* 5 (2016). DOI: 10.12688/F1000RESEARCH.7418.1.

- [25] Santos, R. G. dos and Alencar, A. C. "Biomass-derived syngas production via gasification process and its catalytic conversion into fuels by Fischer Tropsch synthesis: A review". In: *Int. J. Hydrog. Energy*. 45.36 (2020), 18114–18132. DOI: 10.1016/j.ijhydene.2019.07.133.
- [26] Dhakal, N. and Acharya, B. "Syngas fermentation for the production of bio-based polymers: A review". In: *Polymers* (2021). DOI: 10.3390/polym13223917.
- [27] Daniell, J., Köpke, M., and Simpson, S. D. "Commercial biomass syngas fermentation". In: *Energies* 5.12 (2012), 5372–5417. DOI: 10.3390/en5125372.
- [28] Takors, R. et al. "Using gas mixtures of CO, CO₂ and H₂ as microbial substrates: the do's and don'ts of successful technology transfer from laboratory to production scale". In: *Microb. Biotechnol.* 11.4 (2018), 606–625. DOI: 10.1111/1751-7915.13270.
- [29] Barbosa, S. G. et al. "Bioelectrochemical systems (BESs) towards conversion of carbon monoxide/syngas: A mini-review". In: *Renew. sustain. energy rev.* 135 (2021), 110358. DOI: 10.1016/j.rser.2020.110358.
- [30] Anthony, C. "The biochemistry of methylotrophic micro-organisms." In: *Sci. Prog.* 62 (246 1975), 167–206.
- [31] Ochsner, A. M. et al. "*Methylobacterium extorquens*: methylotrophy and biotechnological applications". In: *Appl. Microbiol. Biotechnol.* 99 (2 2015). DOI: 10.1007/s00253-014-6240-3.
- [32] Santolin, L. et al. "Substrate-Flexible Two-Stage Fed-Batch Cultivations for the Production of the PHA Copolymer P(HB-co-HHx) With *Cupriavidus necator* Re2058/pCB113". In: *Front. Bioeng. Biotechnol.* 9 (2021), 217. DOI: 10.3389/fbioe.2021.623890.
- [33] Sánchez-Andrea, I. et al. "The reductive glycine pathway allows autotrophic growth of *Desulfovibrio desulfuricans*". In: *Nat. Commun.* 11 (1 2020). DOI: 10.1038/s41467-020-18906-7.
- [34] Bar-Even, A. "Formate Assimilation: The Metabolic Architecture of Natural and Synthetic Pathways". In: *Biochemistry* 55 (28 2016). DOI: 10.1021/acs.biochem.6b00495.
- [35] Claassens, N. J. "Reductive Glycine Pathway: A Versatile Route for One-Carbon Biotech". In: *Trends Biotechnol.* 39 (4 2021). DOI: 10.1016/j.tibtech.2021.02.005.

- [36] Claassens, N. J. et al. “Engineering the Reductive Glycine Pathway: A Promising Synthetic Metabolism Approach for C1-Assimilation”. In: *One-Carbon Feedstocks for Sustainable Bioproduction*. Ed. by A.-P. Zeng and N. J. Claassens. Springer International Publishing, 2022, 299–350. ISBN: 978-3-031-06854-6. DOI: 10.1007/10_2021_181.
- [37] Bae, J. et al. “Recent progress in the engineering of C1-utilizing microbes”. In: *Curr. Opin. Biotechnol.* 78 (2022), 102836. DOI: 10.1016/j.copbio.2022.102836.
- [38] Dronsella, B. et al. “Engineered synthetic one-carbon fixation exceeds yield of the Calvin Cycle”. In: *bioRxiv* (2022). DOI: 10.1101/2022.10.19.512895.
- [39] Claassens, N. J. et al. “Replacing the Calvin cycle with the reductive glycine pathway in *Cupriavidus necator*”. In: *Metab. Eng.* 62 (2020), 30–41. DOI: 10.1016/J.YMBEN.2020.08.004.
- [40] Bruinsma, L. et al. “Paving the way for synthetic C1- metabolism in *Pseudomonas putida* through the reductive glycine pathway”. In: *Metab. Eng.* 76 (2023), 215–224. DOI: 10.1016/j.ymben.2023.02.004.
- [41] Gleizer, S. et al. “Conversion of *Escherichia coli* to Generate All Biomass Carbon from CO₂”. In: *Cell* 179.6 (2019), 1255–1263. DOI: 10.1016/j.cell.2019.11.009.
- [42] Kim, S. et al. “Growth of *E. coli* on formate and methanol via the reductive glycine pathway”. In: *Nat. Chem. Biol.* 16 (5 2020), 538–545. DOI: 10.1038/s41589-020-0473-5.
- [43] Kim, S. et al. “Optimizing *E. coli* as a formatotrophic platform for bioproduction via the reductive glycine pathway”. In: *Front. Bioeng. Biotechnol.* 11 (2023). DOI: 10.3389/fbioe.2023.1091899.
- [44] Yishai, O. et al. “In Vivo Assimilation of One-Carbon via a Synthetic Reductive Glycine Pathway in *Escherichia coli*”. In: *ACS Synth. Biol.* 7 (9 2018), 2023–2028. DOI: 10.1021/acssynbio.8b00131.
- [45] Chen, F. Y. et al. “Converting *Escherichia coli* to a Synthetic Methylophilic Growing Solely on Methanol”. In: *Cell* 182 (4 2020), 933–946. DOI: 10.1016/j.cell.2020.07.010.
- [46] Woolston, B. M. and Stephanopoulos, G. “Engineering *E. coli* to Grow on Methanol”. In: *Joule* 4.10 (2020), 2070–2072. DOI: 10.1016/j.joule.2020.09.019.
- [47] Keller, P. et al. “Generation of an *Escherichia coli* strain growing on methanol via the ribulose monophosphate cycle”. In: *Nat. Commun.* 13 (1 2022), 1–13. DOI: 10.1038/s41467-022-32744-9.

- [48] Cruz, J. G. D. L. et al. “Core Catalysis of the Reductive Glycine Pathway Demonstrated in Yeast”. In: *ACS Synth. Biol.* 8 (5 2019), 911–917. DOI: 10.1021/ACSSYNBIO.8B00464.
- [49] Marcellin, E. et al. “Low carbon fuels and commodity chemicals from waste gases – systematic approach to understand energy metabolism in a model acetogen”. In: *Green Chem.* 18 (10 2016), 3020–3028. DOI: 10.1039/C5GC02708J.
- [50] Liew, F. et al. “Metabolic Engineering of *Clostridium autoethanogenum* for selective alcohol production”. In: *Metab. Eng.* 40 (2017). DOI: 10.1016/j.ymben.2017.01.007.
- [51] Benito-Vaquero, S. et al. “Modeling a co-culture of *Clostridium autoethanogenum* and *Clostridium kluyveri* to increase syngas conversion to medium-chain fatty-acids”. In: *Comput. Struct. Biotechnol. J.* 18 (2020), 3255–3266. DOI: 10.1016/j.csbj.2020.10.003.
- [52] Song, Y. et al. “Functional cooperation of the glycine synthase reductase and Wood-Ljungdahl pathways for autotrophic growth of *Clostridium drakei*”. In: *PNAS* 117 (13 2020). DOI: 10.1073/pnas.1912289117.
- [53] Lanzillo, F. et al. “Batch Syngas Fermentation by *Clostridium carboxidivorans* for Production of Acids and Alcohols”. In: *Processes* 8.9 (2020). DOI: 10.3390/pr8091075.
- [54] Katsyv, A. and Müller, V. “Overcoming Energetic Barriers in Acetogenic C1 Conversion”. In: *Front. Bioeng. Biotechnol.* 8 (2020), 1420. DOI: 10.3389/fbioe.2020.621166.
- [55] Mock, J. et al. “Energy conservation associated with ethanol formation from H₂ and CO₂ in *Clostridium autoethanogenum* involving electron bifurcation”. In: *J. Bacteriol.* 197 (18 2015). DOI: 10.1128/JB.00399-15.
- [56] Valgepea, K. et al. “H₂ drives metabolic rearrangements in gas-fermenting *Clostridium autoethanogenum*”. In: *Biotechnol. Biofuels* 11 (1 2018), 55. DOI: 10.1186/S13068-018-1052-9.
- [57] Ghadermazi, P. et al. “Metabolic Engineering Interventions for Sustainable 2,3-Butanediol Production in Gas-Fermenting *Clostridium autoethanogenum*”. In: *mSystems* 7 (2 2022). DOI: 10.1128/msystems.01111-21.
- [58] Dykstra, J. C. et al. “Metabolic Engineering of *Clostridium autoethanogenum* for ethyl acetate production from CO”. In: *Microb. Cell Fact.* 21 (1 2022), 1–11. DOI: 10.1186/S12934-022-01964-5.
- [59] Liew, F. E. et al. “Carbon-negative production of acetone and isopropanol by gas fermentation at industrial pilot scale”. In: *Nat. Biotechnol.* 2022 40:3 40 (3 2022), 335–344. DOI: 10.1038/s41587-021-01195-w.

- [60] Diender, M., Parera Olm, I., and Sousa, D. Z. "Synthetic co-cultures: novel avenues for bio-based processes". In: *Curr. Opin. Biotechnol.* 67 (2021), 72–79. DOI: 10.1016/j.copbio.2021.01.006.
- [61] Council, N. R. *Applications of Biotechnology in Traditional Fermented Foods*. The National Academies Press, 1992. ISBN: 978-0-309-04685-5. DOI: 10.17226/1939.
- [62] Vasudevan, D., Richter, H., and Angenent, L. T. "Upgrading dilute ethanol from syngas fermentation to n-caproate with reactor microbiomes". In: *Biore-sour. Technol.* 151 (2014), 378–382. DOI: 10.1016/J.BIORTECH.2013.09.105.
- [63] He, P. et al. "One-step production of C6-C8 carboxylates by mixed culture solely grown on CO". In: *Biotechnol. Biofuels* 11.1 (2018), 1–13. DOI: 10.1186/s13068-017-1005-8.
- [64] Diender, M., Stams, A. J., and Sousa, D. Z. "Production of medium-chain fatty acids and higher alcohols by a synthetic co-culture grown on carbon monoxide or syngas". In: *Biotechnol. Biofuels* 9 (1 2016), 1–11. DOI: 10.1186/S13068-016-0495-0.
- [65] Richter, H. et al. "A Narrow pH Range Supports Butanol, Hexanol, and Octanol Production from Syngas in a Continuous Co-culture of *Clostridium ljungdahlii* and *Clostridium kluyveri* with In-Line Product Extraction". In: *Front. Microbiol.* 7 (2016), 1773. DOI: 10.3389/FMICB.2016.01773.
- [66] Weiss, T. L., Young, E. J., and Ducat, D. C. "A synthetic, light-driven consortium of cyanobacteria and heterotrophic bacteria enables stable polyhydroxybutyrate production". In: *Metab. Eng.* 44 (2017), 236–245. DOI: 10.1016/J.YMBEN.2017.10.009.
- [67] Diender, M. et al. "High Rate Biomethanation of Carbon Monoxide-Rich Gases via a Thermophilic Synthetic Coculture". In: *ACS Sustain. Chem. Eng.* 6 (2 2018). DOI: 10.1021/acssuschemeng.7b03601.
- [68] Diender, M. et al. "Metabolic shift induced by synthetic co-cultivation promotes high yield of chain elongated acids from syngas". In: *Sci. Rep.* 9 (1 2019), 1–11. DOI: 10.1038/s41598-019-54445-y.
- [69] Charubin, K. and Papoutsakis, E. T. "Direct cell-to-cell exchange of matter in a synthetic *Clostridium* syntrophy enables CO₂ fixation, superior metabolite yields, and an expanded metabolic space". In: *Metab. Eng.* 52 (2019), 9–19. DOI: 10.1016/J.YMBEN.2018.10.006.
- [70] Benito-Vaquero, S. et al. "Model-driven approach for the production of butyrate from CO₂/H₂ by a novel co-culture of *C. autoethanogenum* and *C. beijerinckii*". In: *Front. Microbiol.* 13 (2022). DOI: 10.3389/fmicb.2022.1064013.

- [71] Kabimoldayev, I. et al. “Basics of genome-scale metabolic modeling and applications on C1-utilization”. In: *FEMS Microbiol. Lett.* 365.20 (2018). fny241. doi: 10.1093/femsle/fny241.
- [72] Gu, C. et al. “Current status and applications of genome-scale metabolic models”. In: *Genome Biol.* 20 (1 2019), 1–18. doi: 10.1186/S13059-019-1730-3.
- [73] Duman-Özdamar, Z. E. et al. “Tailoring and optimizing fatty acid production by oleaginous yeasts through the systematic exploration of their physiological fitness”. In: *Microb. Cell Fact.* 21 (1 2022), 1–13. doi: 10.1186/S12934-022-01956-5.
- [74] Valgepea, K. et al. “Maintenance of ATP Homeostasis Triggers Metabolic Shifts in Gas-Fermenting Acetogens”. In: *Cell Syst.* 4.5 (2017), 505–515. doi: 10.1016/j.cels.2017.04.008.
- [75] Nilsson, A. and Nielsen, J. “Genome scale metabolic modeling of cancer”. In: *Metab. Eng.* 43 (2017). Engineering approaches to study cancer metabolism, 103–112. doi: <https://doi.org/10.1016/j.ymben.2016.10.022>.
- [76] Machado, D. et al. “Fast automated reconstruction of genome-scale metabolic models for microbial species and communities”. In: *Nucleic Acids Res.* 46 (15 2018), 7542–7553. doi: 10.1093/NAR/GKY537.
- [77] Henry, C. S. et al. “High-throughput generation, optimization and analysis of genome-scale metabolic models”. In: *Nat. Biotechnol.* 28 (9 2010), 977–982. doi: 10.1038/NBT.1672.
- [78] Arkin, A. P. et al. “KBase: The United States department of energy systems biology knowledgebase”. In: *Nat. Biotechnol.* 36 (7 2018). doi: 10.1038/nbt.4163.
- [79] Wang, H. et al. “RAVEN 2.0: A versatile toolbox for metabolic network reconstruction and a case study on *Streptomyces coelicolor*”. In: *PLOS Comput. Biol.* 14.10 (2018), 1–17. doi: 10.1371/journal.pcbi.1006541.
- [80] Aite, M. et al. “Traceability, reproducibility and wiki-exploration for “à-la-carte” reconstructions of genome-scale metabolic models”. In: *PLOS Comput. Biol.* 14.5 (2018), 1–25. doi: 10.1371/journal.pcbi.1006146.
- [81] Aziz, R. K. et al. “The RAST Server: Rapid annotations using subsystems technology”. In: *BMC Genom.* 9 (1 2008), 1–15. doi: 10.1186/1471-2164-9-75.
- [82] Benito-Vaquero, S. et al. “Genome-scale metabolic modelling enables deciphering ethanol metabolism via the acrylate pathway in the propionate-producer *Anaerotignum neopropionicum*”. In: *Microb. Cell Fact.* 21 (1 2022), 1–18. doi: 10.1186/S12934-022-01841-1.

- [83] van Rosmalen, R. et al. “Model reduction of genome-scale metabolic models as a basis for targeted kinetic models”. In: *Metab. Eng.* 64 (2021), 74–84. DOI: 10.1016/j.ymben.2021.01.008.
- [84] Heirendt, L. et al. “Creation and analysis of biochemical constraint-based models using the COBRA Toolbox v.3.0”. In: *Nat. Protoc.* 14 (3 2019), 639–702. DOI: 10.1038/s41596-018-0098-2.
- [85] Ebrahim, A. et al. “COBRApy: CONstraints-Based Reconstruction and Analysis for Python”. In: *BMC Syst. Biol.* 7 (2013), 74. DOI: 10.1186/1752-0509-7-74.
- [86] Orth, J. D., Thiele, I., and Palsson, B. Ø. “What is flux balance analysis?” In: *Nat. Biotechnol.* 28.3 (2010), 245–248. DOI: 10.1038/nbt.1614.
- [87] Mahadevan, R. and Schilling, C. “The effects of alternate optimal solutions in constraint-based genome-scale metabolic models”. In: *Metab. Eng.* 5.4 (2003), 264–276. DOI: 10.1016/j.ymben.2003.09.002.
- [88] Herrmann, H. A. et al. “Flux sampling is a powerful tool to study metabolism under changing environmental conditions”. In: *npj Syst. Biol. Appl.* 2019 5:1 5 (1 2019), 1–8. DOI: 10.1038/s41540-019-0109-0.
- [89] Moreno-Paz, S. et al. “Enzyme-constrained models predict the dynamics of *Saccharomyces cerevisiae* growth in continuous, batch and fed-batch bioreactors”. In: *Microb. Biotechnol.* 15 (5 2022). DOI: 10.1111/1751-7915.13995.
- [90] Mahadevan, R., Edwards, J. S., and Doyle, F. J. “Dynamic Flux Balance Analysis of Diauxic Growth in *Escherichia coli*”. In: *Biophys. J.* 83.3 (2002), 1331–1340. DOI: 10.1016/S0006-3495(02)73903-9.
- [91] Bordbar, A. et al. “Constraint-based models predict metabolic and associated cellular functions”. In: *Nat. Rev. Genet.* 15 (2 2014), 107–120. DOI: 10.1038/NRG3643.
- [92] Zhang, C. and Hua, Q. “Applications of genome-scale metabolic models in biotechnology and systems medicine”. In: *Front. Physiol.* 6 (JAN 2016). DOI: 10.3389/fphys.2015.00413.
- [93] Burgard, A. P., Pharkya, P., and Maranas, C. D. “Optknock: A bilevel programming framework for identifying gene knockout strategies for microbial strain optimization”. In: *Biotechnol. Bioeng.* 84.6 (2003), 647–657. DOI: 10.1002/bit.10803.
- [94] Tepper, N. and Shlomi, T. “Predicting Metab. Eng. knockout strategies for chemical production: accounting for competing pathways”. In: *Bioinformatics* 26.4 (2009), 536–543. DOI: 10.1093/bioinformatics/btp704.

- [95] Sánchez, B. J. et al. “Improving the phenotype predictions of a yeast genome-scale metabolic model by incorporating enzymatic constraints”. In: *Mol. Syst. Biol.* 13.8 (2017), 935. DOI: <https://doi.org/10.15252/msb.20167411>.
- [96] O’Brien, E. J. et al. “Genome-scale models of metabolism and gene expression extend and refine growth phenotype prediction”. In: *Mol. Syst. Biol.* 9.1 (2013), 693. DOI: <https://doi.org/10.1038/msb.2013.52>.
- [97] Heinken, A. and Thiele, I. “Microbiome Modelling Toolbox 2.0: efficient, tractable modelling of microbiome communities”. In: *Bioinformatics* 38.8 (2022), 2367–2368. DOI: [10.1093/bioinformatics/btac082](https://doi.org/10.1093/bioinformatics/btac082).
- [98] Colarusso, A. V. et al. “Computational modeling of metabolism in microbial communities on a genome-scale”. In: *Curr. Opin. Syst. Biol.* 26 (2021), 46–57. DOI: [10.1016/J.COISB.2021.04.001](https://doi.org/10.1016/J.COISB.2021.04.001).
- [99] Scott, W. T. et al. “A Structured Evaluation of Genome-Scale Constraint-Based Modeling Tools for Microbial Consortia”. In: *bioRxiv* (2023). DOI: [10.1101/2023.02.08.527721](https://doi.org/10.1101/2023.02.08.527721).
- [100] Baldini, F. et al. “The Microbiome Modeling Toolbox: from microbial interactions to personalized microbial communities”. In: *Bioinformatics* 35.13 (2018), 2332–2334. DOI: [10.1093/bioinformatics/bty941](https://doi.org/10.1093/bioinformatics/bty941).
- [101] Diener, C., Gibbons, S. M., and Resendis-Antonio, O. “MICOM: Metagenome-Scale Modeling To Infer Metabolic Interactions in the Gut Microbiota”. In: *mSystems* 5 (1 2020). DOI: [10.1128/msystems.00606-19](https://doi.org/10.1128/msystems.00606-19).
- [102] Zomorodi, A. R. and Maranas, C. D. “OptCom: A Multi-Level Optimization Framework for the Metabolic Modeling and Analysis of Microbial Communities”. In: *PLOS Comput. Biol.* 8.2 (2012). DOI: [10.1371/journal.pcbi.1002363](https://doi.org/10.1371/journal.pcbi.1002363).
- [103] Zhuang, K. et al. “Genome-scale dynamic modeling of the competition between *Rhodospirillum rubrum* and *Geobacter* in anoxic subsurface environments”. In: *ISME J.* 5.2 (2011), 305–316. DOI: [10.1038/ismej.2010.117](https://doi.org/10.1038/ismej.2010.117).
- [104] Zomorodi, A. R., Islam, M. M., and Maranas, C. D. “d-OptCom: Dynamic Multi-level and Multi-objective Metabolic Modeling of Microbial Communities”. In: *ACS Synth. Biol.* 3.4 (2014), 247–257. DOI: [10.1021/sb4001307](https://doi.org/10.1021/sb4001307).
- [105] Gomez, J. A., Höffner, K., and Barton, P. I. “DFBALab: a fast and reliable MATLAB code for dynamic flux balance analysis”. In: *BMC Bioinform.* 15.1 (2014), 409. DOI: [10.1186/s12859-014-0409-8](https://doi.org/10.1186/s12859-014-0409-8).
- [106] Harcombe, W. R. et al. “Metabolic Resource Allocation in Individual Microbes Determines Ecosystem Interactions and Spatial Dynamics”. In: *Cell Rep.* 7.4 (2014), 1104–1115. DOI: [10.1016/J.CELREP.2014.03.070](https://doi.org/10.1016/J.CELREP.2014.03.070).

- [107] Foster, C. et al. "Modeling Growth Kinetics, Interspecies Cell Fusion, and Metabolism of a *Clostridium acetobutylicum*/*Clostridium ljungdahlii* Syntrophic Coculture". In: *mSystems* 6 (1 2021). DOI: 10.1128/MSYSTEMS.01325-20.
- [108] Wang, E. X. et al. "Reorganization of a synthetic microbial consortium for one-step vitamin C fermentation". In: *Microb. Cell Fact.* 15 (1 2016), 1–11. DOI: 10.1186/S12934-016-0418-6.
- [109] Zhang, C., Qi, J., and Cao, Y. "Synergistic Effect of Yeast-Bacterial Co-Culture on Bioremediation of Oil-Contaminated Soil". In: *Bioremediat J.* 18 (2014). DOI: 10.1080/10889868.2013.847402.
- [110] Tollefson, J. "Energy: not your father's biofuels". In: *Nature* 451.7180 (2008), 880–883. DOI: 10.1038/451880a.
- [111] Naik, S. N. et al. "Production of First and Second Generation Biofuels: A Comprehensive Review". In: *Renew. Sustainable Energy Rev.* 14 (2010), 578–597. DOI: 10.1016/j.rser.2009.10.003.
- [112] Strong, P. J., Xie, S., and Clarke, W. P. "Methane as a resource: can the methanotrophs add value?" In: *Environ. Sci. Technol.* 49.5 (2015), 4001–4018. DOI: 10.1021/es504242n.
- [113] Pfeifenschneider, J., Brautaset, T., and Wendisch, V. F. "Methanol as carbon substrate in the bio-economy: Metabolic Engineering of aerobic methylotrophic bacteria for production of value-added chemicals". In: *Biofuel Bioprod. Biorefin.* 11.5 (2017), 719–731. DOI: 10.1002/bbb.1767.
- [114] Durre, P. and Eikmanns, B. J. "C1-carbon sources for chemical and fuel production by microbial gas fermentation". In: *Curr. Opin. Biotechnol.* 35 (2015), 63–72. DOI: 10.1016/j.copbio.2015.07.011.
- [115] Jouny, M., Luc, W., and Jiao, F. "General techno-economic analysis of CO₂ electrolysis systems". In: *Ind. Eng. Chem. Res.* 57.6 (2018), 2165–2177. DOI: 10.1021/acs.iecr.7b04222.
- [116] Li, X. et al. "Cocatalysts for selective photoreduction of CO₂ into solar fuels". In: *Chem. Rev.* 119.6 (2019), 3962–4179. DOI: 10.1021/acs.chemrev.8b00400.
- [117] Dincer, I. and Acar, C. "Review and evaluation of hydrogen production methods for better sustainability". In: *Int. J. Hydrog. Energy.* 40.32 (2015), 11094–11111. DOI: 10.1016/j.ijhydene.2014.12.035.
- [118] Alvarez, A. et al. "Challenges in the greener production of formates/formic acid, methanol, and DME by heterogeneously catalyzed CO₂ hydrogenation processes". In: *Chem. Rev.* 117.15 (2017), 9804–9838. DOI: 10.1021/acs.chemrev.6b00816.

- [119] Szima, S. and Cormos, C. C. “Improving methanol synthesis from carbon-free H_2 and captured CO_2 : A techno-economic and environmental evaluation”. In: *J. CO₂ Util.* 24 (2018), 555–563. DOI: 10.1016/j.jcou.2018.02.007.
- [120] Götz, M. et al. “Renewable Power-to-Gas: A technological and economic review”. In: *Renew. Energy* 85 (2016), 1371–1390. DOI: 10.1016/j.renene.2015.07.066.
- [121] Humphreys, C. M. and Minton, N. P. “Advances in Metabolic Engineering in the microbial production of fuels and chemicals from C1 gas”. In: *Curr. Opin. Biotechnol.* 50 (2018), 174–181. DOI: 10.1016/j.copbio.2017.12.023.
- [122] Claassens, N. J. et al. “Towards sustainable feedstocks: A guide to electron donors for microbial carbon fixation”. In: *Curr. Opin. Biotechnol.* 50 (2018), 195–205. DOI: 10.1016/j.copbio.2018.01.019.
- [123] Keryanti, K., Penia, M. T. A., and Setiadi, T. “Evaluation of gas mass transfer in reactor for syngas fermentation”. In: *AIP Conf. Proc.* 020008 (2019). DOI: 10.1063/1.5094986/799202.
- [124] Yasin, M. A. M. et al. “Microbial synthesis gas utilization and ways to resolve kinetic and mass-transfer limitations”. In: *Bioresour. Technol.* 177 (2015), 361–374. DOI: 10.1016/j.biortech.2014.11.022.
- [125] Schrader, J. et al. “Methanol-based industrial biotechnology: current status and future perspectives of methylotrophic bacteria”. In: *Trends. Biotechnol.* 27 (2009), 107–115. DOI: 10.1016/j.tibtech.2008.10.009.
- [126] Upadhyaya, S. et al. “Microbial Protein: A Valuable Component for Future Food Security”. In: *Edited by.* 2016, 259–279. DOI: 10.13140/RG.2.1.1775.8801.
- [127] Babel, W. “The Auxiliary Substrate Concept: From simple considerations to heuristically valuable knowledge”. In: *Eng. Life Sci.* 9 (2009), 285–290. DOI: 10.1002/elsc.200900027.
- [128] Li, H. et al. “Integrated electromicrobial conversion of CO_2 to higher alcohols”. In: *Science* 335 (2012), 1596. DOI: 10.1126/science.1217643.
- [129] Siegel, J. B. et al. “Computational protein design enables a novel one-carbon assimilation pathway”. In: *PNAS* 112.12 (2015), 3704–3709. DOI: 10.1073/pnas.1500545112.
- [130] Claassens, N. J. et al. “Making quantitative sense of electromicrobial production”. In: *Nat. Catal.* 2 (2019), 437. DOI: 10.1038/s41929-019-0272-0.
- [131] Bertsch, J. and Müller, V. “Bioenergetic constraints for conversion of syngas to biofuels in acetogenic bacteria”. In: *Biotechnol. Biofuels* 8 (1 2015), 1–12. DOI: 10.1186/S13068-015-0393-X.

- [132] Heijstra, B. D., Leang, C., and Juminaga, A. "Gas fermentation: Cellular engineering possibilities and scale up". In: *Microb. Cell Fact.* 16 (1 2017). DOI: 10.1186/s12934-017-0676-y.
- [133] Liew, F. et al. "Gas Fermentation-A Flexible Platform for Commercial Scale Production of Low-Carbon-Fuels and Chemicals from Waste and Renewable Feedstocks". In: *Front. Microbiol.* 7 (2016), 694. DOI: 10.3389/fmicb.2016.00694.
- [134] Tschuch, A. and Pfennig, N. "Growth yield increase linked to caffeate reduction in *Acetobacterium woodii*". In: *Arch. Microbiol.* 137.2 (1984), 163–167. DOI: 10.1007/BF00414460.
- [135] Bache, R. and Pfennig, N. "Selective isolation of *Acetobacterium woodii* on methoxylated aromatic acids and determination of growth yields". In: *Arch. Microbiol.* 130 (1981), 255–261. DOI: 10.1007/BF00459530.
- [136] Peters, V., Janssen, P., and Conrad, R. "Efficiency of hydrogen utilization during unitrophic and mixotrophic growth of *Acetobacterium woodii* on hydrogen and lactate in the chemostat". In: *FEMS Microbiol. Lett.* 26.3 (1998), 317–324. DOI: 10.1111/j.1574-6941.1998.tb00516.x.
- [137] Pacaud, S. et al. "Effects of various organic acid supplements on growth rates of *Eubacterium limosum* B2 on methanol". In: *Appl Microbiol Biotechnol* 24.1 (1986), 75–78. DOI: 10.1007/BF00266289.
- [138] Heise, R., Muller, V., and Gottschalk, G. "Sodium dependence of acetate formation by the acetogenic bacterium *Acetobacterium woodii*". In: *J. Bacteriol.* 171.10 (1989), 5473–5478. DOI: 10.1128/jb.171.10.5473-5478.1989.
- [139] Genthner, B. and Bryant, M. "Additional characteristics of one-carbon-compound utilization by *Eubacterium limosum* and *Acetobacterium woodii*". In: *Appl. Env. Microbiol.* 53.3 (1987), 471–476. DOI: 10.1128/aem.53.3.471-476.1987.
- [140] Nicholls, P. "Formate as an inhibitor of cytochrome c oxidase". In: *Biochem. Biophys. Res. Commun.* 67.2 (1975), 610–616. DOI: 10.1016/0006-291x(75)90856-6.
- [141] Zeng, A. "New bioproduction systems for chemicals and fuels: Needs and new development". In: *Biotechnol. Adv.* 37 (2019), 508–518. DOI: 10.1016/j.biotechadv.2019.01.003.
- [142] Pacaud, S. et al. "Organic acid production during methylotrophic growth of *Eubacterium limosum* B2: displacement towards increased butyric acid yields by supplementing with acetate". In: *Appl. Microbiol. Biotechnol.* 23 (1986), 330–335. DOI: 10.1007/BF00257028.

- [143] Datta, R. and Ogeltree, J. A. "Methanol bioconversion by *Butyribacterium methylotrophicum*—batch fermentation yield and kinetics". In: *Biotechnol. Bioeng.* 25.4 (1983), 991–998. doi: 10.1002/bit.260250409.
- [144] Al Rowaihi, I. S. et al. "Poly (3-hydroxybutyrate) production in an integrated electromicrobial setup: Investigation under stress-inducing conditions". In: *PloS one* 13.4 (2018). doi: 10.1371/journal.pone.0196079.
- [145] Grunwald, S. et al. "Kinetic and stoichiometric characterization of organoautotrophic growth of *Ralstonia eutropha* on formic acid in fed-batch and continuous cultures". In: *Microb. Biotechnol.* 8.1 (2015), 155–163. doi: 10.1111/1751-7915.12149.
- [146] Bennett, B. D. et al. "Absolute metabolite concentrations and implied enzyme active site occupancy in *Escherichia coli*". In: *Nat. Chem. Biol.* 5.8 (2009), 593–599. doi: 10.1038/nchembio.186.
- [147] Bar-Even, A. et al. "Thermodynamic constraints shape the structure of carbon fixation pathways". In: *Biochimica et Biophysica Acta (BBA) - Bioenergetics* 1817.9 (2012), 1646–1659. doi: <https://doi.org/10.1016/j.bbabi.2012.05.002>.
- [148] Chistoserdova, L. "Modularity of methylotrophy, revisited". In: *Environ. Microbiol.* 13.10 (2011), 2603–2622. doi: 10.1111/j.1462-2920.2011.02464.x.
- [149] Bennett, R. K. et al. "Expression of heterologous non-oxidative pentose phosphate pathway from *Bacillus methanolicus* and phosphoglucose isomerase deletion improves methanol assimilation and metabolite production by a synthetic *Escherichia coli* methylotroph". In: *Metab. Eng.* 43 (2017), 239–247. doi: 10.1016/j.ymben.2017.11.016.
- [150] Gonzalez, J. E. et al. "Methanol assimilation in *Escherichia coli* is improved by co-utilization of threonine and deletion of leucine-responsive regulatory protein". In: *Metab. Eng.* 42 (2017), 173–181. doi: 10.1016/j.ymben.2017.11.015.
- [151] Muller, J. E. et al. "Engineering *Escherichia coli* for methanol conversion". In: *Metab. Eng.* 28 (2015), 190–201. doi: 10.1016/j.ymben.2015.01.005.
- [152] Price, J. V. et al. "Scaffoldless engineered enzyme assembly for enhanced methanol utilization". In: *PNAS* 113.29 (2016), E4536–E4544. doi: 10.1073/pnas.1601083113.
- [153] Whitaker, W. B. et al. "Engineering the biological conversion of methanol to specialty chemicals in *Escherichia coli*". In: *Metab. Eng.* 39 (2017), 49–59. doi: 10.1016/j.ymben.2016.10.007.

- [154] Chen, C. T. et al. "Synthetic methanol auxotrophy of *Escherichia coli* for methanol-dependent growth and production". In: *Metab. Eng.* 49 (2018), 257–266. DOI: 10.1016/j.ymben.2018.08.005.
- [155] Meyer, F. et al. "Methanol-essential growth of *Escherichia coli*". In: *Nat. Commun.* 9 (2018), 1508. DOI: 10.1038/s41467-018-03937-y.
- [156] Tuyishime, P. et al. "Engineering *Corynebacterium glutamicum* for methanol-dependent growth and glutamate production". In: *Metab. Eng.* 49 (2018), 220–231. DOI: 10.1016/j.ymben.2018.07.011.
- [157] Johnson, E. A. "Biotechnology of non-*Saccharomyces* yeasts—the ascomycetes". In: *Appl. Microbiol. Biotechnol.* 97.2 (2013), 503–517. DOI: 10.1007/s00253-012-4497-y.
- [158] Dai, Z. et al. "Metabolic construction strategies for direct methanol utilization in *Saccharomyces cerevisiae*". In: *Bioresour. Technol.* 245 (2017), 1407–1412. DOI: 10.1016/j.biortech.2017.05.100.
- [159] Lidstrom, M. E. "Aerobic Methylotrophic Prokaryotes". In: *The Prokaryotes*. Ed. by M. Dworkin et al. Springer New York, 2006, 618–634. ISBN: 978-0-387-30742-8. DOI: 10.1007/0-387-30742-7_20.
- [160] Chou, H.-H. et al. "Diminishing returns epistasis among beneficial mutations decelerates adaptation". In: *Science* 332.6034 (2011), 1190–1192. DOI: 10.1126/science.1203799.
- [161] Kim, J. and Copley, S. D. E. "Inhibitory cross-talk upon introduction of a new metabolic pathway into an existing metabolic network". In: *PNAS* 109.30 (2012), E2856–E2864. DOI: 10.1073/pnas.1208509109.
- [162] Yu, H. and Liao, J. C. "A modified serine cycle in *Escherichia coli* converts methanol and CO₂ to two-carbon compounds". In: *Nat. Commun.* 9.1 (2018), 1–11. DOI: 10.1038/s41467-018-06496-4.
- [163] Yishai, O. et al. "Engineered Assimilation of Exogenous and Endogenous Formate in *Escherichia coli*". In: *ACS Synth. Biol.* 6.1 (2017), 172–180. DOI: 10.1021/acssynbio.7b00086.
- [164] Schada von Borzyskowski, L. et al. "Replacing the Ethylmalonyl-CoA Pathway with the Glyoxylate Shunt Provides Metabolic Flexibility in the Central Carbon Metabolism of *Methylobacterium extorquens* AM1". In: *ACS Synth. Biol.* 7.1 (2018), 86–97. DOI: 10.1021/acssynbio.7b00229.
- [165] Khosravi-Darani, K. et al. "Microbial production of poly (hydroxybutyrate) from C₁ carbon sources". In: *Appl. Microbiol. Biotechnol.* 97.4 (2013), 1407–1424. DOI: 10.1007/s00253-012-4649-0.

- [166] Schada von Borzyskowski, L. et al. "A set of versatile brick vectors and promoters for the assembly, expression, and integration of synthetic operons in *Methylobacterium extorquens* AM1 and other alphaproteobacteria". In: *ACS Synth. Biol.* 4.4 (2015), 430–443. DOI: 10.1021/sb500221v.
- [167] Chistoserdova, L. "Applications of methylotrophs: can single carbon be harnessed for biotechnology?" In: *Curr. Opin. Biotechnol.* 50 (2018), 189–194. DOI: 10.1016/j.copbio.2018.01.012.
- [168] Lim, C. K. et al. "Designing and Engineering *Methylorubrum extorquens* AM1 for Itaconic Acid Production". In: *Front. Microbiol.* 10 (2019), 1027. DOI: 10.3389/fmicb.2019.01027.
- [169] Yang, J. et al. "Metabolic Engineering of *Methylobacterium extorquens* AM1 for the production of butadiene precursor". In: *Microb. Cell Fact.* 17.1 (2018), 194. DOI: 10.1186/s12934-018-1042-4.
- [170] Sonntag, F. et al. "Engineering *Methylobacterium extorquens* for de novo synthesis of the sesquiterpenoid α -humulene from methanol". In: *Metab. Eng.* 32 (2015), 82–94. DOI: 10.1016/j.ymben.2015.09.004.
- [171] Barenholz, U. et al. "Design principles of autocatalytic cycles constrain enzyme kinetics and force low substrate saturation at flux branch points". In: *eLife* 6 (2017). DOI: 10.7554/eLife.20667.
- [172] Bar-Even, A. et al. "Design and analysis of metabolic pathways supporting formatotrophic growth for electricity-dependent cultivation of microbes". In: *Biochimica et Biophysica Acta (BBA)-Bioenergetics* 1827 (2013), 1039–1047. DOI: 10.1016/j.bbabi.2012.10.013.
- [173] Figueroa, I. et al. "Metagenomics-guided analysis of microbial chemolithoautotrophic phosphite oxidation yields evidence of a seventh natural CO₂ fixation pathway". In: *PNAS* 115.1 (2018), E92–E101. DOI: 10.1073/pnas.1715549114.
- [174] Kawasaki, H., Sato, T., and Kikuchi, G. "A new reaction for glycine biosynthesis". In: *Biophys. Res. Commun.* 23.3 (1966), 227–233. DOI: 10.1016/0006-291x(66)90532-8.
- [175] Motokawa, Y. and Kikuchi, G. "Glycine metabolism by rat liver mitochondria. Reconstruction of the reversible glycine cleavage system with partially purified protein components". In: *Arch. Biochem. Biophys.* 164.2 (1974), 624–633. DOI: 10.1016/0003-9861(74)90074-5.
- [176] Pasternack, L. B., Laude, D. A. J., and Appling, D. R. "¹³C NMR detection of folate-mediated serine and glycine synthesis in vivo in *Saccharomyces cerevisiae*". In: *Biochem.* 31.34 (1992), 8713–8719. DOI: 10.1021/bi00152a005.

- [177] Bang, J. and Lee, S. Y. "Assimilation of formic acid and CO₂ by engineered *Escherichia coli* equipped with reconstructed one-carbon assimilation pathways". In: *PNAS* 115.39 (2018), E9271–E9279. DOI: 10.1073/pnas.1810386115.
- [178] Lu, X. et al. "Constructing a synthetic pathway for acetyl-coenzyme A from one-carbon through enzyme design". In: *Nat. Commun.* 10.1 (2019), 1–9. DOI: 10.1038/s41467-019-09095-z.
- [179] Ishikawa, K., Kaneko, E., and Ichiyama, A. "Pyridoxal 5'-phosphate binding of a recombinant rat serine: pyruvate/alanine:glyoxylate aminotransferase". In: *J Biochem* 119.5 (1996), 970–978. DOI: 10.1093/oxfordjournals.jbchem.a021337.
- [180] Igarashi, D. et al. "Identification of photorespiratory *glutamate:glyoxylate aminotransferase (GGAT)* gene in *Arabidopsis*". In: *Plant J.* 33.6 (2003), 975–987. DOI: 10.1046/j.1365-313x.2003.01688.x.
- [181] Settembre, E. C. et al. "Structural and mechanistic studies on ThiO, a glycine oxidase essential for thiamin biosynthesis in *Bacillus subtilis*". In: *Biochem.* 42.10 (2003), 2971–2981. DOI: 10.1021/bi026803u.
- [182] Wang, X. et al. "Biological conversion of methanol by evolved *Escherichia coli* carrying a linear methanol assimilation pathway". In: *Bioresour. Bioprocess.* 4.1 (2017), 41. DOI: 10.1186/s40643-017-0165-5.
- [183] Poust, S. et al. "Mechanistic analysis of an engineered enzyme that catalyzes the formose reaction". In: *Chembiochem* 16.10 (2015), 1483–1487. DOI: 10.1002/cbic.201500228.
- [184] Orth, J. D., Fleming, R. M., and Palsson, B. Ø. "Reconstruction and use of microbial metabolic networks: the core *Escherichia coli* metabolic model as an educational guide". In: *EcoSal Plus* 4.1 (2010), 10.1128/ecosalplus.10.2.1. DOI: 10.1128/ecosalplus.10.2.1.
- [185] Bogorad, I. et al. "Building carbon-carbon bonds using a biocatalytic methanol condensation cycle". In: *PNAS* 111.44 (2014), 15928–15933. DOI: 10.1073/pnas.1413470111.
- [186] Krusemann, J. L. et al. "Artificial pathway emergence in central metabolism from three recursive phosphoketolase reactions". In: *FEBS J.* 285.23 (2018), 4367–4377. DOI: 10.1111/febs.14682.
- [187] Carlos, L., Olitta, T., and Nitsche, S. "Ethanol Production in Brazil: The Industrial Process and Its Impact on Yeast Fermentation". In: *Biofuel Production-Recent Developments and Prospects*. 2011. DOI: 10.5772/17047.

- [188] Komives, C. F. et al. "Growth of *Bacillus methanolicus* in seawater-based media". In: *Journal of Industrial Microbiology and Biotechnology* 32.2 (2005), 61–66. DOI: 10.1007/s10295-004-0195-9.
- [189] Purtschert, I., Siegrist, H., and Gujer, W. "Enhanced denitrification with methanol at WWTP Zürich-Werdhölzli". In: *Water Sci. Technol.* 33.12 (1996), 117–126. DOI: 10.1016/0273-1223(96)00465-9.
- [190] Ginige, M. P. et al. "A comparative study of methanol as a supplementary carbon source for enhancing denitrification in primary and secondary anoxic zones". In: *Biodegradation* (2009). DOI: 10.1007/s10532-008-9215-1.
- [191] Bélanger, L. et al. "Production of heterologous protein by *Methylobacterium extorquens* in high cell density fermentation". In: *FEMS Microbiol. Lett.* (2004). DOI: 10.1016/S0378-1097(03)00956-X.
- [192] Brautaset, T. et al. "*Bacillus methanolicus*: A candidate for industrial production of amino acids from methanol at 50°C". In: *Appl. Microbiol. Biotechnol.* (2007). DOI: 10.1007/s00253-006-0757-z.
- [193] Pluschkell, S. B. and Flickinger, M. C. "Dissimilation of ^{13}C methanol by continuous cultures of *Bacillus methanolicus* MGA3 at 50 °C studied by ^{13}C NMR and isotope-ratio mass spectrometry". In: *Microbiology* (2002). DOI: 10.1099/00221287-148-10-3223.
- [194] Choi, J.-H. et al. "Optimization of Growth Medium and Poly- β -hydroxybutyric Acid Production from Methanol in *Methylobacterium organophilum*". In: *Kor. J. Appl. Microbiol. Bioeng.* 17 (1989), 392–396.
- [195] Kim, P., Kim, J. H., and Oh, D. K. "Improvement in cell yield of *Methylobacterium* sp. by reducing the inhibition of medium components for poly- β -hydroxybutyrate production". In: *World J. Microbiol.* (2003). DOI: 10.1023/A:1023969629568.
- [196] Jwanny, E. W. and Rashad, M. M. "Assimilation of methanol by Yeasts". In: *Acta Biotechnol.* (1987). DOI: 10.1002/abio.370070108.
- [197] Warnecke, T. and Gill, R. T. "Organic acid toxicity, tolerance, and production in *Escherichia coli* biorefining applications". In: (2005). DOI: 10.1186/1475-2859-4-25.
- [198] Berríos-Rivera, S. J., Bennett, G. N., and San, K. Y. "Metabolic Engineering of *Escherichia coli*: Increase of NADH availability by overexpressing an NAD $^{+}$ -dependent formate dehydrogenase". In: *Metab. Eng.* (2002). DOI: 10.1006/mben.2002.0227.

- [199] Zaldivar, J. and Ingram, L. O. "Effect of organic acids on the growth and fermentation of ethanologenic *Escherichia coli* LY01". In: *Biotechnol. Bioeng.* (1999). doi: 10.1002/(sici)1097-0290(1999)66:4<203::aid-bit1>3.0.co;2-#.
- [200] Overkamp, K. M. et al. "Functional analysis of structural genes for NAD⁺ - dependent formate dehydrogenase in *Saccharomyces cerevisiae*". In: *Yeast* (2002). doi: 10.1002/yea.856.
- [201] Harris, D. M. et al. "Formate as an auxiliary substrate for glucose-limited cultivation of *Penicillium chrysogenum*: Impact on penicillin G production and biomass yield". In: *Appl. Environ. Microbiol.* (2007). doi: 10.1128/AEM.00093-07.
- [202] Kelly, D. P. et al. "Autotrophic metabolism of formate by *Thiobacillus* strain A2". In: *J. Gen. Microbiol.* (1979). doi: 10.1099/00221287-114-1-1.
- [203] Pronk, J. T. et al. "Growth of *Thiobacillus ferrooxidans* on formic acid". In: *Appl. Environ. Microbiol.* (1991). doi: 10.1128/aem.57.7.2057-2062.1991.
- [204] Solomons, G. L. and Litchfield, J. H. "Single Cell Protein". In: *Crit. Rev. Biotechnol.* 1.1 (1983), 21–58. doi: 10.3109/07388558309082578.
- [205] Behr, A. *Methanol: The Basic Chemical and Energy Feedstock of the Future*. Springer, 2014. ISBN: 978-3-642-39708-0. doi: 10.1002/anie.201409583.
- [206] Escobar, J. C. et al. "Biofuels: Environment, technology and food security". In: *Renew. sustain. energy rev.* 13.6 (2009), 1275–1287. doi: <https://doi.org/10.1016/j.rser.2008.08.014>.
- [207] Bozell, J. J. "Feedstocks for the Future - Biorefinery Production of Chemicals from Renewable Carbon". In: *Clean (Weinh)* 36.8 (2008), 641–647. doi: 10.1002/clen.200800100.
- [208] Lauri, P. et al. "Woody biomass energy potential in 2050". In: *Energy Policy* 66 (2014), 19–31. doi: <https://doi.org/10.1016/j.enpol.2013.11.033>.
- [209] Ragsdale, S. W. and Pierce, E. "Acetogenesis and the Wood–Ljungdahl pathway of CO₂ fixation". In: *Biochim. Biophys. Acta Proteins Proteom.* 1784.12 (2008), 1873–1898. doi: <https://doi.org/10.1016/j.bbapap.2008.08.012>.
- [210] Diender, M., Stams, A. J. M., and Sousa, D. Z. "Pathways and Bioenergetics of Anaerobic Carbon Monoxide Fermentation". In: *Front. Microbiol.* 6 (2015), 1275. doi: 10.3389/fmicb.2015.01275.
- [211] Abrini, J., Naveau, H., and Nyns, E. J. "*Clostridium autoethanogenum*, sp. nov., an anaerobic bacterium that produces ethanol from carbon monoxide". In: *Arch. Microbiol.* 161.4 (1994), 345–351. doi: 10.1007/BF00303591.

- [212] Reddy, M. V., Mohan, S. V., and Chang, Y. C. "Medium-chain fatty acids (MCFA) production through anaerobic fermentation using *Clostridium kluyveri*: effect of ethanol and acetate". In: *Appl. Biochem. Biotechnol.* 185.3 (2018), 594–605. DOI: 10.1007/s12010-017-2674-2.
- [213] Dellomonaco, C., Fava, F., and Gonzalez, R. "The path to next generation biofuels: Successes and challenges in the era of synthetic biology". In: *Microb. Cell Fact.* 9 (2010), 1–15. DOI: 10.1186/1475-2859-9-1.
- [214] Santos, F., Boele, J., and Teusink, B. "A Practical Guide to Genome-Scale Metabolic Models and Their Analysis". In: *Methods in Systems Biology*. Ed. by D. Jameson, M. Verma, and H. V. Westerhoff. Academic Press, 2011, 509–532. DOI: <https://doi.org/10.1016/B978-0-12-385118-5.00024-4>.
- [215] Thompson, R. A. et al. "Elucidating central metabolic redox obstacles hindering ethanol production in *Clostridium thermocellum*". In: *Metab. Eng.* 32 (2015), 207–219. DOI: 10.1016/j.ymben.2015.10.004.
- [216] Stolyar, S. et al. "Metabolic modeling of a mutualistic microbial community". In: *Mol. Syst. Biol.* 3.1 (2007), 92. DOI: 10.1038/msb4100131.
- [217] Hanemaaijer, M. et al. "Systems modeling approaches for microbial community studies: from metagenomics to inference of the community structure". In: *Front. Microbiol.* 6 (2015), 213. DOI: 10.3389/fmicb.2015.00213.
- [218] Li, X. and Henson, M. A. "Metabolic modeling of bacterial co-culture systems predicts enhanced carbon monoxide-to-butyrate conversion compared to monoculture systems". In: *Biochem. Eng. J.* 151 (2019), 107338. DOI: 10.1016/J.BEJ.2019.107338.
- [219] Valgepea, K. et al. "Arginine deiminase pathway provides ATP and boosts growth of the gas-fermenting acetogen *Clostridium autoethanogenum*". In: *Metab. Eng.* 41 (2017), 202–211. DOI: 10.1016/J.YMBEN.2017.04.007.
- [220] Zou, W. et al. "Genome-scale metabolic reconstruction and analysis for *Clostridium kluyveri*". In: *Genome* 61.8 (2018), 605–613. DOI: 10.1139/gen-2017-0177.
- [221] Khandelwal, R. A. et al. "Community Flux Balance Analysis for Microbial Consortia at Balanced Growth". In: *PLoS ONE* 8.5 (2013), e64567. DOI: 10.1371/journal.pone.0064567.
- [222] Gottstein, W. et al. "Constraint-based stoichiometric modelling from single organisms to microbial communities". In: *J. R. Soc. Interface.* 13 (124 2016). DOI: 10.1098/RSIF.2016.0627.
- [223] Flamholz, A. et al. "EQuilibrator - The biochemical thermodynamics calculator". In: *Nucleic Acids Res.* (2012). DOI: 10.1093/nar/gkr874.

- [224] Thauer, R., Rupprecht, E., and Jungermann, K. “The synthesis of one-carbon units from CO₂ via a new ferredoxin dependent monocarboxylic acid cycle”. In: *FEBS Lett.* 8.5 (1970), 304–307. doi: [https://doi.org/10.1016/0014-5793\(70\)80293-9](https://doi.org/10.1016/0014-5793(70)80293-9).
- [225] Thauer, R. K., Fuchs, G., and Jungermann, K. “CHAPTER 5 - Role of Iron-Sulfur Proteins in Formate Metabolism”. In: *Structure and Metabolic Mechanisms*. Ed. by W. Lovenberg. Academic Press, 1977, 121–156. ISBN: 978-0-12-456003-1. doi: <https://doi.org/10.1016/B978-0-12-456003-1.50011-4>.
- [226] Flamholz, A. et al. “eQuilibrator—the biochemical thermodynamics calculator”. In: *Nucleic Acids Res.* 40.D1 (2011), D770–D775. doi: 10.1093/nar/gkr874.
- [227] Hucka, M. et al. “The systems biology markup language (SBML): a medium for representation and exchange of biochemical network models”. In: *Bioinformatics* 19.4 (2003), 524–531. doi: 10.1093/bioinformatics/btg015.
- [228] Hung, S. et al. “SteadyCom: Predicting microbial abundances while ensuring community stability”. In: *PLOS Comput. Biol.* 13 (5 2017). Ed. by N. D. Price, e1005539. doi: 10.1371/JOURNAL.PCBI.1005539.
- [229] Brown, S. D. et al. “Comparison of single-molecule sequencing and hybrid approaches for finishing the genome of *Clostridium autoethanogenum* and analysis of CRISPR systems in industrial relevant Clostridia”. In: *Biotechnol. Biofuels* 7.1 (2014), 40. doi: 10.1186/1754-6834-7-40.
- [230] Seedorf, H. et al. “The genome of *Clostridium kluyveri*, a strict anaerobe with unique metabolic features”. In: *PNAS* 105.6 (2008), 2128–2133. doi: 10.1073/pnas.0711093105.
- [231] Coordinators, N. R. “Database resources of the National Center for Biotechnology Information”. In: *Nucleic Acids Res.* 46.D1 (2017), D8–D13. doi: 10.1093/nar/gkx1095.
- [232] Li, H. and Durbin, R. “Fast and accurate long-read alignment with Burrows–Wheeler transform”. In: *Bioinformatics* 26.5 (2010), 589–595. doi: 10.1093/bioinformatics/btp698.
- [233] Weimer, P. J. and Stevenson, D. M. “Isolation, characterization, and quantification of *Clostridium kluyveri* from the bovine rumen”. In: *Appl. Microbiol. Biotechnol.* 94.2 (2012), 461–466. doi: 10.1007/s00253-011-3751-z.
- [234] Loferer-Krößbacher, M., Klima, J., and Psenner, R. “Determination of bacterial cell dry mass by transmission electron microscopy and densitometric image analysis”. In: *Appl. Environ. Microbiol.* 64.2 (1998), 688–694. doi: 10.1128/aem.64.2.688-694.1998.

- [235] Ebrahim, A. et al. "COBRAPy: CONstraints-Based Reconstruction and Analysis for Python". In: *BMC Syst. Biol.* 7 (2013), 74. doi: 10.1186/1752-0509-7-74.
- [236] Hermann, H. A. et al. "Flux sampling is a powerful tool to study metabolism under changing environmental conditions". In: *npj Syst. Biol. Appl.* 5.32 (2019). doi: 10.1038/s41540-019-0109-0.
- [237] Naama Tepper, T. S. "Predicting Metabolic Engineering knockout strategies for chemical production: accounting for competing pathways". In: *Bioinformatics* 26.4 (2009), 536–543. doi: 10.1093/bioinformatics/btp704.
- [238] Bornstein, B. T. and Barker, H. A. "The Nutrition of *Clostridium kluuyveri*". In: *J. Bacteriol.* 55.2 (1948), 223–230. doi: 10.1128/jb.55.2.223-230.1948.
- [239] Kenealy, W. R. and Waselefsky, D. M. "Studies on the substrate range of *Clostridium kluuyveri*; the use of propanol and succinate". In: *Arch. Microbiol.* 141.3 (1985), 187–194. doi: 10.1007/BF00408056.
- [240] Scherf, U. et al. "Succinate-ethanol fermentation in *Clostridium kluuyveri*: purification and characterisation of 4-hydroxybutyryl-CoA dehydratase/vinyl-acetyl-CoA-isomerase". In: *Arch. Microbiol.* 161 (1994), 239–245. doi: 10.1007/BF00248699.
- [241] Riggs, S. S. and Heindel, T. J. "Measuring Carbon Monoxide Gas Liquid Mass Transfer in a Stirred Tank Reactor for Syngas Fermentation". In: *Biotechnol. Prog.* 22.3 (2006), 903–906. doi: 10.1021/bp050352f.
- [242] Wang, S. et al. "NADP-Specific Electron-Bifurcating [FeFe]-Hydrogenase in a Functional Complex with Formate Dehydrogenase in *Clostridium autoethanogenum* Grown on CO". In: *J. Bacteriol.* 195.19 (2013), 4373–4386. doi: 10.1128/JB.00678-13.
- [243] Charubin, K. and Papoutsakis, E. T. "Direct cell-to-cell exchange of matter in a synthetic *Clostridium* syntrophy enables CO₂ fixation, superior metabolite yields, and an expanded metabolic space". In: *Metab. Eng.* 52 (2019), 9–19. doi: <https://doi.org/10.1016/j.ymben.2018.10.006>.
- [244] Charubin, K. et al. "Interspecies Microbial Fusion and Large-Scale Exchange of Cytoplasmic Proteins and RNA in a Syntrophic *Clostridium* Coculture". In: *mBio* 11.5 (2020). doi: 10.1128/mBio.02030-20.
- [245] Marcellin, E. et al. "Low carbon fuels and commodity chemicals from waste gases - Systematic approach to understand energy metabolism in a model acetogen". In: *Green Chem.* 18 (2016), 3020–3028. doi: 10.1039/C5GC02708J.
- [246] Yin, Y. et al. "Biological caproate production by *Clostridium kluuyveri* from ethanol and acetate as carbon sources". In: *Bioresour. Technol.* 241 (2017), 638–644. doi: 10.1016/J.BIORTECH.2017.05.184.

- [247] Abubackar, H. N. et al. "Impact of cyclic pH shifts on carbon monoxide fermentation to ethanol by *Clostridium autoethanogenum*". In: *Fuel* 178 (2016), 56–62. DOI: <https://doi.org/10.1016/j.fuel.2016.03.048>.
- [248] Agler, M. T. et al. "Chain elongation with reactor microbiomes: upgrading dilute ethanol to medium-chain carboxylates". In: *Energy Environ. Sci.* 5 (8 2012), 8189–8192. DOI: 10.1039/C2EE22101B.
- [249] Du, B. et al. "Genome-scale model of metabolism and gene expression provides a multi-scale description of acid stress responses in *Escherichia coli*". In: *PLOS Comput. Biol.* 15.12 (2019), 1–21. DOI: 10.1371/journal.pcbi.1007525.
- [250] Mahamkali, V. et al. "Redox controls metabolic robustness in the gas-fermenting acetogen *Clostridium autoethanogenum*". In: *PNAS* 117.23 (2020), 13168–13175. DOI: 10.1073/pnas.1919531117.
- [251] Noor, E. et al. "Consistent Estimation of Gibbs Energy Using Component Contributions". In: *PLOS Comput. Biol.* 9.7 (2013), 1–11. DOI: 10.1371/journal.pcbi.1003098.
- [252] Jungermann, K., Thauer, R. K., and Decker, K. "The Synthesis of One-Carbon Units from CO₂ in *Clostridium kluyveri*". In: *European J. Biochem.* 3.3 (1968), 351–359. DOI: 10.1111/j.1432-1033.1968.tb19536.x.
- [253] Tomlison, N. and Barker, H. "Carbon dioxide and acetate utilization by *Clostridium kluyveri*. I. Influence of nutritional conditions on utilization patterns". In: *J. Biol. Chem.* 209.2 (1954), 585–595.
- [254] Richter, H. et al. "A Narrow pH Range Supports Butanol, Hexanol, and Octanol Production from Syngas in a Continuous Co-culture of *Clostridium ljungdahlii* and *Clostridium kluyveri* with In-Line Product Extraction". In: *Front. Microbiol.* 7 (2016), 1773. DOI: 10.3389/fmicb.2016.01773.
- [255] Gonzalez-Garcia, R. A. et al. "Microbial propionic acid production". In: *Fermentation* (2017). DOI: 10.3390/fermentation3020021.
- [256] Ranaei, V. et al. "Propionic acid: Method of production, current state and perspectives". In: *Food Technol. Biotechnol.* (2020). DOI: 10.17113/FTB.58.02.20.6356.
- [257] Boyaval, P. and Corre, C. "Production of propionic acid". In: *Le Lait* 75.4-5 (1995), 453–461. DOI: 10.1016/0023-7302(96)80128-X.
- [258] Blank, L. M. et al. "Biotechnological upcycling of plastic waste and other non-conventional feedstocks in a circular economy". In: *Curr. Opin. Biotechnol.* 62 (2020), 212–219. DOI: 10.1016/j.copbio.2019.11.011.

- [259] Dagle, R. A. et al. "Ethanol as a Renewable Building Block for Fuels and Chemicals". In: *Ind. Eng. Chem.* 59.11 (2020), 4843–4853. DOI: 10.1021/acs.iecr.9b05729.
- [260] Molitor, B. et al. "Carbon recovery by fermentation of CO-rich off gases – Turning steel mills into biorefineries". In: *Bioresour. Technol.* 215 (2016), 386–396. DOI: 10.1016/j.biortech.2016.03.094.
- [261] Stoll, I. K., Boukis, N., and Sauer, J. "Syngas fermentation to alcohols: reactor technology and application perspective". In: *Chem. Ing. Tech.* 92.1-2 (2020), 125–136. DOI: 10.1002/CITE.201900118.
- [262] Köpke, M. and Simpson, S. D. "Pollution to products: recycling of 'above ground' carbon by gas fermentation". In: *Curr. Opin. Biotechnol.* 65 (2020), 180–189. DOI: 10.1016/j.copbio.2020.02.017.
- [263] Ueki, A. et al. "Description of *Anaerotignum aminivorans* gen. Nov., sp. nov., a strictly anaerobic, amino-acid-decomposing bacterium isolated from a methanogenic reactor, and reclassification of *Clostridium propionicum*, *Clostridium neopropionicum* and *Clostridium lactatifermentans* as species of the genus *Anaerotignum*". In: *Int. J. Syst. Evol. Microbiol.* (2017). DOI: 10.1099/ijsem.0.002268.
- [264] Samain, E. "Characterization of a new propionic acid bacterium that ferments ethanol and displays a growth factor-dependent association with a Gram-negative homoacetogen". In: *FEMS Microbiol. Lett.* (1982). DOI: 10.1016/0378-1097(82)90015-5.
- [265] Wielen, P. W. J. J. van der et al. "*Clostridium lactatifermentans* sp. nov., a lactate-fermenting anaerobe isolated from the caeca of a chicken". In: *Int. J. Syst. Evol. Microbiol.* 52 (2002), 921–925. DOI: 10.1099/00207713-52-3-921.
- [266] Laanbroek, H. J., Abee, T., and Voogd, I. L. "Alcohol conversion by *Desulfobulbus propionicus* Lindhorst in the presence and absence of sulfate and hydrogen". In: *Arch. Microbiol.* 133 (1982), 178–184. DOI: 10.1007/BF00414998.
- [267] Stams, A. J. et al. "Pathway of propionate formation in *Desulfobulbus propionicus*". In: *Arch. Microbiol.* 140.4 (1985), 298. DOI: 10.1007/BF00446965.
- [268] Schink, B., Kremer, D. R., and Hansen, T. A. "Pathway of propionate formation from ethanol in *Pelobacter propionicus*". In: *Arch. Microbiol.* 147.4 (1987), 321–327. DOI: 10.1007/BF00406127.
- [269] Moreira, J. P. et al. "Propionate production from carbon monoxide by synthetic cocultures of *Acetobacterium wieringae* and propionigenic bacteria". In: *Appl. Environ. Microbiol.* 87 (14 2021). DOI: 10.1128/AEM.02839-20.

- [270] Reichardt, N. et al. “Phylogenetic distribution of three pathways for propionate production within the human gut microbiota”. In: *ISME J.* 8.6 (2014), 1323–1335. DOI: 10.1038/ismej.2014.14.
- [271] Tholozan, J. L. et al. “*Clostridium neopropionicum* sp. nov., a strict anaerobic bacterium fermenting ethanol to propionate through acrylate pathway”. In: *Arch. Microbiol.* (1992). DOI: 10.1007/BF00245158.
- [272] Machado, D. et al. “Fast automated reconstruction of genome-scale metabolic models for microbial species and communities”. In: *Nucleic Acids Res.* 46.15 (2018), 7542–7553. DOI: 10.1093/nar/gky537.
- [273] Nagarajan, H. et al. “Characterizing acetogenic metabolism using a genome-scale metabolic reconstruction of *Clostridium ljungdahlii*”. In: *Microb. Cell Fact.* 12.118 (2013). DOI: 10.1186/1475-2859-12-118.
- [274] Heffernan, J. K. et al. “Enhancing CO₂-Valorization Using *Clostridium autoethanogenum* for Sustainable Fuel and Chemicals Production”. In: *Front. Bioeng. Biotechnol.* 8 (2020). DOI: 10.3389/fbioe.2020.00204.
- [275] Butler-Wu, S. M. et al. “Genome Sequence of a Novel Species, *Propionibacterium humerusii*”. In: *J. Bacteriol.* 193.14 (2011), 3678–3678. DOI: 10.1128/JB.05036-11.
- [276] Parizzi, L. P. et al. “The genome sequence of *Propionibacterium acidipropionici* provides insights into its biotechnological and industrial potential”. In: *BMC Genom.* 13 (1 2012), 1–20. DOI: 10.1186/1471-2164-13-562.
- [277] Koskinen, P. et al. “Complete genome sequence of *Propionibacterium freudenreichii* DSM 20271T”. In: *Stand. Genom. Sci.* 10 (1 2015). DOI: 10.1186/S40793-015-0082-1.
- [278] Poehlein, A. et al. “Complete Genome Sequence of the Amino Acid-Fermenting *Clostridium propionicum* X2 (DSM 1682)”. In: *Genome Announc.* 4 (2 2016). DOI: 10.1128/GENOMEA.00294-16.
- [279] Wielen, P. W. J. J. van der et al. “*Clostridium lactatifermentans* sp. nov., a lactate-fermenting anaerobe isolated from the caeca of a chicken.” In: *Int. J. Syst. Evol. Microbiol.* 52.3 (2002), 921–925. DOI: <https://doi.org/10.1099/00207713-52-3-921>.
- [280] Beck, M. H. et al. “Draft Genome Sequence of the Strict Anaerobe *Clostridium neopropionicum* X4 (DSM 3847 T)”. In: *Genome Announc.* 4.2 (2016), e00209–16. DOI: 10.1128/genomeA.00209-16.
- [281] Pagani, I. et al. “Complete genome sequence of *Desulfobulbus propionicus* type strain (1pr3T)”. In: *Stand. Genom. Sci.* 4.1 (2011), 100–110. DOI: 10.4056/sigs.1613929.

- [282] Butler, J. E., Young, N. D., and Lovley, D. R. "Evolution from a respiratory ancestor to fill syntrophic and fermentative niches: comparative genomics of six *Geobacteraceae* species". In: *BMC Genom.* 10.1 (2009), 103. DOI: 10.1186/1471-2164-10-103.
- [283] McCubbin, T. et al. "A pan-genome guided metabolic network reconstruction of five *Propionibacterium* species reveals extensive metabolic diversity". In: *Genes* 11.10 (2020), 1115. DOI: 10.3390/genes11101115.
- [284] Navone, L. et al. "Genome-scale model guided design of *Propionibacterium* for enhanced propionic acid production". In: *Metab. Eng. Commun.* 6. June 2017 (2018), 1–12. DOI: 10.1016/j.meteno.2017.11.001.
- [285] Sun, J. et al. "Constraint-based modeling analysis of the metabolism of two *Pelobacter* species." In: *BMC Syst. Biol.* 4 (2010), 174. DOI: 10.1186/1752-0509-4-174.
- [286] Huerta-Cepas, J. et al. "Fast genome-wide functional annotation through orthology assignment by eggNOG-mapper". In: *Mol. Biol. Evol.* (2016). DOI: 10.1101/076331.
- [287] Karp, P. D. et al. "The MetaCyc database". In: *Nucleic Acids Res.* (2002). DOI: 10.1093/nar/30.1.59.
- [288] Schellenberger, J. et al. "BiGG: A Biochemical Genetic and Genomic knowledgebase of large scale metabolic reconstructions". In: *BMC Bioinform.* (2010). DOI: 10.1186/1471-2105-11-213.
- [289] Ogata, H. et al. *KEGG: Kyoto encyclopedia of genes and genomes*. 1999. DOI: 10.1093/nar/27.1.29.
- [290] Davis, J. J. et al. "The PATRIC Bioinformatics Resource Center: expanding data and analysis capabilities". In: *Nucleic Acids Res.* 48 (D1 2020), D606. DOI: 10.1093/NAR/GKZ943.
- [291] Apweiler, R. et al. "UniProt: The universal protein knowledgebase". In: *Nucleic Acids Res.* (2004). DOI: 10.1093/nar/gky092.
- [292] Schomburg, I., Chang, A., and Schomburg, D. "BRENDA, enzyme data and metabolic information". In: *Nucleic Acids Res.* (2002). DOI: 10.1093/nar/30.1.47.
- [293] Bergmann, F. T. et al. "COMBINE archive and OMEX format: One file to share all information to reproduce a modeling project". In: *BMC Bioinform.* 15 (1 2014), 1–9. DOI: 10.1186/S12859-014-0369-Z/TABLES/1.
- [294] Chelliah, V. et al. "BioModels: ten-year anniversary". In: *Nucleic Acids Res.* 43.D1 (2014), D542–D548. DOI: 10.1093/nar/gku1181.

- [295] Milne, C. B. et al. “Metabolic network reconstruction and genome-scale model of butanol-producing strain *Clostridium beijerinckii* NCIMB 8052”. In: *BMC Syst. Biol.* (2011). DOI: 10.1186/1752-0509-5-130.
- [296] Thiele, I. and Palsson, B. “A protocol for generating a high-quality genome-scale metabolic reconstruction”. In: *Nat. Protoc.* 5 (1 2010), 93. DOI: 10.1038/NPROT.2009.203.
- [297] Lee, J. et al. “Genome-scale reconstruction and in silico analysis of the *Clostridium acetobutylicum* ATCC 824 metabolic network”. In: *Appl. Microbiol. Biotechnol.* 80 (5 2008), 849–862. DOI: 10.1007/S00253-008-1654-4.
- [298] Hucka, M. et al. “The Systems Biology Markup Language (SBML): Language Specification for Level 3 Version 1 Core”. In: *J. Integr. Bioinform.* 12 (2 2015), 266. DOI: 10.2390/BIECOLL-JIB-2015-266.
- [299] Lieven, C. et al. “MEMOTE for standardized genome-scale metabolic model testing”. In: *Nat. Biotechnol.* 2020 38:3 38.3 (2020), 272–276. DOI: 10.1038/s41587-020-0446-y.
- [300] Ravikrishnan, A. and Raman, K. “Critical assessment of genome-scale metabolic networks: the need for a unified standard”. In: *Brief. Bioinformatics.* 16 (6 2015), 1057–1068. DOI: 10.1093/BIB/BBV003.
- [301] Ato, M., Ishii, M., and Igarashi, Y. “Enrichment of amino acid-oxidizing, acetate-reducing bacteria”. In: *J. Biosci. Bioeng.* 118.2 (2014), 160–165. DOI: 10.1016/j.jbiosc.2014.02.003.
- [302] Candry, P. et al. “A novel high-throughput method for kinetic characterisation of anaerobic bioproduction strains, applied to *Clostridium kluyveri*”. In: *Sci. Rep.* 8.1 (2018), 9724. DOI: 10.1038/s41598-018-27594-9.
- [303] Dai, Z. et al. “Elucidating the contributions of multiple aldehyde/alcohol dehydrogenases to butanol and ethanol production in *Clostridium acetobutylicum*”. In: *Sci. Rep.* 2016 6:1 6.1 (2016), 1–9. DOI: 10.1038/srep28189.
- [304] Buckel, W. and Thauer, R. K. “Flavin-based electron bifurcation, ferredoxin, flavodoxin, and anaerobic respiration with protons (Ech) or NAD⁺ (Rnf) as electron acceptors: A historical review”. In: *Front. Microbiol.* 9 (2018). DOI: 10.3389/FMICB.2018.00401.
- [305] Westphal, L. et al. “The Rnf complex is an energy-coupled transhydrogenase essential to reversibly link cellular NADH and ferredoxin pools in the acetogen *Acetobacterium woodii*”. In: *J. Bacteriol.* 200.21 (2018). DOI: 10.1128/JB.00357-18.
- [306] Garvie, E. I. “Bacterial lactate dehydrogenases”. In: *Microbiol. Rev.* 44.1 (1980), 106–139. DOI: 10.1128/mr.44.1.106-139.1980.

- [307] Zhu, L. et al. "NADP⁺ -Preferring D-lactate Dehydrogenase from *Sporolactobacillus inulinus*". In: *Appl. Environ. Microbiol.* 81.18 (2015). Ed. by R. M. Kelly, 6294–6301. doi: 10.1128/AEM.01871-15.
- [308] Piwowarek, K. et al. "*Propionibacterium* spp.—source of propionic acid, vitamin B12, and other metabolites important for the industry". In: *Appl. Microbiol. Biotechnol.* 102.2 (2018), 515–538. doi: 10.1007/s00253-017-8616-7.
- [309] Selmer, T., Willanzheimer, A., and Hetzel, M. "Propionate CoA-transferase from *Clostridium propionicum*". In: *European J. Biochem.* 269.1 (2002), 372–380. doi: 10.1046/j.0014-2956.2001.02659.x.
- [310] Hetzel, M. et al. "Acryloyl-CoA reductase from *Clostridium propionicum*: An enzyme complex of propionyl-CoA dehydrogenase and electron-transferring flavoprotein". In: *European J. Biochem.* 270.5 (2003), 902–910. doi: 10.1046/j.1432-1033.2003.03450.x.
- [311] Seeliger, S. "Energetics and kinetics of lactate fermentation to acetate and propionate via methylmalonyl-CoA or acrylyl-CoA". In: *FEMS Microbiol. Lett.* 211.1 (2002), 65–70. doi: 10.1016/S0378-1097(02)00651-1.
- [312] Thauer, R. K., Jungermann, K., and Decker, K. "Energy conservation in chemotrophic anaerobic bacteria". In: *Bacteriol. Rev.* 41.1 (1977), 100–180. doi: 10.1128/br.41.1.100-180.1977.
- [313] Schuchmann, K. and Müller, V. "Autotrophy at the thermodynamic limit of life: a model for energy conservation in acetogenic bacteria". In: *Nat. Rev. Microbiol.* 12.12 (2014), 809–821. doi: 10.1038/nrmicro3365.
- [314] Walter, K. A. et al. "Sequence and arrangement of two genes of the butyrate-synthesis pathway of *Clostridium acetobutylicum* ATCC 824". In: *Gene* 134.1 (1993), 107–111. doi: 10.1016/0378-1119(93)90182-3.
- [315] Vital, M., Howe, A. C., and Tiedje, J. M. "Revealing the Bacterial Butyrate Synthesis Pathways by Analyzing (Meta)genomic Data". In: *mBio* 5.2 (2014). doi: 10.1128/mBio.00889-14.
- [316] Anand, S., Kaur, H., and Mande, S. S. "Comparative in silico analysis of butyrate production pathways in gut commensals and pathogens". In: *Front. Microbiol.* 7 (2016). doi: 10.3389/fmicb.2016.01945.
- [317] Simanshu, D. K., Savithri, H., and Murthy, M. "Crystal structures of ADP and AMPPNP-bound propionate kinase (TdcD) from *Salmonella typhimurium*: Comparison with members of acetate and sugar kinase/heat shock cognate 70/actin superfamily". In: *J. Mol. Biol.* 352.4 (2005), 876–892. doi: 10.1016/j.jmb.2005.07.069.

- [318] Sullivan, L., Cates, M., and Bennett, G. "Structural correlations of activity of *Clostridium acetobutylicum* ATCC 824 butyrate kinase isozymes". In: *Enzyme Microb. Technol.* 46 (2010), 118–124. DOI: 10.1016/j.enzmictec.2009.10.001.
- [319] Liang, J., Huang, H., and Wang, S. "Distribution, evolution, catalytic mechanism, and physiological functions of the flavin-based electron-bifurcating NADH-dependent reduced ferredoxin: NADP⁺ oxidoreductase". In: *Front. Microbiol.* 10 (2019). DOI: 10.3389/FMICB.2019.00373.
- [320] Wang, S. et al. "NADP⁺ reduction with reduced ferredoxin and NADP⁺ reduction with NADH are coupled via an electron-bifurcating enzyme complex in *Clostridium kluyveri*". In: *J. Bacteriol.* 192 (19 2010), 5115–5123. DOI: 10.1128/JB.00612-10.
- [321] Wang, S. et al. "NADP-Specific Electron-Bifurcating [FeFe]-Hydrogenase in a Functional Complex with Formate Dehydrogenase in *Clostridium autoethanogenum* grown on CO". In: *J. Bacteriol.* 195 (19 2013), 4373. DOI: 10.1128/JB.00678-13.
- [322] Shortall, K. et al. "Insights into Aldehyde Dehydrogenase Enzymes: A Structural Perspective". In: *Front. Mol. Biosci.* 8 (2021), 410. DOI: 10.3389/FMOLB.2021.659550.
- [323] Buckel, W. and Thauer, R. K. "Energy conservation via electron bifurcating ferredoxin reduction and proton/Na⁺ translocating ferredoxin oxidation". In: *Biochim. Biophys. Acta Bioenerg.* 1827 (2 2013). DOI: 10.1016/j.bbabi.2012.07.002.
- [324] Buckel, W. and Thauer, R. K. "Flavin-Based Electron Bifurcation, A New Mechanism of Biological Energy Coupling". In: *Chem. Rev.* 118.7 (2018), 3862–3886. DOI: 10.1021/ACS.CHEMREV.7B00707.
- [325] Rangarajan, E. S. et al. "Crystallographic Trapping of the Glutamyl-CoA Thioester Intermediate of Family I CoA Transferases". In: *J. Biol. Chem.* 280.52 (2005), 42919–42928. DOI: 10.1074/JBC.M510522200.
- [326] Choi, S.-H. et al. "*Anaerotignum faecicola* sp. nov., isolated from human faeces". In: *J. Microbiol.* 57.12 (2019), 1073–1078. DOI: 10.1007/s12275-019-9268-3.
- [327] Moazeni, F., Zhang, G., and Sun, H. J. "Imperfect asymmetry of life: Earth microbial communities prefer D-lactate but can use L-lactate also". In: *Astrobiology* 10.4 (2010), 397–402. DOI: 10.1089/ast.2009.0438.
- [328] Ragsdale, S. W. and Pierce, E. "Acetogenesis and the Wood–Ljungdahl pathway of CO₂ fixation". In: *Biochim. Biophys. Acta - Proteins Proteom.* 1784.12 (2008), 1873–1898. DOI: 10.1016/j.bbapap.2008.08.012.

- [329] Diender, M., Olm, I. P., and Sousa, D. Z. “Synthetic co-cultures: novel avenues for bio-based processes”. In: *Curr. Opin. Biotechnol.* 67 (2021), 72–79. DOI: 10.1016/J.COPBIO.2021.01.006.
- [330] Fernández-Blanco, C., Veiga, M. C., and Kennes, C. “Efficient production of n-caproate from syngas by a co-culture of *Clostridium aceticum* and *Clostridium kluyveri*”. In: *J. Environ. Manage.* 302 (2022), 113992. DOI: <https://doi.org/10.1016/j.jenvman.2021.113992>.
- [331] Olm, I. P. and Sousa, D. Z. “Upgrading dilute ethanol to odd-chain carboxylic acids by a synthetic co-culture of *Anaerostignum neopropionicum* and *Clostridium kluyveri*”. In: *Biotechnol. Biofuels* 16 (1 2023), 1–17. DOI: 10.1186/S13068-023-02336-W.
- [332] Arantes, A. L. et al. “Enrichment of Anaerobic Syngas-Converting Communities and Isolation of a Novel Carboxydophilic *Acetobacterium wieringae* Strain JM”. In: *Front. Microbiol.* 11 (2020). DOI: 10.3389/fmicb.2020.00058.
- [333] Moreira, J. P. et al. “Developing a genetic engineering method for *Acetobacterium wieringae* to expand one-carbon valorization pathways”. In: *Biotechnol. Biofuels* 16 (1 2023), 1–16. DOI: 10.1186/S13068-023-02259-6.
- [334] San-Valero, P. et al. “Effect of pH, yeast extract and inorganic carbon on chain elongation for hexanoic acid production”. In: *Bioresour. Technol.* 300 (2020), 122659. DOI: 10.1016/j.biortech.2019.122659.
- [335] Humphreys, C. M. et al. “Whole genome sequence and manual annotation of *Clostridium autoethanogenum*, an industrially relevant bacterium”. In: *BMC Genom.* 16 (1 2015). DOI: 10.1186/s12864-015-2287-5.
- [336] Emms, D. M. and Kelly, S. “OrthoFinder: Phylogenetic orthology inference for comparative genomics”. In: *Genome Biol.* 20 (1 2019). DOI: 10.1186/s13059-019-1832-y.
- [337] Ross, D. E. et al. “Defining Genomic and Predicted Metabolic Features of the *Acetobacterium* Genus”. In: *mSystems* 5.5 (2020). DOI: 10.1128/MSYSTEMS.00277-20.
- [338] Koch, S. et al. “RedCom: A strategy for reduced metabolic modeling of complex microbial communities and its application for analyzing experimental datasets from anaerobic digestion”. In: *PLOS Comput. Biol.* 15.2 (2019). DOI: 10.1371/journal.pcbi.1006759.
- [339] Bertsch, J. and Müller, V. “CO Metabolism in the Acetogen *Acetobacterium woodii*”. In: *Appl. Environ. Microbiol.* 81.17 (2015), 5949–5956. DOI: 10.1128/AEM.01772-15.

- [340] Braun, M. and Gottschalk, G. “*Acetobacterium wieringae* sp. nov., a new species producing acetic acid from molecular hydrogen and carbon dioxide”. In: *Zentralblatt für Bakteriologie Mikrobiologie und Hygiene: I. Abt. Originale C: Allgemeine, angewandte und ökologische Mikrobiologie* 3.3 (), 368–376. doi: 10.1016/S0721-9571(82)80017-3.
- [341] Weghoff, M. C. and Müller, V. “CO Metabolism in the Thermophilic Acetogen *Thermoanaerobacter kivui*”. In: *Appl. Environ. Microbiol.* 82 (2016), 2312–2319. doi: 10.1128/AEM.00122-16.
- [342] Ceccaldi, P. et al. “The hydrogen dependent CO₂ reductase: the first completely CO tolerant FeFe-hydrogenase”. In: *Energy Environ. Sci.* 10.2 (), 503–508. doi: 10.1039/C6EE02494G.
- [343] Allaart, M. T. et al. “Product Inhibition and pH Affect Stoichiometry and Kinetics of Chain Elongating Microbial Communities in Sequencing Batch Bioreactors”. In: *Front. Bioeng. Biotechnol.* 9 (2021), 513. doi: 10.3389/FBIOE.2021.693030.
- [344] Richter, H. et al. “Ethanol production in syngas-fermenting *Clostridium ljungdahlii* is controlled by thermodynamics rather than by enzyme expression”. In: *Energy Environ. Sci.* 9 (7 2016), 2392–2399. doi: 10.1039/C6EE01108J.
- [345] Abubackar, H. N., Veiga, M. C., and Kennes, C. “Carbon monoxide fermentation to ethanol by *Clostridium autoethanogenum* in a bioreactor with no accumulation of acetic acid”. In: *Bioresour. Technol.* 186 (2015), 122–127. doi: 10.1016/J.BIORTECH.2015.02.113.
- [346] Gottinger, A., Ladu, L., and Quitzow, R. “Studying the Transition towards a Circular Bioeconomy—A Systematic Literature Review on Transition Studies and Existing Barriers”. In: *Sustainability* 12 (21 2020). doi: 10.3390/SU12218990.
- [347] Casau, M. et al. “Residual Biomass: A Comprehensive Review on the Importance, Uses and Potential in a Circular Bioeconomy Approach”. In: *Resources* 11 (4 2022), 35. doi: 10.3390/RESOURCES11040035.
- [348] Loow, Y. L. et al. “Typical conversion of lignocellulosic biomass into reducing sugars using dilute acid hydrolysis and alkaline pretreatment”. In: *Cellulose* 23 (3 2016), 1491–1520. doi: 10.1007/S10570-016-0936-8.
- [349] Richardson, Y. et al. “Biomass Gasification to Produce Syngas”. In: *Recent Advances in Thermo-Chemical Conversion of Biomass*. Ed. by A. Pandey et al. Boston: Elsevier, 2015, 213–250. ISBN: 978-0-444-63289-0. doi: 10.1016/B978-0-444-63289-0.00008-9.

- [350] Hwang, H. W. et al. "Two-stage bioconversion of carbon monoxide to biopolymers via formate as an intermediate". In: *Chem. Eng. J.* 389 (2020), 124394. doi: 10.1016/J.CEJ.2020.124394.
- [351] Köpke, M. et al. "Reconstruction of an Acetogenic 2,3-Butanediol Pathway Involving a Novel NADPH-Dependent Primary-Secondary Alcohol Dehydrogenase". In: *Appl. Environ. Microbiol.* 80 (11 2014), 3394. doi: 10.1128/AEM.00301-14.
- [352] Bae, J. et al. "Valorization of C1 gases to value-added chemicals using acetogenic biocatalysts". In: *Chem. Eng. J.* 428 (2022), 131325. doi: 10.1016/j.cej.2021.131325.
- [353] Lee, H. et al. "Engineering Acetogenic Bacteria for Efficient One-Carbon Utilization". In: *Front. Microbiol.* 13 (2022), 1667. doi: 10.3389/FMICB.2022.865168.
- [354] Tracy, B. P. et al. "Clostridia: the importance of their exceptional substrate and metabolite diversity for biofuel and biorefinery applications". In: *Curr. Opin. Biotechnol.* 23 (3 2012), 364–381. doi: 10.1016/J.COPBIO.2011.10.008.
- [355] Yang, Y. et al. "Production of butanol and isopropanol with an immobilized *Clostridium*". In: *Bioprocess Biosyst. Eng.* 39 (3 2016), 421–428. doi: 10.1007/S00449-015-1525-1.
- [356] Liao, C. et al. "Integrated, systems metabolic picture of acetone-butanol-ethanol fermentation by *Clostridium acetobutylicum*". In: *PNAS* 112 (27 2015), 8505–8510. doi: 10.1073/PNAS.1423143112.
- [357] Du, Y. et al. "Advances and Applications of *Clostridium* Co-culture Systems in Biotechnology". In: *Front. Microbiol.* 11 (2020), 2842. doi: 10.3389/FMICB.2020.560223.
- [358] Bengelsdorf, F. R. et al. "Bacterial Anaerobic Synthesis Gas (Syngas) and CO₂ + H₂ Fermentation". In: *Adv. Appl. Microbiol.* 103 (2018), 143–221. doi: 10.1016/BS.AAMBS.2018.01.002.
- [359] Diallo, M., Kengen, S. W., and López-Contreras, A. M. "Sporulation in solventogenic and acetogenic Clostridia". In: *Appl. Microbiol. Biotechnol.* 105 (9 2021), 3533–3557. doi: 10.1007/S00253-021-11289-9.
- [360] Kuit, W. et al. "Disruption of the acetate kinase (ack) gene of *Clostridium acetobutylicum* results in delayed acetate production". In: *Appl. Microbiol. Biotechnol.* 94 (3 2012), 729. doi: 10.1007/S00253-011-3848-4.
- [361] Monot, F. et al. "Acetone and butanol production by *Clostridium acetobutylicum* in a synthetic medium". In: *Appl. Environ. Microbiol.* (1982). doi: 10.1128/aem.44.6.1318-1324.1982.

- [362] Brändle, J., Domig, K. J., and Kneifel, W. "Relevance and analysis of butyric acid producing Clostridia in milk and cheese". In: *Food Control* (2016). DOI: 10.1016/j.foodcont.2016.02.038.
- [363] Dwidar, M. et al. "The future of butyric acid in industry". In: *Sci. World J.* 2012 (2012). DOI: 10.1100/2012/471417.
- [364] Dash, S. et al. "Capturing the response of *Clostridium acetobutylicum* to chemical stressors using a regulated genome-scale metabolic model". In: *Biotechnol. Biofuels* 7 (1 2014), 1–16. DOI: 10.1186/S13068-014-0144-4.
- [365] Chan, S. H. J., Simons, M. N., and Maranas, C. D. "SteadyCom: Predicting microbial abundances while ensuring community stability". In: *PLOS Comput. Biol.* 13.5 (2017), 1–25. DOI: 10.1371/journal.pcbi.1005539.
- [366] Kremp, F., Roth, J., and Müller, V. "The Sporomusa type Nfn is a novel type of electron-bifurcating transhydrogenase that links the redox pools in acetogenic bacteria". In: *Sci. Rep.* 10 (1 2020). DOI: 10.1038/S41598-020-71038-2.
- [367] Diez-Gonzalez, F., Russell, J. B., and Hunter, J. B. "The role of an NAD-independent lactate dehydrogenase and acetate in the utilization of lactate by *Clostridium acetobutylicum* strain P262". In: *Arch. Microbiol.* 164 (1 1995), 36–42. DOI: 10.1007/BF02568732.
- [368] Agyeman-Duah, E. et al. "Glycerol Utilization as a Sole Carbon Source Disrupts the Membrane Architecture and Solventogenesis in *Clostridium beijerinckii* NCIMB 8052". In: *Fermentation* 8.7 (2022). DOI: 10.3390/fermentation8070339.
- [369] Croux, C. et al. "Autolysis of *Clostridium acetobutylicum* ATCC 824". In: *J. Gen. Microbiol.* 138.5 (1992), 861–869. DOI: 10.1099/00221287-138-5-861.
- [370] Diallo, M. et al. "Transcriptomic and phenotypic analysis of a spoIIIE mutant in *Clostridium beijerinckii*". In: *Front. Microbiol.* 11.September (2020), 1–19. DOI: 10.3389/fmicb.2020.556064.
- [371] Keis, S., Sullivan, J. T., and Jones, D. T. "Physical and genetic map of the *Clostridium saccharobutylicum* (formerly *Clostridium acetobutylicum*) NCP 262 chromosome". In: *Microbiology* 147 (7 2001), 1909–1922. DOI: 10.1099/00221287-147-7-1909.
- [372] Patakova, P. et al. "Acidogenesis, solventogenesis, metabolic stress response and life cycle changes in *Clostridium beijerinckii* NRRL B-598 at the transcriptomic level". In: *Sci. Rep.* 9 (1 2019), 1–21. DOI: 10.1038/s41598-018-37679-0.

- [373] Chen, C. K. and Blaschek, H. P. "Effect of acetate on molecular and physiological aspects of *Clostridium beijerinckii* NCIMB 8052 solvent production and strain degeneration". In: *Appl. Environ. Microbiol.* 65 (2 1999), 499–505. DOI: 10.1128/AEM.65.2.499-505.1999.
- [374] Ibarbalz, F. M. et al. "The bias associated with amplicon sequencing does not affect the quantitative assessment of bacterial community dynamics". In: *PLoS ONE* 9.6 (2014), 1–12. DOI: 10.1371/journal.pone.0099722.
- [375] Kim, H., Jeon, B. S., and Sang, B.-I. "An efficient new process for the selective production of odd-chain carboxylic acids by simple carbon elongation using *Megasphaera hexanoica*". In: *Sci. Rep.* 9.1 (2019), 11999. DOI: 10.1038/s41598-019-48591-6.
- [376] García-Jiménez, B., Torres-Bacete, J., and Nogales, J. "Metabolic modelling approaches for describing and engineering microbial communities". In: *Comput. Struct. Biotechnol. J.* 19 (2021), 226. DOI: 10.1016/J.CSBJ.2020.12.003.
- [377] Im, C. et al. "*Clostridium ljungdahlii* as a biocatalyst in microbial electrosynthesis – Effect of culture conditions on product formation". In: *Bioresour. Technol. Rep.* 19 (2022), 101156. DOI: 10.1016/J.BITEB.2022.101156.
- [378] Drake, H. L. and Daniel, S. L. "Physiology of the thermophilic acetogen *Moorella thermoacetica*". In: *Res. Microbiol.* (2004). DOI: 10.1016/j.resmic.2004.03.003.
- [379] Mook, A. et al. "Autotrophic lactate production from H₂ + CO₂ using recombinant and fluorescent FAST-tagged *Acetobacterium woodii* strains". In: *Appl. Microbiol. Biotechnol.* 106 (4 2022), 1447–1458. DOI: 10.1007/S00253-022-11770-Z.
- [380] Sar, T. et al. "Potential utilization of dairy industries by-products and wastes through microbial processes: A critical review". In: *Sci. Total Environ.* 810 (2022), 152253. DOI: 10.1016/J.SCITOTENV.2021.152253.
- [381] Xu, Z. et al. "Spoilage lactic acid bacteria in the brewing industry". In: *J. Microbiol. Biotechnol.* 30 (7 2020). DOI: 10.4014/jmb.1908.08069.
- [382] Chen, Y., Sharma-Shivappa, R. R., and Chen, C. "Ensiling agricultural residues for bioethanol production". In: *Appl. Biochem. Biotechnol.* 143 (1 2007). DOI: 10.1007/s12010-007-0030-7.
- [383] Sakarika, M. et al. "Production of microbial protein from fermented grass". In: *Chem. Eng. J.* 433 (2022), 133631. DOI: 10.1016/J.CEJ.2021.133631.

- [384] Detman, A. et al. "Cell factories converting lactate and acetate to butyrate: *Clostridium butyricum* and microbial communities from dark fermentation bioreactors". In: *Microb. Cell Factories* 18.1 (2019), 1–12. DOI: 10.1186/S12934-019-1085-1.
- [385] Show, K. Y. et al. "Biohydrogen production: Current perspectives and the way forward". In: *Int. J. Hydrog. Energy* 37 (20 2012), 15616–15631. DOI: 10.1016/J.IJHYDENE.2012.04.109.
- [386] Freier, D. and Gottschalk, G. "L(+)-lactate dehydrogenase of *Clostridium acetobutylicum* is activated by fructose-1,6-bisphosphate". In: *FEMS Microbiol. Lett.* 43 (2 1987), 229–233. DOI: 10.1111/j.1574-6968.1987.tb02128.x.
- [387] Siemerink, M. A. et al. "Comparative genomic analysis of the central metabolism of the solventogenic species *Clostridium acetobutylicum* ATCC 824 and *Clostridium beijerinckii* NCIMB 8052". In: *Systems Biology of Clostridium*. Ed. by P. Dürre. Imperial College Press, 2014, 193–219. ISBN: 978-1-78326-441-4. DOI: 10.1142/9781783264414_0008.
- [388] Sreekumar, S. et al. "Production of an acetone-butanol-ethanol mixture from *Clostridium acetobutylicum* and its conversion to high-value biofuels". In: *Nat. Protoc.* 10 (3 2015), 528–537. DOI: 10.1038/nprot.2015.029.
- [389] Schwalm, N. D. et al. "Developing a Microbial Consortium for Enhanced Metabolite Production from Simulated Food Waste". In: *Fermentation* 5 (4 2019), 98. DOI: 10.3390/fermentation5040098.
- [390] Goers, L., Freemont, P., and Polizzi, K. M. "Co-culture systems and technologies: taking synthetic biology to the next level". In: *J. R. Soc. Interface.* 11 (96 2014). DOI: 10.1098/RSIF.2014.0065.
- [391] Jia, X. et al. "Design, analysis and application of synthetic microbial consortia". In: *Synth. Syst. Biotechnol.* 1.2 (2016), 109–117. DOI: <https://doi.org/10.1016/j.synbio.2016.02.001>.
- [392] Cho, J. S. et al. "Designing Microbial Cell Factories for the Production of Chemicals". In: *J. Am. Chem. Soc.* 2 (8 2022), 1781–1799. DOI: 10.1021/JACSAU.2C00344.
- [393] Kleerebezem, R. and Loosdrecht, M. C. van. "Mixed culture biotechnology for bioenergy production". In: *Curr. Opin. Biotechnol.* 18.3 (2007), 207–212.
- [394] Senne de Oliveira Lino, F. et al. "Complex yeast–bacteria interactions affect the yield of industrial ethanol fermentation". In: *Nat. Commun.* 12.1 (2021), 1498. DOI: 10.1038/s41467-021-21844-7.

- [395] Alper, H. and Stephanopoulos, G. “Engineering for biofuels: exploiting innate microbial capacity or importing biosynthetic potential?” In: *Nat. Rev. Microbiol.* 7.10 (2009), 715–723. DOI: 10.1038/nrmicro2186.
- [396] Hu, J. et al. “Design and composition of synthetic fungal-bacterial microbial consortia that improve lignocellulolytic enzyme activity”. In: *Bioresour. Technol.* 227 (2017), 247–255. DOI: 10.1016/j.biortech.2016.12.058.
- [397] Cabau-Peinado, O., Straathof, A. J., and Jourdin, L. “A general model for biofilm-driven microbial electrosynthesis of carboxylates from CO₂”. In: *Front. Microbiol.* 12 (2021), 669218. DOI: 10.3389/fmicb.2021.669218.
- [398] Baas, P. et al. “Phosphorus mobilizing consortium Mammoth PTM enhances plant growth”. In: *PeerJ* 4 (2016), e2121. DOI: 10.7717/peerj.2121.
- [399] Herrera Paredes, S. et al. “Design of synthetic bacterial communities for predictable plant phenotypes”. In: *PLoS Biol.* 16.2 (2018), e2003962. DOI: 10.1371/journal.pbio.2003962.
- [400] Hu, J. et al. “Probiotic diversity enhances rhizosphere microbiome function and plant disease suppression”. In: *MBio* 7.6 (2016), e01790–16. DOI: 10.1128/mBio.01790-16.
- [401] Vrancken, G. et al. “Synthetic ecology of the human gut microbiota”. In: *Nat. Rev. Microbiol.* 17.12 (2019), 754–763. DOI: 10.1038/s41579-019-0264-8.
- [402] Szulc, A. et al. “The influence of bioaugmentation and biosurfactant addition on bioremediation efficiency of diesel-oil contaminated soil: feasibility during field studies”. In: *J. Environ. Manage.* 132 (2014), 121–128. DOI: 10.1016/j.jenvman.2013.11.006.
- [403] Piccardi, P., Vessman, B., and Mitri, S. “Toxicity drives facilitation between 4 bacterial species”. In: *PNAS* 116.32 (2019), 15979–15984. DOI: 10.1073/pnas.190617211.
- [404] Roell, G. W. et al. “Engineering microbial consortia by division of labor”. In: *Microb. Cell Fact.* 18 (2019), 1–11. DOI: 10.1186/s12934-019-1083-3.
- [405] Thommes, M. et al. “Designing metabolic division of labor in microbial communities”. In: *MSystems* 4.2 (2019), e00263–18. DOI: 10.1128/mSystems.00263-18.
- [406] Hays, S. G. et al. “Better together: engineering and application of microbial symbioses”. In: *Curr. Opin. Biotechnol.* 36 (2015), 40–49. DOI: 10.1016/j.copbio.2015.08.008.
- [407] Erkus, O. et al. “Multifactorial diversity sustains microbial community stability”. In: *ISME J.* 7.11 (2013), 2126–2136. DOI: 10.1038/ismej.2013.108.

- [408] Sanchez, A. et al. “The community-function landscape of microbial consortia”. In: *EcoEvoRxiv* (2022). DOI: 10.1016/j.cels.2022.12.011.
- [409] Widder, S. et al. “Challenges in microbial ecology: building predictive understanding of community function and dynamics”. In: *ISME J.* 10.11 (2016), 2557–2568. DOI: 10.1038/ismej.2016.45.
- [410] Passi, A. et al. “Genome-scale metabolic modeling enables in-depth understanding of big data”. In: *Metabolites* 12 (1 2022), 14. DOI: 10.3390/METABO12010014.
- [411] Chen, J. et al. “Spatiotemporal modeling of microbial metabolism”. In: *BMC Syst. Biol.* (2016). DOI: 10.1186/s12918-016-0259-2.
- [412] Dukovski, I. et al. “A metabolic modeling platform for the computation of microbial ecosystems in time and space (COMETS)”. In: *Nat. Protoc.* 16 (11 2021). DOI: 10.1038/s41596-021-00593-3.
- [413] Biggs, M. B. and Papin, J. A. “Novel Multiscale Modeling Tool Applied to *Pseudomonas aeruginosa* Biofilm Formation”. In: *PLOS ONE* 8.10 (2013), null. DOI: 10.1371/journal.pone.0078011.
- [414] Bauer, E. et al. “BacArena: Individual-based metabolic modeling of heterogeneous microbes in complex communities”. In: *PLOS Comput. Biol.* 13 (5 2017), e1005544. DOI: 10.1371/JOURNAL.PCBI.1005544.
- [415] Borer, B. et al. “Modeling metabolic networks of individual bacterial agents in heterogeneous and dynamic soil habitats (IndiMeSH)”. In: *PLOS Comput. Biol.* 15.6 (2019), 1–21. DOI: 10.1371/journal.pcbi.1007127.
- [416] Heinken, A., Basile, A., and Thiele, I. “Advances in constraint-based modelling of microbial communities”. In: *Curr. Opin. Syst. Biol.* 27 (2021), 100346. DOI: 10.1016/J.COISB.2021.05.007.
- [417] Ang, K. S. et al. “Metabolic Modeling of Microbial Community Interactions for Health, Environmental and Biotechnological Applications.” In: *Curr. Genomics* 19.8 (2018), 712–722. DOI: 10.2174/1389202919666180911144055.
- [418] Shoaie, S. et al. “Quantifying Diet-Induced Metabolic Changes of the Human Gut Microbiome”. In: *Cell Metab.* 22 (2 2015), 320–331. DOI: 10.1016/J.CMET.2015.07.001.
- [419] Mendoza, S. N. et al. “A systematic assessment of current genome-scale metabolic reconstruction tools”. In: *Genome Biol.* 20 (1 2019), 1–20. DOI: 10.1186/s13059-019-1769-1.
- [420] Wilkinson, M. D. et al. “The FAIR Guiding Principles for scientific data management and stewardship”. In: *Sci. Data* 3 (1 2016), 1–9. DOI: 10.1038/sdata.2016.18.

- [421] Katz, D. S., Gruenpeter, M., and Honeyman, T. “Taking a fresh look at FAIR for research software”. In: *Patterns* 2.3 (2021), 100222. doi: <https://doi.org/10.1016/j.patter.2021.100222>.
- [422] Barker, M. et al. “Introducing the FAIR Principles for research software”. In: *Sci. Data* 9.1 (2022), 1–6. doi: [10.1038/s41597-022-01710-x](https://doi.org/10.1038/s41597-022-01710-x).
- [423] Bengtsson-Palme, J. “Microbial model communities: To understand complexity, harness the power of simplicity”. In: *Comput. Struct. Biotechnol. J.* 18 (2020), 3987–4001. doi: [10.1016/j.csbj.2020.11.043](https://doi.org/10.1016/j.csbj.2020.11.043).
- [424] Eng, A. and Borenstein, E. “Microbial community design: methods, applications, and opportunities”. In: *Curr. Opin. Biotechnol.* 58 (2019), 117–128. doi: [10.1016/j.copbio.2019.03.002](https://doi.org/10.1016/j.copbio.2019.03.002).
- [425] Aguirre de Cárcer, D. “Experimental and computational approaches to unravel microbial community assembly”. In: *Comput. Struct. Biotechnol. J.* 18 (2020), 4071–4081. doi: <https://doi.org/10.1016/j.csbj.2020.11.031>.
- [426] Stolyar, S. et al. “Metabolic modeling of a mutualistic microbial community”. In: *Mol. Syst. Biol.* 3.1 (2007), 92. doi: <https://doi.org/10.1038/msb4100131>.
- [427] Cai, J., Tan, T., and Chan, S. H. “Predicting Nash equilibria for microbial metabolic interactions”. In: *Bioinformatics* 36 (24 2021), 5649–5655. doi: [10.1093/BIOINFORMATICS/BTAA1014](https://doi.org/10.1093/BIOINFORMATICS/BTAA1014).
- [428] Louca, S. and Doebeli, M. “Calibration and analysis of genome-based models for microbial ecology”. In: *eLife* 4 (2015). doi: [10.7554/ELIFE.08208](https://doi.org/10.7554/ELIFE.08208).
- [429] Succurro, A., Segrè, D., and Ebenhöf, O. “Emergent Subpopulation Behavior Uncovered with a Community Dynamic Metabolic Model of *Escherichia coli* Diauxic Growth”. In: *mSystems* 4 (1 2019). doi: [10.1128/msystems.00230-18](https://doi.org/10.1128/msystems.00230-18).
- [430] Popp, D. and Centler, F. “ μ BialSim: Constraint-Based Dynamic Simulation of Complex Microbiomes”. In: *Front. Bioeng. Biotechnol.* 8 (2020), 574. doi: [10.3389/FBIOE.2020.00574](https://doi.org/10.3389/FBIOE.2020.00574).
- [431] García-Jiménez, B. et al. “Dynamic simulations of microbial communities under perturbations: opportunities for microbiome engineering”. In: *Research Square Preprints* (2020). doi: [10.21203/rs.2.24431/v1](https://doi.org/10.21203/rs.2.24431/v1).
- [432] Brunner, J. D. and Chia, N. “Minimizing the number of optimizations for efficient community dynamic flux balance analysis”. In: *PLOS Comput. Biol.* 16.9 (2020), 1–20. doi: [10.1371/journal.pcbi.1007786](https://doi.org/10.1371/journal.pcbi.1007786).
- [433] Gardner, J. J., Hodge, B. M. S., and Boyle, N. R. “Multiscale Multiobjective Systems Analysis (MiMoSA): an advanced metabolic modeling framework for complex systems”. In: *Sci. Rep.* 9 (1 2019). doi: [10.1038/s41598-019-53188-0](https://doi.org/10.1038/s41598-019-53188-0).

- [434] Karimian, E. and Motamedian, E. “ACBM: An Integrated Agent and Constraint Based Modeling Framework for Simulation of Microbial Communities”. In: *Sci. Rep.* 10 (1 2020). DOI: 10.1038/s41598-020-65659-w.
- [435] Angeles-Martinez, L. and Hatzimanikatis, V. “Spatio-temporal modeling of the crowding conditions and metabolic variability in microbial communities”. In: *PLOS Comput. Biol.* 17 (7 2021). DOI: 10.1371/journal.pcbi.1009140.
- [436] Hanly, T. J. and Henson, M. A. “Dynamic flux balance modeling of microbial co-cultures for efficient batch fermentation of glucose and xylose mixtures”. In: *Biotechnol. Bioeng.* 108.2 (2011), 376–385.
- [437] Vlassis, N., Pacheco, M. P., and Sauter, T. “Fast Reconstruction of Compact Context-Specific Metabolic Network Models”. In: *PLOS Comput. Biol.* 10.1 (2014), 1–10. DOI: 10.1371/journal.pcbi.1003424.
- [438] Olivier, B. et al. *CBMPy release 0.8.2*. Version 0.8.2. 2021. DOI: 10.5281/zenodo.5546608.
- [439] Klamt, S., Saez-Rodriguez, J., and Gilles, E. D. “Structural and Functional Analysis of Cellular Networks with CellNetAnalyzer”. In: *BMC Syst. Biol.* 1.1 (2007), 2. DOI: 10.1186/1752-0509-1-2.
- [440] Wang, H. et al. “RAVEN 2.0: A versatile toolbox for metabolic network reconstruction and a case study on *Streptomyces coelicolor*”. In: *PLOS Comput. Biol.* 14.10 (2018), 1–17. DOI: 10.1371/journal.pcbi.1006541.
- [441] Palsson, B. Ø. *Systems Biology: Constraint-based Reconstruction and Analysis*. Cambridge University Press, 2015. ISBN: 9781139854610. DOI: 10.1017/CBO9781139854610.
- [442] Keating, S. M. et al. “SBML Level 3: an extensible format for the exchange and reuse of biological models”. In: *Mol. Syst. Biol.* 16.8 (2020), e91110. DOI: 10.15252/msb.20199110.
- [443] Zelezniak, A. et al. “Metabolic dependencies drive species co-occurrence in diverse microbial communities”. In: *PNAS* 112.20 (2015), 6449–6454. DOI: 10.1073/pnas.1421834112.
- [444] Giannari, D., Ho, C. H., and Mahadevan, R. “A gap-filling algorithm for prediction of metabolic interactions in microbial communities”. In: *PLOS Comput. Biol.* 17.11 (2021), e1009060. DOI: 10.1371/journal.pcbi.1009060.
- [445] Bekiaris, P. S. and Klamt, S. “Designing microbial communities to maximize the thermodynamic driving force for the production of chemicals”. In: *PLOS Comput. Biol.* 17.6 (2021), e1009093. DOI: 10.1371/journal.pcbi.1009093.

- [446] García-Jiménez, B., García, J. L., and Nogales, J. “FLYCOP: metabolic modeling-based analysis and engineering microbial communities”. In: *Bioinformatics* 34.17 (2018), i954–i963. doi: 10.1093/bioinformatics/bty561.
- [447] Luo, H. et al. “Modeling the metabolic dynamics at the genome-scale by optimized yield analysis”. In: *Metab. Eng.* 75 (2023), 119–130. doi: 10.1016/j.ymben.2022.12.001.
- [448] Heinken, A. et al. “Genome-scale metabolic reconstruction of 7,302 human microorganisms for personalized medicine”. In: *Nat. Biotechnol.* (2023), 1–12. doi: 10.1038/s41587-022-01628-0.
- [449] Bäumlner, M. et al. “Synthetic co-culture of autotrophic *Clostridium carboxidivorans* and chain elongating *Clostridium kluyveri* monitored by flow cytometry”. In: *Microb. Biotechnol.* 15 (5 2022). doi: 10.1111/1751-7915.13941.
- [450] Anton, M. et al. “standard-GEM: standardization of open-source genome-scale metabolic models”. In: *bioRxiv* (2023). doi: 10.1101/2023.03.21.512712.
- [451] Lachance, J.-C. et al. “BOFdat: Generating biomass objective functions for genome-scale metabolic models from experimental data”. In: *PLOS Comput. Biol.* 15.4 (2019), e1006971. doi: 10.1371/journal.pcbi.1006971.
- [452] Scott, W. T. et al. “Dynamic genome-scale modeling of *Saccharomyces cerevisiae* unravels mechanisms for ester formation during alcoholic fermentation”. In: *Biotechnol. Bioeng.* (2023). doi: 10.1002/bit.28421.
- [453] Schuetz, R., Kuepfer, L., and Sauer, U. “Systematic evaluation of objective functions for predicting intracellular fluxes in *Escherichia coli*.” In: *Mol. Syst. Biol.* 3 (2007), 119. doi: 10.1038/msb4100162.
- [454] Scott, W. T. et al. “Metabolic flux sampling predicts strain-dependent differences related to aroma production among commercial wine yeasts”. In: *Microb. Cell Fact.* 20.1 (2021), 1–15. doi: 10.1186/s12934-021-01694-0.
- [455] Wiback, S. J. et al. “Monte Carlo sampling can be used to determine the size and shape of the steady-state flux space”. In: *J. Theor. Biol.* 228.4 (2004), 437–447. doi: 10.1016/j.jtbi.2004.02.006.
- [456] Zomorodi, A. R. and Segrè, D. “Synthetic ecology of microbes: mathematical models and applications”. In: *J. Mol. Biol.* 428.5 (2016), 837–861. doi: 10.1016/j.jmb.2015.10.019.
- [457] Duarte, N. C., Herrgård, M. J., and Palsson, B. Ø. “Reconstruction and validation of *Saccharomyces cerevisiae* iND750, a fully compartmentalized genome-scale metabolic model”. In: *Genome Res.* 14.7 (2004), 1298–1309. doi: 10.1101/gr.2250904.

- [458] Reed, J. L. et al. “An expanded genome-scale model of *Escherichia coli* K-12 (iJR904 GSM/GPR)”. In: *Genome Biol.* 4.9 (2003), 1–12. doi: 10.1186/gb-2003-4-9-r54.
- [459] King, Z. A. et al. “BiGG Models: A Platform for Integrating, Standardizing and Sharing Genome-Scale Models”. In: *Nucleic Acids Res.* 44.D1 (2016), D515–D522. doi: 10.1093/nar/gkv1049.
- [460] Montgomery, D. C. *Design and analysis of experiments*. John Wiley & sons, 2017. ISBN: 978-1-119-49244-3.
- [461] Orth, J. D. et al. “A Comprehensive Genome-Scale Reconstruction of *Escherichia Coli* Metabolism”. In: *Mol. Syst. Biol.* 7.1 (2011), 535–535. doi: 10.1038/msb.2011.65.
- [462] Raghunathan, A. et al. “Constraint-based analysis of metabolic capacity of *Salmonella typhimurium* during host-pathogen interaction”. In: *BMC Syst. Biol.* 3.1 (2009), 1–16. doi: 10.1186/1752-0509-3-38.
- [463] Fernández-Naveira, Á. et al. “Production of chemicals from C1 gases (CO, CO₂) by *Clostridium carboxidivorans*”. In: *World J. Microbiol.* 33 (3 2017), 1–11. doi: 10.1007/S11274-016-2188-Z.
- [464] Neuendorf, C. S. et al. “A quantitative metabolic analysis reveals *Acetobacterium woodii* as a flexible and robust host for formate-based bioproduction”. In: *Metab. Eng.* 68 (2021), 68–85. doi: 10.1016/j.ymben.2021.09.004.
- [465] Rafieenia, R., Atkinson, E., and Ledesma-Amaro, R. “Division of labor for substrate utilization in natural and synthetic microbial communities”. In: *Curr. Opin. Biotechnol.* 75 (2022), 102706. doi: 10.1016/j.copbio.2022.102706.
- [466] De Groof, V. et al. “Medium Chain Carboxylic Acids from Complex Organic Feedstocks by Mixed Culture Fermentation”. In: *Molecules* 24.3 (2019). doi: 10.3390/molecules24030398.
- [467] Charubin, K. et al. “Interspecies Microbial Fusion and Large-Scale Exchange of Cytoplasmic Proteins and RNA in a Syntrophic *Clostridium* Coculture”. In: *mBio* 11 (5 2020), 1–20. doi: 10.1128/MBIO.02030-20.
- [468] Milanese, A. et al. “Microbial abundance, activity and population genomic profiling with mOTUs2”. In: *Nat. Commun.* 2019 10:1 10 (1 2019), 1–11. doi: 10.1038/s41467-019-08844-4.
- [469] Li, J. et al. “Surface enhanced Raman scattering (SERS)-active bacterial detection by Layer-by-Layer (LbL) assembly all-nanoparticle microcapsules”. In: *Colloids Surf. A Physicochem. Eng. Asp.* 650 (2022). doi: 10.1016/j.colsurfa.2022.129547.

- [470] Deev, D. et al. “When Beneficial Biofilm on Materials Is Needed: Electrostatic Attachment of Living Bacterial Cells Induces Biofilm Formation”. In: *Front. Mater.* 8 (2021). DOI: 10.3389/fmats.2021.624631.
- [471] Johnston, T. G. et al. “Compartmentalized microbes and co-cultures in hydrogels for on-demand bioproduction and preservation”. In: *Nat. Commun.* 11 (1 2020). DOI: 10.1038/S41467-020-14371-4.
- [472] Sánchez-Clemente, R. et al. “Carbon source influence on extracellular pH changes along bacterial cell-growth”. In: *Genes* 11 (11 2020). DOI: 10.3390/genes11111292.
- [473] Ribeling, V., Jungermann, K., and Thauer, R. K. “The Internal-Alka-line pH Gradient, Sensitive to Uncoupler and ATPase Inhibitor, in Growing *Clostridium pasteurianum*”. In: *European J. Biochem.* 55 (2 1975). DOI: 10.1111/j.1432-1033.1975.tb02181.x.
- [474] Huang, L., Gibbins, L. N., and Forsberg, C. W. “Transmembrane pH gradient and membrane potential in *Clostridium acetobutylicum* during growth under acetogenic and solventogenic conditions”. In: *Appl. Environ. Microbiol.* 50 (4 1985). DOI: 10.1128/aem.50.4.1043-1047.1985.
- [475] Salvy, P. et al. “pyTFA and matTFA: a Python package and a Matlab toolbox for Thermodynamics-based Flux Analysis”. In: *Bioinformatics* 35.1 (2018), 167–169. DOI: 10.1093/bioinformatics/bty499.
- [476] Handler, R. M. et al. “Life Cycle Assessments of Ethanol Production via Gas Fermentation: Anticipated Greenhouse Gas Emissions for Cellulosic and Waste Gas Feedstocks”. In: *Ind. Eng. Chem.* 55 (12 2015), 3253–3261. DOI: 10.1021/ACS.IECR.5B03215.
- [477] Stamatopoulou, P. et al. “Fermentation of Organic Residues to Beneficial Chemicals: A Review of Medium-Chain Fatty Acid Production”. In: *Processes* 8.12 (2020). DOI: 10.3390/pr8121571.
- [478] Global Market Insights Inc. *Butyric Acid Market Size By Application (Animal Feed, Chemical Intermediate, Food & Flavor, Pharmaceutical, Personal Care & Cosmetics), Industry Analysis Report, Regional Outlook, Growth Potential, Price Trends, Competitive Market Share & Forecast, 2020 - 2026*. <https://www.gminsights.com/industry-analysis/butyric-acid-market>. Accessed on March 8, 2023. 2020.
- [479] Research and Markets. *Caproic Acid: Global Strategic Business Report 2021-2026*. <https://www.researchandmarkets.com/reports/5302114/caproic-acid-global-strategic-business-report>. Accessed on March 8, 2023. 2021.

- [480] Perimenis, A. et al. "Comparison of the acidogenic and methanogenic potential of agroindustrial residues". In: 72 (2018), 178–185. DOI: 10.1016/J.WASMAN.2017.11.033.
- [481] Scarborough, M. J. et al. "Increasing the economic value of lignocellulosic stillage through medium-chain fatty acid production". In: *Biotechnol. Biofuels* 11 (1 2018). DOI: 10.1186/s13068-018-1193-x.
- [482] Jain, D. S. et al. *Global potential of Biogas*. Research Report. The World Biogas Association, 2019, 56 p.
- [483] Groof, V. D. et al. "Medium chain carboxylic acids from complex organic feedstocks by mixed culture fermentation". In: *Molecules* 24 (3 2019). DOI: 10.3390/molecules24030398.
- [484] Nzeteu, C. O. et al. "Reproducible, high-yielding, biological caproate production from food waste using a single-phase anaerobic reactor system". In: *Biotechnol. Biofuels* (2018). DOI: 10.1186/s13068-018-1101-4.
- [485] Otten, J. K., Zou, Y., and Papoutsakis, E. T. "The potential of caproate (hexanoate) production using *Clostridium kluyveri* syntrophic cocultures with *Clostridium acetobutylicum* or *Clostridium saccharolyticum*". In: *Front. Bioeng. Biotechnol.* 10 (2022). DOI: 10.3389/fbioe.2022.965614.
- [486] Rigouin, C. et al. "Increasing medium chain fatty acids production in *Yarrowia lipolytica* by Metabolic Engineering". In: *Microb. Cell Fact.* (2018). DOI: 10.1186/s12934-018-0989-5.
- [487] Lauer, I., Philipps, G., and Jennewein, S. "Metabolic Engineering of *Clostridium ljungdahlii* for the production of hexanol and butanol from CO₂ and H₂". In: *Microb. Cell Fact.* 21 (1 2022), 1–18. DOI: 10.1186/S12934-022-01802-8.
- [488] Stark, C. et al. "The Potential of Sequential Fermentations in Converting C1 Substrates to Higher-Value Products". In: *Front. Microbiol.* 13 (2022). DOI: 10.3389/fmicb.2022.907577.
- [489] Reddy, M. V. et al. "Review on the production of medium and small chain fatty acids through waste valorization and CO₂ fixation". In: *Bioresour. Technol.* 309 (2020). DOI: 10.1016/j.biortech.2020.123400.

List of publications

Selçuk Aslan, Elad Noor, **Sara Benito-Vaquerizo**, Steffen N. Lindner, Arren Bar-Even (2020). “Design and engineering of *E. coli* metabolic sensor strains with a wide sensitivity range for glycerate.” *Metab. Eng.*, 57, 96-109.

Charles AR. Cotton*, Nico J. Claassens*, **Sara Benito-Vaquerizo***, Arren Bar-Even (2020). “Renewable methanol and formate as microbial feedstocks.” *Curr. Opin. Biotechnol.*, 162, 168-180.

Sara Benito-Vaquerizo, Martijn Diender, Ivette Parera Olm, Peter J. Schaap, Diana Z. Sousa, Vitor A.P. Martins dos Santos, Maria Suarez-Diez (2020). “Modeling a co-culture of *Clostridium autoethanogenum* and *Clostridium kluyveri* to increase syngas conversion to medium-chain fatty-acids.” *CSBJ*, 18, 3255-3266.

Sara Benito-Vaquerizo*, Ivette Parera Olm*, Thijs de Vroet, Peter J. Schaap, Diana Z. Sousa, Vitor A.P. Martins dos Santos, Maria Suarez-Diez (2022). “Genome-scale metabolic modelling enables deciphering ethanol metabolism via the acrylate pathway in the propionate-producer *Anaerotignum neopropionicum*.” *Microb. Cell Factories* 21, 1-18.

Beau Dronsella, Enrico Orsi, **Sara Benito-Vaquerizo**, Timo Glatter, Arren Bar-Even, Tobias J. Erb, Nico J. Claassens (2022). “Engineered synthetic one-carbon fixation exceeds yield of the Calvin Cycle.” *bioRxiv*. doi: 10.1101/2022.10.19.512895.

Sara Benito-Vaquerizo*, Niels Nouse*, Peter J. Schaap, Jeroen Hugenholtz, Stanley Brul, Ana M. López-Contreras, Vitor A.P. Martins dos Santos, Maria Suarez-Diez (2022). “Model-driven approach for the production of butyrate from CO₂/H₂ by a novel co-culture of *C. autoethanogenum* and *C. beijerinckii*.” *Front. Microbiol.* 13.

William T. Scott Jr.*, **Sara Benito-Vaquerizo***, Johannes Zimmerman, Djordje Bajić, Almut Heinken, Maria Suarez-Diez, Peter J. Schaap (2023). “A structured evaluation of genome-scale constraint-based modeling tools for microbial consortia.” *bioRxiv*. 10.1101/2023.02.08.527721.

Mihail Anton, Eivind Almaas, Rui Benfeitas, **Sara Benito-Vaquerizo**, Lars M. Blank, Andreas Dräger, John M. Hancock, Matthias König, Hongzhong Lu, Ulf W. Liebal, Hongwu Ma, Radhakrishnan Mahadevan, Adil Mardinoglu, Jens Nielsen, Juan Nogales, Marco Pagni, Jason A. Papin, Nathan D. Price, Jonathan L. Robinson, Benjamín J. Sánchez, Maria Suarez-Diez, Snorre Sulheim, L. Thomas Svensson, Bas Teusink, Wanwipa Vongsangnak, Hao Wang, Ahmad A. Zeidan, Eduard J. Kerkhoven (2023). “Standard-GEM: standardization of open-source genome-scale metabolic models.” *bioRxiv*. doi:10.1101/2022.10.19.512895.

**Contributed equally*

Overview of completed training activities

Discipline-specific activities

Machine Learning for Bioinformatics & Systems Biology	2019
Wageningen PhD Symposium: Science with Impact	2019
Closed Cycles Meeting	2020
BioSB 2020	2020
BioSB 2021	2021
B-Wise Seminar	2022
Clostridium XVI Conference	2022
Netherlands Biotechnology Congress	2022
MB8.0 Microbial Biotechnology Symposium	2022
Symposium: The expanding world of biological One-carbon fixation - made by nature & engineers	2022
BioSB 2023	2023

General courses

PhD Workshop Carousel	2019
VLAG PhD week	2019
Masterclass on Data Visualization	2019
Project and Time Management	2020
Scientific Writing	2021
How to present online?	2021
Brain friendly working	2021
Teaching and Supervising Thesis students	2022

Assisting in teaching and supervision activities

MSc course 'Metabolic Engineering of Industrial Microorganisms'	2020
MSc course 'Molecular Systems Biology'	2021-2023
Research talk at the BioSB course 'Integrated modelling and optimization'	2021
Supervision of four MSc and one BSc thesis	2020-2022
Co-supervision of a student in MSc course 'Toolbox in Systems and Synthetic Biology'	2022

Other activities

Preparation of research proposal	2019
SSB Seminar series	2019-2023
CSB meetings	2019-2023
SynValue project meetings	2019-2023
PhD trip	2022
Microbial Synthetic Metabolism meetings	2022-2023

About the author

Sara's journey resembles her curious, free, restless, indecisive and adventurous mind. Sara was born on August 25th 1988 in Segovia, a world Heritage city by UNESCO in Spain. She went to the same school next to her house for fourteen years, but she would never have this comfort again. After finishing high school, she moved to Madrid and studied her degree in Chemical Engineering at the Technical University. During her degree, she went on Erasmus to Athens. She really enjoyed meeting people from all over the world and that experience really changed her mind. When she went back from Erasmus, she did her final thesis at the Spanish National Research Council in Madrid where she worked on a project to produce light olefins from sustainable sources.



After obtaining her degree, she got a Leonardo Da Vinci fellowship to work at NIZO, and she moved to the Netherlands. This was the first time that Sara discovered the special city of Wageningen. Once her fellowship finished, she went back to Spain and found a job on a business consulting. This experience woke up her interest in the computing side, but she was missing science and being abroad. Thus, she gave it a try and moved to Utrecht to work in Danone. After this experience, she decided to push her career learning new things, so she studied a MSc in Bioinformatics at Wageningen University. She had the chance to do her MSc thesis at SSB and got her first experience with synthetic biology, modeling and microbial metabolism. She wanted to continue on this path, so, she went to Germany to do her internship in the Systems and Synthetic metabolism group at the Max Planck Institute in Golm. During her internship she discovered the fascinating world of One-Carbon fixation, which she continued working on during her PhD. Sara really enjoyed working on her PhD because she was motivated to contribute to something valuable.

As expected, Sara doesn't know where her next adventure will bring her, but she has something clear, that she will always go back to her favourite place in the world, her small, cozy and marvelous village: Muñoveros.

Acknowledgements

First of all, thank you all for going through ~~the entire thesis a part of my thesis~~ the acknowledgements. You did it! You managed to ~~read skip~~ pass 266 pages. Anyway, I am happy if you are just reading this because that means that you have been an important part of this journey for me. However, I know that there is at least one person who had to read it all, and that person is Maria, my supervisor.

Maria, thanks a lot for everything. Having a good supervision cannot be taken for granted, and I feel the luckiest person to have had you as my supervisor. When I first did my MSc thesis with you, I did not have confidence in myself, and you managed to change that by caring for me and showing faith in me. I was very happy I could force you later to be my PhD supervisor (sorry for that btw ;)). I am deeply grateful for everything you have taught me throughout these years, both scientifically and personally. Thank you for supporting me, and for listening to me (I know, you saved me some therapy!). I am glad I could see you becoming chair of SSB, you fully deserve it, and I hope we will always be in touch.

Vitor, thanks for all the support and your experience to shape and boost the importance of the modeling work and always promote collaboration. Diana, thanks for giving me the chance of discovering this field, and your valuable insights in our group meetings and our projects. Peter, thanks for the discussions, your insights and for believing in my work. Ana, thanks for the valuable insights, for helping me visualize our work together and for showing interest in my future career. Jeroen, thanks a lot for the fruitful SynValue meetings.

There were two key pieces in this project and they were Ivette and Niels. You really did the hardest work and I owe you everything. You have taught me a lot and I am very happy we shared this project together. Ivette, you have helped me immensely and I will always be grateful. I could have avoided opening many melons, but I am happy we could eat most of them together. We were a great team. Niels, thanks a lot for being so open about your work and for sharing such a nice discussions. I appreciate you never gave up and fully trusted in our project.

I would like to thank all my colleagues and friends that I have met during these years in SSB: Enrique, Lyon, Christos, Maria, Silvia, Marco, Sara, Wasin, Rik, Marco, Sonja, Edo, Willemijn, Cristina, Rob, Bart, Jasper, William, Efsun, Sabine, Sanjee, Maria, Peter, Vitor, Brett, Architha, Alex, Tom, Henk, Jenny, Claudia, Anna, Nhung, Linde, Erika, Nong and all the students that have passed by SSB. The pass years were definitely difficult for SSB. Many people left and there was a lot of uncertainty,

but the hardest was to be apart from each other for two years. Covid really hit us hard, but it is nice to see how we are reconnecting as a group. I really appreciated every time I went to the office and I could share moments with you, and of course, everything I could learnt from the wide variety of cool projects that you work on. You made me feel very comfortable and at home, and this is the best feeling when your real home is actually far. Thanks for all your help and for listening to me. I will definitely miss SSB.

Maria, I am happy I got to know how special you are, you transmit positive energy and happiness everywhere you go. Lyon and you are the best tandem. Lyon, thanks for all the help and for always bringing fun to the group. Sanjee, I am glad we shared many years of this journey together. Thanks for always being there and willing to help. Willemijn, you are a vital part of SSB. Thank you for always being so helpful, for being so caring and for the nice chats. Thanks to my office mates, Marco and Wasin. I know I left you many times alone, but I was very happy to share the office with you and laugh out loud to face stress together. Wasin, I have missed you. You were the calm that I needed in many moments, thanks a lot. Silvia, it was great to have met you and I like to see that you are enjoying your time in SSB. Thanks to Marco and Sonja, you were a great discovery of the PhD trip in California. Marco, thanks for all the fun moments together. William, thanks for giving me the chance to work together. Bart, thanks a lot for your help in many projects.

Special thanks to my paranymphs: Sara, Sabine and Efsun. I know these are busy times for you and yet, you have always been there, supporting me and making time to make my defense day special. I love that we always help and respect each other. I am so happy to have met you all, you mean a lot to me. Sara, I always told you that thanks to you, wet and dry lab blended. You are a big example for all of us, you stood up in a bad moment and offered everyone your friendship when most needed. I will be eternally grateful for giving me the chance to be your friend. Sabientje, you are joy! You always have a good word for everyone and know how to cheer us up. I like your enthusiasm for everything and how you enjoy every small detail of life. Efsun, thanks for your kindness and for putting all the love in organizing everything. Thanks for opening the doors of your house here and in Istanbul. I love you 'mis chicas' and I hope we keep on sharing many good moments together.

I want to thank all the students I had the opportunity to supervise: Bram, Thijs, Matylda, Emma, Rensco and Vindhya. I enjoyed it a lot!

Thanks to everyone I have collaborated with, specially to Arren and Nico. Arren, I would have loved you could have witnessed this important moment. I learnt a lot from you. Thanks a lot for being a great mentor, for sharing your passion about the C1 world, but most of all, for giving me the chance to work together. Nico, thanks a lot for always thinking in me and giving me the chance of being part of such nice projects and group meetings. I have learnt a lot from you. Arren would be happy to

see how you are continuing his legacy.

Everyone that has ever had the chance to live in Wageningen knows how special Wageningen is. Specially, when you live the experience surrounded by friends that become your family. I was very lucky to meet Irene, Iame, Curro, Peer, Simon, Alba, Alfonso, Patri, Maira, Thais, Alba and the offspring. Thanks a lot for all the nice moments together. Chulis, you are home to me. Sometimes it is hard to believe how you can give so much love to everyone. I am so happy we have lived together twice. The break up was hard, but we have found our way to continue being there for each other. Alba and Alfonso, you broke my heart when you left. As I said sometimes, everything was easier when you were here, but I am happy we are still sharing great moments and that you are finally together. Albi, you have always been one of my biggest support in the Netherlands, always so helpful and supportive, love you. Simoncito, I miss you tons, but I am happy to see how happy you are with your new life with Theresa. It was great to discover how terrific you are, so fun, so Simon! I miss a lot the intellectual/fun/wild dinners we had with our moving out group. Iamecita and Curro, thanks a lot for being such lovely people. You are always so welcoming and kind with everyone. I am happy to see the wonderful family you have created. Ire and Peer, I am lucky I have met you and seen how your lovely girls grow. Thanks for always being there. Ire, you are a warrior my friend. If you would believe how valuable you are, you could not afford yourself. Mi Patri, it was great to have you back again, thanks a lot for keeping visiting us all the time, be always willing to do things together and be there for me. Jens is very lucky to have you.

During these years, I have also lived in Utrecht and I had the opportunity to make wonderful friends. Thanks to Desi, Eugene, Isma, Claudia, Miguel, Miguel, Álvaro, Claudia, Said, Alberto, Marina and Maria. Desi, you are my sister. Thanks for always being there for me, no matter how busy you were, or whether I was living in Wageningen or Utrecht. I am so happy you met Eugene. You definitely deserve each other. I gained another friend and a new nephew, Theito :). Isma, I am so glad I went to that language café and met you there. Thanks for believing in me, understanding me and being a good friend. Thanks for introducing us the adorable Flo. Claudia, I am so happy we moved out close to each other and became closer. You are an inspiring woman and I am glad to have you as a friend. Maria, thanks for the good moments together and for sharing your courage. The little Alicia has wonderful parents. Thanks to Said and Claudia for all the years of friendship, all the fun and good moments together and the ones that are yet to come ;). Thanks to Miguel malo and Miguel bueno. I was so lucky to end up living in Abraham Bloemaertstraat. I will never forget all the great moments we have lived together and I hope we continue doing so my friends. Alberto and Marina, it was a great discovery to meet you. Thanks for being always that open and willing to organize and do things together. Álvaro, thanks for bringing always your humour and your

positive energy to the group.

Thanks to Iris and Sebastian. I am thrilled I got to know you more. You are amazing people and hope we continue sharing good moments together.

Thanks to my friend Clara. Clara, you are an adorable person, always so positive, kind and caring. I am very happy you came to live in the Netherlands and met such a special guy as Victor. Jonas is very lucky to have such lovely parents.

I would like to thank my friend Laura. Thanks a lot for everything. If I managed to get here today is also because of you. I would have loved to see you among the audience and celebrate this special day with you. However, someone told me that unfortunately, the most special people leave us first.

Thanks a lot to all the great people I could also meet along the way: Cami, Thijs, Nino, Vania, Righe, Enrica and the new Spanish-Italian crew.

I want to thank Joost, Beppie, Linus, Sara, Mika, Bram and the rest of the Koning-Fontijn family for treating me as one more of you. I am very grateful to have met Bram and have gained a new family. I have really learned a lot from your admirable values and the respect you have for each other. Thank you all for the affection, help and love you have given me and my family.

Bramcito, thanks a lot for your unconditional support and for being by my side all these years. Meeting you has been the best thing that has ever happened to me. You are way beyond of what someone can dream of. Sometimes I am a lot, but you always manage to understand me, calm me and make me smile. You have always believed in me and that gave me wings to get till the end. I love you.

Esta aventura ha sido muy especial pero también ha sido duro estar lejos de mis amigos de España y de mi familia. Quisiera agradecer a todos los amigos que siguen ahí a pesar del tiempo y la distancia. A mis amigos de Muñoveros y de Madrid, en especial a mis amigas Lucía y Raquel, porque cada vez que he ido a España me han recibido con los brazos abiertos. Brindo por todos esos buenos momentos, por nuestra mágica conexión y por nuestra amistad infinita. Gracias a mi tsunami (Pili, Rutch, Bea, Sara y el pollo). Sois lo más amigas. No me cansaré de revivir una y otra vez todos esos momentazos juntas, y los que nos quedan. También a mis amigas de la uni, abrazo oso (Galle, Clara, Martis, Ana, Raquel e Irene). Hemos pasado por momentos duros pero ha sido una suerte compartirlos juntas. Me alegro que aunque cada una estemos en un lugar del mundo, sigamos en contacto. Gracias a las pickys pickys (Moni, Martita, San, Andre, Refe y Nata), mis amigas de toda la vida. Gracias por hacer cómo si el tiempo no pasara en nuestra amistad y por estar siempre ahí.

Finalmente, quiero agradecer a mi familia su apoyo incondicional. A mis padres por dárme todo. Gracias por darme una educación, unos valores, por enseñarme a creer, a no rendirme, a valorar cada cosa y a disfrutar de la vida. Sois mi ejemplo de superación y de lucha y gracias a vosotros, hoy soy quien soy. Sé que es difícil estar separados y sé que no lo he puesto fácil, pero aún así, siempre habéis estado ahí. Me

alegro que siempre creyeráis en mi hermana y en mí desde pequeñas, que nunca nos pusiérais límites y siempre nos apoyárais para perseguir nuestros sueños. Gracias a mi hermana María. Gracias chusqui por siempre ser la primera en venir a verme a todos lados, por quererme, valorarme y apoyarme por encima de todo, aunque eso suponga estar separadas. Ojalá pronto estemos juntas y podamos recuperar todo lo que la distancia nos ha quitado. Te quiero. Gracias a mi persona favorita, la tia Ale, por seguir a mi lado. Qué felicidad fue entregar la tesis y poder ir a celebrar tus 100 años! 100 maravillosos años repartiendo felicidad y amor, te adoro. Gracias a mis tias de oro, Maria, Fuen y Marina, por mimarme y quererme siempre de esa forma tan especial. Gracias a mis tios Jose y Rosi por todo el cariño. Gracias también a todos mis primos y en especial, a mi tío Nemesio. Tío, sé que estarías muy orgulloso de mí y me hubiera encantado que hubieras vivido este momento conmigo. Te echo mucho de menos. Este trabajo va por ti.

The research described in this thesis was financially supported by the Netherlands Science Foundation (NWO) under the Programme 'Closed Cycles' (Project nr. AL-WGK.2016.029) and the Netherlands Ministry of Education, Culture and Science under the Gravitation Grant nr. 024.002.002.

Financial support from Wageningen University for printing this thesis is gratefully acknowledged.

